State of Art for
"Phase Sensitive Methods to Detect Cathodic Disbondment"

DOT/PHMSA Other Transaction Agreement DTPH56-06-T-000020

Submitted to:

The U.S. Department of Transportation
Pipeline and Hazardous Materials Safety Administration
400 7TH Street, S.W.
Washington, D.C. 20590-0001

DOT Technical Manager: Allan Beshore

Prepared by:
Gas Technology Institute
1700 S Mount Prospect Rd.
Des Plaines, IL 60018

GTI Project Manager: Max Kieba
GTI Technical Coordinator: Chris Ziolkowski
GTI Principal Investigator: Joe McCarty

Report Issue Date: November 2006

This research was funded in part under the Department of Transportation, Pipeline and Hazardous Materials Safety Administration's Pipeline Safety Research and Development Program. The views and conclusions contained in this document are those of the authors and should not be interpreted as representing the official policies, either expressed or implied, of the Pipeline and Hazardous Materials Safety Administration, or the U.S. Government.

Introduction

This document serves as a state of the art for technologies used to detect cathodic disbondment on steel pipe. The object of the proposed work is to develop a technology that could detect coating disbondment on steel pipe from above ground, thus identifying potential corrosion locations before the pipeline fails. Ideally this technology would detect a coating disbondment at a very early stage, when there is little or no corrosion associated with it.

There is currently no method to detect or locate a disbonded coating from above ground. Existing pipeline potential gradient surveys, both DC and AC voltage, make use of only amplitude data. While amplitude methods can detect an active holiday (break) in the coating, a disbonded coating can shield active corrosion from both detection and cathodic protection. Stated another way, the space between a disbonded coating and the pipe can house an active corrosion cell. Until there is an actual holiday in the coating, the corrosion cell cannot be detected with existing technology. A holiday will allow increased cathodic protection current to flow to the pipe in the immediate vicinity of the holiday, but may not reach the extremities of a large disbondment. Internal methods, such as magnetic flux leakage (MFL) pigging may detect wall thinning but will not differentiate causes. MFL pigging is expensive and may not be possible on lines with bends or diameter changes.

A patent search was performed, and no technologies relating to Phase Sensitive Methods to Detect Cathodic Disbondment were found. There are, however, other technologies that may detect cathodic disbondment by other means. There are also techniques that may infer the presence of cathodic disbondment by detecting its effects, such as shielded corrosion cells.

The general result of the state-of-the-art survey is that there is a great deal of technology that is focused on identifying and locating active corrosion. There is little technology that can identify flaws early on.

Standards

The technology being researched will aim to address a number of standards. It is understood that properly coated pipe will follow one or more of these practices, listed in the project proposal, but not directly referenced elsewhere in this document.

NACE International:	NACE Standard RP0105-2005 Standard Recommended Practice Liquid-Epoxy Coatings for External Repair, Rehabilitation, and Weld Joints on Buried Steel Pipelines
	NACE Standard RP0303-2003 Standard Recommended Practice Field-Applied Heat-Shrinkable Sleeves for Pipelines: Application, Performance, and Quality Control
American Petroleum Institute (API):	API 5L Standard American Petroleum Institute Specification for Line Pipe
American Society of Mechanical Engineers (ASME):	ASME B31.3 Standard American Society of Mechanical Engineers Process Piping
	ASME B31.4 Standard American Society of Mechanical Engineers Pipeline Transportation Systems for Liquid Hydrocarbons and Other Liquids

The research will also aim to address the following standards related to direct assessment and measurement. These standards are cited elsewhere in this document.

- NACE Standard RP0502: Item No. 21097. Pipeline External Corrosion Direct Assessment Methodology.
- NACE Standard TM0102: Item No. 21241. Measurement of Protective Coating Electrical Conductance on Underground Pipelines.

Existing Technologies

The existing technologies can be roughly divided into two categories: gradient surveys and waveform analysis. By existing, these authors mean that there is commercial, off-the-shelf equipment available. Gradient surveys take a measurement of a single parameter, such as pipe to soil potential, at various points along the pipe being surveyed. Waveform analysis, by contrast, captures the voltage or current waveform to a high resolution. The waveform is then analyzed to extract information about the state of the pipeline.

Because of its simplicity, the Direct Current Voltage Gradient (DCVG) survey is probably the most commonly used survey method. There are a large number of manufacturers and contractors that support this type of survey. If the pipeline has cathodic protection (CP) test stations in place, the DCVG survey can be performed with a half-cell and a digital multimeter (DMM). The DCVG survey is not intrinsically sensitive to disbondment. The DCVG will find existing holidays of a reasonable size by detecting the change in pipe to soil potential along the pipe. An abrupt change in potential as a function of location infers that there is a breach in the coating. The holiday so found may be the end result of a disbondment that shielded a corrosion pocket. NACE TM0102 (NACE International, 2002) describes survey techniques for measuring the conductance of pipeline coatings. A disbondment is expected to change the capacitance of the coating, and may have no effect on the conductance.

In Line Inspection (ILI) methods, such as magnetic flux leakage (MFL) pigging can be regarded as surveys with extremely fine spatial resolution. It must be noted that not all pipelines are accessible to ILI methods. This is a well-established method supported by numerous vendors. ILI can detect wall thinning but does not differentiate the causes. If a disbondment contains an active corrosion cell, then there may be wall thinning associated with the corrosion. It is important to note that the wall thinning may not be present during the early stages of a disbondment. Properly applied ILI will locate indications along the pipeline with very good spatial accuracy. ILI may infer the presence of a well-established disbondment but does not directly detect it.

The Alternating Current Voltage Gradient (ACVG) and Current Attenuation (ACCA) may be able to detect large disbondments. Because these techniques measure only the signal amplitude,

however, it may be difficult to distinguish between an extensive disbondment and a small holiday. These methods inject a known AC signal into the pipeline over and above the existing CP current. The ACVG measures the AC signal at various locations along the pipeline by the use of probes in contact with the soil. The ACCA uses a hand held magnetometer or search coil to get the measurement without the requirement of soil contact. Anomalies in the coating will cause the AC current to drain off at rate different than pristine coating. These techniques detect the difference. The Radiodetection Pipeline Current Mapper is an example of a modern ACCA instrument (Parker, 2002 and 2004.)

The first type of waveform analysis to be considered makes use of the half-wave rectified sinusoid that is the commonly used on impressed current systems. EUPEC Risk Management Systems (formerly TransWave International) offers the system commercially (Flanery et al, 2000; EUPEC Risk Management Systems, n.d.) In this case, data is taken at hard wired test stations along a pipeline that is under impressed current protection. A digital oscilloscope is used to capture the rectified power waveform. The waveform is then analyzed for its extreme values and features. This provides more information than the simple average voltage given by a DMM. A pipeline may have an average CP voltage that is appropriate while the extreme negative excursion of the rectifier waveform may be in a region that can produce excess hydrogen and promote disbondment. Once again, the technique can provide inferential evidence that a disbondment is present but does not directly detect the disbondment. The technique has a unique advantage in that it uses an excitation waveform that is commonly available on many pipelines.

Time Domain Reflectometry (TDR) is commonly used in the telecom industry to detect faults in electrical cables, both buried and overhead. It has seen some limited use in geotechnical applications such as bridge tendon inspection (Chajes et al, 2002.) There are numerous vendors supporting TDR for wire and cable applications. The Infrastructure Technology Institute at Northwestern University (Evanston, IL) and the University of Delaware (Newark, DE) are at the forefront of applying TDR to civil and geotechnical engineering.

In TDR, an electrical pulse is launched into the conductor one wishes to inspect through a direct connection. The injection point is monitored using a high-speed digital oscilloscope. Various features along the conductor will cause reflections of the pulse that can be observed at the

injection point. The time delay between launch and reflection gives the distance from the injection point to the flaw. The phase and amplitude of the reflection provide information about the geometry of the flaw.

TDR does require some calibration to give accurate results. The velocity of pulse propagation in the conductor must be characterized to give accurate linear location. Various features such as flaws, branches, stubs, etc will give their own characteristic reflections. These characteristics must be catalogued. Once calibrated for pipelines, TDR may be able to directly detect and distinguish cathodic disbondment. The drawback to TDR is that its range may be limited in the pipeline environment. TDR typically uses sharp pulses that contain high frequency components that would be susceptible to dispersion. Using lower frequency excitation can extend the range at the expense of lowering the resolution. Both the spatial location accuracy and size of flaw detection would be affected.

Current Research

Spread Spectrum Time Domain Reflectometry (SSTDR) systems are currently under development (Smith et al, 2005.) SSTDR uses a unique train of pulses to excite the pipeline under test. The use of a complex waveform can improve the noise immunity and spatial resolution over that of single pulse TDR. Correlation techniques are used to bring about the improvement. Because the complex signal is known at the transmitter, the receiver can correlate the echoes with a replica of the sent signal. The correlation technique will be much more robust in the presence of noise.

The corrosion process itself generates electrochemical noise (EN) and potentials. Once again, it is important to note that a coating disbondment in its very early stages may not contain corrosion. A variety of techniques are described in the patents cited. These use auxiliary electrical signals to excite the pipe or specimen under test. These auxiliary signals are used to overcome the polarization potentials caused by corrosion, and by doing so, measure it. In other instances the auxiliary signals provided a scaling and calibration of the attenuation along the pipeline allowing accurate scaling of the EN being observed. The importance of EN techniques is that they recognize the pipe-to-soil boundary as having complex impedance. The technique that GTI proposes seeks to find impedance anomalies in the pipeline coating.

Patents

Below are the abstracts of U.S. patents believed to be relevant to the current research. The patents are included in their entirety the Appendix.

1.0 Monitoring the Corrosion of Pipelines by Evaluating the Noise in Data Signals Transmitted via the Pipeline" (US 6,718,267, Jones; Issued April 6, 2004)

(57) **ABSTRACT**

When a pipeline is used as a medium for data transmission using a VLP or ELF Electro-magnetic signal the presence of corrosion effects on the pipeline lead to noise signals appearing in the received data signal. The present invention relates to a method of separating out this noise signal and analyzing it to determine the corrosion status of the pipeline. Both the type and location of the corrosion effect can be determined in this way.

2.0 Method of Detecting Corrosions in Pipelines and the Like by Comparative Pulse Propagation Analysis (US 6,298,732, Burnett; Issued October 9, 2001)

(57) **ABSTRACT**

A method of detecting corrosion on an elongate member, such as a pipe. Far side and near side electric pulses (waves) are transmitted into a magnetically permeable pipe at spaced locations to travel toward one another. These are synchronized to intersect at various locations on the pipe. The resulting wave forms are analyzed by combining adjacent wave forms resulting from pulses intersection at spaced locations. Two combined wave forms are analyzed by subtracting one from the other to produce a difference wave form and the difference wave forms are compared to detect corrosion.

3.0 Electrochemical Impedance Spectroscopy Method for Evaluating Corrosion Inhibitor Performance (US 5,370,776, Chen/Chevron Research and Technology Company; Issued Dec 6, 1994)

[57] **ABSTRACT**

A simple, expedient method for measuring the effectiveness of a corrosion inhibitor provided to a metallic surface by a surface layer, wherein the layer is formed by use of the corrosion inhibitor is a corrosive fluid. The method employs the measuring of a high frequency phase angle as an indicator of inhibitor effectiveness.

List of Acronyms

ACVG Alternating Current Voltage Gradient

ACCA Alternating Current – Current Attenuation

ECDA External Corrosion Direct Assessment

ICDA Internal Corrosion Direct Assessment

SCCDA Stress Corrosion and Cracking (Direct Assessment)

DMM Digital Multimeter

CIS Close Interval Survey

DCVG Direct Current Voltage Gradient or Direction Current Voltage Gradient

PCM Pipeline Current Mapper

SCM Stray Current Mapper

TDR Time Domain Reflectometry

SSTDR Spread Spectrum Time Domain Reflectometry

IEEE Institute of Electronic & Electrical Engineers

NACE National Association of Corrosion Engineers

References

ANSI/NACE Standard RP0502: Item No. 21097. “Pipeline External Corrosion Direct Assessment Methodology.” ISBN 1-57590-156-0. Copyright 2002, NACE International. Approved August 22, 2003.

Chajes, Michael et al. “Void Detection in Grouted Post-Tensioned Bridges Using Time Domain Reflectometry.” Transportation Research Board Annual Meeting. August 2002.

EUPEC Risk Management Systems. “Full Wave Form Analysis and ECDA Requirements.” Date Unknown.

Flanery, Mark et al. “New Waveform Technology for the Diagnostic Survey and Remote Monitoring of Cathodically protected Underground Pipelines.” June 16, 2000.

NACE Standard TM0102: Item No. 21241. “Measurement of Protective Coating Electrical Conductance on Underground Pipelines.” ISBN 1-57590-155-2. Copyright 2002, NACE International.

Parker, G.W. “New Electromagnetic Methods to Locate and Assess Buried CP Problems.” NACE International Conference. Quebec, Canada. August 26-27, 2002.

Parker, G.W. “Pipeline Coating: Aboveground Techniques for the Underground Evaluation of Condition.” NACE Conference. Seattle, WA. 2004.

Smith, Paul et al. “Analysis of Spread Spectrum Time Domain Reflectometry for Wire Fault Location.” IEEE Sensors Journal, Vol. 5, No. 6, December 2005.

Appendix – Patents and References

Note: Only summaries (available free to the public) for the NACE standards are included. The full standards can be downloaded and distributed for free only to NACE members. If copies of these standards are desired, please contact NACE International directly to purchase.

US006718267B1

(12) **United States Patent**
Jones

(10) **Patent No.: US 6,718,267 B1**
(45) **Date of Patent: Apr. 6, 2004**

(54) **MONITORING THE CORROSION OF PIPELINES BY EVALUTING THE NOISE IN DATA SIGNALS TRANSMITTED VIA THE PIPELINE**

(76) Inventor: **Greg Jones**, c/o Kairua Limited, 7a Ferryhill Place, Aberdeen AB11 2SE (GB)

(*) Notice: Subject to any disclaimer, the term of this patent is extended or adjusted under 35 U.S.C. 154(b) by 0 days.

(21) Appl. No.: **09/762,496**

(22) PCT Filed: **Aug. 9, 1999**

(86) PCT No.: **PCT/GB99/02621**

§ 371 (c)(1),
(2), (4) Date: **Feb. 23, 2001**

(87) PCT Pub. No.: **WO00/08438**

PCT Pub. Date: **Feb. 17, 2000**

(30) **Foreign Application Priority Data**

Aug. 8, 1998 (GB) 9817221

(51) **Int. Cl.**[7] **G01B 5/28**; G01N 27/26

(52) **U.S. Cl.** **702/38**; 702/33; 702/35; 204/404

(58) **Field of Search** 204/404; 205/775.5; 702/33–35, 36–38, 45, 47, 50–54; 324/207.12, 207.24, 72; 73/86, 570, 597, 627

(56) **References Cited**

U.S. PATENT DOCUMENTS

4,575,678 A	*	3/1986	Hladky	204/404
4,658,365 A		4/1987	Syrett et al.	
4,886,360 A		12/1989	Finlan	
5,139,627 A	*	8/1992	Eden et al.	204/404
5,370,776 A		12/1994	Chen	
6,298,732 B1	*	10/2001	Burnett	73/579

FOREIGN PATENT DOCUMENTS

GB	1 341 426 A		12/1973
GB	WO 93 26115	*	12/1993
WO	WO 93 26115 A		12/1993
WO	WO 94 12862 A		6/1994

OTHER PUBLICATIONS

Lynn et al., *Introductory Digital Signal Processing*, Wiley, ISBN 0 471 97631 8. , pp. 316, 317, and 333–337.

Tadeusz et al., *Signal and Noise Separation: Art and Science*, Geophysics, vol. 64, No. 5., pp. 1648–1656.

Lacey, *Assessment of Noise Characteristics of Different Corrosion Processes in a Pipeline*, CAPCIS Reference BPJLGY/R1, Jun., 1999., 18 Pages.

Dougherty, P.E. et al., "Use of electrochemical noise measurement in the evaluation of materials for steam generators, " Proceedings of the 1994 1st International.

Dickie Neil, "Corrosion monitoring in remote or hostile locations," Anticorrosion Methods and Materials, Jan.–Feb. 1997 MCB University Press LTD, Bradford, England, vol. 44, No. 1, pp. 41–43.

* cited by examiner

Primary Examiner—Bryan Bui
(74) *Attorney, Agent, or Firm*—Shalom Wertsberger; Saltamar Innovations

(57) **ABSTRACT**

When a pipeline is used as a medium for data transmission using a VLP or ELF Electro-magnetic signal the presence of corrosion effects on the pipeline lead to noise signals appearing in the received data signal. The present invention relates to a method of separating out this noise signal and analyzing it to determine the corrosion status of the pipeline. Both the type and location of the corrosion effect can be determined in this way.

8 Claims, 2 Drawing Sheets

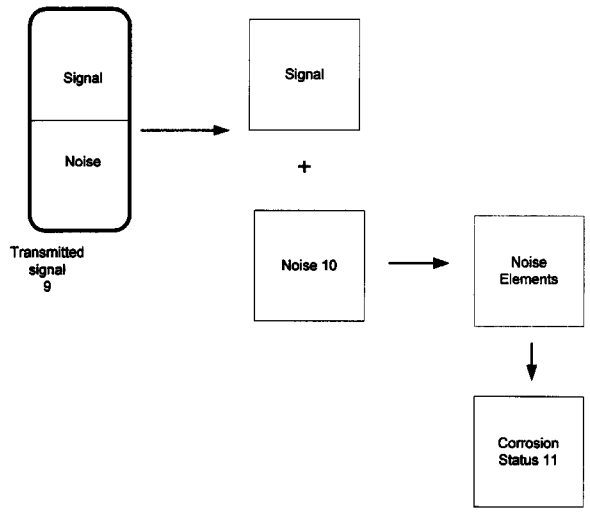

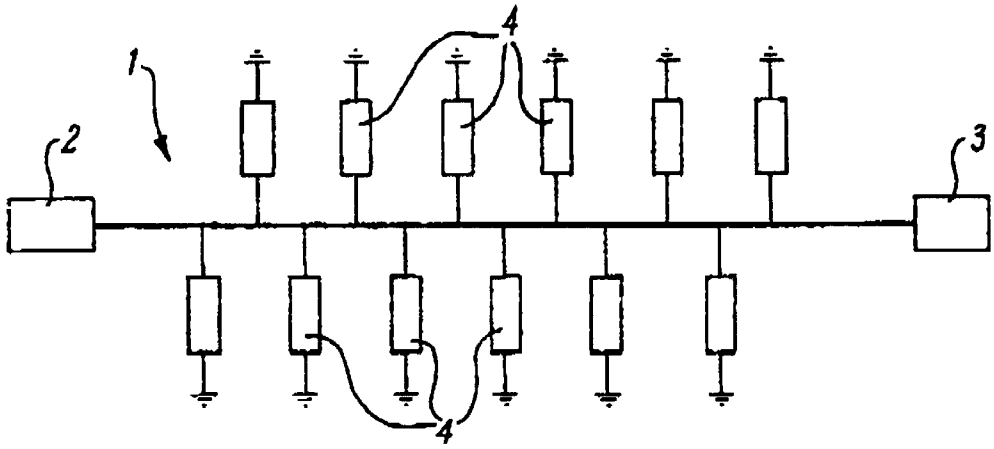

FIG. 1

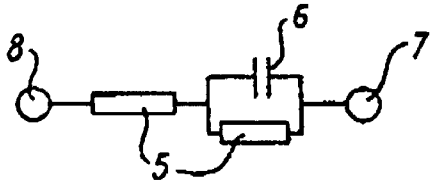

FIG. 2

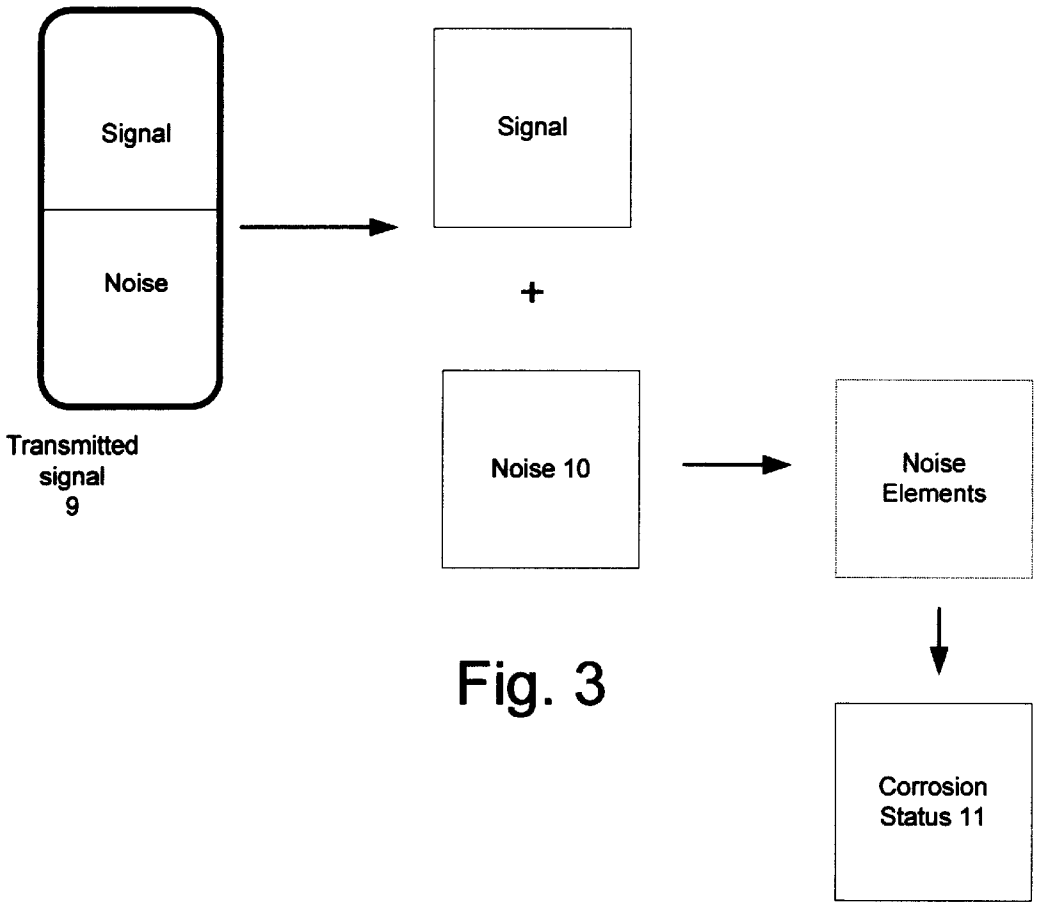
Signal
Noise
Transmitted signal 9
Signal
+
Noise 10
Noise Elements
Corrosion Status 11

Fig. 3

MONITORING THE CORROSION OF PIPELINES BY EVALUTING THE NOISE IN DATA SIGNALS TRANSMITTED VIA THE PIPELINE

This invention relates to a method of detecting and monitoring corrosion on both onshore and offshore pipelines especially but not exclusively by utilising low frequency signal propagation communication systems.

BACKGROUND OF THE INVENTION

Pipelines used for the transport of oil both on and offshore are subject to corrosion effects both from the material being transported and from the external environment. In order to ensure that the mechanical integrity of the pipeline is not compromised there is a need to monitor any corrosion that takes place. In certain circumstances, visual inspection of the pipeline is possible. However internal inspection and inspection of offshore pipelines in this way is generally not practical.

It is known that corrosion effects in a metallic pipeline will have an effect on electrical signals that are transmitted along a section of pipeline. Various proposals have previously been made to make use of electrical effects to monitor and measure corrosion rates in metal structures. Examples of methods for monitoring and measuring corrosion in metal structures using electrical techniques are described in U.S. Pat. Nos. 4,575,678, 4,658,365, 5,139,627 and 5,370,776. In each of these there is either a dedicated electrical connection made to the structure using parts of the structure to form electrodes or special electrodes attached to the structure. Various techniques are used for applying and analyzing electrical signals to obtain some measure of corrosion effects.

All of these techniques however share the disadvantage and limitation that they rely on the addition of extra components and specific dedicated external circuitry to the pipeline or structure in order to apply and measure electrical signals. In certain circumstances, for example offshore, this may be difficult to achieve.

SUMMARY OF THE INVENTION

It is an object of the present invention to provide a means of analyzing the electrical effects caused by corrosion in metal structures without the addition of extra external connections and circuitry.

According to the present invention there is provided a method of corrosion monitoring of pipelines comprising separating out a noise signal from a reference signal transmitted on a pipeline and analyzing said noise signal to provide an indication of the presence of corrosion effects.

Preferably the reference signal comprises a data communications signal.

The reference signal may be a DC signal or a low frequency AC signal. Most preferably, the reference signal has a signal frequency of around 100 Hz.

Preferibly also, the noise signal is separated out into elements representative of specific corrosion effects on the pipeline.

More preferably, the separate noise elements are analysed by comparison to noise signals representative of a range of corrosion effects to identify the presence and extent of any of said corrosion effects.

Most preferably, the separate noise elements are additionally analysed to determine the positional source of each noise element and so identify the location on the pipeline of each corrosion effect.

This may, for example, be by transmitting signals in both directions and analyzing their interaction.

The corrosion effects being monitored may for example include general corrosion, localised corrosion, sacrificial anode cathodic protection, CO_2 corrosion and seawater corrosion.

BRIEF DESCRIPTION THE DRAWINGS

Embodiments of the present invention will now be described by way of example with reference to the accompanying drawings in which:

FIG. **1** is a schematic diagram illustrating the manner in which corrosion cells on a pipeline effectively create additional electrical inputs to a, signal being transmitted on said pipeline; and

FIG. **2** is an effective circuit diagram of the corrosion cell that exists between the pipeline and seawater or ground.

FIG. **3** is a schematic diagram illustrating separating out of a noise signal from a transmitted reference signal and further obtaining a corrosion status from the noise signal according to an embodiment of the present invention

DETAILED DESCRIPTION OF THE PREFERRED EMBODIMENT (S)

International Patent application number PCT/GB93/01272 describes a system for data transmission on pipelines. The system described is a low frequency communications system in which digital signals are transmitted along both onshore and offshore pipelines. Data is transmitted in either direction between a master platform and a remote, usually offshore, facility via communication channels formed by the electrically conducting material of the pipelines. The data is transmitted in the form of a VLF or ELF Electron-magnetic signal which comprises changes of voltage level oscillating about the DC voltage level of pipe so that the mean level of the signal is the DC voltage level of the pipe. The signal frequency is of the order of 100 Hz and as part of the data transmission system the received signal is analysed, using a series of signal processing algorithms, to remove noise picked up during transmission to produce a clean signal for data purposes. The presence of this noise is, at least partially, a result of corrosion effects on the surface, both internally and externally, of the pipeline. Thus while for data transmission purposes this noise is undesirable its very presence is on the other hand an indication of corrosion effects on the pipeline. While the above application recognises the cause of noise, its main concern is the removal of the noise effect from the data transmission.

Referring to the drawings the present invention is concerned with the analysis of the noise signal **10** that occurs in the transmitted signal **9** to provide a picture of the corrosion status **11** of the pipeline. The noise picked up on the transmitted signal is low frequency noise of typically <1 Hz. The noise has the spontaneous non-stoiochmetric electrochemical signal of low frequency (<1 Hz) and low amplitude (<10 mv) which is characteristic of the corrosion process and corrosion kinetics occurring on the metal surface. Thus by detailed analysis of the noise signal the presence of corrosion on the pipeline between the signal transmitter and receiver can be determined. Further developments may allow detailed analysis of the extent, type and location of the corrosion.

More specifically the noise can be considered as the effect of the numerous parallel and series paths of corrosion cells

associated with the pipeline. The electrochemical noise generated by these corrosion cells is effectively added to the data transmission signal. This can be seen in FIGS. **1** & **2** where a data transmission system is shown generally at **1** with a data transmitter **2** and a receiver **3** at respective ends of the system. A series of corrosion cells are represented by **4**. The effective circuit of each corrosion cell **4** is shown generally in FIG. **2** being effectively a combination of resistive **5** and capacitive **6** elements between a pipeline **7** and ground **8**.

Of course the noise signal is itself a composite signal representative of the cumulative effects of the various corrosion call paths. This noise signal will be made up of electrochemical noise associated with natural corrosion processes both generally and localised on joins and welds etc. both internally and externally and the effect of noise generated by sacrificial anodes.

By building up a database of the characteristics of the different electrochemical noises generated from different corrosion processes it is possible to have a means of identifying these corrosion processes when they occur in practice. Examples include general corrosion, localised corrosion, sacrificial anode cathodic protection, CO_2 corrosion, and seawater corrosion.

The present system analyses the noise signal to separate out and identify these individual noise elements in order that a picture can be created of the corrosion state of the section of pipeline. The analysis can be more or less complex depending on the level of detail required in the report to be created

Modifications and improvements may be made without departing from the scope of the invention herein intended. For example although the embodiment described makes use of a data transmission system on the pipeline it is also envisaged that the system can be adapted for use on pipelines where no such data transmission system is in use. In such circumstances alternative arrangements can be provided for transmitting and receiving reference signals along the pipeline.

I claim:

1. A method of corrosion monitoring of pipelines comprising separating out a noise signal from a reference signal transmitted on a pipeline, separating out the noise signal into noise elements, and analyzing said noise elements by comparison to noise signals representative of a range of corrosion effects, to provide an indication of the presence of corrosion effects in the pipeline.

2. A method of corrosion monitoring of pipelines as claimed in claim **1**, wherein the reference signal comprises a data communications signal.

3. A method of corrosion monitoring of pipelines as claimed in claim **1**, wherein the reference signal has a signal frequency of around 100 Hz.

4. A method of corrosion monitoring of pipelines as claimed in claim **1**, wherein the separate noise elements are analysed to determine the positional source of each noise element to identify the location on the pipeline of each corrosion effect.

5. A method of corrosion monitoring of pipelines as claimed in claim **4**, wherein the signals are transmitted in both directions and interaction analysed to determine the positional source of each noise element.

6. A method of corrosion monitoring of pipelines as claimed in claim **1**, wherein the corrosion effects being monitored include general corrosion, localised corrosion, sacrificial anode cathodic protection, CO_2 and seawater corrosion.

7. A method of corrosion monitoring of pipelines as claimed in claim **1**, wherein said step of analyzing is conducted on a noise signal having a frequency of less than 1 Hz.

8. A method of corrosion monitoring of pipelines as claimed in claim **1**, wherein said step of analyzing is conducted on a noise signal having an amplitude of less than 10 mV.

* * * * *

US006298732B1

(12) **United States Patent**
Burnett

(10) **Patent No.: US 6,298,732 B1**
(45) **Date of Patent: *Oct. 9, 2001**

(54) **METHOD OF DETECTING CORROSION IN PIPELINES AND THE LIKE BY COMPARATIVE PULSE PROPAGATION ANALYSIS**

(76) Inventor: **Gale D. Burnett**, 9191 Northwood Rd., Lynden, WA (US) 98264

(*) Notice: Subject to any disclaimer, the term of this patent is extended or adjusted under 35 U.S.C. 154(b) by 0 days.

This patent is subject to a terminal disclaimer.

(21) Appl. No.: **09/576,865**

(22) Filed: **May 22, 2000**

Related U.S. Application Data

(63) Continuation of application No. 09/090,800, filed on Jun. 4, 1998, now Pat. No. 6,065,348.
(60) Provisional application No. 60/048,660, filed on Jun. 4, 1997.

(51) **Int. Cl.**[7] **G01N 29/04**
(52) **U.S. Cl.** **73/801**; 73/579; 73/600
(58) **Field of Search** 73/801, 592, 597, 73/600, 577, 621, 625, 638; 324/637

(56) **References Cited**

U.S. PATENT DOCUMENTS

4,181,882	*	1/1980	Isaacs et al.	205/775.5
4,393,711	*	7/1983	Lapides	73/592
4,970,476	*	11/1990	Kitagawa	333/12
5,456,113	*	10/1995	Kwun et al.	73/587
5,497,661	*	3/1996	Stripf et al.	73/611
5,526,691	*	6/1996	Latimer et al.	73/592
6,065,348	*	5/2000	Burnett	73/801

* cited by examiner

Primary Examiner—Max Noori
(74) *Attorney, Agent, or Firm*—Robert B. Hughes; Hughes & Schacht, PLLC

(57) **ABSTRACT**

A method of detecting corrosion on an elongate member, such as a pipe. Far side and near side electric pulses (waves) are transmitted into a magnetically permeable pipe at spaced locations to travel toward one another. These are synchronized to intersect at various locations on the pipe. The resulting wave forms are analyzed by combining adjacent wave forms resulting from pulses intersection at spaced locations. Two combined wave forms are analyzed by subtracting one from the other to produce a difference wave form and the difference wave forms are compared to detect corrosion.

9 Claims, 13 Drawing Sheets

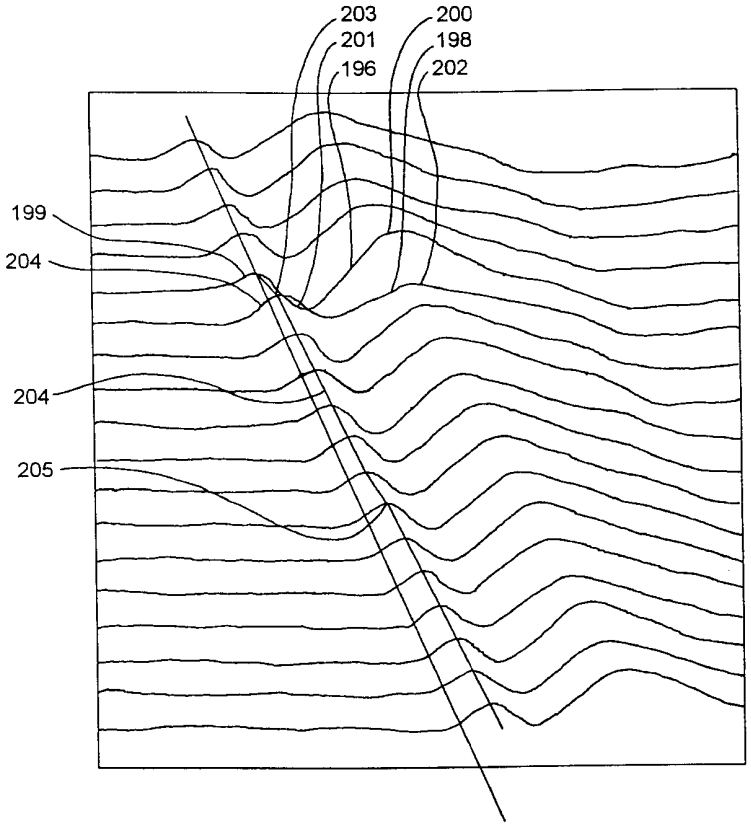

FIG. 1

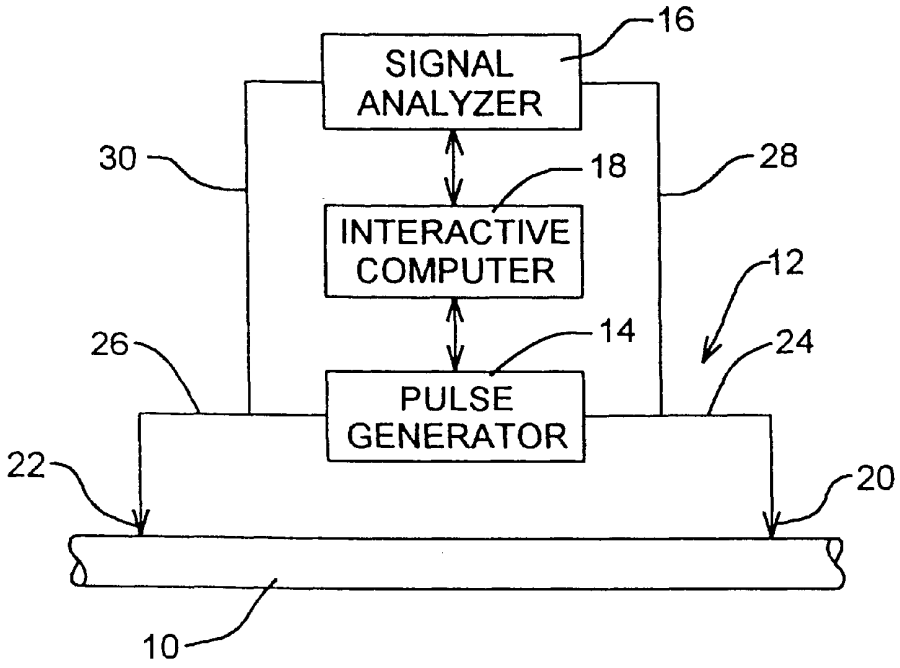

FIG.2A
PRIOR ART

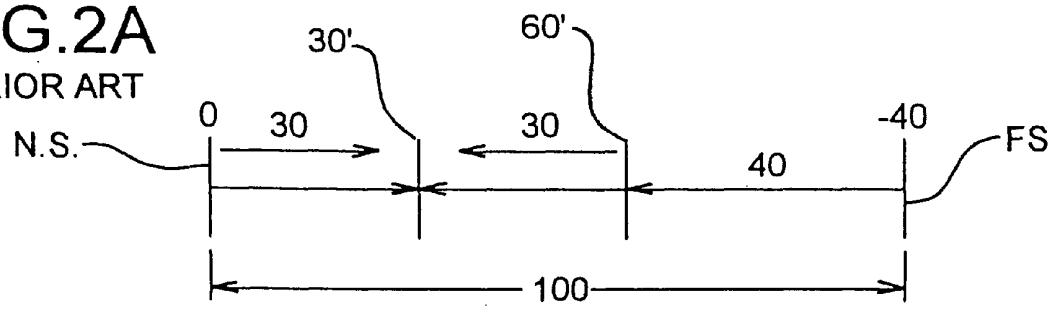

FIG. 2B
PRIOR ART

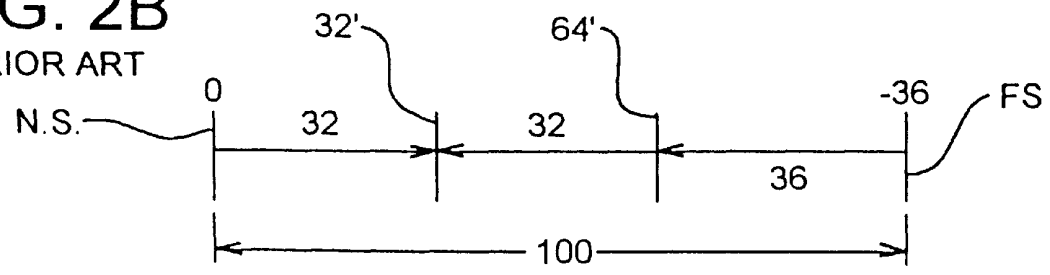

FIG. 3

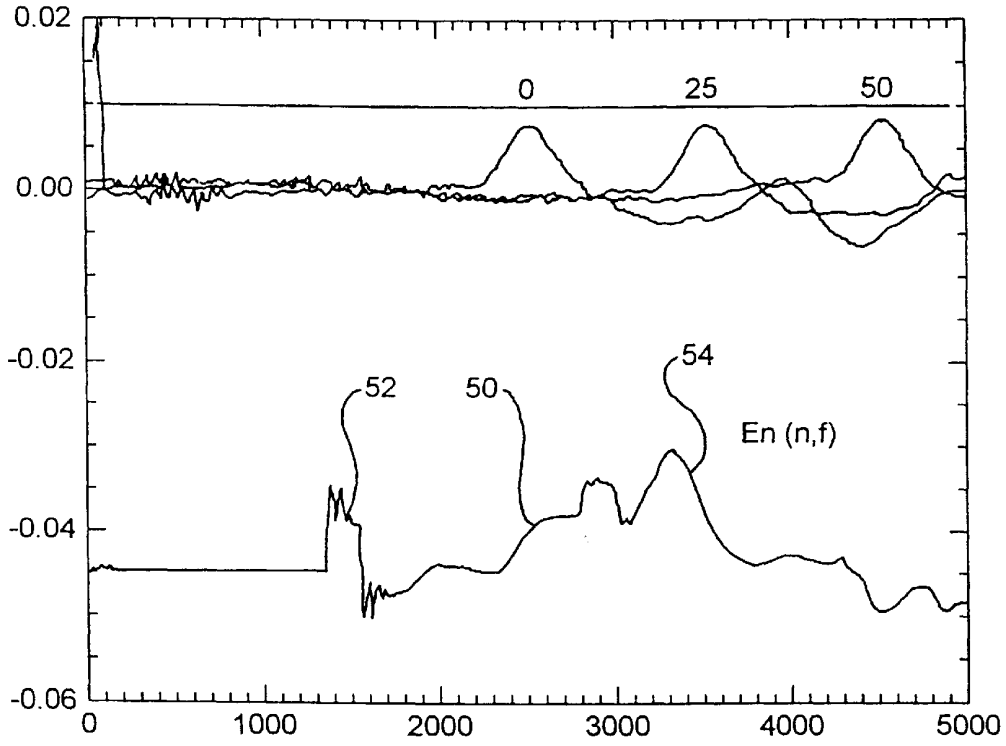
0.02
0.00
-0.02
-0.04
-0.06
0
25
50
52
50
54
En (n,f)
0
1000
2000
3000
4000
5000

FIG. 4

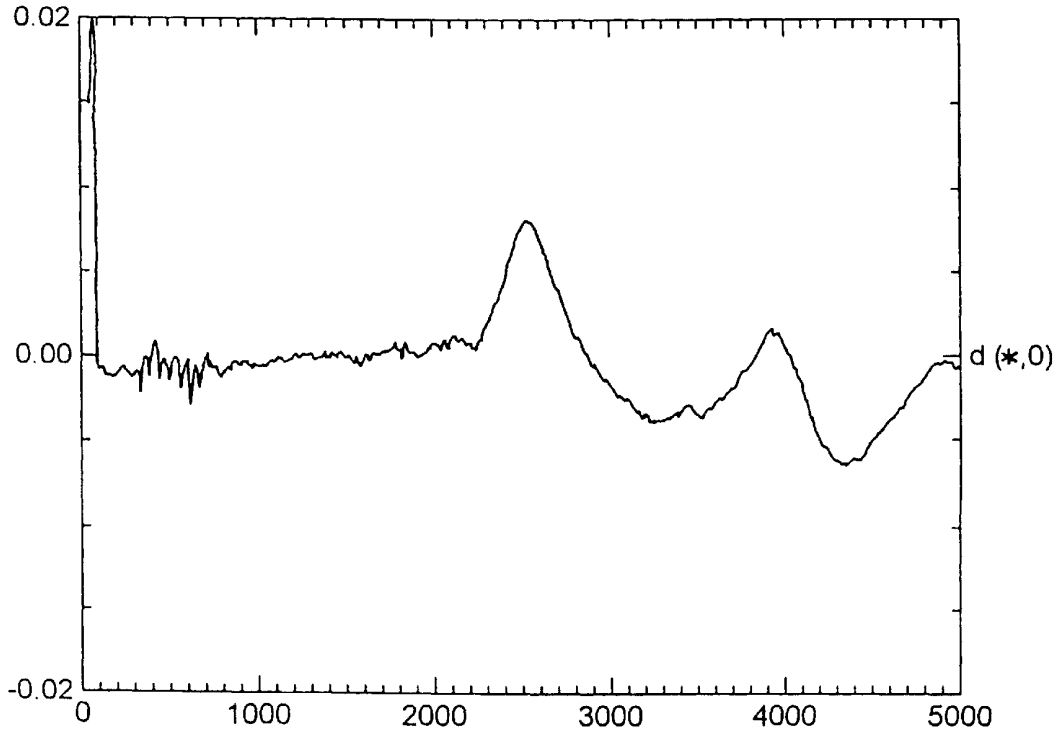
0.02
0.00
-0.02
d (*,0)
0
1000
2000
3000
4000
5000

FIG. 5

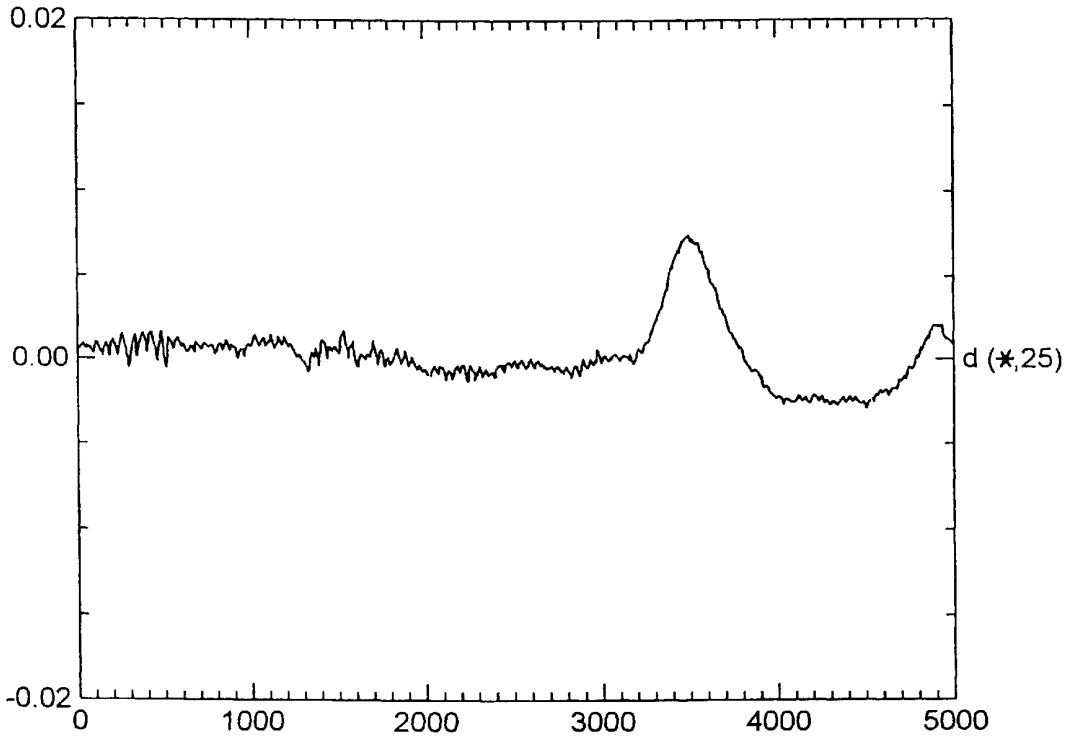
0.02
0.00
-0.02
0
1000
2000
3000
4000
5000
d (*,25)

FIG. 6

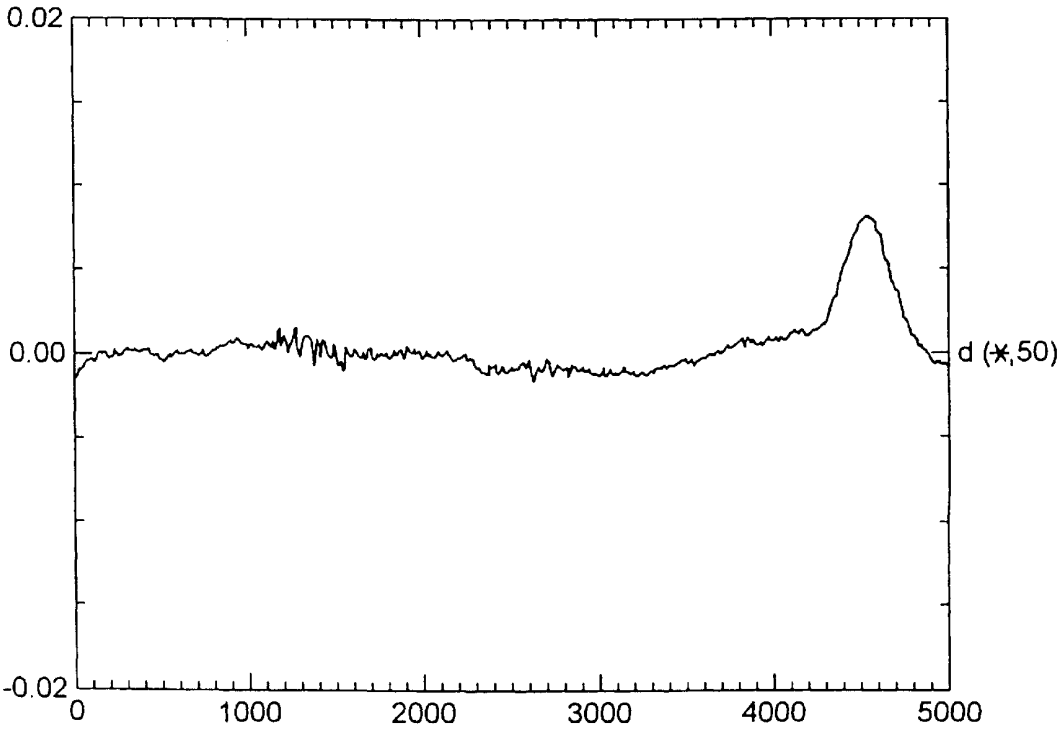
0.02
0.00
-0.02
0
1000
2000
3000
4000
5000
d (*,50)

FIG. 7A

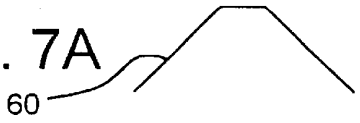

FIG. 7B

FIG. 7C

FIG. 7D

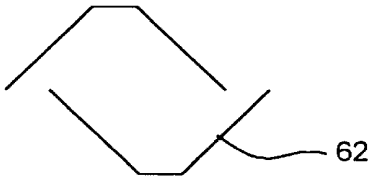

FIG. 7E

FIG. 7F

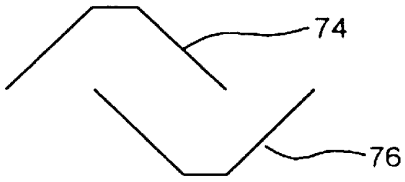

FIG. 7G

FIG. 7H

FIG. 7I

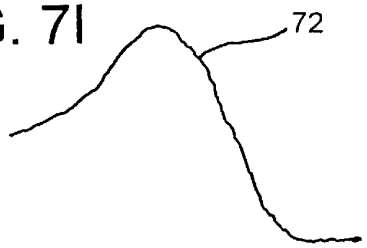

FIG. 8A

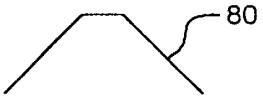

FIG. 8B

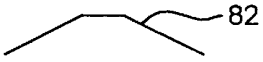

FIG. 8C

FIG. 8D

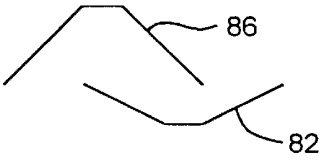

FIG. 8E

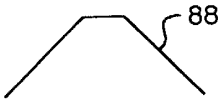

FIG. 9A

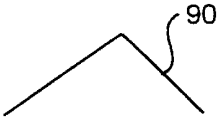

FIG. 9B

FIG. 9C

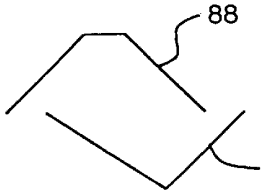

FIG. 9D

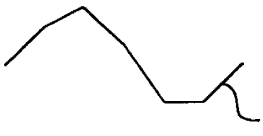

FIG. 9E

FIG. 10
PRIOR ART

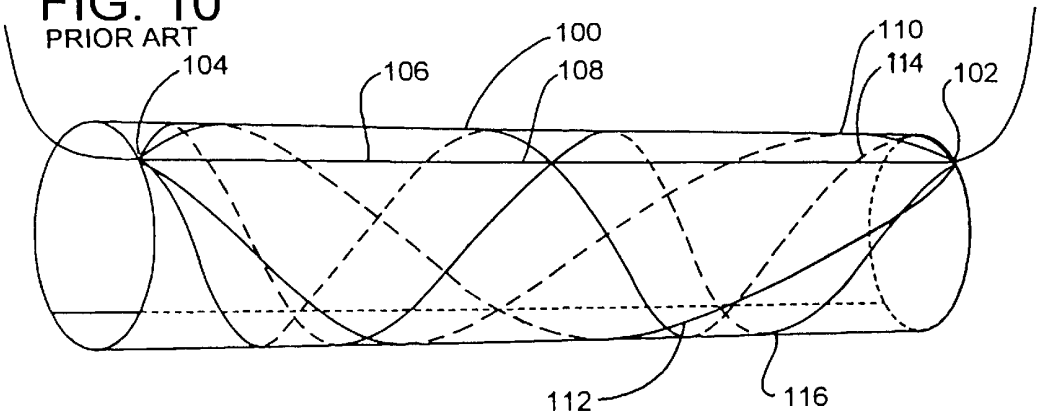

FIG. 11

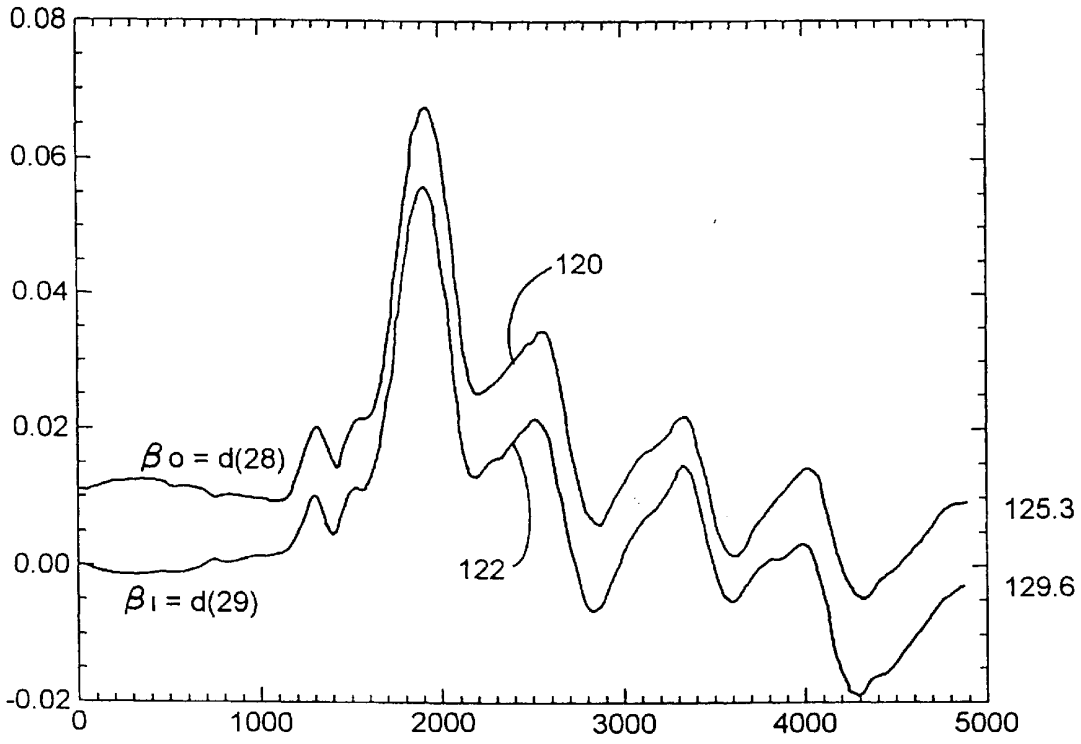
0.08
0.06
0.04
0.02
0.00
-0.02
0
1000
2000
3000
4000
5000
120
122
βo = d(28)
βI = d(29)
125.3
129.6

FIG. 12

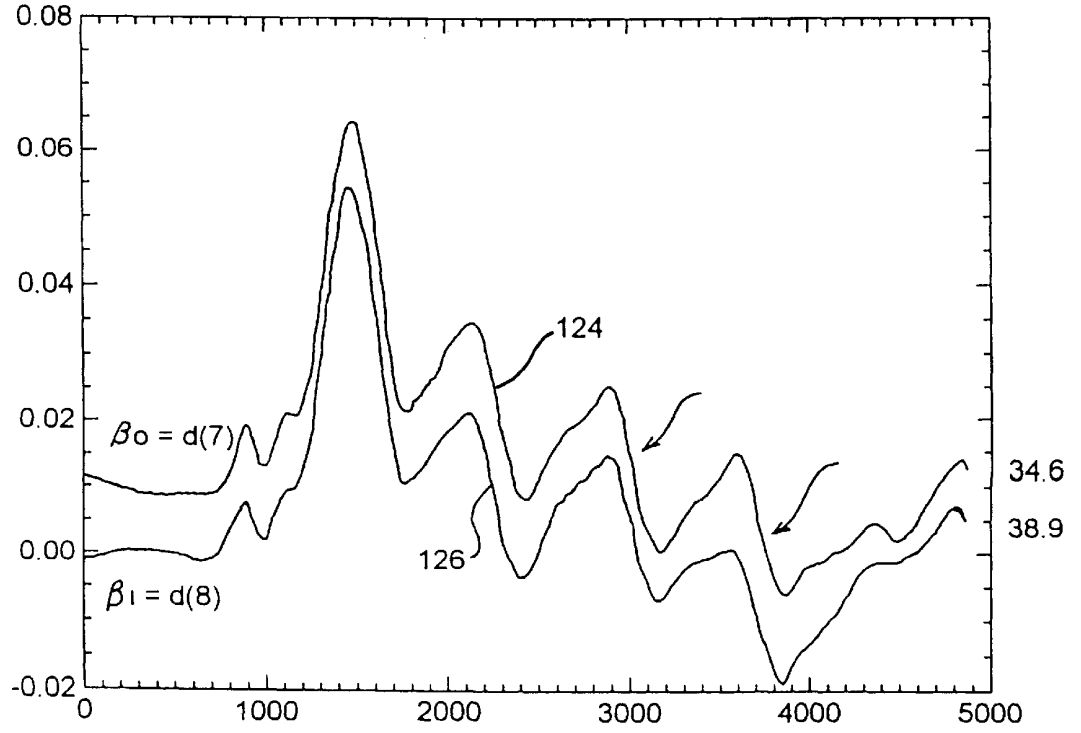
0.08
0.06
0.04
0.02
0.00
-0.02
0
1000
2000
3000
4000
5000
124
126
βo = d(7)
βI = d(8)
34.6
38.9

FIG. 13

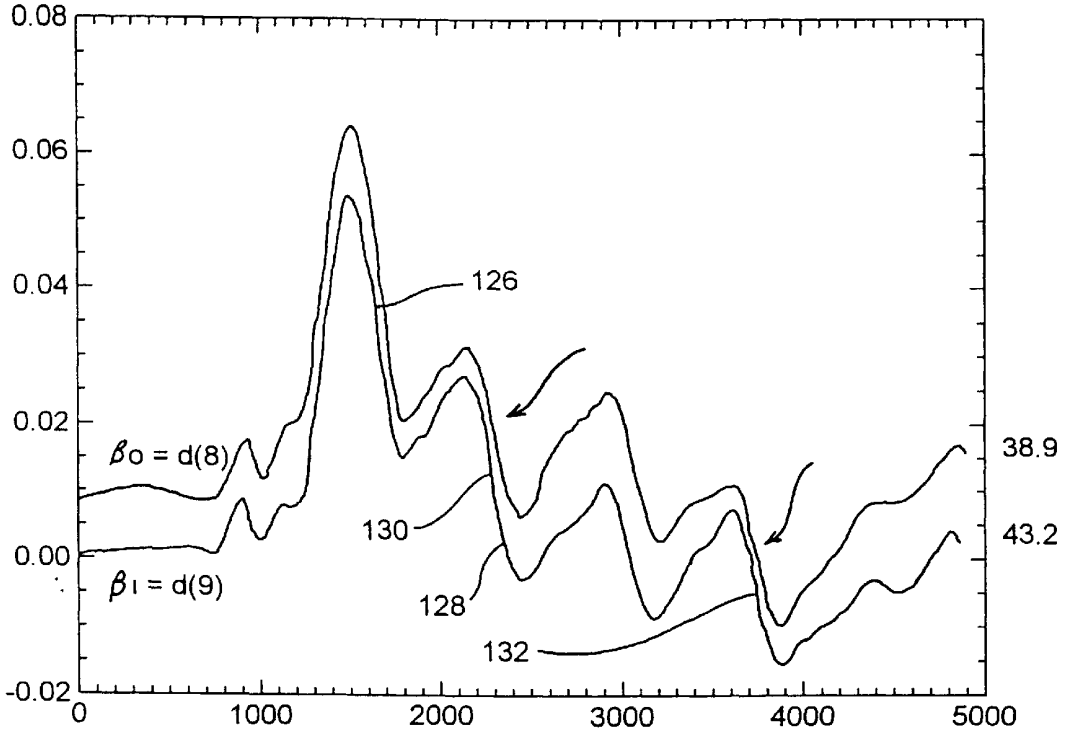
0.08
0.06
0.04
0.02
0.00
-0.02
0
1000
2000
3000
4000
5000
126
130
128
132
βo = d(8)
β1 = d(9)
38.9
43.2

FIG. 14

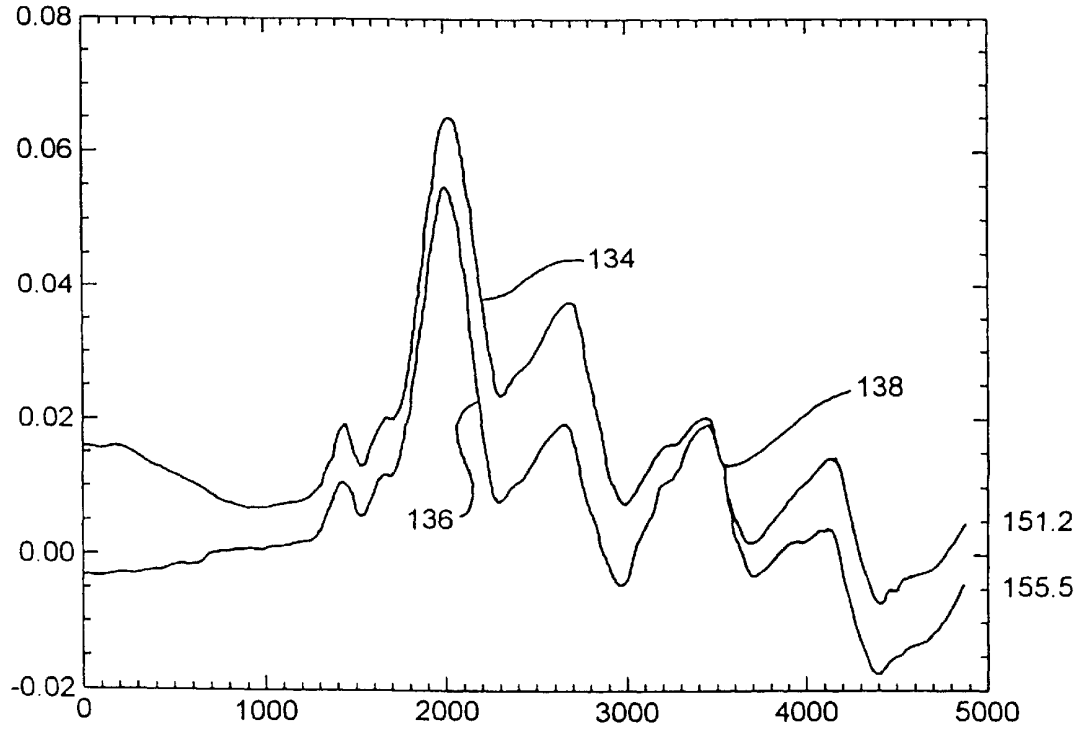
0.08
0.06
0.04
0.02
0.00
-0.02
0
1000
2000
3000
4000
5000
134
138
136
151.2
155.5

FIG. 15

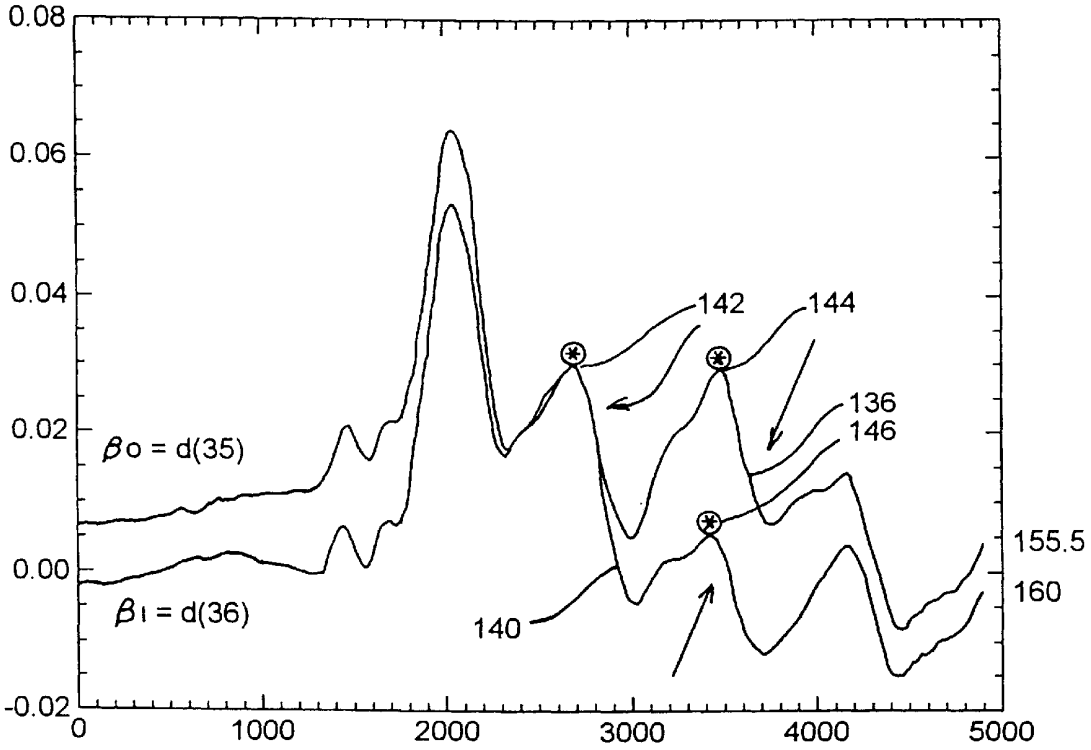
0.08
0.06
0.04
0.02
0.00
-0.02
0
1000
2000
3000
4000
5000
βo = d(35)
βI = d(36)
142
144
136
146
140
155.5
160

FIG. 16

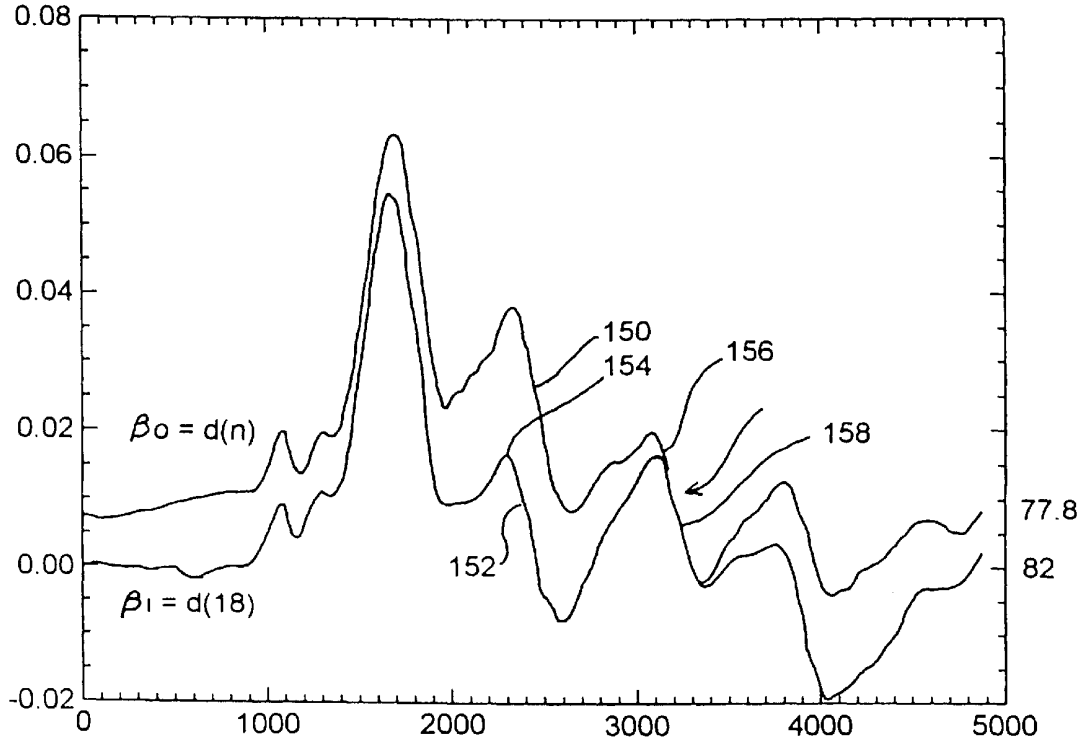
0.08
0.06
0.04
0.02
0.00
-0.02
0
1000
2000
3000
4000
5000
βo = d(n)
βI = d(18)
150
154
156
158
152
77.8
82

FIG. 17

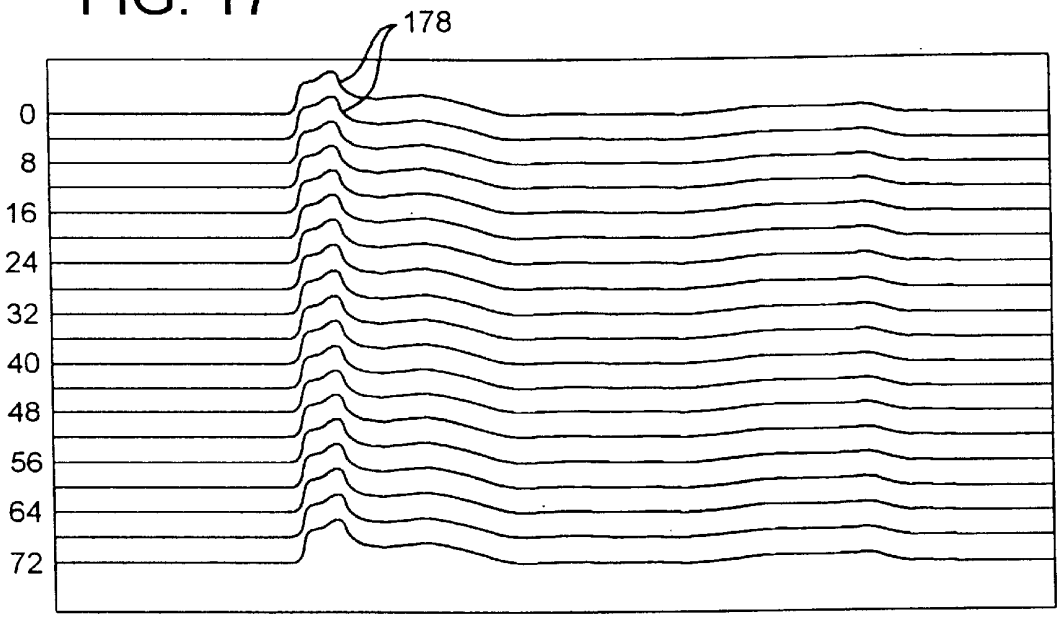

FIG. 18

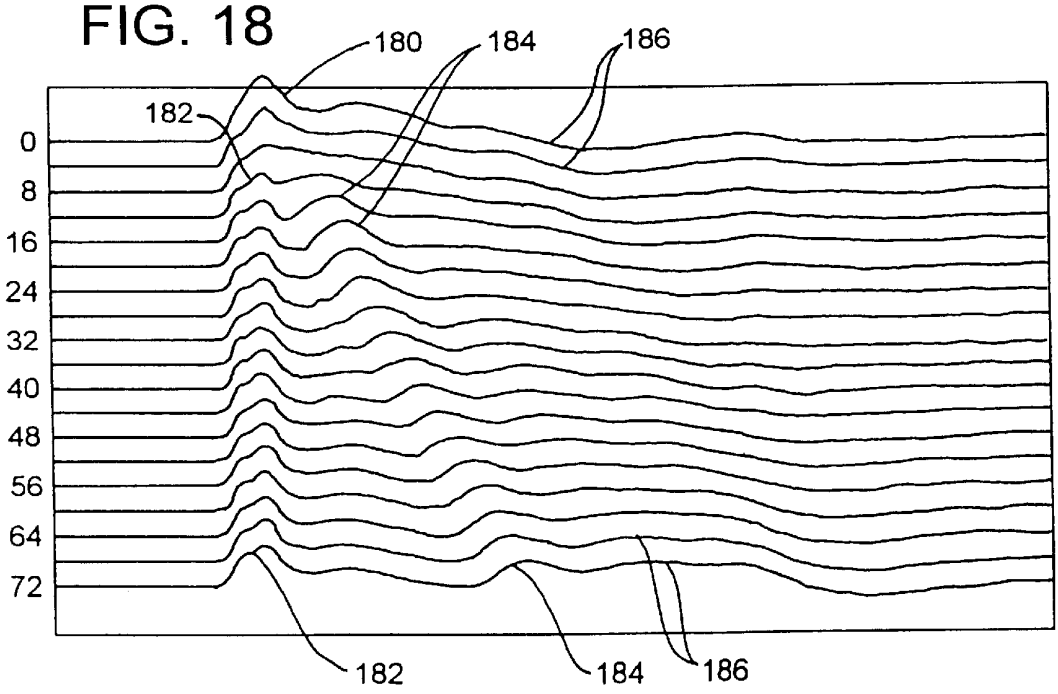

FIG. 19

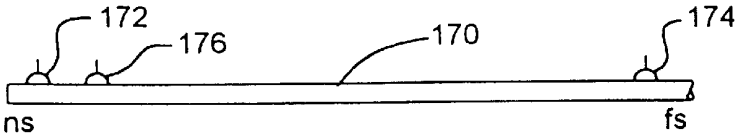

FIG. 20

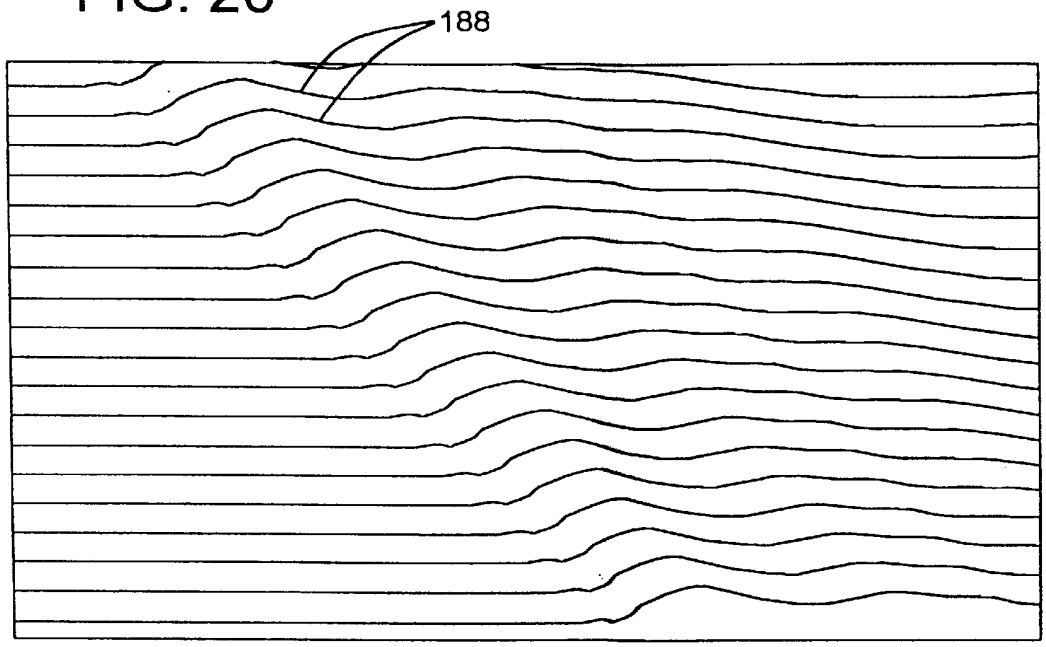

FIG. 21

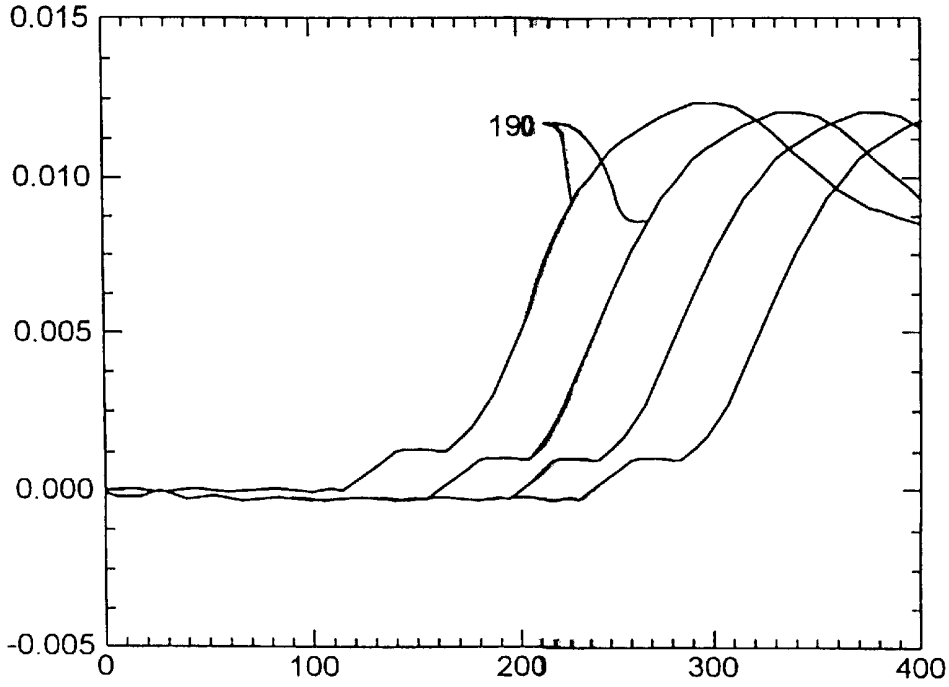

FIG. 22

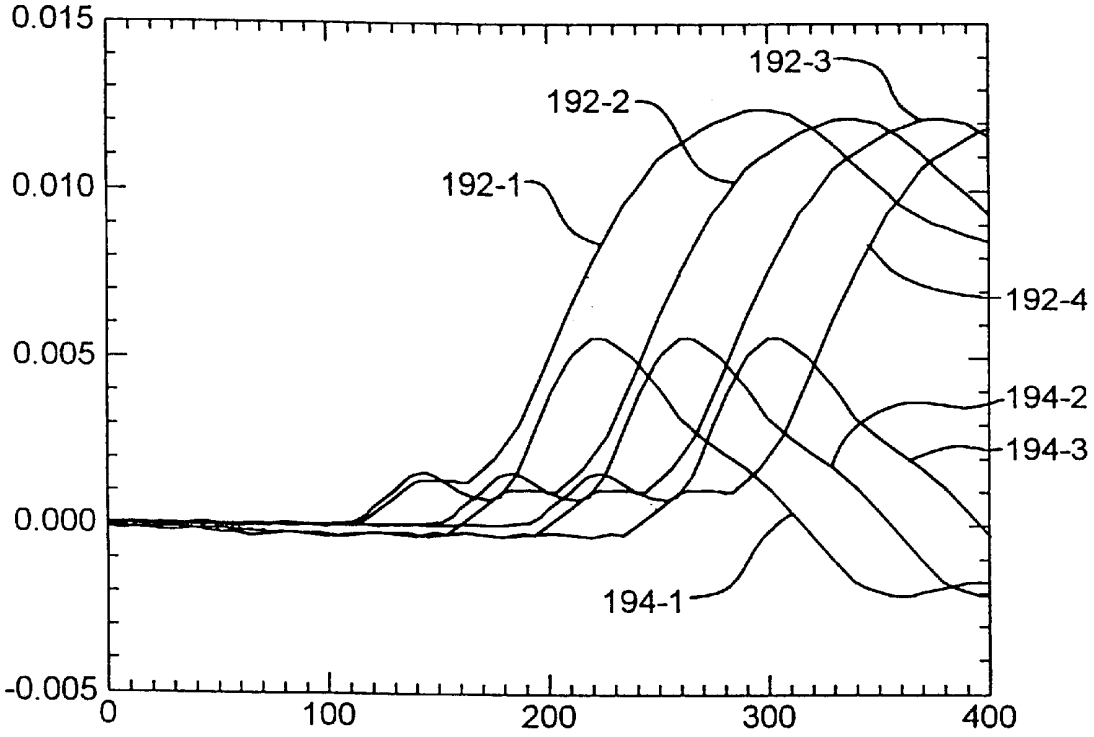
0.015
0.010
0.005
0.000
-0.005
0
100
200
300
400
192-3
192-2
192-1
192-4
194-2
194-3
194-1

FIG. 23

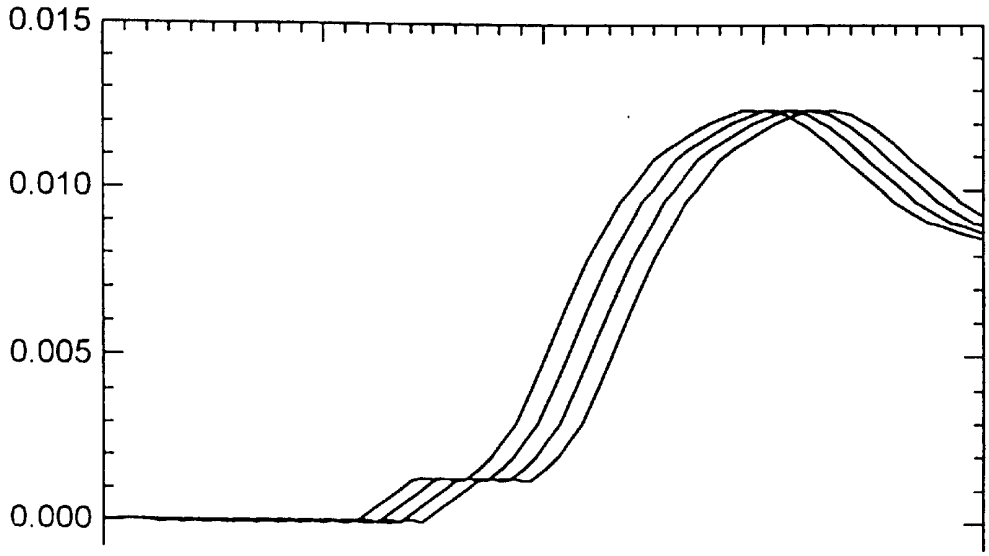
0.015
0.010
0.005
0.000

FIG.24

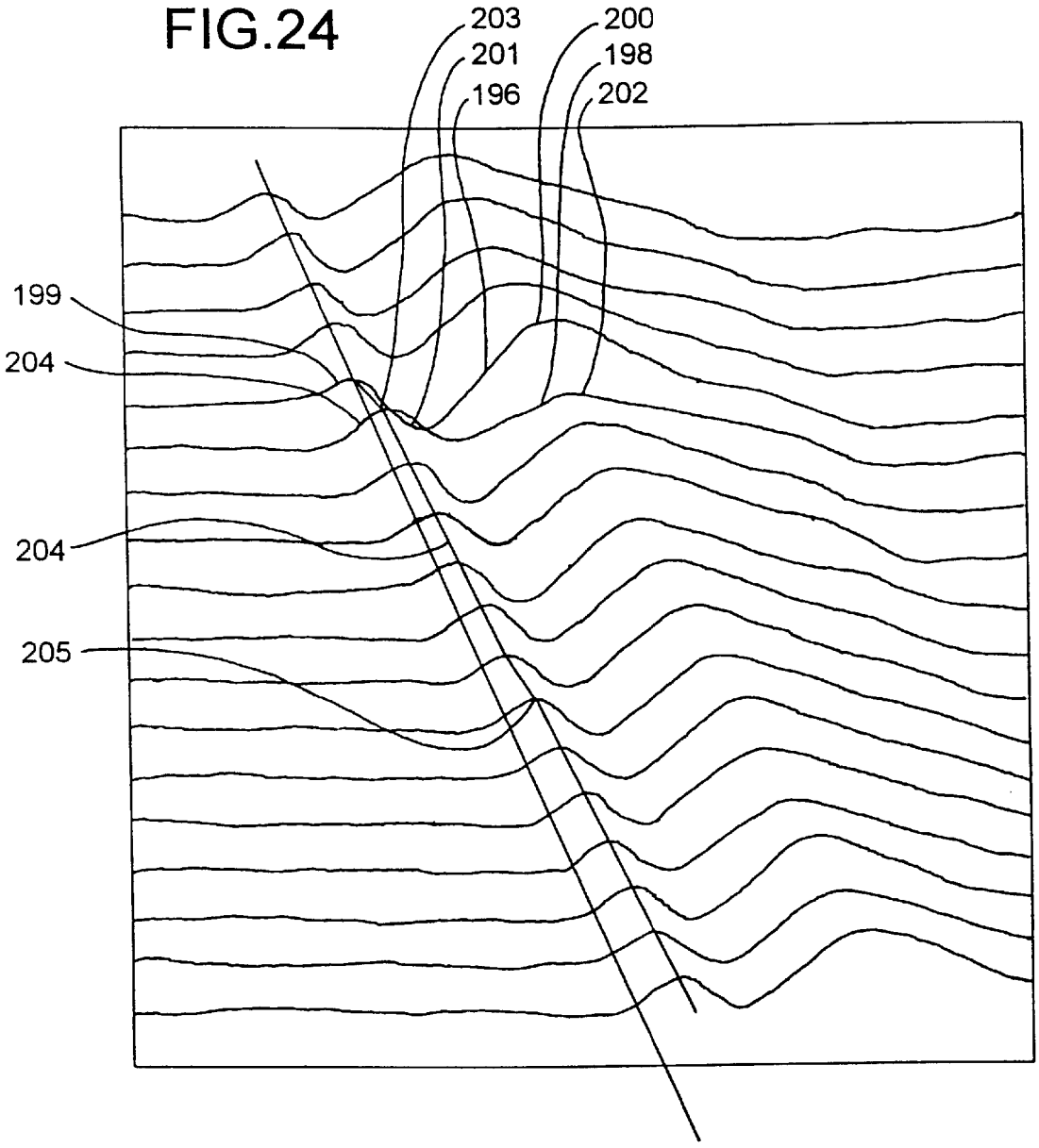

FIG. 25

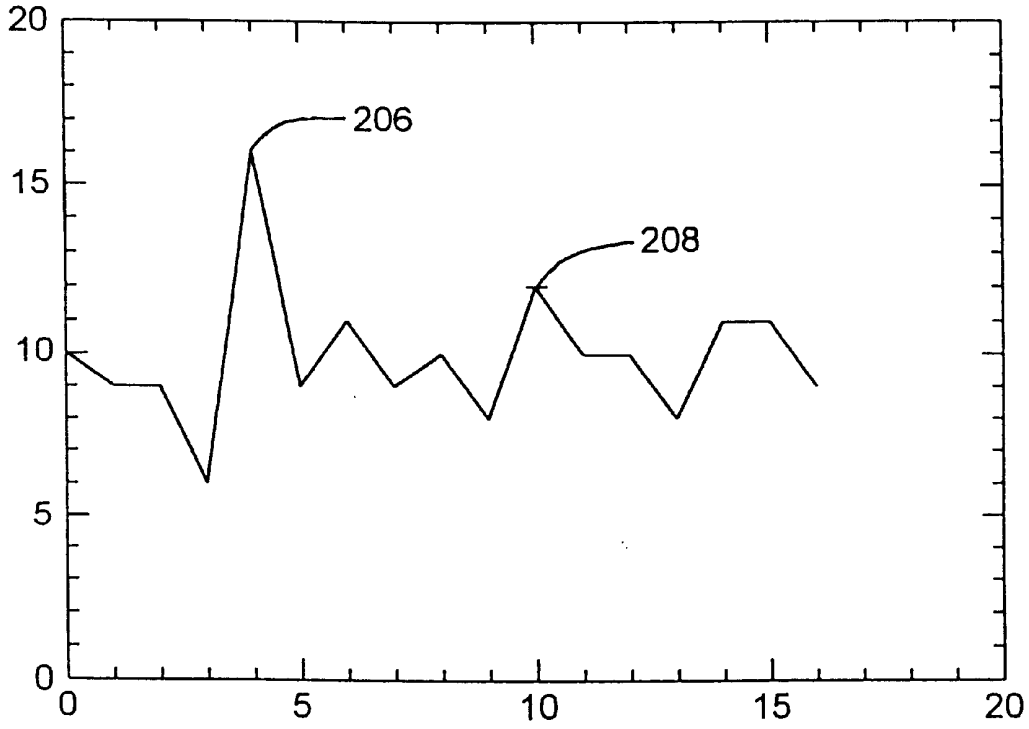

FIG. 26

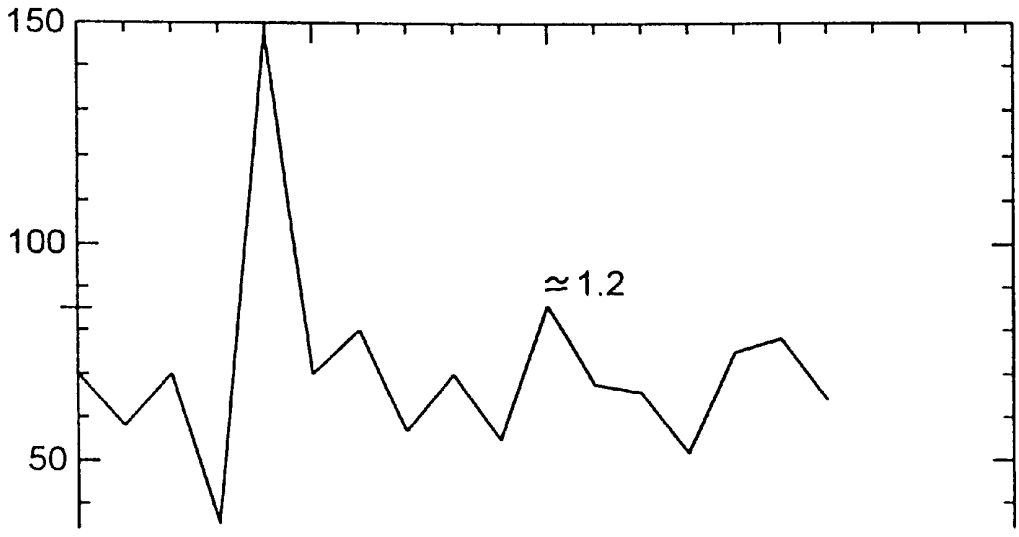

METHOD OF DETECTING CORROSION IN PIPELINES AND THE LIKE BY COMPARATIVE PULSE PROPAGATION ANALYSIS

This application is a continuation of Ser. No. 09/090,800 filed Jun. 4, 1998, U.S. Pat. No. 6,065,348 which colims benefit of Prov. No. 60/048,660 filed Jun. 4, 1997.

BACKGROUND OF THE INVENTION

a) Field of the Invention

The present invention relates to a system, apparatus and method for testing elongate objects, such as pipe, and is directed toward the problem of detecting corrosion, defects or other anomalies to the pipe under conditions where access and/or visual inspection of the pipe is either not possible or impractical.

b) Background Art

In petroleum processing and petrochemical plants and other industrial environments, it is common to have numerous pipes extending between various locations in the plant, with these pipes carrying fluid or gas (e.g.petroleum products), often under high heat and pressure. These pipes are commonly made of steel, and can have an inside diameter ranging anywhere from two to sixty inches, or even outside of this range. The exterior of these pipes are often insulated, with the insulating layers being as great as approximately ⅛ to 5 inches in thickness, or outside of this range.

For a number of reason, (safety, environmental considerations, avoiding costly shut-downs, etc.), the integrity of these pipes must be maintained. Defects in the pipe can occur for a number of reasons. One is that moisture can collect between the insulating layer and the pipe, thus causing corrosion (i.e.rust). Visual inspection of the steel pipe that is encapsulated in insulation is not possible unless the layers of insulation are removed, and then replaced. However, this is expensive and time consuming, and as a practical matter it would be economically unfeasible to accomplish the inspections with reasonable frequency.

It is the object of the present invention to provide a means of inspecting pipes under the circumstances given above in a manner that corrosion, other defects and/or anomalies can be detected with a relatively high degree of reliability, and in a manner that the various difficulties of inspection, such as those mentioned above, can be diminished and/or alleviated.

SUMMARY OF THE INVENTION

The method of the present invention enables corrosion on an elecromagnetical permeable elongate member, such has a pipe, to be detected quite effectively. More specifically, this method enables much of the irrelevant information (reflections, electromagnetic noise) to be eliminated from the wave form, and then the wave forms processed in a particular manner to enable clearer identification of variations in the wave form that would indicate corrosion.

In the method of the present invention, a nearside and far side electric or electromagnetic pulses (waves) are transmitted from, respectively, nearside and farside spaced transmitting locations on the elongate member. The pulses (waves) travel toward one another to intersect at intersecting locations on the elongate member.

The farside pulses are received as wave forms at a receiving location after intersection with related nearside pulses. The transmission of the nearside and farside pulses are synchronized so that the intersections of the near side and far side pulses (waves) occur at spaced intersecting locations on the elongate member.

The wave forms of at least two of the far side pulses (waves) which are spaced from one another are combined to form a composite wave form. A variation of variations are ascertained from the composite wave form as a means of detecting corrosion.

In the preferred form, one of the wave forms of the two wave forms that are to be combined is inverted and then added to the other of the waveforms being combined to create a difference waveform, and variations in the difference wave form are ascertained as a means of detecting corrosion.

Also, in the preferred form, the nearside pulses which pass through points of intersection that are adjacent to one another are considered to be sequential nearside pulses, with the order of sequence being the same as the order in which the points of intersection are spaced along the elongate member. The combining of the nearside waveforms is accomplished in a pattern such that first and second adjacent wave forms are combined to make a first composite waveform, the second waveform and an adjacent third waveform are combined to make a second composite waveform, the third waveform is combined with an adjacent fourth waveform to make a third composite waveform, with the pattern repeating itself with subsequent pairs of waveforms from adjacent farside pulses. Adjacent composite wave forms are compared with another as a means of detecting corrosion.

A reference wave form is established by creating composite wave forms resulting from pulses that intersect at non-corroded areas of the elongate member, and identifying composite waveforms that differ from the reference composite waveform by a phase shift and/or dispersion and/or amplitude and and/or wave distortion.

Corrosion that is present between two adjacent points of intersection on the elongate member is detected by comparing a composite wave form resulting from combining the difference waveform overlapping the point of intersection with difference wave forms on opposite sides of the overlapping composite waveform.

Also, corrosion that is present at a point of intersection of two wave forms can be detected by deriving two difference waveforms by combining the waveform at the point of corrosion with adjacent waveforms to form two difference wave forms which are then compared.

Also, two additional difference wave forms that are on opposite sides of, and adjacent to, the two difference waveforms which are analyzed to detect the corrosion are compared with the two difference waveforms which are combined at the point of intersection as a means of detecting corrosion.

Other features of the present invention would become apparent from the following detailed description.

BRIEF DESCRIPTION OF THE DRAWINGS

FIG. **1** is a somewhat schematic view of the system of the present invention being in its operative position where it is being used in testing a length of insulated pipe;

FIG. **2** is a graph illustrating one way in which data can be taken and presented in accordance with the present invention, this graph plotting propagation time against distance from A to B and again from B to A giving a reversed profile;

FIGS. **2**A and **2**B are schematic drawings showing the intersection of two pair of pulses at adjacent spaced locations;

FIG. **3** is a graph which displays a curve in the lower part of the graph which represents a composite wave form resulting from both the near side of far side pulses traveling along the pipe section under test, and the curves at the upper part of FIG. **1** showing resulting wave forms at different locations, using the method of the present invention;

FIG. **4** is a graph which is similar to the upper part of the graph of FIG. **3**, displaying separately a first resulting wave form identified at the zero location shown in FIG. **3**;

FIG. **5** is a graph similar to FIG. **4**, but showing separately the resulting wave form identified at the 25 location shown in FIG. **3**;

FIG. **6** is a graph similar to both FIGS. **4** and **5**, but showing separately the resulting wave form at the 50 location of FIG. **3**;

FIGS. **7**A through **7**I are a series of simplified illustrations of wave forms to demonstrate certain principles of different wave forms;

FIGS. **8**A through **8**E and FIGS. **9**A through **9**E are two series of Figures similar to those of FIGS. **7**A through **7**E, and to illustrate further the certain principles of difference wave forms;

FIG. **10** is an illustration of the paths of the electromagnetic wave components traveling along a section of pipe; and

FIGS. **11**–**16** are presentations of wave forms illustrating the difference wave forms produced in accordance with the method of the present invention.

FIG. **17** is a graph illustrating the wave forms in the first step of third embodiment of the present inventions;

FIG. **18** is a graph similar to FIG. **17**, showing the wave forms of a subsequent step in this third embodiment;

FIG. **19** is a schematic drawing of the place for the antennas in this third embodiment;

FIG. **20** is a graph similar to FIGS. **17** and **18** illustrating a third step in the third embodiment;

FIG. **21** is a graph showing three of the wave forms of FIG. **20**, drawn to a scale emphasizing the vertical dimension of the waves;

FIG. **22** is a graph similar to FIG. **21** showing the wave forms of FIG. **21** and also the difference wave forms derived therefrom;

FIG. **23** is a graph similar to FIG. **21** showing three of the waves moved together;

FIG. **24** is a graph showing a plurality of difference wave forms, where two areas of corrosion are being detected;

FIG. **25** is a graph derived from the earlier wave forms illustrating the difference in amplitude of the difference waves where corrosion exists;

FIG. **26** is a graph based on FIG. **24**, further emphasizing the differences in amplitude.

DESCRIPTION OF THE PREFERRED EMBODIMENTS

The basic testing apparatus and method of the present invention will now be described with reference to FIG. **1**. There is shown a pipe **10** having a section **11** which is under test. This pipe **10** is or may be a pipe or pipeline that would typically be used in the petroleum or petrochemical industry, where the pipe is made of steel and surrounded by a coat or layer of insulation.

The apparatus **12** of the present invention is shown somewhat schematically in its operating position, testing the section **11** of the pipe **10**. This apparatus **12** comprises a pulse generator **14**, a signal analyzer **16**, and interactive computer **18**, and two transmitting/receiving antennas **20** and **22**. There are two cables **24** and **26** (or other signal or pulse transmitting means) interconnecting the antennas **20** and **22**, respectively, to the pulse generator **14**. There is a second pair of cables or other transmitting means **28** and **30** connected between the cables **24** and **26**, respective, and to the signal analyzer **16**.

When the transmitted pulse is received by one or the other of the antennas **20** or **22**, this pulse is in turn transmitted to the signal analyzer. Certain analysis can immediately take place in the signal analyzer **16**. Alternatively, the information relating to the pulse can be stored and analyzed at a later time. The computer performs certain control functions in the proper transmission and reception of the pulses and other functions.

There are several ways in which an apparatus, such as the apparatus **12**, can be used in detecting corrosion in pipes, and two of these will be discussed below.

There is a first method where a single pulse is transmitted from the pulse generator **16** to one or the other of the antennas **20** or **22** to cause the wave form to travel from the location of that antenna **20** or **22** along the pipe **10** to the location of the other antenna **20** or **22** where the signal from the wave form is received. The distance between the sending location 20 and the receiving location 22 is ascertained accurately, and the timing of the time of transmission of the pulse from the antenna **20** or **22** to the other antenna **20** or **22** is measured very accurately (desirably to a fraction of a nanosecond or even to a very small fraction of a nanosecond). If the section between the two test locations 20 and 22 is non-corroded, and if the pipe is uniform along its length, then the pulse will arrive at the receiving location 22 in a wave form which is in the same general pattern (except possibly for disturbances, such as a near by magnetic field, electromagnetic noise, etc.). Also, the rate of travel of the pulse would remain substantially constant, provided the pipe remains uncorroded and uniform.

However, when corrosion is encountered between the points **20** and **22**, the corrosion will affect the wave form by retarding its velocity diminishing its amplitude, and also possibly changing the actual wave form itself.

One method of utilizing this technique is to send the pulse from the transmitting location to the receiving location over an uncorroded section of pipe of a know length and diameter, and known characteristics, relative to its transmission of electromagnetic waves. This would establish the time of travel of the wave from the transmitting to receiving location and the expected configuration of the wave form at the receiving location.

Then various sections of the pipe are tested, as illustrated in FIG. **1**. When there is a delay in the predicted arrival time of the wave form and/or deviations from the reference wave form for uncorroded pipe, then this will presumed to be due to corrosion on the pipe. However, it should also be understood that some other disturbance (e.g. nearby electromagnetic noise, presence of some other object that would disturb the electromagnetic field) could also affect the wave form, and this should be accounted for.

The second method which will be discussed further in this text is what is termed the "dual pulse" method, described in U.S. Pat. No. 4,970,467. In this method, the same apparatus as shown in FIG. **1** can be used. However, instead of using

a single pulse or series of single pulses, as in the method described above, both antennas **20** and **22** are used as both transmitting and receiving antennas in the same timeframe. Thus, as one pulse is transmitted from the antenna **20**, one is also transmitted from the antenna **22**. These pulses travel toward one another and "collide" at some intermediate location along the pipe. This meeting of the pulses will cause variations in both of the wave forms as they move through the area of collision toward the other antenna which is its receiving location.

By properly coordinating the precise time at which the pulses are transmitted from the two locations 20 and 22, the point of collision along the length of the pipe can be caused to occur at any desired location along the length of the pipe. Then by changing the relative time transmissions of the pulses in small increments, this point of collision can be stepped along the length of the pipe.

As described in the above noted patent, when the point of collision occurs at a location where there is corrosion, the wave form resulting from the collision will be different from a reference wave form which would occur where the collision point is at a non-corroded section of pipe. Thus, not only is there a means of detecting corrosion, but also a means of determining the location of such corrosion.

Also, the antennas **20** and **22** could be used only as transmitting antennas and two additional antennas could be used as receiving antennas. Further, other transmitting and receiving devices could be used, such as by making a direct electrical connection to the pipe.

The present invention is particularly adapted for extracting information from the wave forms resulting from the dual pulse method described above.

A first embodiment of the method of the present invention is described in the following text, with reference to FIGS. **2**A–**2**B through FIGS. **9**A–**9**E. A second embodiment is also disclosed later herein, using in part the same principles as the first embodiment, and this will be described later with reference to FIGS. **10**–**16**.

Reference is first made to FIGS. **2**A and **2**B which are schematic illustrations of the operation of the dual pulse method. In FIG. **2**A, there is schematically shown a one hundred foot length of pipe. It will be assumed that the pulse travels along the length of the uncorroded pipe at the rate of one foot per nanosecond.

In FIG. **2**A, the near side pulse is transmitted into the pipe at the location NS (near side location) at a point in time indicated at zero. The second pulse is transmitted into the pipe at the far side location (designated FS), and in this particular example, it is assumed that the second far side pulse is transmitted into the pipe forty nanoseconds earlier than the time the near side pulse is transmitted into the NS location.

Therefore, it can be seen that when the far side pulse has traveled along the length of the pipe for forty nanoseconds to reach a location indicated at the sixty foot location, the near side pulse is transmitted at time zero from the near side location.

The near side and the far side pulses travel toward one another, each traveling thirty feet until they intersect at the thirty foot location on the one hundred foot pipe. At the intersection, the two pulses interact with one another, and the far side pulse continues it path of travel to the near side (NS) location. Also, the near side pulse after passing through the point of intersection continues its course of travel toward the far side (FS) location.

At this time, it is important to note that each of the pulses is a somewhat complex wave form. First, as a wave form travels along the length of the pipe, it is subject to attenuation, distortion, interference and dispersion. Further, each wave can be considered as having what we might term wave components made up of earlier and later arrivals. There is a first arrival which will travel the shortest course from the transmitting to the receiving location. Thus, if both the transmitter and the receiver are on top of the pipe, the first arrival will travel along the top surface of the pipe in a straight line. Then there are second arrivals which are pulse components which follow a helical path once around the pipe to arrive at a short time later. Then there are third, fourth, fifth, . . . etc. arrivals which come at yet later times. Further, there are quite commonly outside sources of interference, such as sources of electromagnetic radiation, nearby objects which may interact with the wave form traveling along the pipe, and thus become activated and in turn transmit their own electromagnetic radiation back into the pipe under test. Further, there are reflections and refractions.

To return to FIG. **2**A, let us first assume that the one hundred foot section of pipe which is under test is free of corrosion. After the near side and far side pulses intersect at the thirty foot location, there is a resulting wave form which reaches the near side receiving location, which is the composite of both the original near side pulse and the far side pulse, with these having been modified or affected to some extent by reason of intersecting.

It has been found that if the intersection of the near side and far side pulses takes place at a location on a pipe which is noncorroded, then the resulting pulse which travels through the location of intersection will have certain characteristics typical of a situation where the intersection takes place at a non-corroded area of pipe. However, if the intersection of the near side and far side pulses take place at a location where there is corrosion, the two pulses interact in a rather different manner, and the resulting wave form of each of the intersected pulses has different characteristics.

However, the analysis of the wave form as a means of detecting corrosion is difficult to quantify. There are features such as rise time, slope, amplitude, and phase change, all of these being relevant characteristic of the wave form.

To illustrate this, reference is made to the lower curve shown in FIG. **3**. This curve, designated **50**, is a composite curve which results from the combination of both the near side and the far side pulses. In this instance, one transmission takes place at the near side, and the receiving antennae is also located at the near side. The portion of the curve indicated at **52** represents the near side pulse being transmitted into the pipe at the transmitting location.

The portion of the curve indicated at the general area of **54** represents a portion of the composite wave that arrives at the near side receiving location, this being a combination of the far side wave and near side wave components. As indicated above, there are reflections, refractions, late arrivals, etc., which complicate the wave form.

Reference is now made to FIG. **2**B, which shows a second dual pulse operation where the transmission time of the far side pulse has been delayed by four nanoseconds, so that it is transmitted thirty six nanoseconds before the transmission of the near side pulse. It can be seen that after the far side pulse has traveled thirty six feet, the transmission of the near side pulse takes place. Thus when the near side pulse is transmitted, the far side pulse is at the sixty four foot location, and the two pulses intersect at the thirty two foot location.

With the foregoing being presented, the method of the present invention will now be described. Let us assume that

the dual pulse testing method is being accomplished and that the near side and far side pulses are timed (as indicated in FIG. **2**A) so that there is intersection at the thirty foot location on the one hundred foot pipe. Let it further be assumed that the wave form which is received at the near side location looks the same, or similar to, that shown in the bottom part of FIG. **3**.

Now let us assume that a second testing operation is to be initiated and the far side pulse is delayed by four nanoseconds. However, the transmission at the near side location remains constant, in terms of time, and is still transmitted at zero time. As illustrated in FIG. **2**B, the intersection takes place at the thirty two foot location. What this would effectively mean is that the portion of the composite curve which is attributable to the far side pulse would have been delayed, relative to the time of transmission of the near side pulse, and that, with reference to the lower curve of FIG. **3**, the portion of the composite wave form contributed by the far side pulse would have shifted to the right somewhat, from what is shown in the lower curve of the graph of FIG. **3**.

In order to extract meaningful information about the condition of the pipe, the following is done. First, the composite wave form which results from the transmission and intersection of pulses as shown in FIG. **2**A is stored in the memory. Next, the second composite wave form resulting from the transmission of the near side and far side pulses in accordance with FIG. **2**B is also received. Then the second composite wave form resulting from the test operation of Figure B is subtracted from the composite wave resulting from the test operation in FIG. **2**A.

At this point, it is very important to keep in mind that the near side pulse has in both instances (in the operation of FIG. **2**A and the operation of FIG. **2**B) been transmitted at zero time. Thus, in both the FIG. **2**A and FIG. **2**B operation, the near side pulse has not changed position. From this, it becomes apparent that the contribution of the near side pulse to the composite wave form is essentially subtracted out of the composite wave form resulting from the operation of FIG. **2**A. Now, let us turn our attention to the far side pulses of the test operation of FIG. **2**A and FIG. **2**B. With the far side pulse having been delayed by four nanoseconds, the wave component of the far side pulse has now shifted from the first location in the first operation of FIG. **2**A four nanoseconds to a second position composite curve of the second test operation of FIG. **2**B.

With the entire first composite curve being subtracted from the entire second composite curve, there remains what can be termed a "difference wave form". It has been found that if in the two dual pulse operations where the intersecting locations are stepped within a reasonably close distance from one another, and if uncorroded pipe is encountered at both intersecting locations, the resultant difference wave form is a reasonably well defined and identifiable peak.

Reference is now made to FIG. **3**. It can be seen that the curve in the upper part of FIG. **3** shows three separate peaks designated "zero", "twenty five", and "fifty", respectively. Each of these peaks is the result of using the method of the present invention where the point of intersection for the two adjacent dual pulse operations has been stepped by an interval of about 5 feet.

To provide cleaner representations of the wave forms, FIG. **4** illustrates the single curve indicated at "0" in FIG. **3**; FIG. **5** illustrates only the curve indicated at "25" in FIG. **3**; and FIG. **6** illustrates only the curve indicated at "50" in FIG. **3**.

It should be noted that the wave forms indicated at "0", "25", and "50" in the top part of FIG. **3** are actual wave forms extracted from adjacent wave forms similar to the ones shown in the lower part of FIG. **3**. It is important to note that if the composite wave form is not formatted correctly, the difference between adjacent wave forms does not provide the "effect" wave forms shown in FIG. **3**.

To review how to format the data correctly, consider the two active wave forms on the pipe, one from the near side (NS), and the other from the far side (FS). When the data analyzer is synchronized with the near side pulse, the near side component of the composite pulse will not move (i.e. shift position). However, the FS (far side) pulse, which is synchronized to the master clock, will move across the screen from left to right and will modify the composite wave form for each intersection along the pipe. When the composite wave forms are subtracted from each other, two significant things happen:

1. The effect of the NS pulse, which has a very large amplitude with respect to the FS pulse, is cancelled, since this NS component in the composite wave form is fixed in time.

2. The resulting difference wave form represents the difference between the two adjacent FS pulses that have intersected with the NS pulses at two different points on the pipe.

When this difference occurs, then the "effect" (time rise, slope, amplitude, dispersion and absolute time, among many parameters that are effected by corrosion) influence the shape of the different wave form. The difference wave form will be displaced in time with respect to other adjacent pairs. This time displacement is a good indication of the condition of the pipe, provided it can be meaningfully interpreted. The difference wave forms shown here are examples of the wave forms that are well defined, but are very difficult to extract real time information. (See FIGS. **4**, **5** and **6**. Note particularly FIG. **6** at the "knee" of the wave form is not well defined, and could be selected anywhere from a point near thirty two hundred to forty two hundred, a range of one hundred nanoseconds. Automating a selection of the absolute time location of the knee is very difficult and sometimes impossible. However, the peak is well defined. The peak is not just a voltage difference between two different response wave forms, but it is determined by the shape factors involved with the leading edge of the two adjacent wave forms.

For example, if the two adjacent wave forms are displaced more in time than any two other adjacent wave forms, it will result in an increase of amplitude. Hence, "Δ" (peak) is a function of time. It is also a function of actual amplitude difference between two different wave forms. Also, if the leading edge of one wave form is distorted as a result of corrosion, this distortion will result in a change of amplitude in the difference wave form and a shift in the position of the peak with respect of time. When the pipe is very good, the peak is very sharp and the shape of the difference wave forms extremely uniform. When the pipe has anomalies (e.g. corrosion), the shape of the difference wave form is significantly altered and the corrosion effect (CE) displaced by major differences in the leading edge. These differences result in an effective peak shift that can be related directly to pipeline quality.

This peak shift is much easier to instrument and measure than other parameters. Also this peak shift is an indicator of the cumulative effect of all individual parameters and effect the electromagnetic response, even if they might be very

difficult to measure individually. As the pipe degrades, the peak distorts more readily because of the complex contribution of all driving forces. In a perfect system, every difference pulse should be identical. Hence, measuring the time associated with the first peak occurring after an indefinite knee of a differential pair, provides an effective way of extracting critical information and measuring the corrosion effect.

Obviously, a stable source is required and is being used for this system. From the wave forms included, it should be obvious that measuring the peak is easier than measuring the time related to the knee. When the peak is not well defined, it will indicate different anomalies on the pipe. The process of measuring the corrosion effect is designed to impose the quality of data and reduce the time required to collect and analyze the data in the field.

To illustrate in a rather simplified fashion certain aspects of the present invention, relative to subtraction of one wave form from another, reference is now made to FIGS. **7**A through **7**G, and also FIGS. **7**H and **7**I.

FIG. **7**A shows a rather simple wave form **60** which is drawn, for convenience, in straight lines. FIG. **7**B shows the same wave form at **62**, but offset one unit from the wave form **60**. FIG. **7**C shows the summation of the wave forms **60** and **62** as the wave form **64**. It is possible to drive meaningful information from the wave form in FIG. **7**C where the wave forms are added, but it is preferred to first one of the wave forms and then add the two together. This is done in FIG. **7**D which shows the wave form **60**, with the offset wave form **62** inverted, and the summation of the wave **60** and the inverted wave **62** accomplishes a subtraction of the wave forms of FIG. **7**A and **7**B. This results in the difference in the difference wave form **66** shown in Figure E.

As indicated above, these curves are somewhat artificial, and in actuality, these simple wave forms would not be formed with these straight lines. Rather FIGS. **7**H and **7**I would be more realistic, where we see the wave form **68** and a very similar wave form **70** offset in the wave form **68**. In **7**I, there is shown a difference wave form **72** which would result from subtracting the wave **70** from the wave form **68**. It can be seen that the difference wave form **72** forms in a rather well defined peak.

For purposes of further analysis, in FIG. **7**F, the wave form **74** is shown, exactly in the same form and position as the wave form **60** of FIG. **7**A. Then the same wave form is shown in FIG. **7**F at **76**, inverted and shifted two units from the wave form **74**. Then when the wave form **76** is subtracted from the wave form **74**, there is the difference wave form **78** shown in FIG. **7**G. It will be noted that with the wave form **76**, spaced two units away from the wave form **74** (instead of one unit, as in FIGS. **7**A and **7**B) has an amplitude which is twice the amplitude Of the difference wave form **66**. This illustrates that if the time displacement of the wave forms increases, the amplitude of the difference wave form would be expected to increase. This is simply by way of illustration, and relates to only one particular facet of detecting corrosion from the difference wave form.

For purposes of further analysis, reference is made to FIGS. **8**A through **8**E and to FIGS. **9**A through **9**E.

In FIG. **8**A, there is shown a wave form **80**, and in FIG. **8**B a second advanced wave form **82** which has been attenuated and delayed, presumably because of encountering corrosion in the pipe. FIG. **8**C shows the summation of these, this being the wave form **84**. FIG. **8**D shows the same wave form **80** and the adjacent wave form **82** inverted. FIG. **8**E shows a difference wave form **86** which results by subtracting the wave form **82** of FIG. **8**B from the wave form **80** of FIG. **8**A.

In FIG. **9**A, these same steps are followed. FIG. **9**A shows a wave form **88** which is the same as the wave form **80** of FIG. **8**A. FIG. **9**B shows a second wave form **90** delayed by one unit, and having a different slope along the leading edge. FIG. **9**C shows the summation wave form at **92**. FIG. **9**D shows the wave form **88** and the second wave form **90** inverted. FIG. **9**E shows the difference wave form at **94**.

In reviewing FIGS. **7**A through **7**I, FIGS. **8**A through **8**E, and also FIGS. **9**A through **9**E, four of the figures show difference wave forms, these being the difference wave form **66** in FIG. **7**E, the difference wave form **78** in FIG. **7**G, the difference wave form **86** in FIG. **8**E, and the difference wave form **94** FIG. **9**E. It can be seen that the different characteristics of these difference wave forms emphasize the difference between the adjacent wave forms.

It should be kept in mind that these wave forms of FIGS. **7**A–**7**I, **8**A–**8**E and **9**A–**9**E are not the more complex composite wave forms such as shown at **50**. These are simplified wave forms provided simply to show some of the principles involved.

What the method of the present invention accomplished is the elimination of a great deal of the irrelevant information. There is the tendency of the near side pulse to swamp out the far side pulse, mainly because the near side pulse has a substantially larger amplitude, since it is closer to the transmitting location. The components of the near side pulses are substantially eliminated. Beyond this, by subtracting the shifted wave components attributable to the far side pulses from one another is that a difference comparison is provided. If the pipe is substantially uniform along its length (non-corroded), and if the intersecting point of the pulses is stepped in even increments along the pipe, then the same or very similar difference waves are expected to be obtained. As indicated previously, the difference curves shown in the upper part of FIG. **3** are quite similar, indicating no corrosion or possibly minimal corrosion. Thus, the difference curves as shown in FIGS. **4** through **6** provide the meaningful information, without being cluttered by extraneous wave components.

A second embodiment of the present invention will now be described relative to FIGS. **10** through **16**. By way of introduction, much of the focus on the analysis of the wave forms to detect corrosion has been directed toward the leading dge of the wave form or at least the early arrival portion of the wave form. To some extent, it has been recognized (or at least conjectured) that valuable information would be contained in the later arriving portions of the wave form. However, the problem is how such information could be identified and/or extracted.

As indicated earlier in this text, the propagating wave form can be considered to be a composite of a number of wave components made up at least in part of early and late arrivals. To illustrate this graphically, reference is made to FIG. **10** which shows a relatively short section of pipe, where there is a transmitting location 102 and receiving location 104. In this instance, these locations 102 and 104 are both at the top of the pipe and aligned. The straight line lengthwise axis between the points **102** and **104** is indicated at **106**. Since this axis **106** is the shortest path between the points **102** and **104**, the first arrival path would be along the path indicated at **108**, which is coincident with the axis **106**.

In addition to the first arrival wave component **108**, there are two second arrival wave components, the travel paths of

which are indicated at **110** and **112**. It can be seen that each of these are helical paths, which travel longitudinally and through a helical curve of 360°. Then the third arrivals are indicated at **114** and **116**, and these also are helical paths, but with a total circumferential component of travel of 720°.

Obviously, the second arrival has a longer path of travel than the first arrival, the third arrival has a yet longer path of travel than the second arrival, etc. If there is corrosion on the pipe, at least some of these later arrival pulse components will pass through the area or areas of corrosion and that path component will be delayed, attenuated, and/or otherwise modified.

With the foregoing being given as background information, reference is now made to FIG. **11**, which illustrates the wave forms obtained by the second embodiment of the present invention. In FIG. **11**, the vertical axis represents voltage (measured in volts), and the horizontal axis measures time, with each increment representing ten nanoseconds. Thus, the numeral one thousand actually represents one hundred nanoseconds, the numeral two thousand represents two hundred nanoseconds, etc. It can be seen that the wave forms presented in FIG. **11** extend over a full five hundred nanoseconds.

The particular tests from which these curves were developed were done over a pipe section one hundred and sixty feet length (i.e. the transmitting location was one hundred and sixty feet away from the receiving location). Further, the dual pulse method was utilized, as indicated above. Since the entire pipe is encircled by electromagnetic energy, the effect of corrosion anywhere on the pipe will appear in the difference wave form obtained by intersection of the pulses at the location of corrosion.

The first steps in the second embodiment in the method of the present invention are substantially the same as those of the first embodiment. More specifically, a first testing operation was performed by transmitting the near side and far side pulse in timed relationship so that these would meet at a predetermined point of intersection. There is a composite wave form resulting from this first test operation and that is stored. Then, as described in the presentation of the first embodiment, there is a second operation in timing of the far side pulse so that it was either advanced or delayed so that the point of intersection was shifted, and the result was a composite wave being recorded that had components of the far side pulse shifted somewhat from the previous composite wave. As described in the first embodiment of this method of the present invention, one of the composite wave forms is subtracted from the other to get a difference wave form.

These steps are performed in the second embodiment of the present invention, and it will be recognized, of course, that these are substantially the same steps as described in the first embodiment. From this point on in the method of the second embodiment, a further analysis is conducted as will be described below.

For purposes of description, we shall consider the sequence of the difference wave forms and designate these as difference wave form **1**, difference wave form **2**, difference wave form **3**, etc. It will be evident that the difference wave form **1** results from processing composite wave forms **1** and **2** which result from the first and second dual pulse test operations; difference wave form **2** is a result of processing the composite wave forms **2** and **3** resulting from the second and third dual pulse operations; etc.

In FIG. **11**, there is first plotted the difference wave form **120**, and this wave form is about five hundred nanoseconds in length. The next step is to plot the second difference wave form **122**, but the second difference wave form **122** is shifted to the left, and is also lowered somewhat so that the second difference wave form **122** is aligned with and a short distance below, the first difference wave form **120**. It will be observed in the wave form representation of FIG. **11** that the two wave forms **120** and **122** match each other rather closely. These two difference wave forms **120** and **122** were derived from adjacent composite wave forms, and both of these composite wave forms resulted from a dual pulse operation where the pulse is intersected at a noncorroded area (or at least a very lightly corroded area) of the pipe under test. As indicated at the right side of FIG. **11**, the upper composite wave results from a difference wave form where a reference point of intersection was that at the 125.3 feet mark, while the second difference wave form **122** was made up of adjacent composite wave forms at a reference location 129.6.

FIG. **12** shows two other reference wave forms **124** and **126**, resulting from two adjacent pair of composite wave forms at reference locations at the 34.6 and 38.9 foot locations on the pipe section under test. These composite wave forms also resulted from the far side and near side pulses of each test operation intersecting at a noncorroded (or very lightly corroded) area of the pipe section under test.

Reference is now made to FIG. **13**, where there is shown as the upper wave form the same wave form **126**, as shown in FIG. **12**, this difference wave form having a reference location of 38.9 feet on the pipe. The lower wave form **128** has a reference of 43.2. This was at a somewhat corroded pipe section having a corrosion index of 1.0262. (The corrosion index is a scale which is utilized by the inventor in rating areas of corrosion. A rating of 1.000 would be no corrosion and the higher the number, the greater the severity of corrosion).

It will be noted in FIG. **13** that the lower wave form **128** has at two areas something of a phase shift, indicated at **130** and **132**.

Reference is now made to FIG. **14**, where there are two adjacent reference wave forms at locations along the pipe section at the 151.2 foot location and the 155.5 foot location. There was a corrosion index of 1.055, which is higher than in FIGS. **11**, **12** and **13**. These wave forms are indicated at **134** and **136**. It can be seen that at the location **138** there is a rather substantial phase shift.

Next, attention is directed toward FIG. **15** which shows as the upper wave form the same wave form **136** which is the lower wave form in FIG. **14**, and a new difference wave form **140** taken at a reference location of 160 feet on the pipe. These wave forms resulted from composite wave forms developed with the intersecting locations being at more highly corroded areas. Several features should be noted. In observing the peak location at **142**, and the two peak locations at **144** and **146**, it can be seen that there are substantial amplitude differences with regard to the second and third peaks between these curves **136** and **140**. In addition there is significant phase shift indicative of corrosion anomalies.

It is enlightening to observe the difference curve **134** which is at the reference location 151.2 (FIG. **14**) and the curve **140** which is at the reference location 160 (FIG. **15**). It can be seen by matching up the curves **134** and **140** that these correspond fairly closely to one another, at least much more closely to one another than each matches up with the curve **136**. This would indicate that the corrosion area is more likely in the area of the reference location 155.5, presumably somewhere between the **153** to the **158** area.

Finally, reference is made to FIG. **16**, where there are two difference wave forms **150** and **152**. It can be seen that the difference wave form **152** has substantial similarities to the curve **136** (see FIGS. **14** and **15**). Further, it can be seen the match up between the wave forms **150** and **152** are rather similar to the matching of the wave forms of **134** and **136** in FIG. **14**. More specifically, it can be seen that the second and third peaks **154** and **156**, respectively, of the wave form **152** are of nearly equal amplitude, and then there is the phase shift at the area **158**. This is a pattern quite similar to that shown at area **138** in FIG. **14**.

Thus, it can be seen that with the method of the second embodiment of the present invention, the presence of corrosion is detected by a method which might be termed "whole wave analysis", which involves looking not only at the leading portion of the wave, but also a much greater time span of the wave form which also contains significant information. It also becomes apparent that valuable information is obtained from portions of the wave form as far along the wave form as two hundred to four hundred nanoseconds or longer from the first arrival of the electromagnetic pulse. Further, the location of the corrosion can be located within reasonably close tolerances by properly synchronizing the pulses so that the point of intersection is known.

Also, it should be noted that these readings were taken on the same section of pipe, but with the intersection being moved to different locations. Therefore, all of the wave forms developed for the data of FIGS. **11** through **16** passed over the same pipe section. The key difference is that the point of intersection was moved. When the point of intersection of the wave forms which were combined to make the difference wave forms were at an area of corrosion, the variations of the different wave forms become apparent.

A third embodiment of the method of the present invention will now be described. In this third embodiment, as in the prior embodiments, the pulses will be transmitted from the far side and near side locations, and in this particular embodiment, the wave form which is to be analyzed to detect corrosion is the far side pulse arriving at a receiving location adjacent to the transmitting location at the near side. Also, in this third embodiment , the time intervals between the transmissions of the far side pulse will remain constant. Thus, to synchronize the pulses so that the point of intersection stepped along the length of the pipe, for each transmission, the near side pulses shall be advanced in timing by a short increment so that the point of intersection of the pulses will be stepped in a left to right direction across FIG. **18**. In the first step of this further embodiment, the far side transmitter is shut down, and a series of pulses are transmitted from the near side and these are picked up by the near end receiving antenna that is closely adjacent to the near side transmitter. The timing of the transmission of the near side pulses is timed relative to a sender except that each subsequent transmission is advanced one additional increment of time, and in this particular example we will assume that it is being advanced by four nanoseconds for each pulse transmission.

The first step in the method of this preferred embodiment will now be described with reference to FIGS. **17** and **19**. In FIG. **19**, there is shown a section of pipe **170** having a Near side transmitting antenna **172** and a far side transmitting antenna **174**. There is a receiving antenna **176** spaced from the transmitting antenna **172** a short distance toward the far side transmitting antenna **174**.

Initially, the far side transmitter remains inactive so that the far side transmitting antenna **174** is not transmitting any signal. The near side transmitter is activated to transmit a series of timed pulses which are synchronized with regular time intervals. This is done in a manner that each subsequent pulse is advanced four nanoseconds relative to the preceding pulse.

For example, if the near side pulses are to be transmitted every two seconds, less the time of the advance of the timing, the first pulse would be sent at 0 seconds. The second pulse would be transmitted four nanoseconds before the two second interval. The third pulse would be sent eight nanoseconds sooner than the four second interval. The first pulse would be sent twelve seconds before the 8 second interval, etc.

Thus, as can be seen in FIG. **17**, the first pulse is transmitted at 0 nanoseconds, the next pulse indicating as having a four nanosecond advance, the third pulse at 8 nanoseconds advance, with these advances continuing on down to the 18th pulse which has been advanced by 72 nanoseconds relative to the initial pulse at 0.

Each pulse from the near side antenna **172** passes by the receiving antenna **176**, and the pulse is recorded, with the wave forms indicated at **178**. It is to be recognized that in most all instances, there is a certain amount of outside electromagnetic, electrical noise, echoes, refractions, etc. that tend to obscure or "clutter" the signal. Each of these pulses **178** is recorded in the memories of the control unit, including all the various extraneous influences on the signal, plus the portion of the signal attributable to the pulse itself. As will be discussed subsequently herein, these pulses **178** that are recorded are used as reference pulses which are subtracted in a subsequent step in the method of the third embodiment.

The next step will now be described with reference to FIG. **18**. The far side transmitter is activated so that regularly timed pulses are transmitted from the antenna **174** into the pipe section **170** i.e. without any advancing or delay in the timing. Each transmission at the near side is synchronized with the transmission at the far side. However, each time the near side transmits a pulse, the next pulse from the near side is advanced four nanoseconds from the designated time period from the previous pulse. Thus, at the zero location in FIG. **18**, the far side pulse is transmitted at a time period so that the pulses from the near side and far side antennas **174** intersect at the location of the receiving antenna **176**. The next pair of pulses are transmitted with the Near side pulse being advanced by four seconds, so the point of intersection is spaced two nanoseconds closer to the far side. The third pulse is advanced by eight seconds so that the intersection of the spaced and additional two nanoseconds toward the far side.

It can be seen that the first pair of pulses intersecting at the antenna **176** that the peaks of theses pulses come close to coinciding. It can be seen that subsequent pairs of pulses are transmitted and with the near side pulses being advanced four nanoseconds on each transmission, relative the far side pulse,the pattern of the wave which is received at the antenna **176** comprises a first peak **182** which is attributable to the near side pulse passing by the antenna **176**, and a second peak **184** which is attributable to the near side pulse reaching the antenna at a later time.

In this third embodiment, the far side pulse that is received by the antenna **176** is the one which is analyzed to determine whether the corrosion exists. To accomplish this, the following procedure is followed. Each of the wave forms **186** that result from the second step of this method are also stored in memory. Then the wave forms **178** (showed in FIG.

17) are each subtracted from the corresponding wave forms shown in FIG. **18** with the resulting wave forms being shown in at **188**, FIG. **20**.

What has occurred is that when the wave forms of FIG. **17** are subtracted from the corresponding wave forms of FIG. **18**, the wave form from the near side, along with the extraneous noise, echoes, etc. is cancelled out so that what is left is the wave form **188** that essentially represents the far side wave form which is "uncluttered." The overall result is that this facilitates the detection of variations in the wave form that originated from the far side.

It should be noted that if there is a relatively smaller amount of corrosion, its effect on the wave forms which intersect at the location of the corrosion is more difficult to detect. By performing the first three steps as described with reference to FIGS. **17**, **18** and **20**, these more subtle variations in the wave form resulting from the far side pulse intersecting with the near side pulse at the area of corrosion can be detected more easily.

FIG. **21** shows four adjacent wave forms **190** which are the same wave forms **188** of FIG. **20**, except that vertical dimension has been increased substantially so that the slope of these wave forms **190** is steeper. It can be seen in FIG. **21** that each of these four wave forms **190** are very similar to one another. This would indicate that there is little or no corrosion in the area where the wave forms **190** have intersected.

Now a fourth step in the method of the present invention is performed to further enhance the ability to analyze the wave forms to detect corrosion, and this will be explained first with reference to FIG. **22**. FIG. **22** represents four adjacent wave forms resulting from four pulse transmissions which follow one after the other in sequence. These waves are designated **192-1**, **192-2**, **192-3** and **192-4**. Each wave form is subtracted from the preceding wave to obtain a difference wave form.

This is accomplished by first inverting the wave form **192-2** and then adding this inverted wave form to the wave form **192-1** to obtain a difference wave form which is **194-1** (this **194-1** being the difference wave form of the two wave forms **192-1** and **192-2**). In a similar manner, a second difference wave form **194-2** is obtained by inverting the wave form **192-3** and adding this to the wave form **192-2** to obtain the difference wave form **194-2**. The third difference wave form **194-3** is obtained in the same way by inverting the wave form **194-4** and adding this to the wave form **192-3**.

It can be seen in FIG. **22** that each of the three different wave forms **194-1**, **194-2** and **194-3** are very similar to one another and have substantially the same amplitude.

FIG. **23** illustrates another technique utilized in this third embodiment. The four wave forms **194-1** through **194-4** are moved closer together, while leaving the wave forms unchanged. By moving these wave forms closer together, it is much easier to detect variations in the wave forms. Also, the different wave forms which would result from the arrangement of the wave forms in FIG. **23** would be a much smaller attitude. The effect of this is, however, that differences in amplitude between the peaks does not decrease when the wave forms are moved closer together. This further accentuates the differences in the wave forms.

To illustrate the wave forms where corrosion is being detected, reference is now made to FIG. **24**. There are shown **18** adjacent difference wave forms such as shown at **194-1**, **194-2**, and **194-3** in FIG. **22**. It can be seen that the fourth wave form **196** and the fifth wave form **198** are configured rather differently than the adjacent wave forms shown immediately above and below these two wave forms **196** and **198**. It will be noted that between the initial "hump" **199** and the second "hump" **200** of the wave form **196** there is a substantial dip at **201**.

In addition, it will be noted that the second peak or "hump" **202** of the wave form **198** has a much smaller amplitude. Further, it can be seen that the peak **203** of the first rise or "hump" **204** of the wave form **198** is shifted to the right. An alignment line **204** is drawn to show the shift from the alignment line at the left.

It will also be noted that there is a shift in the peak **205** of a wave form which is the twelfth wave form from the top. This is also an indication of a corrosion, but a smaller degree of corrosion in comparison with the corrosion detected in the area of the fifth and sixth wave forms.

FIG. **25** is a graph where the points of peak amplitude for adjacent difference wave forms has been prepared by drawing lines connecting adjacent peak points. It can be seen that the peak indicator at **206** is much greater than the rest of the peak points, and this would indicate an area of corrosion. The peak indicated at **208**, while not having the height of the peak at **206**, still rises above the others. This would indicate that corrosion would likely be encountered at the location at the pipe represented by the point **208** which would be the peak of the difference wave form of two adjacent wave forms where the corrosion was at or near the location of intersection.

FIG. **26** is a graph similar to FIG. **25**, where the amplitude of the points in FIG. **25** have been amplified in a matter to further accentuate the differences.

It is to be understood that the terms "near side" and "far side" can be reversed. Further, it is to be understood that while the third embodiment has been described, with the far side pulse being the pulse which is analyzed, and the near side pulse which has been advanced to cause the point of intersection to be stepped along the elongate number (pipe), this arrangement could be reversed. Further, in an actual testing operation, both the near side pulses arriving at the far side, and the far side pulses arriving at the near side could each be received and analyzed.

Also, it is to be understood that various modifications to be made in the present invention without departing from the basic teachings thereof. Further, the terminology used in this description should, in the following claims, be given an interpretation commensurate with the scope of the invention and should not be interpreted as being limited to the specific procedures and operating components described herein.

What is claimed is:

1. A method of identifying corrosion on an electromagnetically permeable member, said method comprising:

a. transmitting near side and far side electric or electromagnetic pulses (waves) from, respectively, near side and far side spaced transmitting locations on said member, with said pulses (waves) travelling toward one another to intersect at intersecting locations on said elongate member,

b. Receiving said far side pulses (waves) as wave forms at a receiving location after intersection with related nearside pulses (waves),

c. Synchronizing transmission of the near side and far side pulses (waves) so that the intersections of the near side and far side pulses (waves) occur at spaced intersecting locations on said member;

d. combining the wave forms of at least two of said far side pulses (waves) which are spaced from one another to form a composite wave form;

e. ascertaining a variation or variations in said composite wave form as a means of detecting corrosion.

2. The method as recited in claim **1**, wherein far side pulses (waves) which pass through points of intersection that are adjacent to one another are considered to be sequential far side pulses, with order of sequence being the same as the order in which the points of intersection are spaced along the elongate member, and combining of the far side wave forms is accomplished in a pattern such that first and second adjacent wave forms are combined to make a first composite wave form, the second wave form and an adjacent third wave form are combined to make a second composite wave form, the third wave form is combined with an adjacent fourth wave form to make a third composite wave form, with the pattern repeating itself with subsequent pairs of wave forms from adjacent far side pulses.

3. The method as recited in claim **2**, wherein far side pulses which pass through points of intersection that are adjacent to one another are considered to be sequential far side pulses, with the order of sequence being the same as the order in which the points of intersection are spaced along the elongate member, and combining of the far side wave forms is accomplished in a pattern such that first and second adjacent wave forms are combined to make a first composite wave form, the second wave form and an adjacent third wave form are combined to make a second composite wave form, the third wave form is combined with an adjacent fourth wave form to make a third composite wave form, with the pattern repeating itself with subsequent pairs of wave forms from adjacent far side pulses.

4. The method recited in claim **3**, wherein adjacent composite wave forms are compared with one another as a means of detecting corrosion.

5. The method as recited in claim **4**, wherein a reference wave form is established by creating composite wave forms resulting from pulses that intersect away from a corroded areas of the elongate member and identifying composite wave forms that differ from the reference composite wave form in phase shift, dispersion, amplitude, wave distortion, or combinations of these.

6. The method as recited in claim **5**, wherein corrosion that is present between two adjacent points of intersection on the member, is detected by examining a composite wave form resulting from combining the difference wave form overlapping the point of intersection with difference wave forms on opposite sides of the overlapping composite wave form.

7. The method as recited in claim **5**, wherein corrosion is present at a point of intersection of two wave forms, and two difference wave forms are derived by combining the wave form at the point of corrosion with adjacent wave forms, and these are compared with one another wave form to ascertain corrosion.

8. The method as recited in claim **7** wherein two additional difference wave forms that are on opposite sides of, and adjacent to, the two wave forms which are compared to detect the corrosion are also compared with the two difference wave forms which are combined at the point of intersection, as a means of detecting corrosion.

9. The method as recited in claim **1**, wherein far side pulses (waves) which pass through the points of intersection that are adjacent to one another are considered to be sequential far side pulses (waves), with the order of sequence being the same as the order in which the points of intersection are spaced along the member, the combining of the far side wave forms being accomplished in a pattern such that the wave form resulting from the first and second adjacent nearside pulses intersecting with related far side pulses are combined to make a first composite wave form, wave forms of the second and third near side pulses that are combined with the related far side pulses are combined to make composite wave forms, with this pattern repeating itself for subsequent pulses.

* * * * *

US005370776A

United States Patent [19]

Chen

[11] Patent Number: 5,370,776

[45] Date of Patent: Dec. 6, 1994

[54] **ELECTROCHEMICAL IMPEDANCE SPECTROSCOPY METHOD FOR EVALUATING CORROSION INHIBITOR PERFORMANCE**

[75] Inventor: **Huey-Jyh Chen**, Santa Ana, Calif.

[73] Assignee: **Chevron Research and Technology Company**, San Francisco, Calif.

[21] Appl. No.: **139,593**

[22] Filed: **Oct. 20, 1993**

[51] **Int. Cl.**[5] **G01N 17/02**

[52] **U.S. Cl.** **204/153.11**; 204/404; 324/71.2; 324/425; 324/700

[58] **Field of Search** 204/153.11, 404; 324/425, 71.2, 700

[56] **References Cited**

U.S. PATENT DOCUMENTS

4,095,176	6/1978	Maes	204/153.11
4,238,298	12/1980	Tsuru et al.	204/153.11
4,266,187	5/1981	Slough	204/153.11
4,658,365	4/1987	Syrett et al.	364/496
4,800,165	1/1989	Oka et al.	436/6
4,831,324	5/1989	Asakura et al.	324/615
4,881,037	11/1989	Bellingham et al.	324/425
5,,006,786	4/1991	McKubre et al.	324/71.2

Primary Examiner—Aaron Weisstuch

Attorney, Agent, or Firm—M. W. Carson; W. K. Turner; D. J. Power

[57] **ABSTRACT**

A simple, expedient method for measuring the effectiveness of a corrosion inhibitor provided to a metallic surface by a surface layer, wherein the layer is formed by use of the corrosion inhibitor is a corrosive fluid. The method employs the measuring of a high frequency phase angle as an indicator of inhibitor effectiveness.

12 Claims, 7 Drawing Sheets

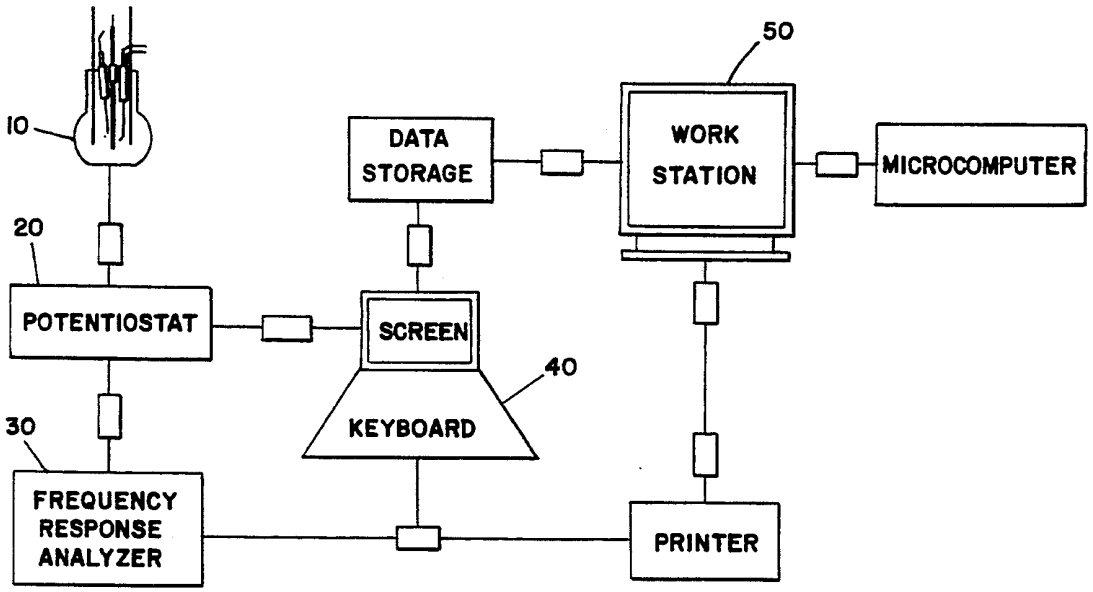

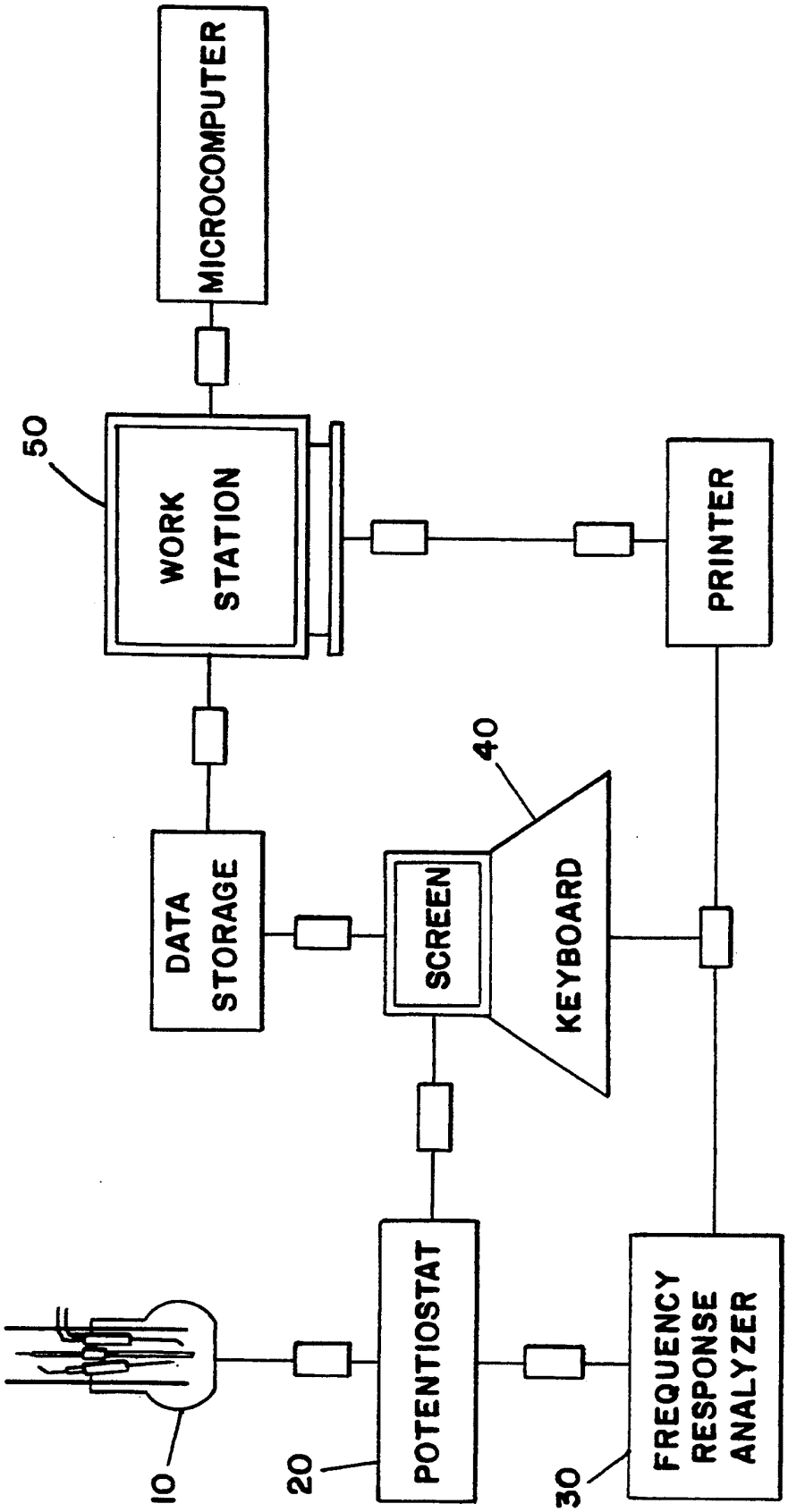
MICROCOMPUTER
50
WORK STATION
PRINTER
40
DATA STORAGE
SCREEN
KEYBOARD
10
20
POTENTIOSTAT
30
FREQUENCY RESPONSE ANALYZER

FIG_1

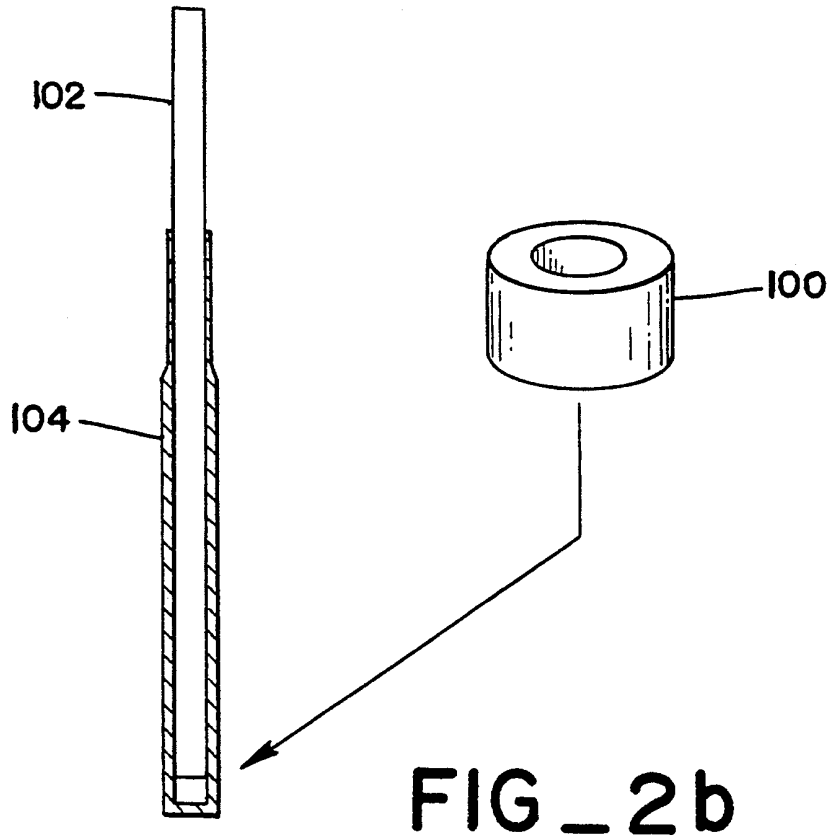

FIG_2b

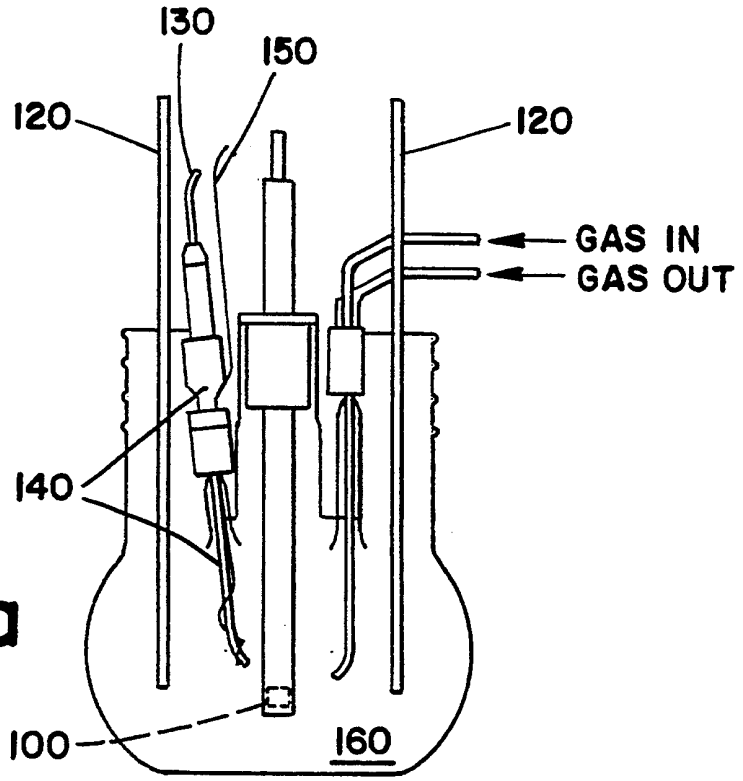

FIG_2a

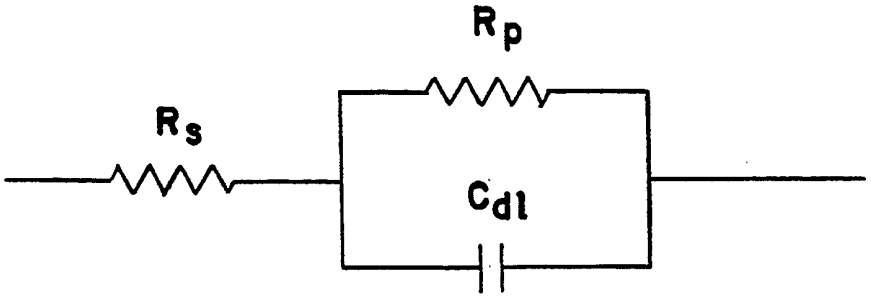

R_s – SOLUTION RESISTANCE
R_p – POLARIZATION RESISTANCE
C_{dl} – DOUBLE LAYER CAPACITANCE

FIG_3

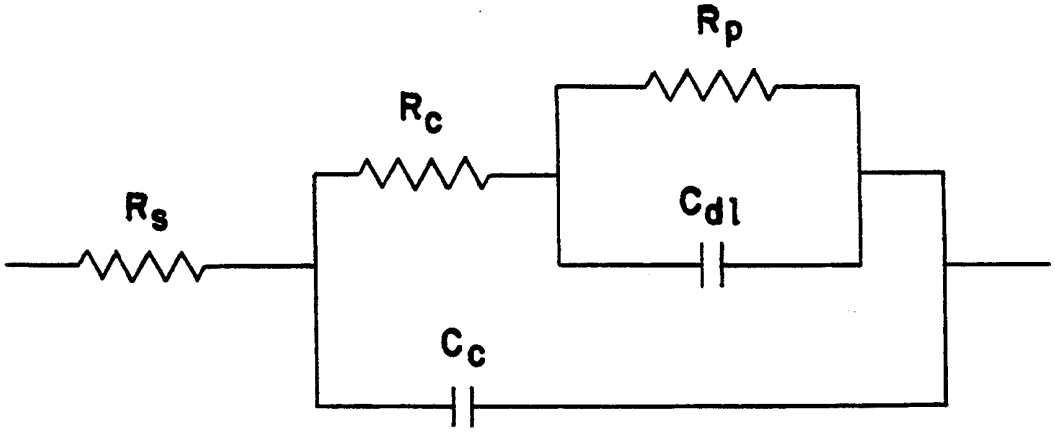

R_s – SOLUTION RESISTANCE
R_p – POLARIZATION RESISTANCE
C_{dl} – DOUBLE LAYER CAPACITANCE
R_c – COATING (INHIBITOR FILM) PORE RESISTANCE
C_c – COATING (INHIBITED FILM) CAPACITANCE

FIG_4

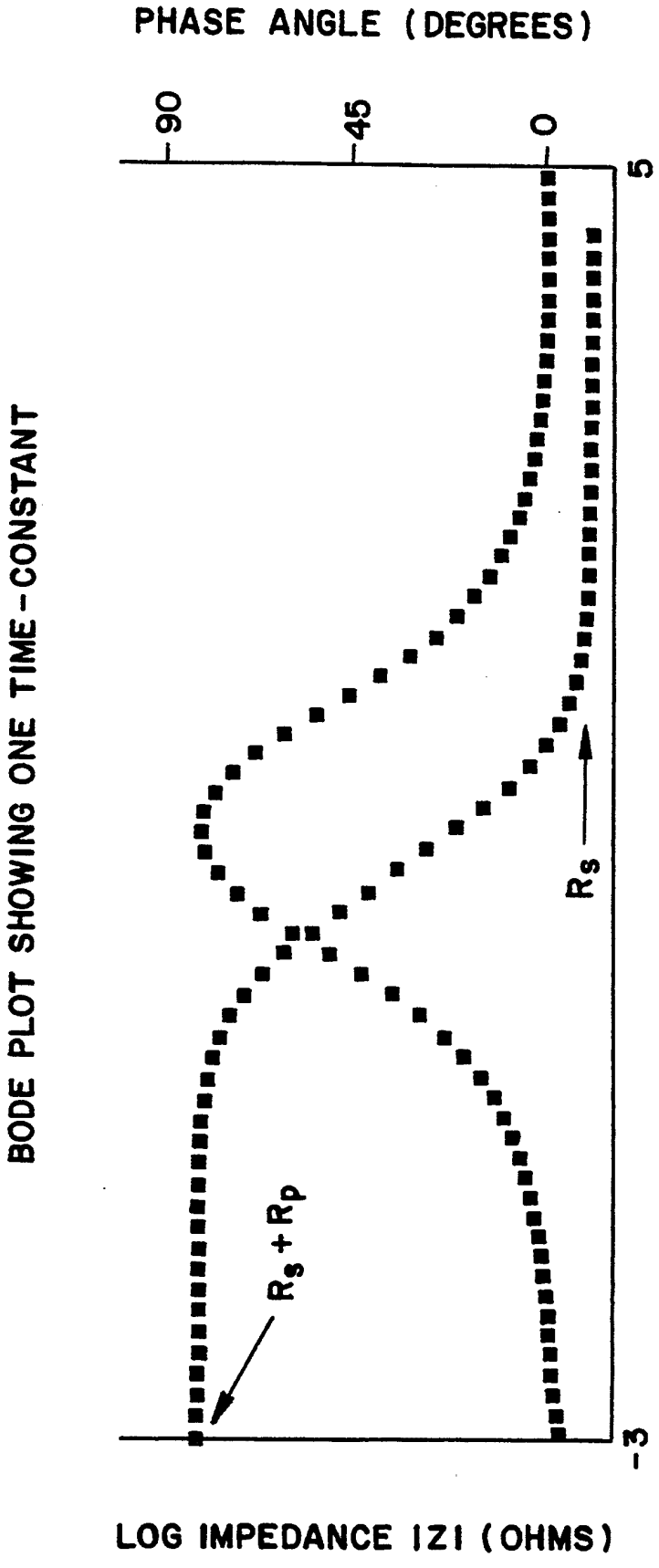
PHASE ANGLE (DEGREES)
90
45
0
5
-3
R_s
$R_s + R_p$
BODE PLOT SHOWING ONE TIME-CONSTANT
LOG FREQUENCY (Hz)
LOG IMPEDANCE IZI (OHMS)

FIG_5

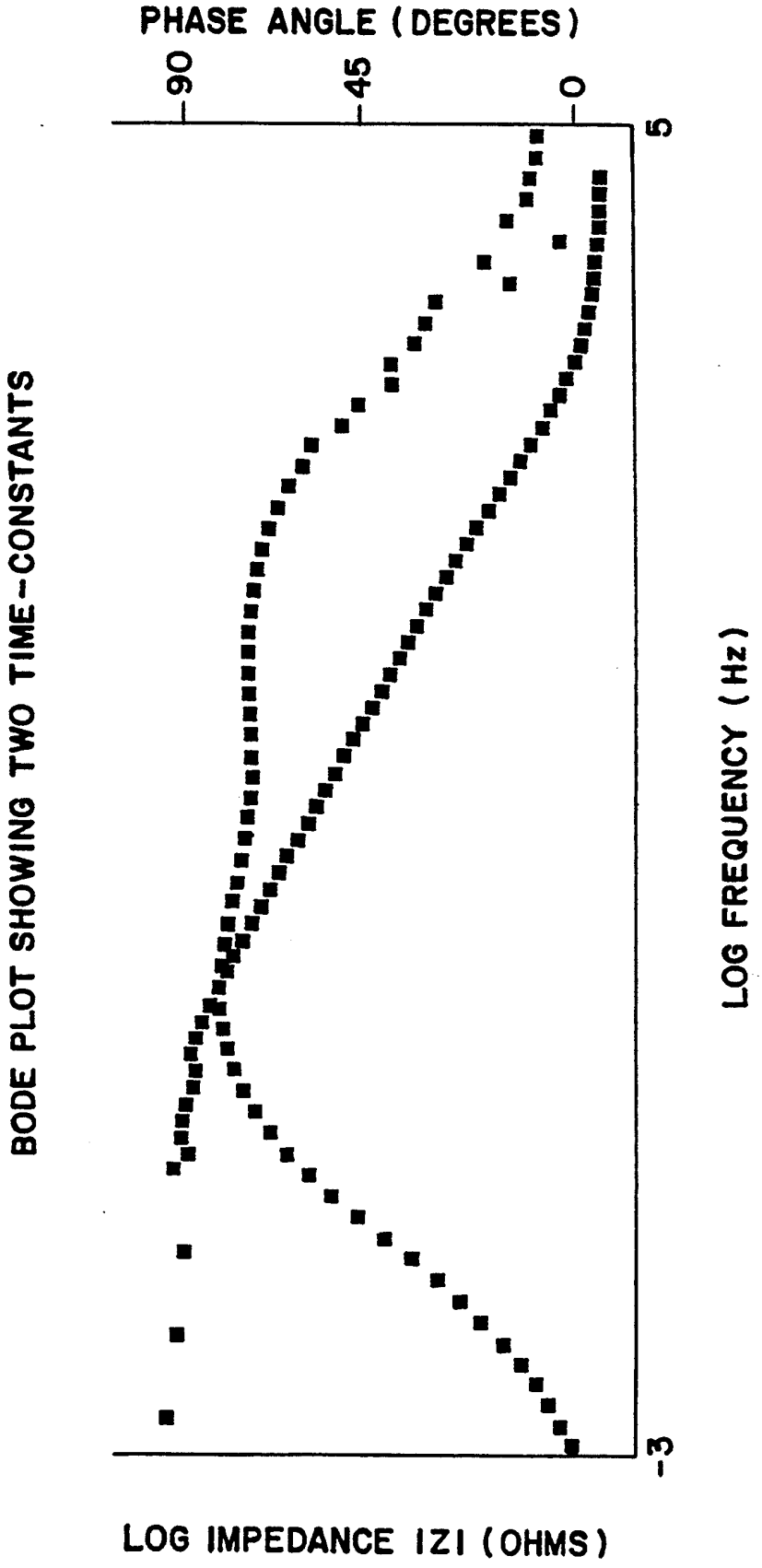
PHASE ANGLE (DEGREES)
90
45
0
5
-3
BODE PLOT SHOWING TWO TIME-CONSTANTS
LOG FREQUENCY (Hz)
LOG IMPEDANCE IZI (OHMS)

FIG_6

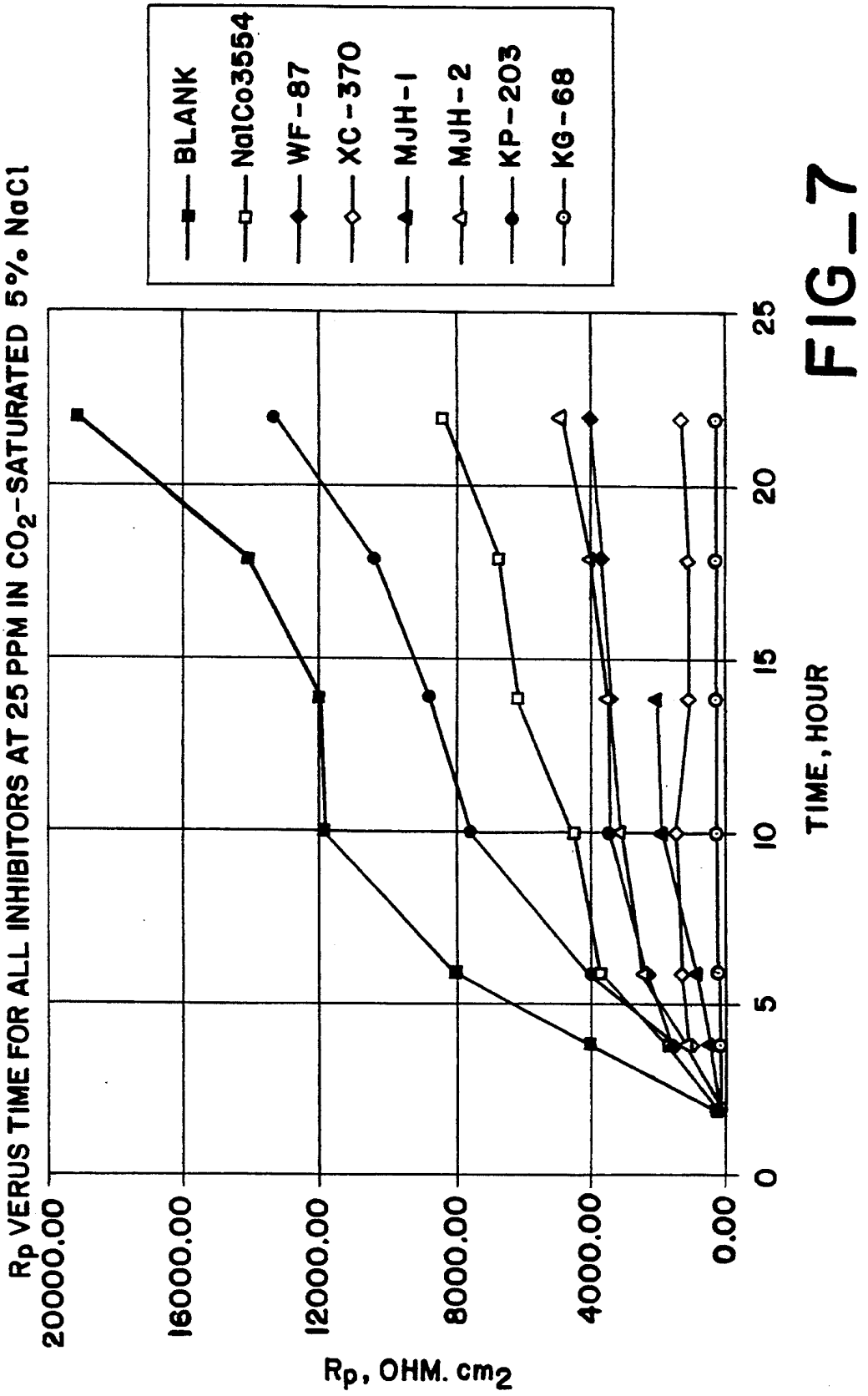
Rp VERUS TIME FOR ALL INHIBITORS AT 25 PPM IN CO_2-SATURATED 5% NaCl
BLANK
NalCo3554
WF-87
XC-370
MJH-1
MJH-2
KP-203
KG-68
20000.00
16000.00
12000.00
8000.00
4000.00
0.00
Rp, OHM. cm_2
0
5
10
15
20
25
TIME, HOUR

FIG_7

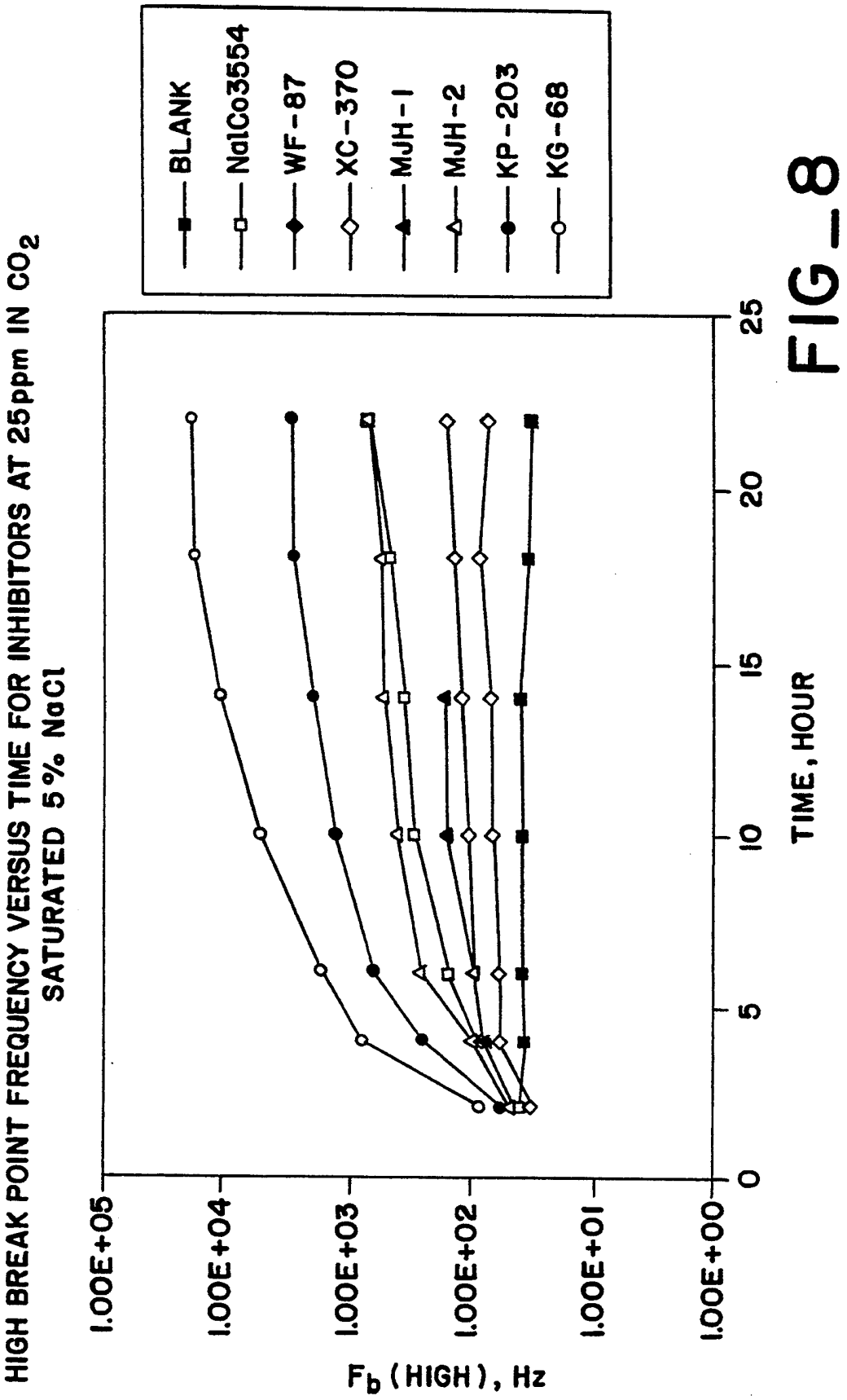
HIGH BREAK POINT FREQUENCY VERSUS TIME FOR INHIBITORS AT 25ppm IN CO_2
SATURATED 5% NaCl
BLANK
NalCo3554
WF-87
XC-370
MJH-1
MJH-2
KP-203
KG-68
1.00E+05
1.00E+04
1.00E+03
1.00E+02
1.00E+01
1.00E+00
F_b (HIGH), Hz
0
5
10
15
20
25
TIME, HOUR

FIG_8

ELECTROCHEMICAL IMPEDANCE SPECTROSCOPY METHOD FOR EVALUATING CORROSION INHIBITOR PERFORMANCE

FIELD OF THE INVENTION

This invention relates to a method and apparatus for the evaluation of corrosion protection afforded by a corrosion inhibiting material. More specifically, it deals with an alternative measurement technique utilizing a high frequency at a varying phase angle as an indicator for monitoring inhibitor effectiveness.

DESCRIPTION OF THE PRIOR ART

Metallic surfaces are detrimentally affected by corrosive fluids in many fields of industry. For example, in the petroleum industry corrosion of metallic surfaces by petroleum materials occurs at all stages of production and distribution. To reduce this corrosion, inhibitors are often utilized as a control method, particularly in the oil and gas industry. There are various inhibitors which work in different ways, as well as various screening procedures used for the selection of inhibitors. Some inhibitors work by neutralizing active ions, others by reducing ion mobility and others by changing the ion transport numbers. In all cases the electrical conductivity of the corrosive fluid is altered, and various electrical parameters contributing to the overall corrosion mechanism will be affected. Accordingly, by using the corrosive fluid as an electrolyte in which two electrodes are immersed, and by measuring electrical characteristics of the electrolytic circuit, it is possible to derive an indication of the level of corrosion which continues to occur.

Until now, corrosion rates have been evaluated and monitored by measuring the polarization current, wherein a working electrode and a measuring electrode of a different metal are immersed in the corrosive fluid, and a D.C. voltage is applied across the two operative electrodes. By correlating potential difference increments, against current increments, a measure of the polarization current can be derived. Typically the use of linear polarization and potentiodynamic polarization are the D.C. methods used to determine corrosion rate.

In practice, however, the measurement of polarization current does not give a reliable evaluation of corrosion protection. Although the measurement may indicate very Little residual corrosion at the working electrode, the measurements taken a short distance away from the working electrode indicate that substantial corrosion may still be occurring. Other methods, based upon measured circuit characteristics such as solution resistivity and electrode capacitance, as well as polarization current, have been devised in an attempt to provide a more reliable evaluation technique for corrosion control. An example of a method utilizing electrode capacitance is disclosed in U.S. Pat. No. 4,095,176 to Maes et al., incorporated herein.

More recently, the use of electrochemical impedance spectroscopy (EIS) data has been developed as a new tool for conducting corrosion research. Using an equivalent electrical circuit comprised of a network of resistor, capacitor, inductor and constant phase elements, which are correlated to the physical and electrochemical properties of the system, allows the application of EIS data to various electrochemical properties, particularly corrosion and corrosion inhibition processes. In addition to mechanistic processes, EIS analysis can provide corrosion rate information, and has the advantage of allowing measurements to be conducted in low conductivity solutions where conventional D.C. techniques are subject to serious measurement error. This analysis is based upon the measurement of the polarization resistance of the system through the use of a low amplitude sinusoidal voltage in an extremely low frequency region, applied over a long period of time, and using this resistance measure to calculate the corrosion current density for the system.

This analysis, however, requires a significant amount of time to measure the polarization resistance, making it difficult for use in a field environment. It is therefore an object of the present invention to provide an expedient means for determining polarization resistance to allow for a timely and accurate measure of inhibition performance.

SUMMARY OF THE INVENTION

The present invention concerns a test method for evaluating the performance of a corrosion inhibitor utilizing the novel direct correlation method discovered to exist between the high "break point frequency", the frequency which occurs at 45° phase angle, and the corrosion rate for a given system. By the method of the present invention, the results of an EIS data analysis for a corrosive system are categorized into specific parameters; those related to the corrosion process such as polarization resistance (R_p) and double layer capacitance (C_{dl}), those related to inhibited film properties such as pore resistance (R_c) and film capacitance (C_{-c}) and those parameters related to the specific system being studied such as the maximum phase angle (θ_{max}) frequency at maximum phase angle ($f_{\theta max}$), and the breakpoint frequency (f_b). These parameters can then be used to evaluate and rank the performance of various corrosion inhibitors introduced to the system. The present method recognizes that when a ranking based on the corrosion process parameter of polarization resistance (R_p) is compared to a ranking based on the system parameter of high breakpoint frequency (f_b), each ranking is identical. The present method exploits this correlation by measuring the high frequency at 45° phase angle of a corrosive system before and after the addition of a corrosion inhibitor, and measuring the inhibitor's effectiveness by comparison. Because of the excellent correlation, the higher the high frequency at 45° phase angle measurement in the inhibited system, the higher the polarization resistance and the lower the corrosion rate.

BRIEF DESCRIPTION OF THE DRAWINGS

FIG. **1** depicts the data acquisition and analysis system used in conducting EIS analysis.

FIG. **2***a* depicts the electrochemical cell used in the EIS measurement.

FIG. **2***b* is the electrode assembly used in the electrochemical cell of FIG. **2***a*.

FIG. **3** is a circuit model corresponding to a simple electrochemical corrosion cell.

FIG. **4** is a circuit model corresponding to a coated (or inhibited film) metal electrolyte system.

FIG. **5** is a Bode plot of impedance Z and phase angle θ as a function of frequency for a simple electrochemical corrosion cell.

FIG. **6** is a Bode plot of impedance Z and phase angle θ as a function of frequency for a coated metal system.

FIG. 7 is a plot of polarization resistance R_p versus immersion time for inhibitors listed in Table 1.

FIG. 8 is a plot of high breakpoint frequency versus time for the inhibitors listed in Table 1.

DETAILED DESCRIPTION OF THE INVENTION

An important method for permitting the determination of inhibitor effectiveness in a corrosive system in an expedient manner is of particular value, particularly in the selection of inhibitors and the optimization of treating programs. By providing a method and/or system according to this invention, the monitoring of inhibitor effectiveness may be employed in the field environment to avoid over-treating a particular system with a particular inhibitor, as well as use as a tool to evaluate the overall corrosion processes.

In identifying the unique correlation between polarization resistance (R_p) and the frequency measurement at high frequency at 45° phase angle (f_b), EIS analysis was conducted utilizing the data acquisition and analysis system depicted in FIG. **1**. As shown in FIG. **1** an electrochemical cell **10** is connected to an EG&G Model 273 potentiostat **20** and a Solartron Model 1255 frequency response analyzer **30**; both of which are interfaced to an HP 9836S computer **40** and UNIX workstation **50** for data acquisition and analysis. EIS measurements were carried out at open circuit potential with an amplitude of 10 mv in the frequency range of about 5.5 mHz to about 55 KHz.

The electrochemical cell is shown in detail in FIG. **2***a* wherein cylindrical test coupons of C-1018 mild steel, having a total area of about 3.0 cm^2, are used as working electrode **100**. The working electrodes are affixed to an electrode assembly shown in FIG. **2***b*, which comprises an isolated ¼" steel shaft **102** having a 12 mm Kel-F insulation jacket **104** on the lower portion subjected to the corrosive media of the cell. Referring again to the electrochemical cell of FIG. **2***a*, graphite counter electrodes **120** are shown in conjunction with a Saturated Calomel Electrode (SCE) acting as the reference electrode **130**, which is connected to salt bridge **140**. A platinum wire **150** is placed alongside the salt bridge and is coupled to the reference electrode through a 1.0 nf capacitor (not shown) to minimize the high frequency phase shift in the EIC measurements due to the slow response of the SCE. The corrosive media **160** used was approximately 900 ml of 5% NaCl brine which was deaerated with nitrogen and purged for 30 minutes with CO_2 to ensure CO_2 saturation of the brine. EIS measurements were conducted, utilizing the data acquisition and analysis set up at FIG. **1**, two hours after the coupons were immersed and precorroded to establish the baseline data. An inhibitor of desired concentration was next injected into the cell, after which EIS measurements were again taken, followed by subsequent measurements every 2 to 4 hours. The EIS spectra obtained for the corrosion inhibitor evaluation were based upon the circuit models shown in FIGS. **3** and **4**. FIG. **3** is an equivalent circuit corresponding to a simple electrochemical corrosion cell having a one time constant impedance spectrum, wherein R_s is assigned as solution resistance, R_p is the polarization resistance, and C_{dl} is the double-layer capacitance between the metal and solution interface. FIG. **4** is the equivalent circuit for a coated or inhibited film-metal electrolyte system having a two-time constant impedance spectrum, wherein R_c is assigned as the pore resistance of the inhibitor film, and C_c is the capacitance of the coating or inhibitor film.

When conducting the EIS analysis, the first step is the determination of the polarization resistance, R_p. It is well known that the polarization resistance is related to corrosion rate by calculating the corrosion current density I_{corr} according to the Stern-Geary equation:

$$I_{corr} = \frac{\beta_a * \beta_c}{2.303\,(\beta_a + \beta_c) R_p} = \frac{k}{R_p} \quad (1)$$

where β_a and β_c are the anodic and cathodic Tafel constants, respectively, of the corrosion system, and K is a system constant related to the Tafel constraints. For the determination of R_p in EIS, the potentiostat **20** of FIG. **1**, develops a sinusoidal potential perturbation of very small amplitude, of about 10 mv, which is applied as a function of frequency. This slight excitation ensures that the measurement is performed in the linear region of the system, generally between about 100 kHz and 1 mHz. The impedance spectrum is then displayed as a Bode plot, displaying the impedance Z and phase angle θ, each as a function of frequency f as shown in FIG. **5**. The use of a Bode plot allows the capacitance (frequency-dependent) and resistance (frequency-independent) regions to be clearly distinguished; with the frequency dependence of the phase angle made apparent.

For a simple system with only one time constant impedance spectrum, as depicted in FIG. **5** and represented by the equivalent circuit of FIG. **3**, polarization resistance, R_p, is determined by the difference between the impedance at a very high ($Z \rightarrow R_s$; R_s is solution resistance) and a very low ($Z \rightarrow R_s + R_p$) frequency measured at corrosion potential. In a system having more than one time constant impedance spectrum, as depicted in FIG. **6** and represented by the equivalent circuit of FIG. **4**, R_p can be calculated by fitting the impedance data to the equivalent circuit of FIG. **4** using a nonlinear least-square fitting software program, such as LEVM, developed by J. R. MacDonald.

The effectiveness of a given corrosion inhibitor, in terms of percent protection, can be determined from the corrosion rate with or without the presence of a corrosion inhibitor. Since corrosion rate is inversely proportional to polarization resistance, the inhibition efficiency can be determined from the polarization resistance as shown in equation (2):

$$\%\ \text{Protection} = \frac{R_{p(CI)} - R_{p(B)}}{R_{p(CI)}} * 100\% \quad (2)$$

where $R_{p(CI)}$ and $R_{p(B)}$ are polarization resistances with and without the presence of a corrosion inhibitor;respectively. Therefore, since polarization resistance, R_p, is related to corrosion rate as shown in equation (1); and assuming that the K value for the corrosive system is the same with or without the presence of an inhibitor, the corrosion inhibition of a particular inhibitor can be determined from equations (2).

FIG. 7 shows the plot of polarization resistance R_p versus immersion time for the inhibitors listed in Table 1.

TABLE 1

Chemistries of Inhibitors Studies

Inhibitors	Solubility	Description
Nalco3554	water soluble	Fatty acid imidazoline, quaternary

TABLE 1-continued

Chemistries of Inhibitors Studies

Inhibitors	Solubility	Description
		compound and arylsulfonic acid in alcohols
Petrolite WF-87	water soluble	Fatty quaternary ammonium chloride in methanol, isopropanol and water
Petrolite XC-370	water soluble	Oxydiethylene Bis(alkyl dimethyl ammonium chloride) in methanol and water
Chevron MJH-1	water soluble	C-14 polyamine quaternized with benzyl chloride in isopropanol
Chevron MJH-2	water soluble	MJH-1 plus nonyl phenol ethoxylate surfactant in isopropanol
Petrolite KP-203	oil soluble	Cyclic aliphatic amine, oxyalkylated alkyphenols and a thiazole derivative
Petrolite KG-68	oil soluble	Cyclic aliphatic amines, a highly sulfurized polyolefin and oxyalkylated alkylphenols

The inhibitors were each studied at 25 ppm in the corrosive CO_2-saturated, 5% NaCl solution, and as evidenced in FIG. 7, each showed corrosion rates which decreased over time, indicating an increase in inhibitor effectiveness.

For each of the inhibitors studied there are two frequencies at 45° phase angle or "breakpoint frequency". The low breakpoint frequency occurs at a frequency lower than 13 Hz, and the high breakpoint frequency appears at a frequency higher than 30 Hz. A plot of high breakpoint frequency versus time for inhibitors in the corrosive solution is depicted in FIG. 8.

As shown in FIG. 8, high breakpoint frequency increases with increasing immersion time, with the order of increase the same as the corrosion rate profile for the inhibitors shown in FIG. 7. The higher the high breakpoint frequency, therefore, the higher the polarization resistance for the inhibitor and the lower the resulting corrosion rate. A comparison of FIGS. 7 and 8 verifies this direct correlation between, and identical ranking of, the high breakpoint frequency and the corrosion rate.

A mathematical correlation between polarization resistance, R_p, and breakpoint frequency, f_b, for a one time constant model as represented by the circuit of FIG. 3 and observed from the Bode plot of FIG. 5, is as follows:

$$Z_{tot} = R_S + R_p/\{1.0 + j\omega R_p C_{dl}\} \quad (3)$$

$$= R_S + R_p(1.0 - j\omega R_p C_{dl})/\{1.0 - (j\omega R_p C_{dl})^2)\}$$

$$= R_S + R_p(1.0 - j\omega R_p C_{dl})/\{1.0 + (\omega R_p C_{dl})^2)\}$$

$$= R_S + R_p/\{1.0 + (\omega R_p C_{dl})^2\} -$$

$$j\omega R_p^2 C_{dl}/\{1.0 + (\omega R_p C_{dl})^2\}$$

where

Z_{tot} is the total impedance in ohm;

R_s is solution resistance in ohm;

R_p is polarization resistance in ohm;

C_{dl} double layer capacitance in farad;

ω is angular frequency and equals $2\pi f$ rad/s;

f is the frequency in Hz and j equals $\sqrt{-1}$.

At frequencies of 45 degree phase angle, f_b, the following relations hold.

$$Z_{real} = |Z_{imag}| \quad (4)$$

$$|\text{Phase angle}| = 45° \quad (5)$$

and

$$Z_{real} = R_s + R_p/\{1.0 + (\omega R_p C_{dl})^2\} \quad (6)$$

$$|Z_{imag}| = \omega R_p^2 C_{dl}/\{1.0 + (\omega R_p C_{dl})^2\} \quad (7)$$

Combining Equations (4) , (5) , (6) and (7) , one has

$$R_s + R_p/\{1.0 + (\omega R_p C_{dl})^2\} = \omega R_p^2 C_{dl}/\{1.0 + (\omega R_p C_{dl})^2\} \quad (8)$$

Case I—$R_s << R_p$

For $R_s << R_p$, we have

$$R_s + R_p \approx R_p \quad (9)$$

Equation (8) becomes

$$R_s R_p^2 C_{dl}^2 \omega^2 + R_p = \omega R_p^2 C_{dl} \quad (10)$$

and

$$R_s R_p C_{dl}^2 \omega^2 - R_p C_{dl} \omega + 1.0 = 0 \quad (11)$$

Let

$$\tau_1 = R_s C_{dl} \quad (12)$$

$$\tau_2 = R_p C_{dl} \quad (13)$$

Eqn. (11) becomes

$$\tau_1 \tau_2 \omega^2 - \tau_2 \omega + 1.0 = 0 \quad (14)$$

The angular frequencies of 45 degree phase angle at high and low frequencies can be obtained by solving Eqn. (14) and the results are shown below:

$$\omega_b = \frac{\tau_2 \pm \text{sqrt}(\tau_2^2 - 4\tau_1\tau_2)}{2\tau_1\tau_2} \quad (15)$$

and

$$\omega_b = \frac{1.0 \pm \text{sqrt}(1.0 - 4\tau_1/\tau_2)}{2\tau_1} \quad (16)$$

The frequencies of 45 degree phase angle, f_b, are obtained using Eqn. (17).

$$f_b = \frac{1.0 \pm \text{sqrt}(1.0 - 4\tau_1/\tau_2)}{4\pi\tau_1} \quad (17a)$$

or

$$f_b = \frac{1.0 \pm \text{sqrt}(1.0 - 4R_s/R_p)}{4\pi R_s C_{dl}} \quad (17b)$$

It is obvious that both high and low frequencies at 45 degree phase angle are related with R_s, C_{dl} and R_p. The increase of R_p and the decrease of C_{dl} move the high frequency at 45 degree phase angle to a higher frequency direction. Eqns. (17a) and (17b) are valid only at $R_s << R_p$. Since R_s is an independent parameter which is determined by the conductivity of the electrolyte, therefore, a large R_s value can be reduced by deconvolution. In this way, Eqn. (17) is also applicable to system with a low electric conductivity.

For a two-time constant model, represented by the equivalent circuit shown in FIG. 4, a mathematical correlation is derived as follows, where R_s is solution

resistance, R_{po} is pore resistance, indicative of the conductive path of the coating, R_p is the polarization resistance or coating resistance, C_c is the coating capacitance and C_{dl} is the double layer capacitance:

$$Z_{real}=R_s+R_{po}/(1+\omega^2\tau_2^2)+R_p(1-\omega^2\tau_2\tau_4)/\{(1+\omega^2\tau_2^2)(1+\omega^2\tau_4^2)\} \quad (18)$$

and

$$|Z_{imag}|=\omega R_{po}\tau_2/(1+\omega^2\tau_2^2)+\omega R_p(\tau_2+\tau_4)/\{(1+\omega^2\tau_2^2)(1+\omega^2\tau_4^2)\} \quad (19)$$

with

$$\tau_2=R_{po}C_c$$

$$\tau_4=R_pC_{dl}$$

At 45 degree phase angle, we have

$$Z_{real}=|Z_{imag}| \quad (20)$$

The fourth-order equation of ω is shown as follows:

$$a'\omega^4+b'\omega^3+c'\omega^2+d'\omega+e'=0 \quad (21)$$

where

$a'=R_s\tau_2^2\tau_4^2$;
$b'=-R_{po}\tau_2\tau_4^2$;
$c'=R_s(\tau_2^2+\tau_4^2)+R_{po}\tau_4^2-R_p\tau_2\tau_4$;
$d'=-(R_{po}\tau_2+R_p\tau_2+R_p\tau_4)$;
$e'=R_s+R_{po}+R_p$.

By dividing a' on both sides of Eqn. (21), Eqn. (22) can be used to get the four real roots if they are available.

$$\omega^4b\omega^3+c\omega^2+d\omega+e=0 \quad (22)$$

The four roots of ω are listed below:

$$\omega^2+\{b+\sqrt{(8y+b^2-4c)}\}\omega/2+\{y+(by-d)/\sqrt{(8y+b^2-4c)}\}=0 \quad (23a)$$

$$\omega^2+\{b-\sqrt{(8y+b^2-4c)}\}\omega/2+\{y-(by-d)/\sqrt{(8y+b^2-4c)}\}=0 \quad (23b)$$

and y is any real root of Eqn. (24).

$$8y^3-4cy^2+(2bd-8e)y+e(4c-b^2)-d^2=0 \quad (24)$$

In order to solve Eqns. (22) to (24) for a real root, the following conditions are necessary.

$R_{po}>>R_s$;

$R_p>>R_{po}$;

$C_{dl}>>C_c$;

The complete solution is time-consuming, however, if we consider Eqn. (22) without R_s term (it is reasonable for polymer coating at $f_{b,1}$ occurs at very high frequency and $R_s<<R_{po}$), we have

$$a''\omega^3+b''\omega^2+c''\omega+d''=0 \quad (25)$$

with

$$a''=R_{po}\tau_2\tau_4^2;$$

$$b''=-(R_{po}\tau_4^2-R_p\tau_2\tau_4);$$

$$c''=+(R_{po}\tau_2+R_p\tau_2+R_p\tau_4);$$

$$d''=-(R_{po}+R_p).$$

Eqn. (25) can be solved by a standard methods well known, by using for example derivations provided by G. A. Korn and T. A. Korn in their reference text "Mathematical Handbook for Scientists and Engineers", McGraw-Hill, 1968.

According to the deviation in one-time constant model, the following method is provided as a solution for the two-time constant model:

Branch 1—elements R_9 and C_c;
Branch 2—elements R_{po} and C_c;
Branch 3—elements R_{po} and C_{dl};
Branch 4—elements R_p abd C_{dl}

The approximation of the f_b at each branch is calculated as follows:

$$f_{b,1}=\{1+\sqrt{(1-4\tau_1/\tau_2)}\}/4\pi\tau_1 \quad (33a)$$

$$f_{b,1}=\{1+\sqrt{(1-4R_s/R_{po})}\}/4\pi R_sC_c \quad (33b)$$

$$f_{b,2}=\{1-\sqrt{(1-4\tau_1/\tau_2)}\}/4\pi\tau_1 \quad (33c)$$

$$f_{b,2}=\{1-\sqrt{(1-4R_s/R_{po})}\}/4\pi R_sC_c \quad (33d)$$

$$f_{b,3}=\{1+\sqrt{(1-4\tau_3/\tau_4)}\}/4\ \pi\tau_3 \quad (33e)$$

$$f_{b,3}=\{1+\sqrt{(1-4R_{po}/R_p)}\}/4\pi R_{po}C_{dl} \quad (33f)$$

$$f_{b,4}=\{1-\sqrt{(1-4\tau_3/\tau_4)}\}/4\pi\tau_3 \quad (33g)$$

$$f_{b,4}=\{1-\sqrt{(1-4R_{po}/R_p)}\}/4\pi R_{po}C_{dl} \quad (33h)$$

with

$\tau_1=R_sC_c$;
$\tau_3=R_{po}C_{dl}$.

The direct correlation of high breakpoint frequency and corrosion rate therefore allows for the evaluation of corrosion inhibitor performance by direct measurement of the high frequency at 45 degree phase angle. This method of evaluation is a great improvement and more expedient measurement of inhibitor performance than the determination of polarization resistance, which must be conducted at extremely low frequencies and can require as much as a ten fold increase in time to complete as compared to the present method. While the present method utilized the high breakpoint frequency, it will be recognized by those skilled in the art that other phase angles at high frequency, within a range of about 30° to 60° could also be used in conjunction with the method provided herein.

While particular embodiments of the present invention have been described above in considerable detail in accordance with the applicable statues, this is not to be taken as in any way limiting the invention by merely as being descriptive thereof.

What is claimed is:

1. A method of evaluating corrosion protection afforded to a metallic surface by a surface layer thereon, wherein said metallic surface is contacted by a corrosive fluid, said method comprising the steps of:

establishing a circuit path through a working electrode and a reference electrode in the corrosive fluid;

causing a small sinusoidal potential perturbation at a high breakpoint frequency to flow in said circuit path;

measuring a reference high frequency at said high breakpoint frequency; and

introducing a corrosion inhibitor to said corrosive fluid and measuring a response high frequency shift, said response high frequency being indicative of inhibitor efficiency.

2. The method according to claim **1** wherein the corrosion inhibitor is water soluble.

3. The method according to claim **1** wherein the corrosion inhibitor is oil soluble.

4. The method according to claim **1** wherein the sinusoidal potential perturbation has an amplitude of about 10 mV.

5. The method according to claim **4** wherein the frequency range of said perturbation is about 5.5 mHz to about 55 kHz.

6. The method according to claim **1** further comprising the step of correlating said response high frequency with a measured polarization resistance.

7. A method of evaluating corrosion protection afforded to a metallic surface by a surface layer thereon, wherein said metallic surface is subjected to a corrosive fluid having a corrosion inhibitor contained therein, said method comprising the steps of

establishing a circuit path through a working electrode and a reference electrode in the corrosive fluid

causing a small sinusoidal potential perturbation at a high-phase shifted frequency to flow in said circuit path

measuring a high frequency response at said high-phase shifted frequency at differing time intervals to monitor changes in said high frequency response, said changes being indicative of changes in inhibitor efficiency.

8. The method according to claim **7** wherein the sinusoidal potential perturbation has an amplitude of about 10 mV and the frequency range of said perturbation is about 5.5 mHz to about 55 kHz.

9. The method according to claim **8** wherein the high-phase shifted frequency is a breakpoint frequency.

10. The method according to claim **7** wherein the inhibitor is water soluble.

11. The method according to claim **7** wherein the inhibitor is oil soluble.

12. The method of claim **7** wherein the frequency phase shift is between about 30° and 60°.

* * * * *

ANSI/NACE Standard RP0502-2002
Item No. 21097

Standard
Recommended Practice

Pipeline External Corrosion Direct Assessment Methodology

Approved 2002-10-11
NACE International
1440 South Creek Dr.
Houston, Texas 77084-4906
+1 (281)228-6200

ISBN 1-57590-156-0

An American National Standard
Approved August 22, 2003

Foreword

External corrosion direct assessment (ECDA) is a structured process that is intended to improve safety by assessing and reducing the impact of external corrosion on pipeline integrity. By identifying and addressing corrosion activity and repairing corrosion defects and remediating the cause, ECDA proactively seeks to prevent external corrosion defects from growing to a size that is large enough to impact structural integrity.

ECDA as described in this standard recommended practice is specifically intended to address buried onshore pipelines constructed from ferrous materials. Other methods of addressing external corrosion on onshore ferrous pipelines, such as pressure testing and in-line inspection (ILI), are not covered in this standard but are covered in other industry standards. Users of this standard must be familiar with all applicable pipeline safety regulations for the jurisdiction in which the pipeline operates. This includes all regulations requiring specific pipeline integrity assessment practices and programs. This standard is intended for use by pipeline operators and others who must manage pipeline integrity.

ECDA is a continuous improvement process. Through successive ECDA applications, a pipeline operator should be able to identify and address locations at which corrosion activity has occurred, is occurring, or may occur. One of the advantages of ECDA is that it can locate areas where defects could form in the future rather than only areas where defects have already formed.

Pipeline operators have historically managed external corrosion using some of the ECDA tools and techniques. Often, data from aboveground inspection tools have been used to locate areas that may be experiencing external corrosion. The ECDA process takes this practice several steps forward and integrates information on a pipeline's physical characteristics and operating history (pre-assessment) with data from multiple field examinations (indirect inspections) and pipe surface evaluations (direct examinations) to provide a more comprehensive integrity evaluation with respect to external corrosion (post assessment).

This standard was prepared by Task Group (TG) 041 on Pipeline Direct Assessment Methodology. TG 041 is administered by Specific Technology Group (STG) 35 on Pipelines, Tanks, and Well Casings. This standard is issued by NACE under the auspices of STG 35.

In NACE standards, the terms *shall*, *must*, *should*, and *may* are used in accordance with the definitions of these terms in the *NACE Publications Style Manual*, 4th ed., Paragraph 7.4.1.9. *Shall* and *must* are used to state mandatory requirements. The term *should* is used to state something considered good and is recommended but is not mandatory. The term *may* is used to state something considered optional.

NACE International
Standard
Recommended Practice

Pipeline External Corrosion Direct Assessment Methodology

Void Detection in Grouted Post-tensioned Bridges Using Time Domain Reflectometry

Michael Chajes, Professor and Chair[1]
Department of Civil & Environmental Engineering
301 DuPont Hall
University of Delaware
Newark, DE 19716
Voice (302) 831-6056
Fax (302) 831-3640
chajes@ce.udel.edu

Robert Hunsperger, Professor
Department of Electrical & Computer Engineering
214 Evans Hall
University of Delaware
Newark, DE 19716
Voice (302) 831-8031
Fax (302) 831-4316
hunsperg@ee.udel.edu

Wei Liu, Graduate Assistant
Department of Electrical & Computer Engineering
University of Delaware
Newark, DE 19716
Voice (302) 831-0678
Fax (302) 831-4316
wliu@ee.udel.edu

Jian Li, Graduate Assistant
Department of Electrical & Computer Engineering
University of Delaware
Newark, DE 19716
Voice (302) 831-0678
Fax (302) 831-4316
jian@mail.eecis.udel.edu

Eric Kunz, President
Vetek Systems Corporation
6 Oak Road
Elkton, MD 21921
Voice (410) 398-7131
VETEKsys@aol.com

Word Count 5860

August 1, 2002

[1] Corresponding Author

ABSTRACT

The presence of voids is a serious problem in grouted post-tensioned bridges because voids greatly reduce the corrosion-protective capabilities of the grout. Current methods for void detection suffer several significant drawbacks. A new method utilizing time domain reflectometry (TDR) is discussed in this paper. TDR is a well-developed method for detecting discontinuities in electrical transmission lines. A recent study has shown that TDR can be used as an effective nondestructive damage detection method for concrete bridges. A void changes the electrical properties of transmission lines and therefore introduces electrical discontinuities. It can be detected and analyzed by TDR. Experiments on grouted post-tensioning ducts with built-in voids demonstrated the effectiveness of TDR as a void detection method.

INTRODUCTION

Void detection is an important aspect of nondestructive evaluation of post-tensioned concrete bridges, as the presence of a void leaves a section of post-tensioning strands vulnerable to corrosion. Both the US and the UK have developed significant concerns regarding the condition of post-tensioned segmental concrete bridges. The problem revolves around the fact that it is difficult to ensure proper grouting of post-tensioning tendons. When post-tensioned ducts are not completely grouted and voids are present, the steel tendons are left vulnerable to premature corrosion (1). This very issue led to the declaration of a moratorium on the construction of post-tensioned bridges by the UK's Department of Transport in 1992 (2).

More recently, distress and failure of post-tensioning tendons due to improper grouting were found in Florida on the Mid-Bay Bridge. These problems were reported in a preliminary report issued by the Florida Department of Transportation on February 8, 2001 (3). The report states that "on August 28, 2000, during a routine inspection of the Mid-Bay Bridge, a post-tensioning tendon in Span 28 was observed to be significantly distressed." The discovery "led to an immediate *walk-through* inspection to verify if other post-tensioning tendons were exhibiting similar signs of distress. A post-tensioning tendon in Span 57 was found completely failed at the north end of the tendon as evidenced by pull out of the tendon from the expansion joint diaphragm." Subsequent examination of the two distressed/failed tendons revealed that "the condition of the grout for these two tendons was suspect. Air cavities, bleed water trails and soft, chalky grout characteristics were observed." The report goes on to say that "significant voids in grout or a highly porous grout can reduce the corrosion protective capabilities of this system … (and) there is a consistent presence of voids in the tendons." Figure 1 shows a typical post-tensioning tendon and the location of the voided area that was discovered in the failed tendon of the Mid-Bay Bridge.

While it is well known that incomplete grouting of ducts (i.e., voids) can leave tendons vulnerable to corrosion (1,2,3), effective and economical methods for detecting voids in post-tensioning ducts are not readily available. While some void inspection methods, such as bore scope, impact-echo, and ground-penetrating radar inspections, do exist, each has its drawbacks.

In order to perform a bore scope inspection, a hole is drilled on the grout element and a flexible bore scope is inserted. A still image or video can be captured through the bore scope. However, this is not a nondestructive method, and it may affect the long-term integrity of the structure.

The basic principle of the impact-echo technique is that a stress pulse is introduced into the structure from an impact source, such as a hammer or ball drop. The resulting stress waves are monitored by an ultrasonic transducer also on the surface of the structure. These stress waves travel back and forth between the surface and the voids that may exist in the structure. By observing the resonant frequency, the distance from the surface to the void can be determined. Impact-echo techniques have been shown to be fairly effective for locating large voids. However, smaller voids are difficult to detect with this technique due to the relatively low frequencies involved.

In a test using ground-penetrating radar, a high-frequency electromagnetic wave is emitted via an antenna into the structure under evaluation. The reflected energy caused by changes in the electromagnetic properties of the material is detected by a receiver antenna and analyzed. However, in order to obtain a usable signal, the antenna needs to be placed within very close proximity to the concrete structure.

Other advanced methods have also been used to detect corrosion and voids. However, they have met with limited success due to the skill needed to analyze the data as well as the expense of the equipment.

To help ensure that new post-tensioned, segmental concrete bridges will not prematurely deteriorate, which could result in major economic losses as well as potentially threatening the safety of the traveling public, new NDE methods are needed to ensure proper grouting in post-tensioned applications. This paper describes research conducted in an effort to develop such a method. Specifically, a novel and economical nondestructive evaluation technique using time domain reflectometry (TDR) is demonstrated. TDR is an electrical measurement technique that has been used since the 1940s to determine the spatial location and nature of faults in transmission lines (4). It involves sending an electrical pulse along a transmission line and using an oscilloscope to observe the echoes returning back from the device under test. The embedded steel cable can be modeled as an asymmetric, twin-conductor transmission line by applying a sensor wire along with the cable (5). Physical defects of the cable or the grout surrounding the cable will change the electromagnetic properties of the line and can be detected by TDR.

The effectiveness of TDR corrosion detection has already been verified through both small-scale laboratory tests (6) and field demonstration (7). This paper focuses on the use of the TDR method to detect voids in grouted post-tensioning ducts.

TWO-WIRE TRANSMISSION LINE MODEL

TDR was introduced recently as a corrosion detection method for post-tensioning strands by applying a sensor wire alongside the steel strand to establish an asymmetric two-conductor transmission line. A distributed parameter model is used to study the wave propagation in this transmission line. Wave propagation is described in terms of voltage and current by utilizing the equivalent circuit shown in Figure 2.

The four distributed parameters of the steel strand transmission line are calculated from the geometry and material parameters of the cable and are given in Table 1.

At very high frequencies, R increases as the square root of f, whereas ωL increases directly as f, and the ratio $R/\omega L$ decreases as the square root of f. Series resistance can be neglected in the frequency range of TDR operation. Additionally, $G/\omega C$ can be considered to be zero, since the conductance is quite small for grout with low water content. Under these circumstances, the characteristic impedance is given to a high degree of accuracy by the simplified expression

$$Z_0 = \sqrt{\frac{R + j\omega L}{G + j\omega C}} \approx \sqrt{\frac{L}{C}}$$

Upon substituting for C and L the following expression for Z_0 results:

$$Z_0 = \frac{1}{2\pi}\sqrt{\frac{\mu}{\varepsilon}}\cosh^{-1}\left(\frac{d^2 - a^2 - b^2}{2ab}\right) \approx \frac{60}{\sqrt{\varepsilon_r}}\cosh^{-1}\left(\frac{d^2 - a^2 - b^2}{2ab}\right)$$

Note that the characteristic impedance of the line depends on the radius of the steel cable. Therefore, any physical damage to the steel cable will change the impedance. This change can be detected with TDR. More important to this work is that the impedance is also a function of ε_r, which is the dielectric constant of the surrounding material.

VOID DETECTION

TDR can detect not only damage to steel strands but also voids in the surrounding grout. This is due to the fact that a void in the grout dramatically changes the dielectric constant of the medium through which the transmission line passes, thereby affecting the characteristic impedance of the line.

To demonstrate this, several samples were fabricated with built-in voids. Thin-walled hollow balls of two different diameters (3.7 cm and 5.6 cm) were used to create voids that extend across a single, 7-wire strand with a length of 1 m, a diameter of 12.77 mm, and a yield value of 1860 MPa. Holes with the same diameter as the strand were drilled in the balls on opposite sides, and the strand was passed through the holes. The openings were sealed with silicon sealant to prevent water and grout from getting into the void. The voids were located one-third of the way down the strand. Figure 3 shows the bare strand with the 5.6-cm rubber ball prior to grouting. The strand and void assembly was then placed in a 10-cm-diameter polyvinylchloride (PVC) duct and filled with grout. To increase the applicability of the laboratory testing, a typical grout used in cable-stayed bridges was used. After some initial TDR tests, a hole was drilled on the side of the specimen to provide access to the void. The properties of the void were studied, and a set of electrochemical corrosion experiments was conducted in the void. The two specimens used in the void experiments are listed in Table 2.

The laboratory experiments focused on voids that extend across the strand, since this type of void leaves the strands most susceptible to corrosion. Voids far away from the strand/wire transmission line might be difficult to detect due to their negligible effect on the line impedance. However, these voids are of less concern and will be the focus of future studies.

Figure 4 shows the TDR result from void specimen 1. Note that the diameter of the spherical void is 5.6 cm, which corresponds to 31% of the cross-sectional area of the duct. As stated before, the characteristic impedance of the line depends on ε_r. Since $\varepsilon_{r\ concrete} > \varepsilon_{r\ air}$, an electrical discontinuity is introduced by the void.

In evaluating the signal produced by TDR and shown in Figure 4, it is useful to understand the setup and operation of the test. The specimen was connected to a TDR measuring system through a short section of coaxial cable. The TDR system generated a fast-rising step pulse at t=1ns. The pulse was launched into the coaxial cable, whose characteristic impedance is 50Ω. At t=9 ns, the pulse reached the connection between the coaxial cable and the specimen (marker: start). Since the connection itself was a discontinuity, a reflection was recorded there. The reflection at 13 ns was caused by the void (marker: void), and the step at 20 ns corresponded to the end of the specimen (marker: end). Note that all the times mentioned here are roundtrip times. One can see that the location of the void is easily determined based on the travel time. In this case, the total roundtrip travel time along the strand is 11 ns, while it is only 4 ns to the void. This would indicate that the void is 4/11 or 36% of the way down the strand (close to the one-third location).

Sensitivity to Void Size

Figure 5 shows a TDR reading from void specimen 2, which has a 3.7-cm void (14% of the total area of the duct). Clearly, the reflection magnitude is related to void size: a larger void tends to generate a bigger reflection. Larger voids can significantly alter the localized effective dielectric constant and therefore introduce relatively large electrical discontinuities. Even though the reflection is relatively small for this void size, it is still distinguishable.

Effect of Void Contents on Reflection

The reflection magnitude is also related to the content of the void, since different materials have different electrical properties. Figure 6 shows the TDR return from specimen 1 when the void was filled with dry sand. Basically, it has the a very similar shape and magnitude as the signal shown in Figure 4, which was taken while the void was filled with air. This is the case because the dielectric constant of dry sand is very close to 1, the dielectric constant of air. As close as the two signals are, changes in waveform can still be recognized from a differential comparison with Figure 4, which is also shown in Figure 6.

Once the concrete specimen is instrumented, TDR readings should be repeatable, since the material and geometrical parameters that affect transmission line properties will remain unchanged. A differential comparison of stored signals with newly measured ones can reveal changes that occurred between the two measurements. The difference between an air-filled void and a sand-filled void is small but detectable. While filled with sand, the void gives off a slightly smaller reflection.

Porous grouts should have electrical properties similar to those of sand-filled voids. The result in Figure 6 indicates that a region of chalky and porous grout can be detected by TDR. This is of practical importance, since highly porous grouts can also seriously reduce the corrosion protective capabilities of the grout.

Next, the content of the void was changed from air to water. In this case, the TDR reflection from the void changed substantially, as shown in Figure 7. While the electrical property of water is much different from air, demonstrated by the comparison with Figure 4, it is very similar to the surrounding wet concrete. For this reason, only a negligible reflection was detected at the void site.

In the above void detection tests, a steel strand was used as a part of the transmission line to enable future corrosion monitoring for the strand. However, this is not necessary; if the purpose of the nondestructive evaluation is void detection only, a section of standard transmission line, such as the inexpensive 300Ω television cable, can be used. The cable needs to be run inside the duct, and recent experiments indicate that this approach can give better results than the steel strand/wire line, since a standard transmission line is used. Any void close to the line can be easily detected. One may combine this method with corrosion detection by applying a two-wire transmission line alongside the steel cable. Voids are detected by TDR on this two-wire line, while corrosion damage is detected using either one of the two wires with the steel cable. Note that shielded transmission lines such as coaxial cables are not suitable for this purpose, since their electric field is confined and does not extend into the grout.

CORROSION IN THE VOID

Typically, voids in the surrounding grout will not change the strength of the reinforcing cable. However, their presence can greatly reduce the corrosion protective capacities of the system and leave sections of the cable vulnerable to corrosion. The TDR method can not only detect the existence of voids but also monitor the corrosion progress in the void.

A set of electrochemical corrosion experiments was conducted with the void specimen. Salty water was added to the void. A piece of copper strip was inserted through the hole into the void. The steel strand was connected to the anode of a constant-current source while the copper strip was connected to the cathode. The strand was corroded under a constant current of 2A. Several TDR readings taken over time are shown in Figure 8. Note that the void was drained and dried before each measurement. The reflections at around 13 ns were generated from the corrosion site. The reflection magnitude increased gradually as the electrochemical corrosion continued. The extent of damage was controlled by the corrosion time and current. The TDR measurements clearly show the increase in corrosion. More details regarding the corrosion tests are given by Liu et al. (8).

CONCLUSIONS

Time domain reflectometry can be utilized as a novel nondestructive evaluation technique for grouted post-tensioned bridge ducts. An analytical model was developed, which represents the steel strand as an asymmetric two-wire transmission line by introducing an insulated conductive sensor alongside a steel strand. TDR is capable of detecting both corrosion and voids. The effectiveness of TDR as a void detection method was demonstrated through tests on specimens with built-in voids. Several factors affecting void detection were identified. Among them are void size, void content, and corrosion. The ability to monitor the progression of electrochemical corrosion inside of a void by TDR is also shown. Future testing will focus on the ability to detect voids that do not intersect the strands.

REFERENCES

1. Bungey, J.H., S. G. Millard, and M. R. Shaw, (1997). "Radar Assessment of Post-Tensioned Concrete," *Proceedings of Structural Faults & Repair '97*, Edinburgh, Scotland, 1997, pp. 331-339.
2. Shaw, J.D.N and J. Keble, J. "Durable Grouted Post-Tensioned Bridges Development of a Special Grout," *Proceedings of Structural Faults & Repair '97*, Edinburgh, Scotland, 1997, pp. 295-298.
3. Corven Engineering. "Mid-Bay Bridge: Post-Tensioning Evaluation," Florida Department of Transportation, Draft Report, February 8, 2001.
4. "Time Domain Reflectometry Theory." *Hewlett-Packard Application Note 1304-2*, Hewlett-Packard Company, Palo Alto, Calif., 1998.
5. Bhatia, S. K., R. G. Hunsperger, and M. J. Chajes. "Modeling Electromagnetic Properties of Bridge Cables for Non-destructive Evaluation." *Proc. of Int. Conference on Corrosion and Rehabilitation of Reinforced Concrete Structures*, Orlando, Florida, 1998.
6. Liu, W., R. G. Hunsperger, K. J. Folliard, M. J. Chajes, and E. Kunz. "Detection and Characterization of Corrosion of Bridge Cables by Time Domain Reflectometry," *Proceedings of SPIE*, vol. 3587, 1999, pp 28-39, Newport Beach, Calif.
7. Liu, W., R. G. Hunsperger, M. J. Chajes, D. Li, and E. Kunz. "Nondestructive Corrosion Monitoring of Prestressed HPC Bridge Beams Using Time Domain Reflectometry," *Proc. of TRB 80th Annual Meeting*, Washington, DC, 2001.
8. Liu, W. "Electromagnetic Modeling of Embedded Metallic Structures for Nondestructive Evaluation Using Time Domain Reflectometry," PhD dissertation, University of Delaware, 2001.

LIST OF FIGURES AND TABLES

Figures

Tables

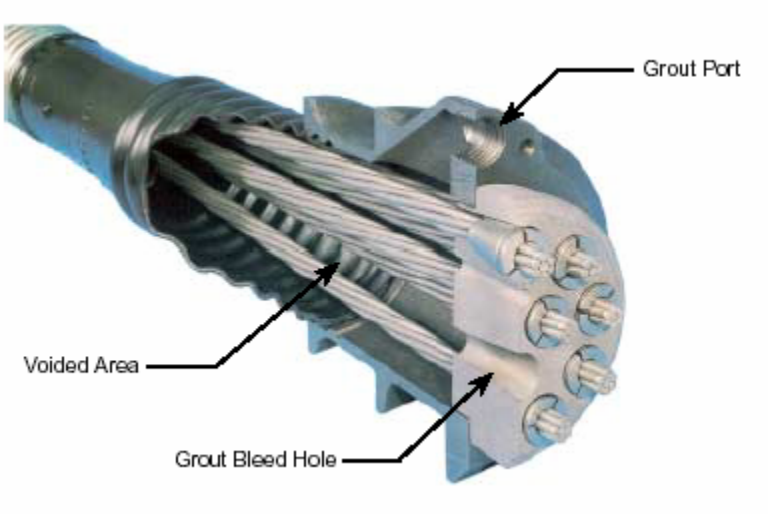

FIGURE 1 Typical Post-Tensioning Tendon Anchor with Void (3).

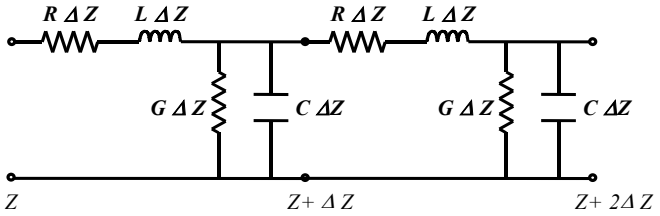

FIGURE 2 Distributed parameter equivalent circuit for the steel cable transmission line.

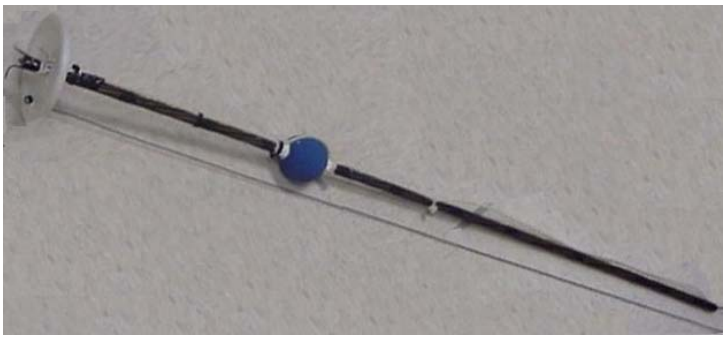

FIGURE 3 Fabrication of a Void Specimen, with a Rubber Ball Used to Simulate a Void.

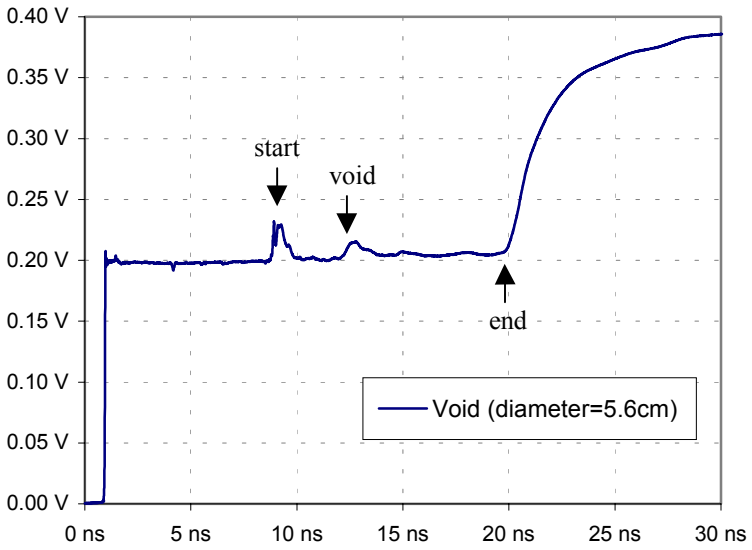

FIGURE 4 TDR Reflection from a 1-meter Specimen with Built-in Void (Specimen 1). The Reflection at 13ns is Due to the Presence of a Void.

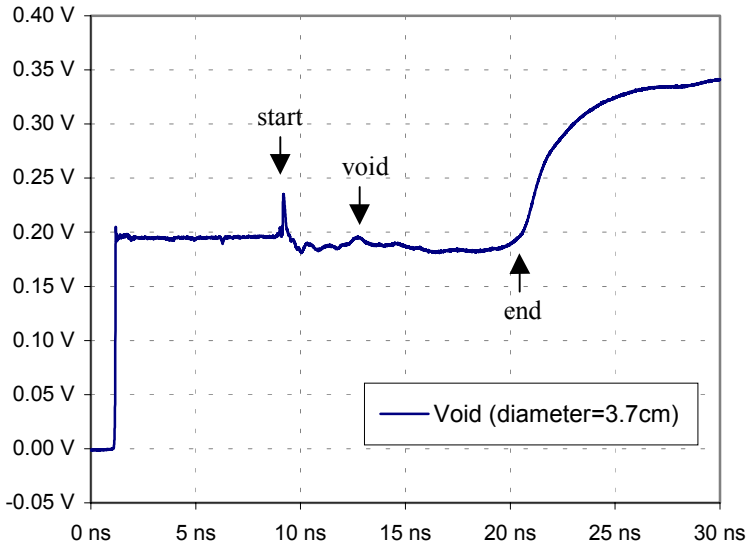

FIGURE 5 TDR Reflection from a 1-Meter Specimen (Specimen 2), which Has a Smaller Void than Specimen 1.

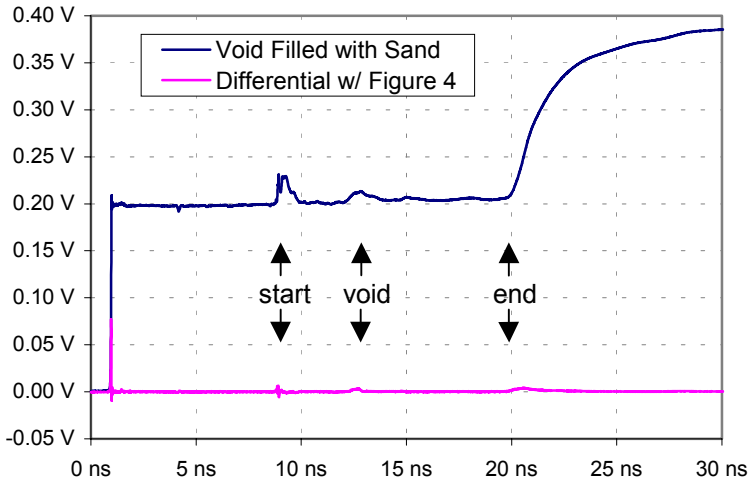

FIGURE 6 TDR Return from a Void Sample (Specimen 1) When the Void Was Filled with Sand.

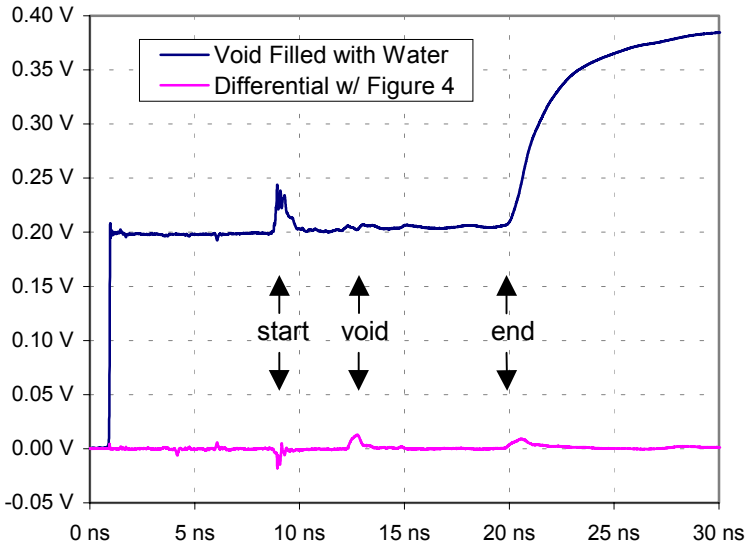

FIGURE 7 TDR Return from a Void Sample (Specimen 1) When the Void Was Filled with Water.

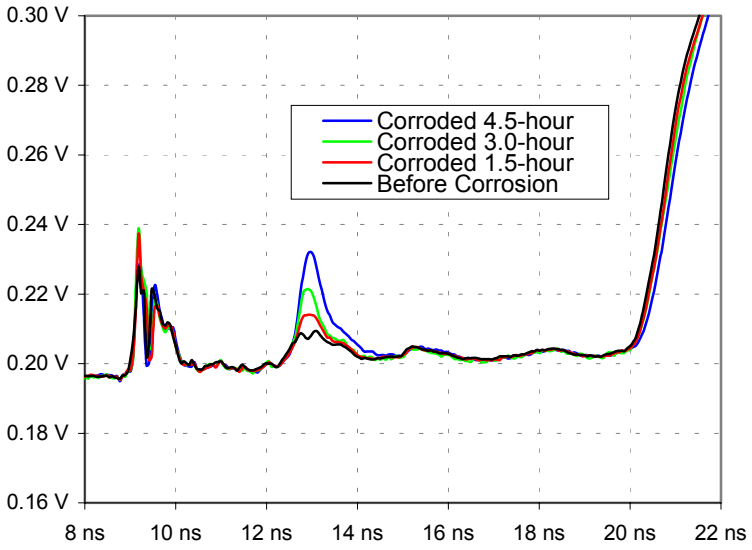

FIGURE 8. TDR Readings from Specimen 1 During the Progress of Electrochemical Corrosion.

TABLE 1 Distributed Parameters of the Steel Cable Transmission Line.

Distributed Parameters	Two-wire Transmission Line
shunt capacitance C	$C = \frac{2\pi\varepsilon}{\cosh^{-1}\left(\frac{d^2 - a^2 - b^2}{2ab}\right)}$
series inductance L	$L = \frac{\mu}{2\pi}\cosh^{-1}\left(\frac{d^2 - a^2 - b^2}{2ab}\right)$
series resistance R	$R = \sqrt{\frac{f\mu}{4\pi}}\left(\frac{1}{a\sqrt{\sigma_a}} + \frac{1}{b\sqrt{\sigma_b}}\right)$
shunt conductance G	G is negligible for insulated sensor wire in dry grout

TABLE 2 Two Void Specimens Used in the Experimental Study.

Specimen	Length	Diameter	Void		
			Position	Diameter	Percentage of cross-sectional area at maximum
1	100 cm	10 cm	33 cm	5.6 cm	31%
2	100 cm	10 cm	36 cm	3.7 cm	14%

FULL WAVE FORM ANALYSIS AND ECDA REQUIREMENTS

EUPEC RMS RISK MANAGEMENT SYSTEMS

EUPEC RMS
Pipeline Risk Management

What problems are identified via ECDA?

1. **Coating anomalies.**
2. **Interference.**
3. **Rectifiers performing out of specification**

Illustrated below are a few typical cathodic protection signatures. Only EUPEC RMS Cathodic Protection Signal Analysis can identify these signatures.

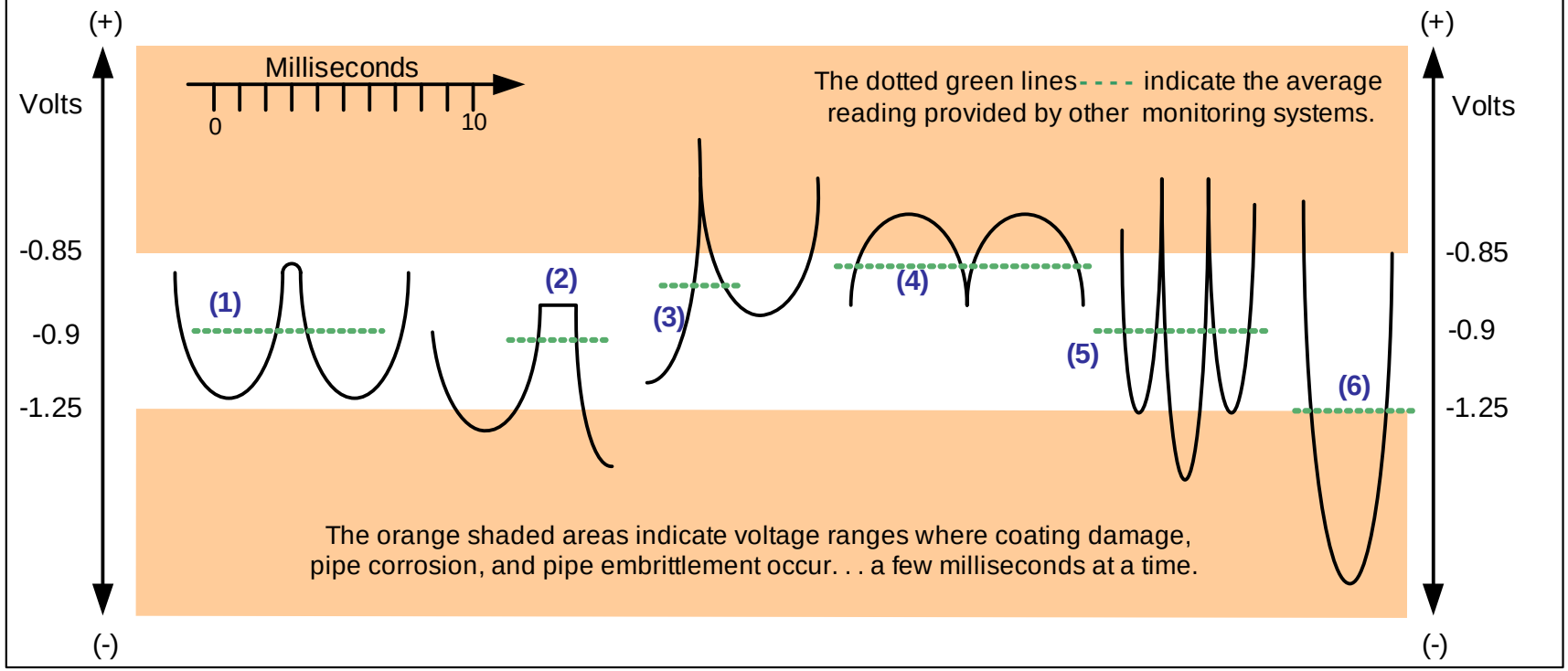

CP Signal Characteristics

EUPEC RMS RISK MANAGEMENT SYSTEMS

(1) This is the “perfect” cathodic protection signature on a well coated pipeline.

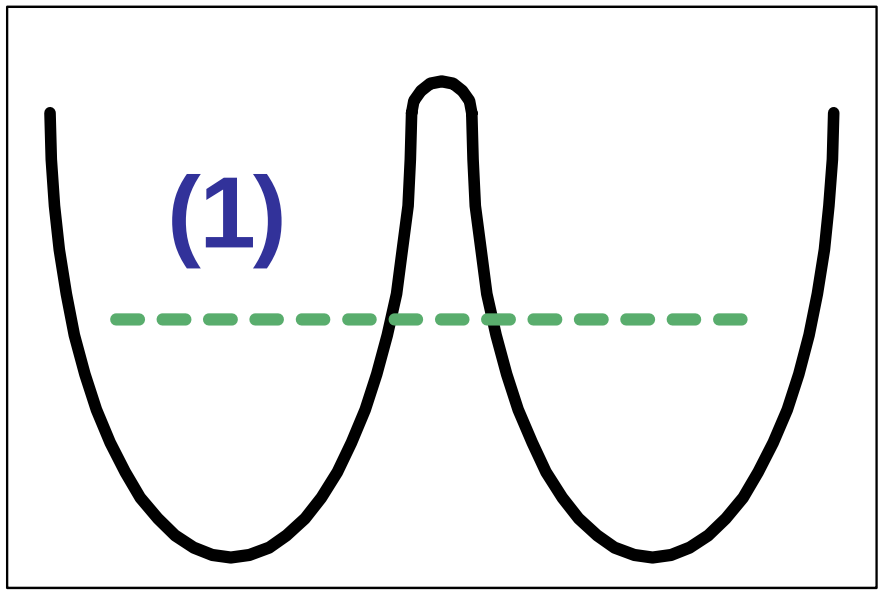

CP Signal Characteristics

EUPEC RMS RISK MANAGEMENT SYSTEMS

(2) The flat area illustrates the instant-off potential

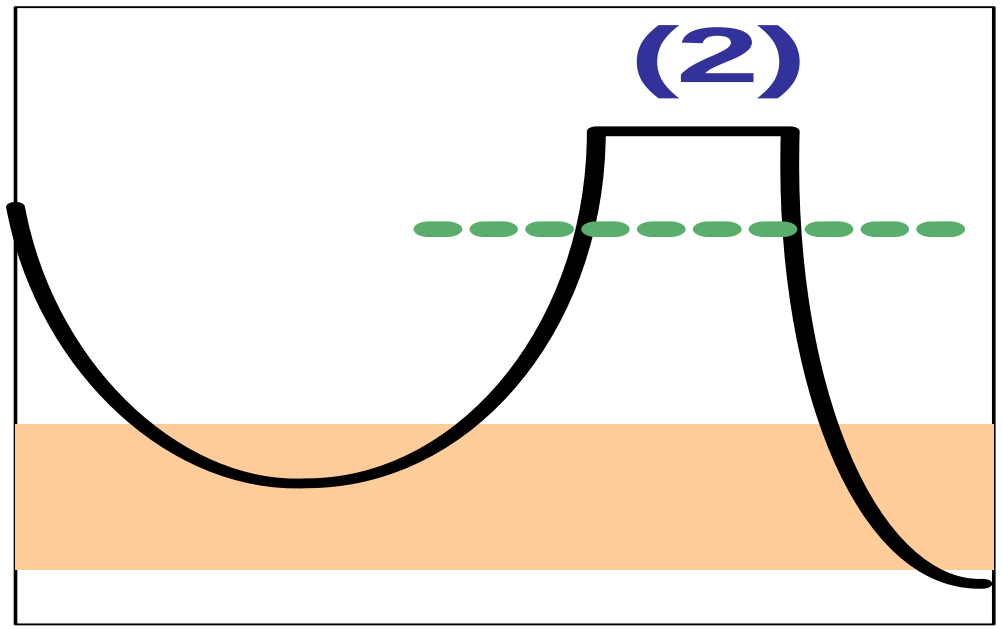

CP Signal Characteristics

EUPEC RMS RISK MANAGEMENT SYSTEMS

(3) This particular waveform indicates positive spiking. EUPEC RMS is working to determine if corrosion actually occurs during these milliseconds.

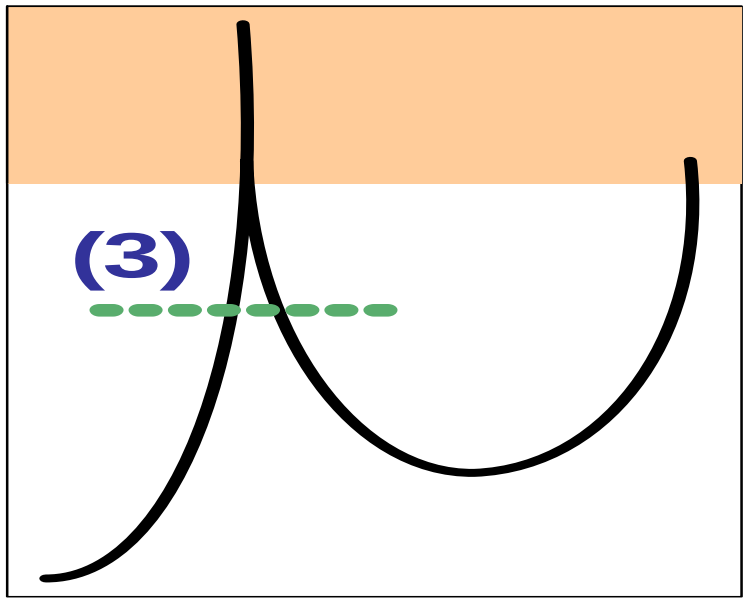

EUPEC RMS RISK MANAGEMENT SYSTEMS

(4) This wave form identifies interference from a foreign source. Note the inverting of of the signal.

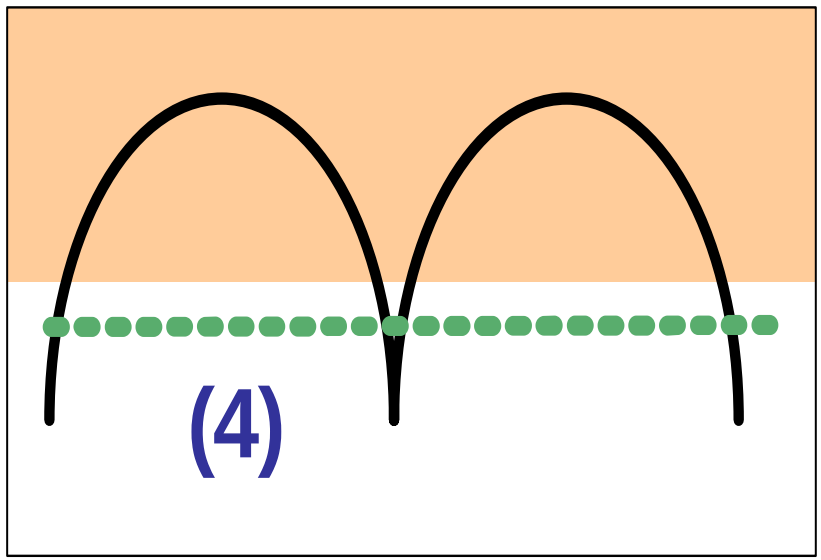

(5) Wave form interference from a DC train passing in the vicinity of the line.

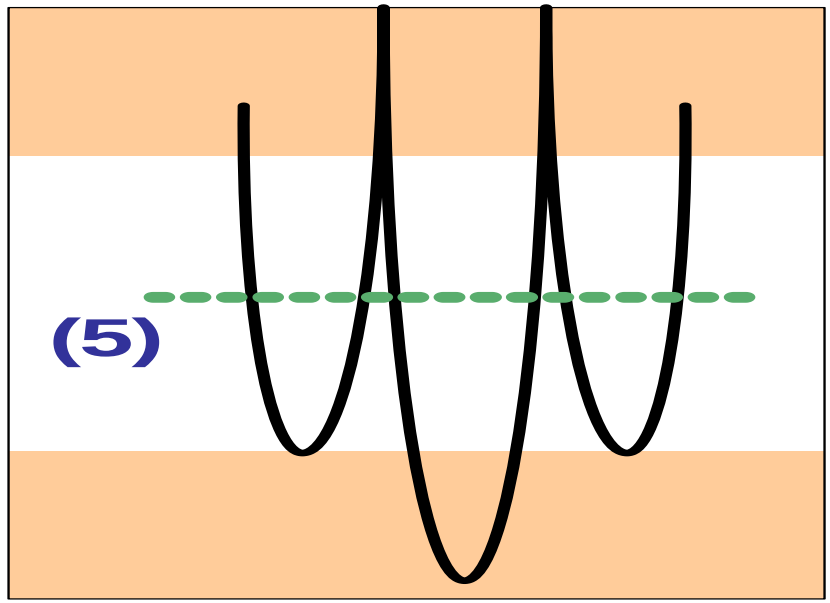

(6) This illustration shows off-potentials more negative than 1.2 volts which could cause the production of excessive hydrogen that can attack both the and the pipe.

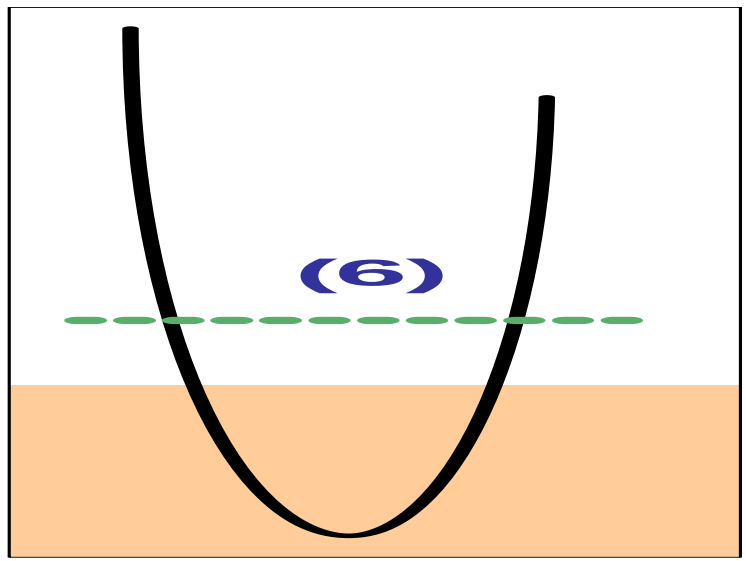

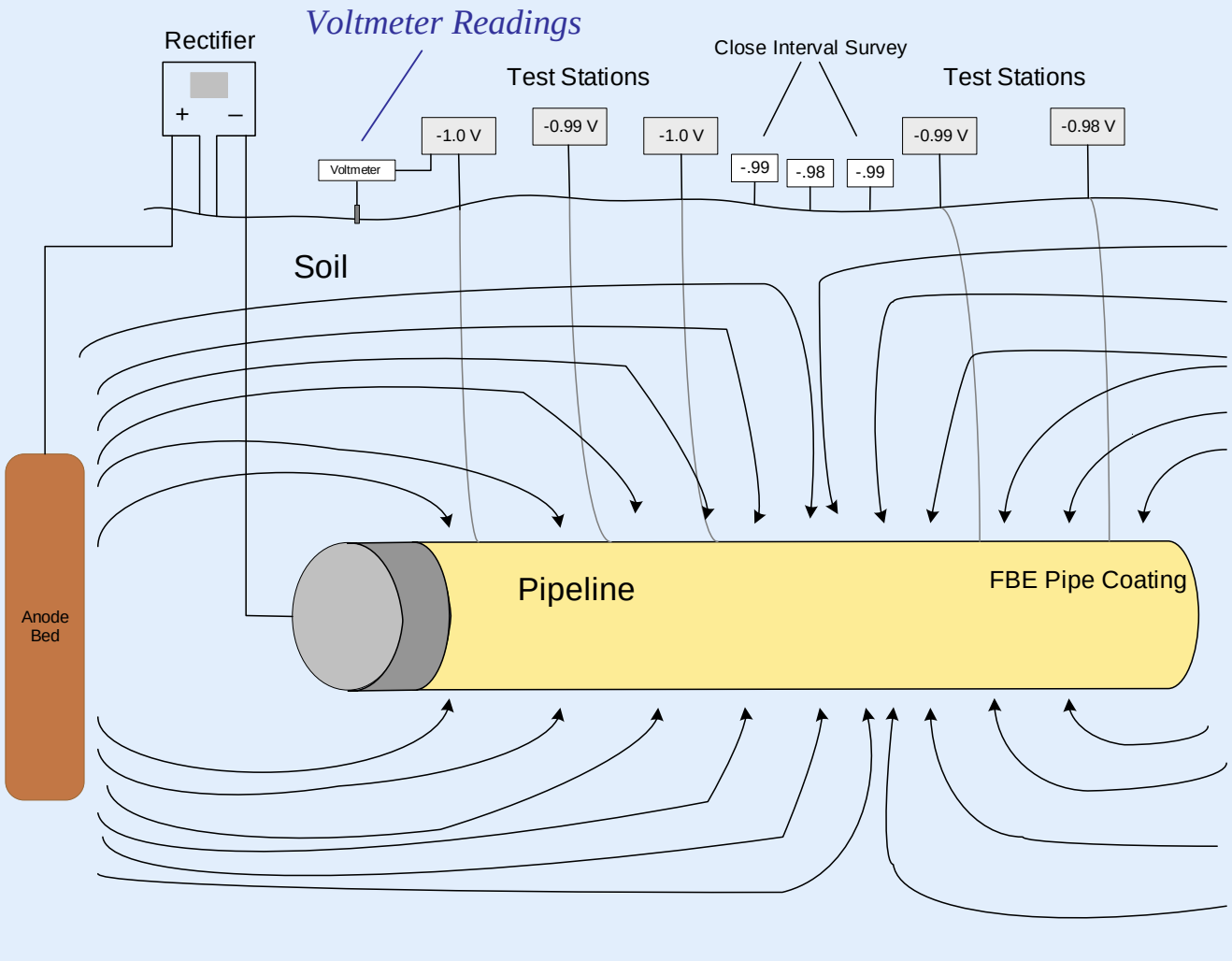

CP System: well coated pipe

- No anomalies
- No interference
- Consistent pipe to soil potentials

EUPEC RMS RISK MANAGEMENT SYSTEMS

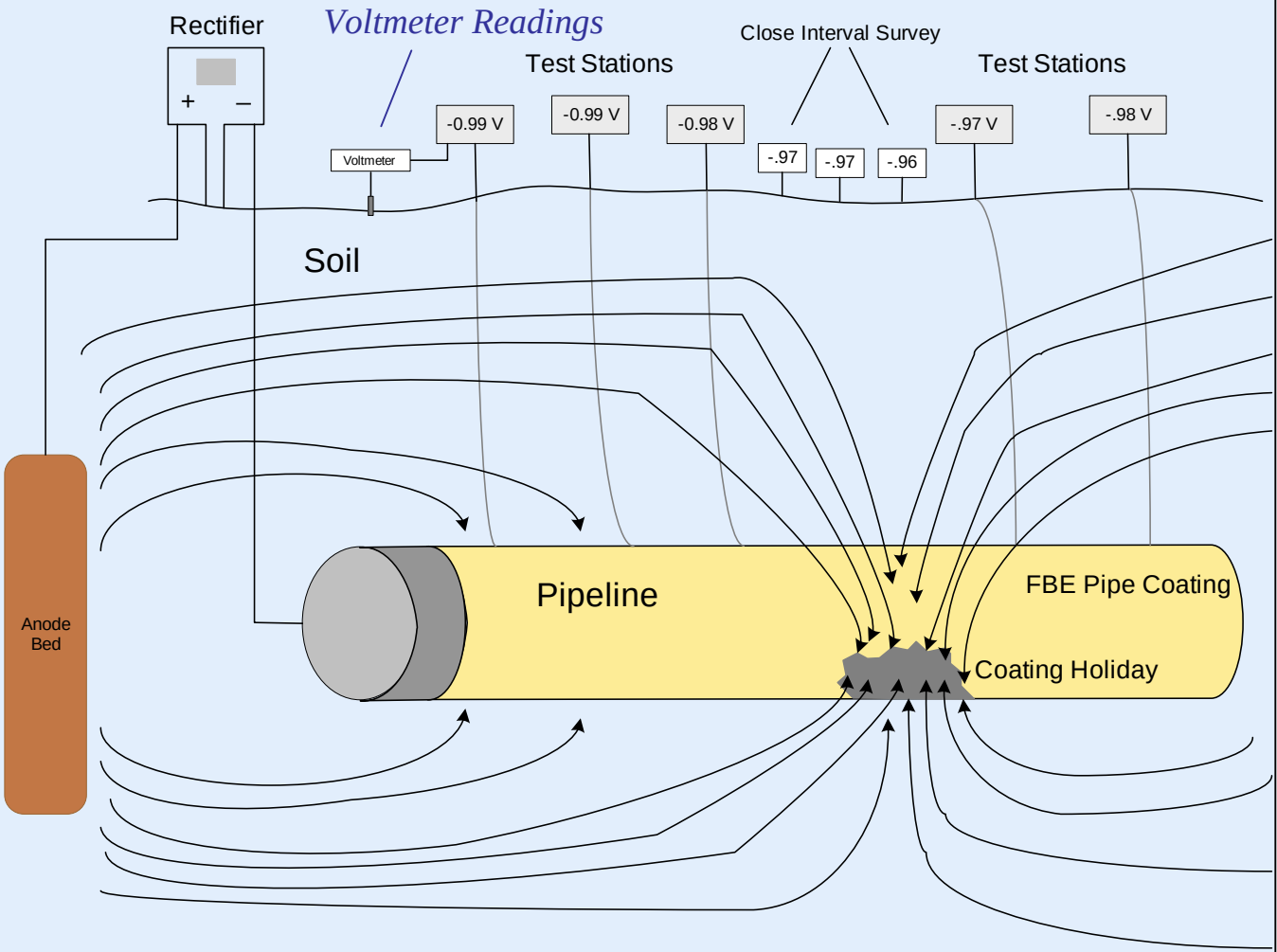

CP System: coated pipe with Holiday

- Hole in coating
- Pipe exposed
- No interference
- Inconsistent pipe to soil potentials

EUPEC RMS RISK MANAGEMENT SYSTEMS

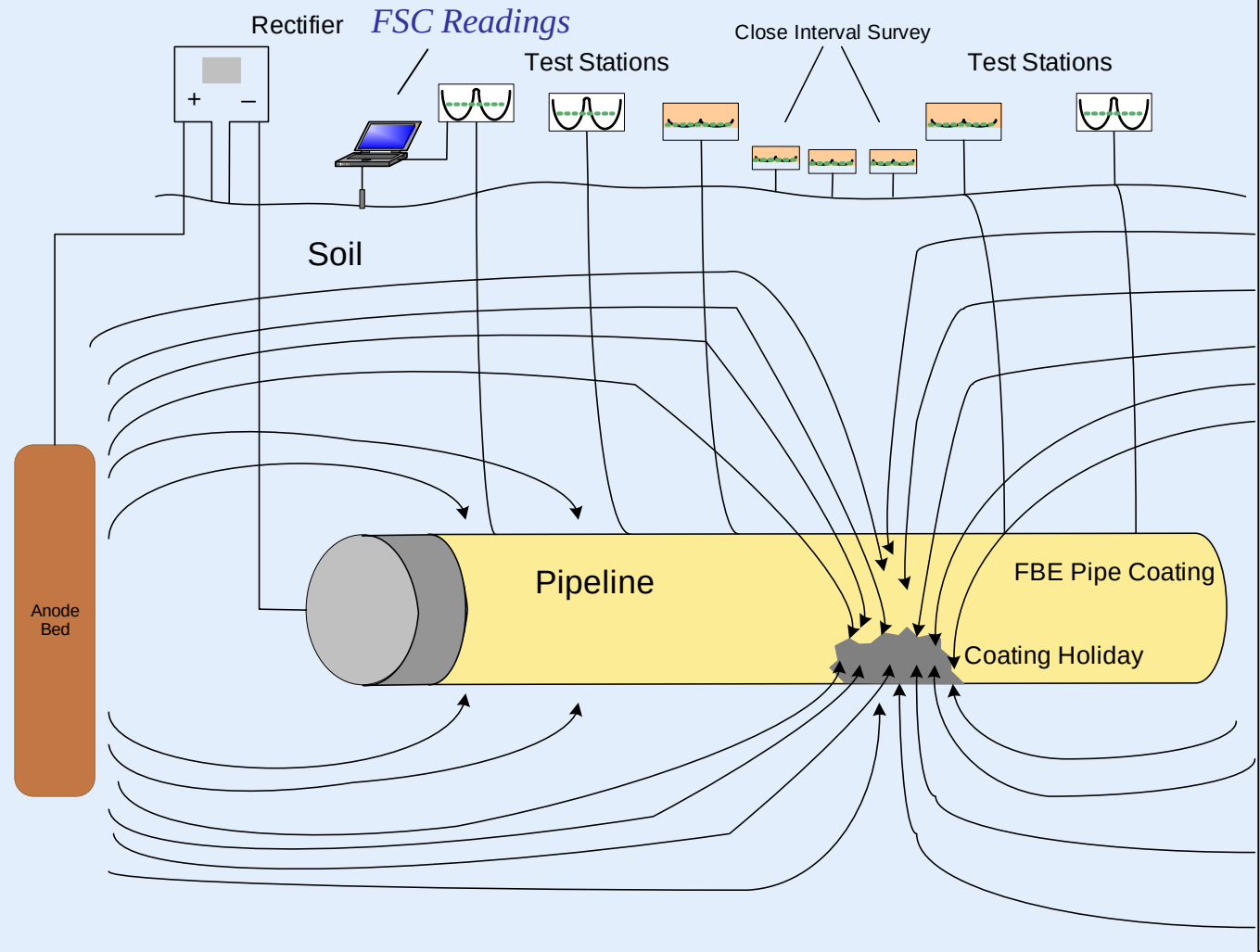

EUPEC RMS CP Signal Analysis:

- Holiday
- No interference
- Inconsistent pipe to soil potentials more efficiently identified with amplitude shift and decibel change.

FSC = Field Survey Computer

EUPEC RMS RISK MANAGEMENT SYSTEMS

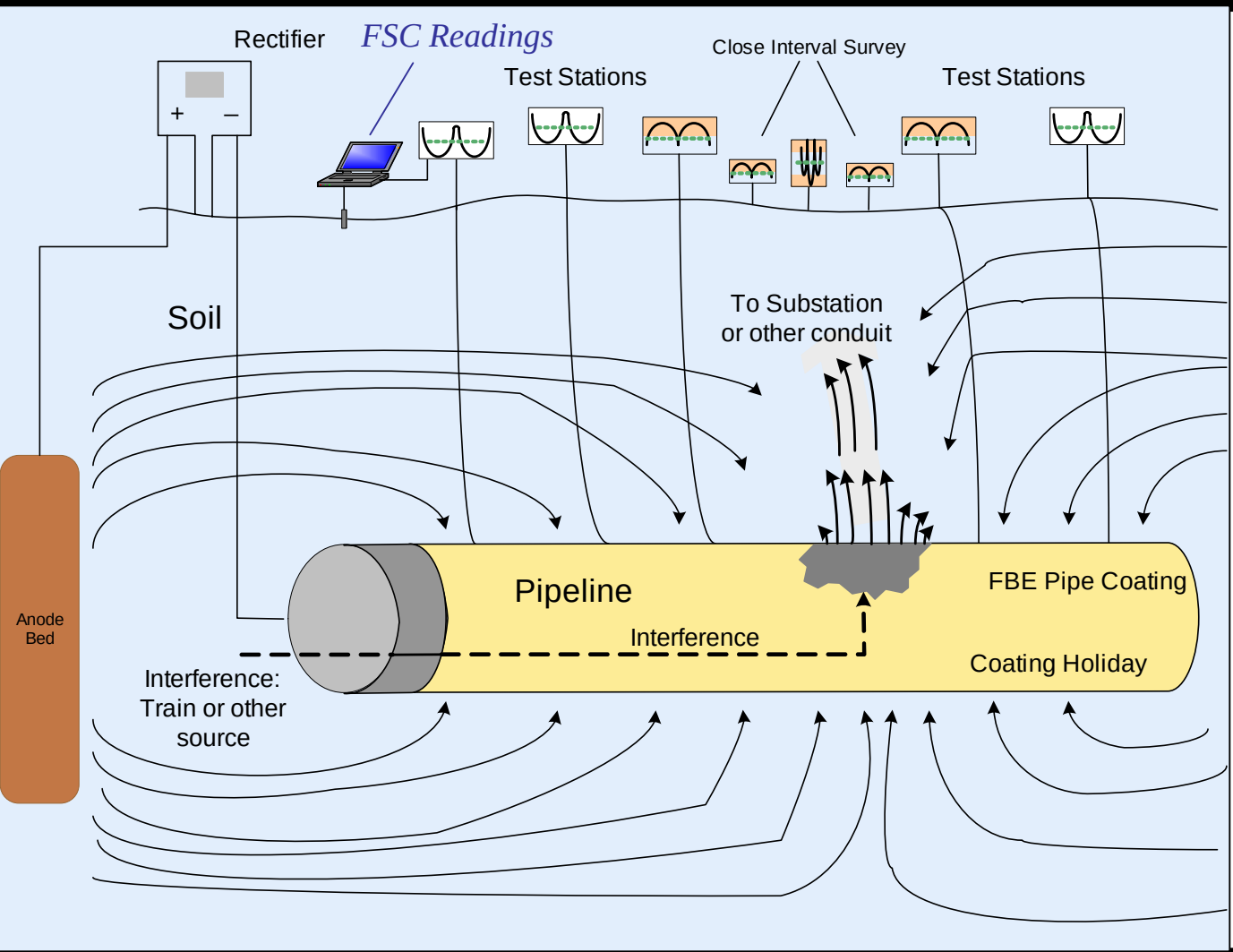

EUPEC RMS
CP Signal Analysis:

- Holiday
- Interference present
- Interference identified with signal characteristic change.

EUPEC RMS

Field Service Computer (FSC)

- **Extensive processing of data.**
- **Captures entire CP signal.**
- **Analyzes change.**
- **Identifies holidays.**
- **Spectrum analysis**
- **Identifies interference.**

EUPEC RMS

Delta Survey

- **Utilizes EUPEC RMS FSC.**
- **Identifies waveform.**
- **Also uses PSM, SCM, & soil resistivity**
- **Analyzes change.**
- **Identifies holidays.**
- **Identifies interference.**

EUPEC RMS RISK MANAGEMENT SYSTEMS

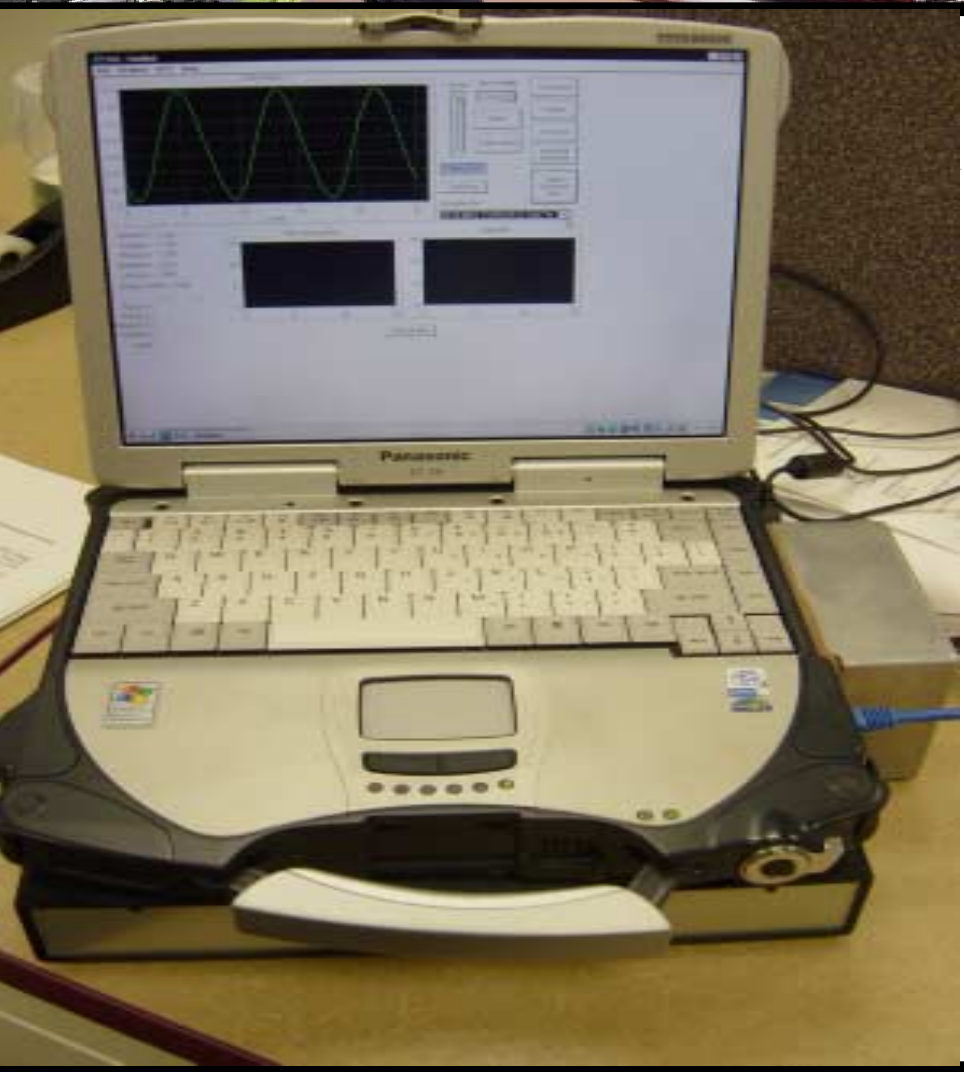

EUPEC RMS

Field Survey Computer

- **Monitors more than single average**
- **Extensive processing of data**
- **Improved anomaly identification**
- **Spectrum Analysis**
- **Improved Interference Identification**
- **Direct assessment assistance**
- **Improved compliance**

EUPEC RMS
RISK MANAGEMENT SYSTEMS

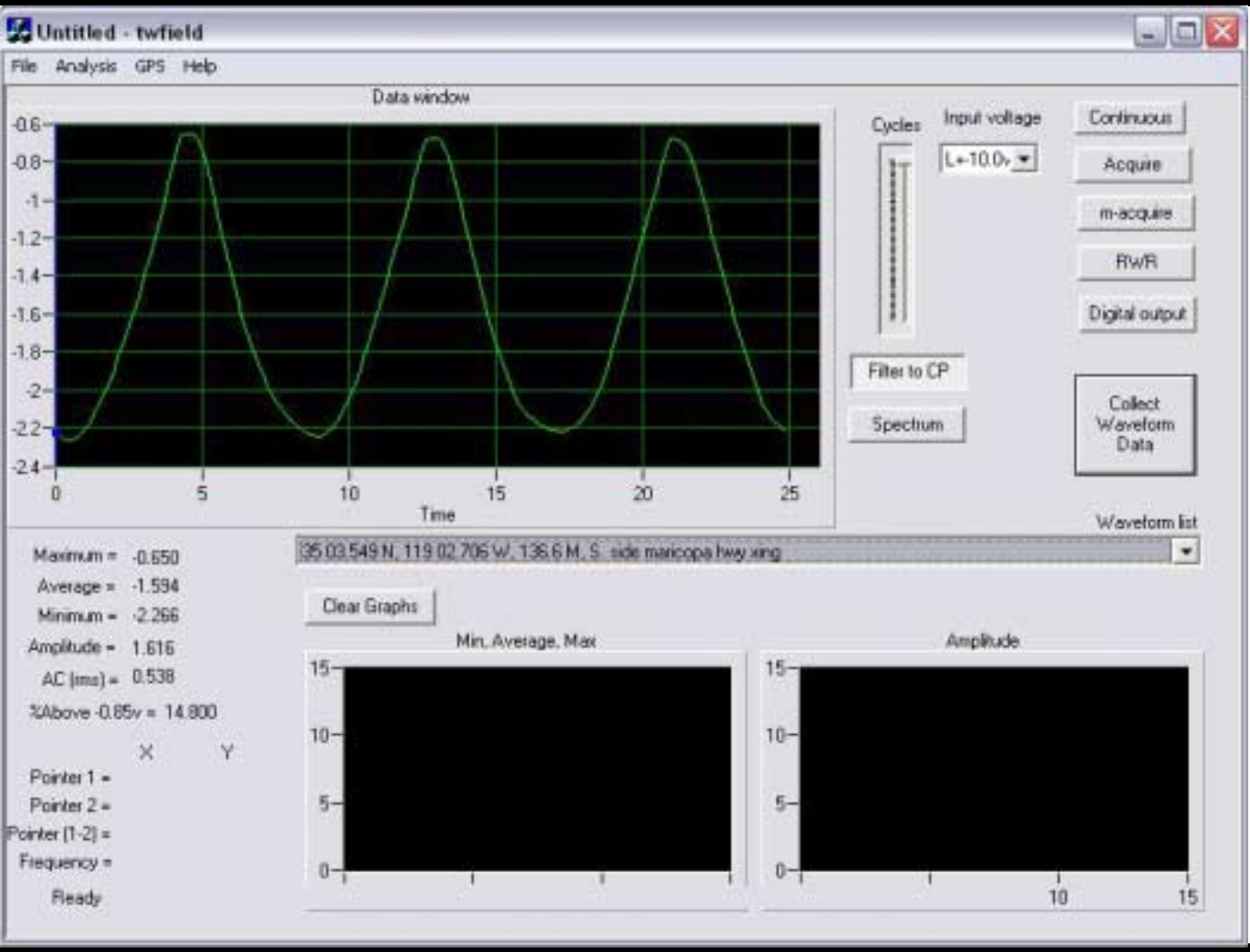

EUPEC RMS FSC with Good Signal

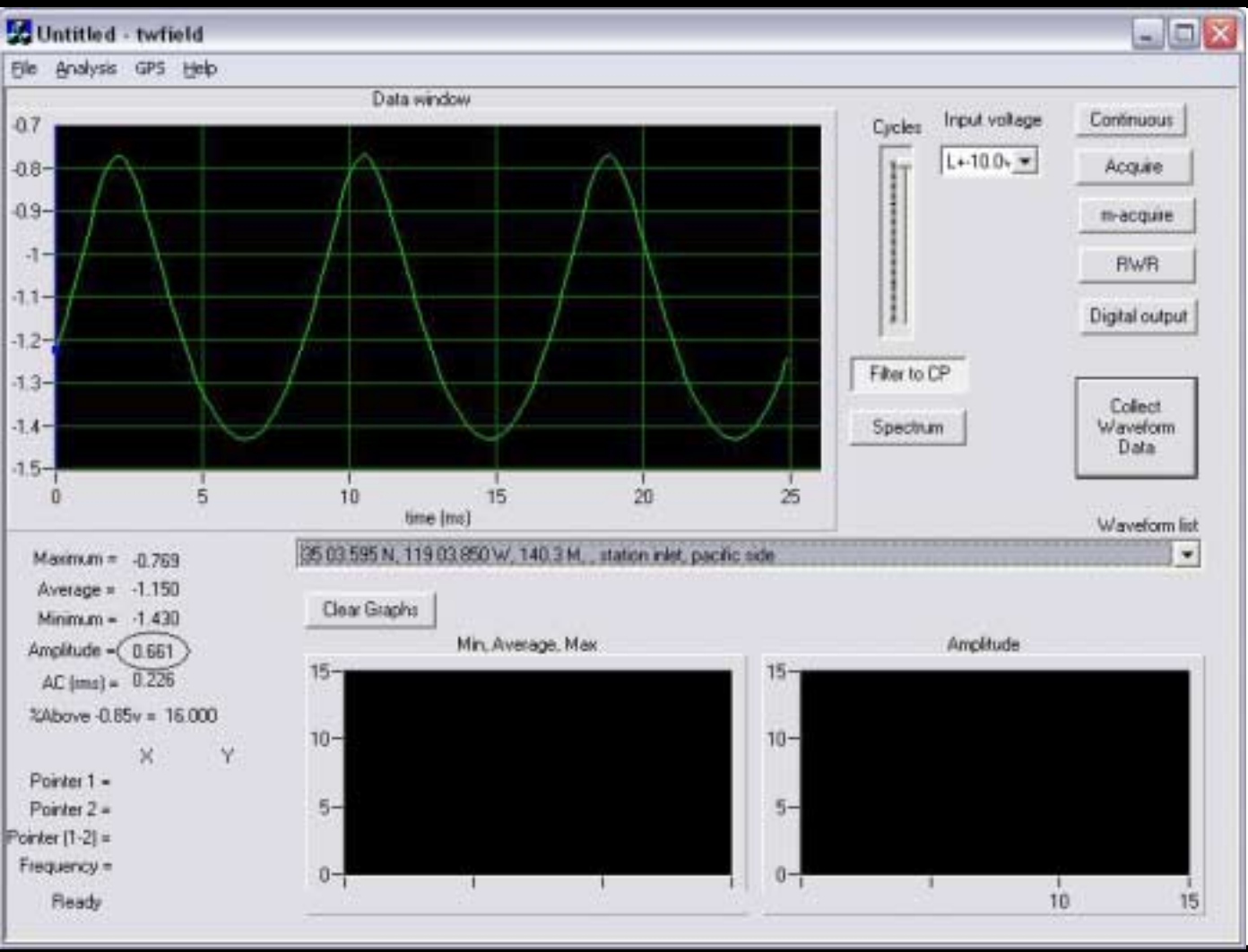

EUPEC RMS FSC with Anomaly Indication

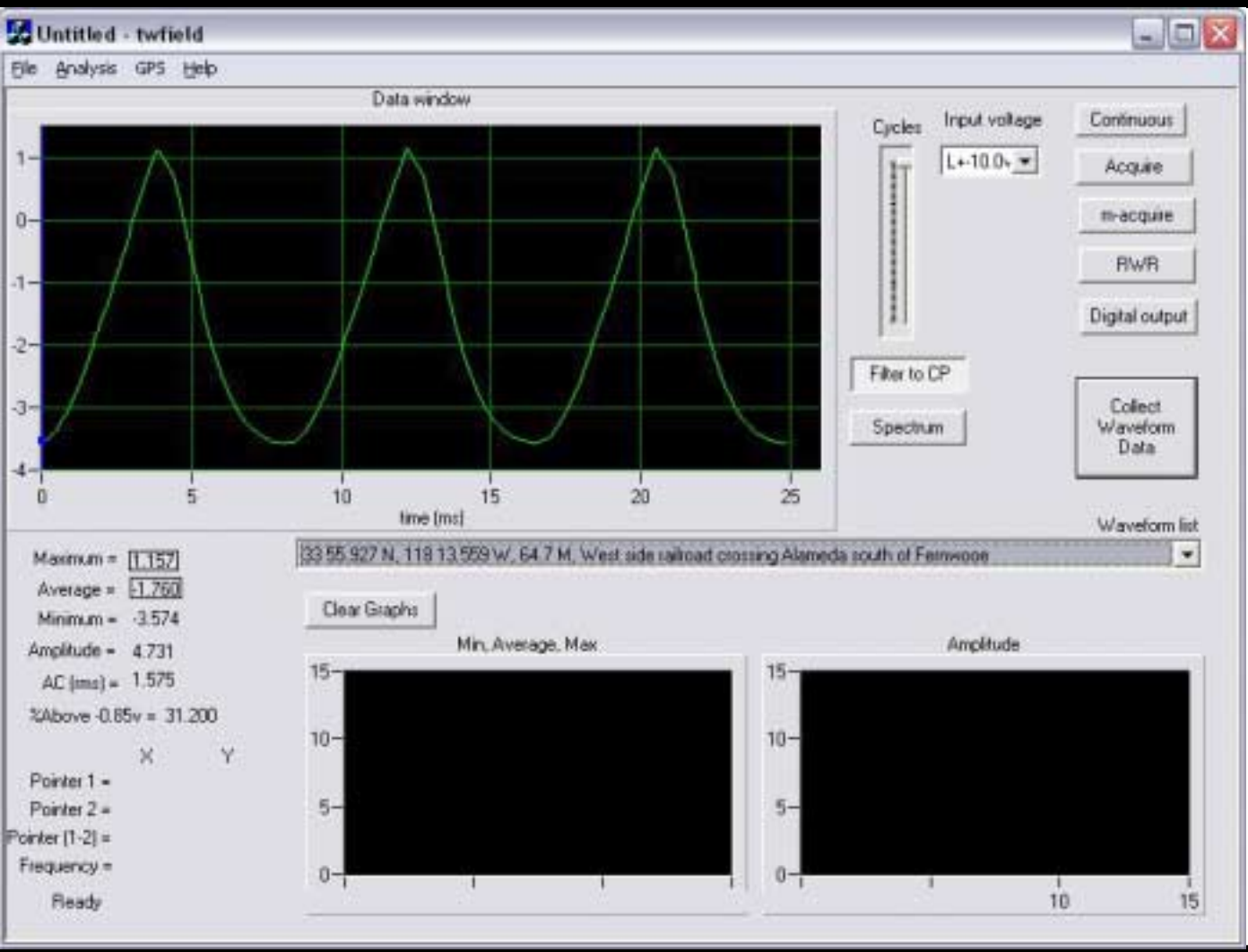

EUPEC RMS FSC with Positive Spiking

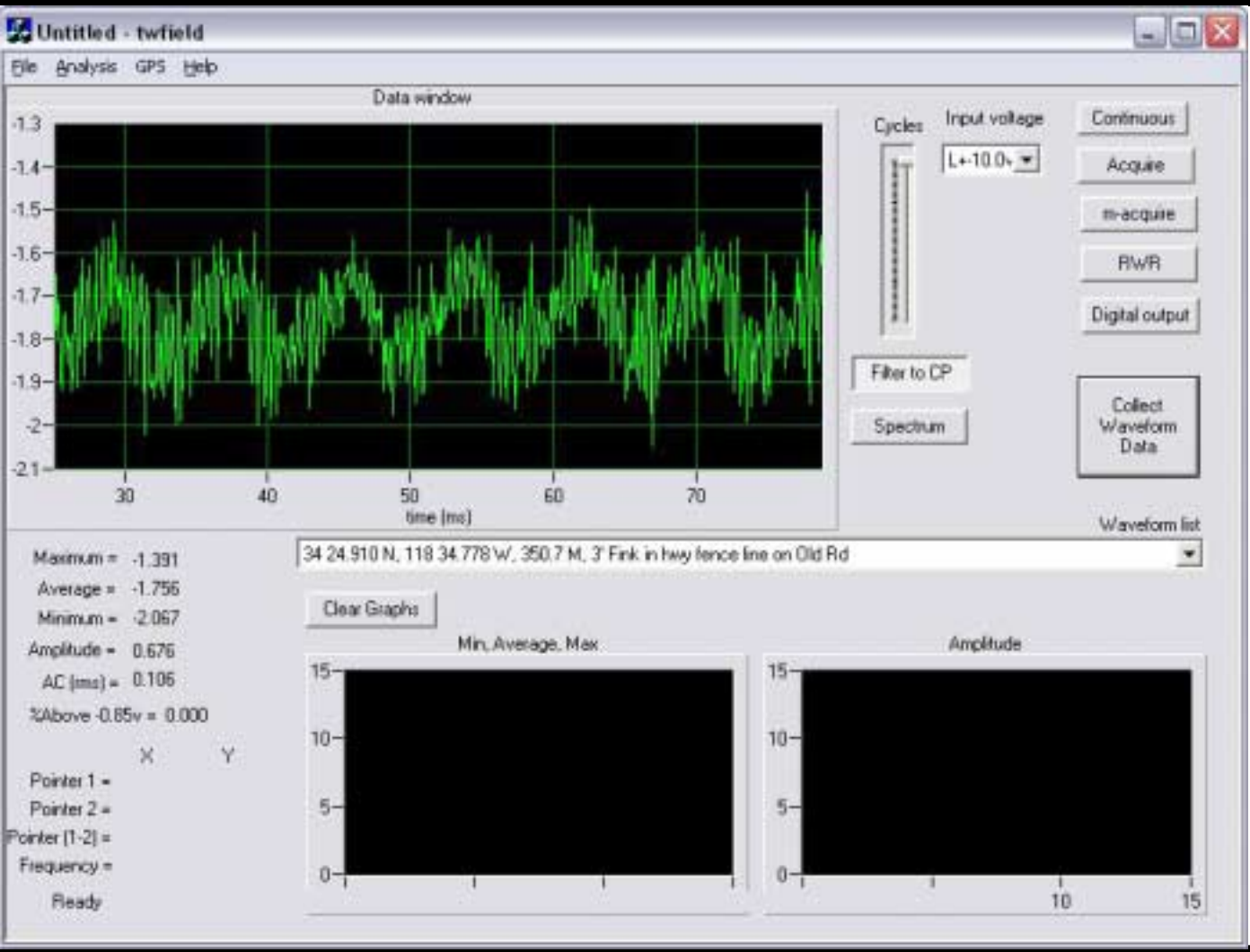

EUPEC RMS FSC with Interference Waveform

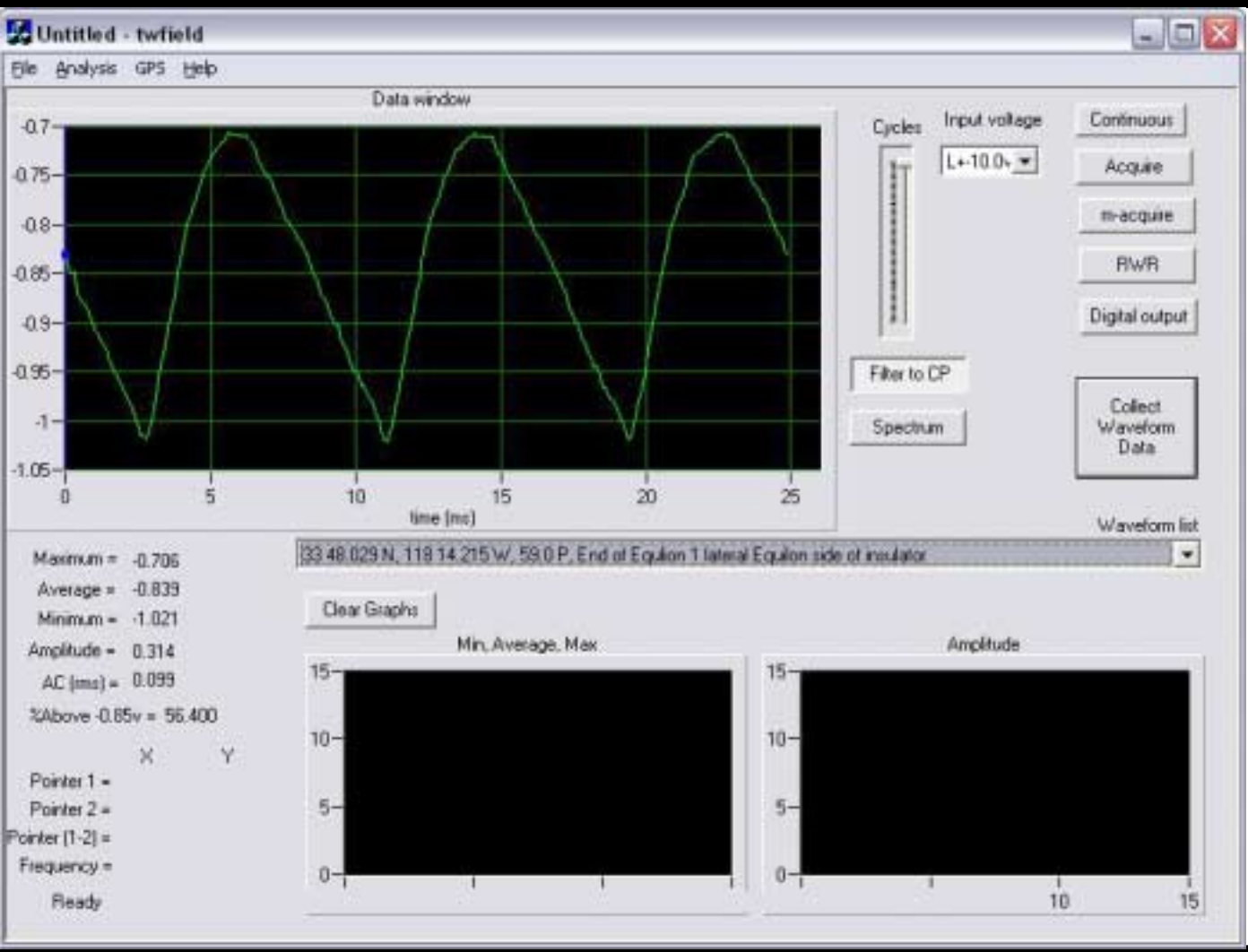

EUPEC RMS FSC with Inverted Waveform

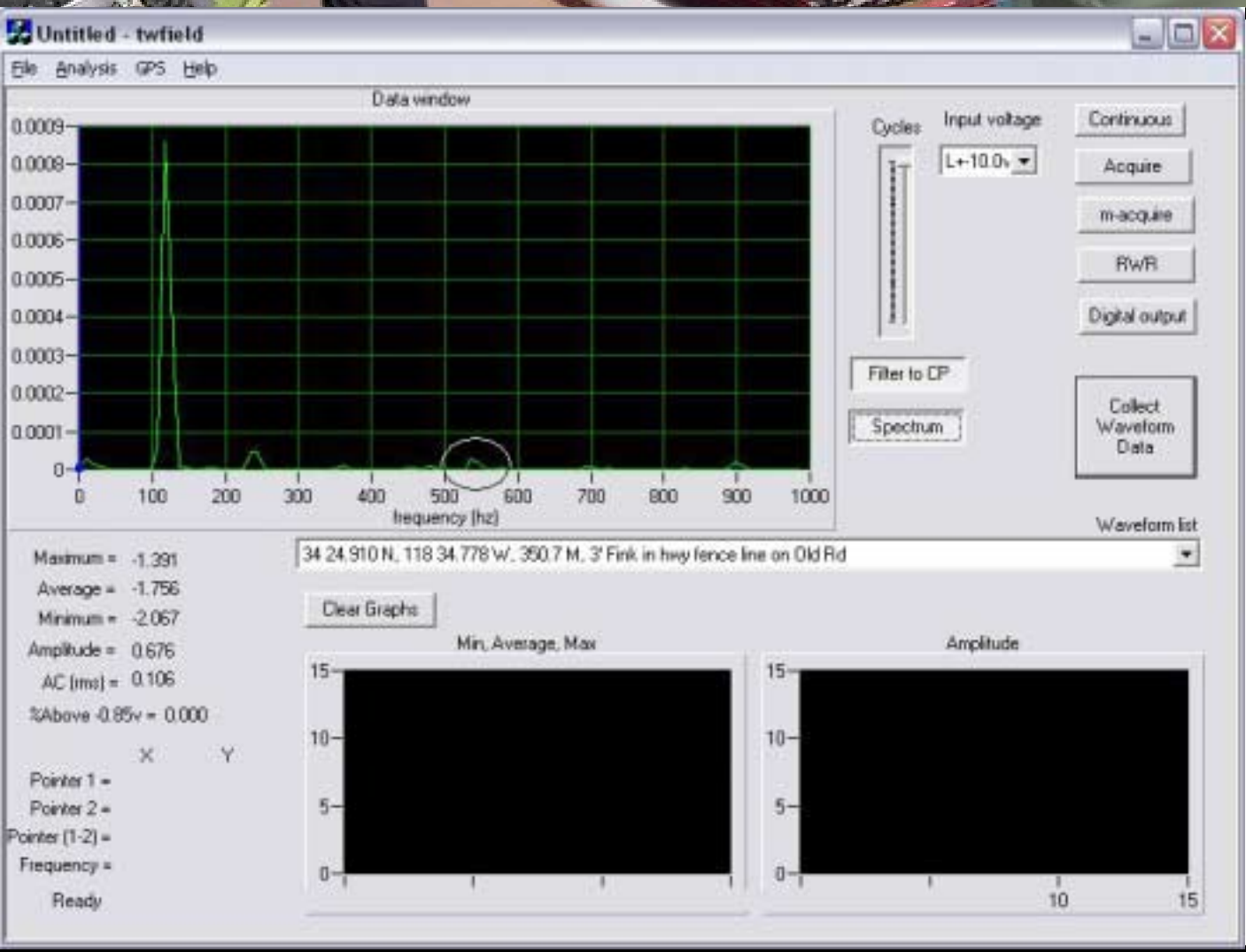

EUPEC RMS FSC with Spectrum Analysis

CP Signal Analysis with amplitude shift

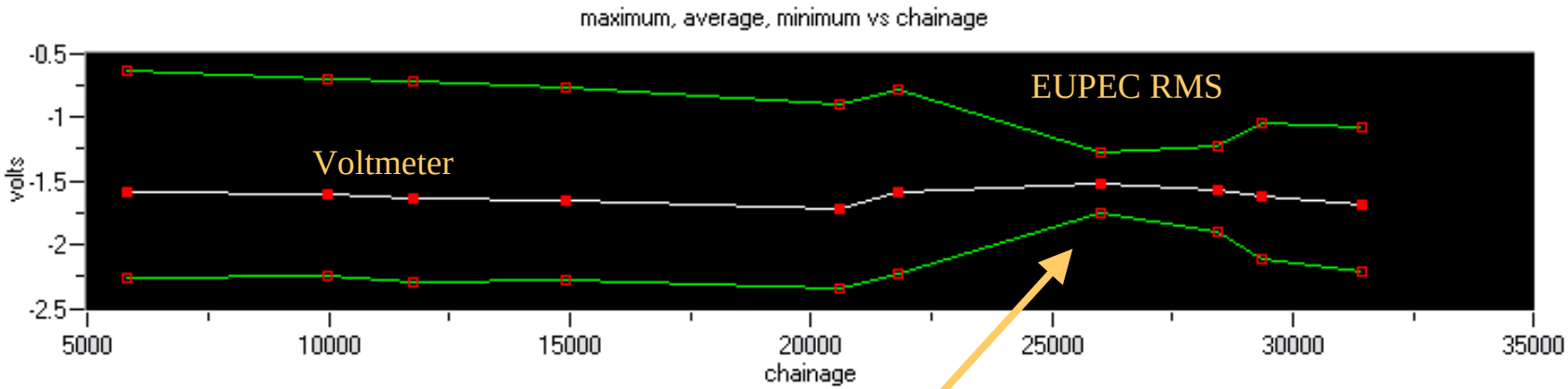

Potential Holiday

- Delta amplitude provides more clarity than delta average

CP Signal Analysis with Amplitude Shift and dB change

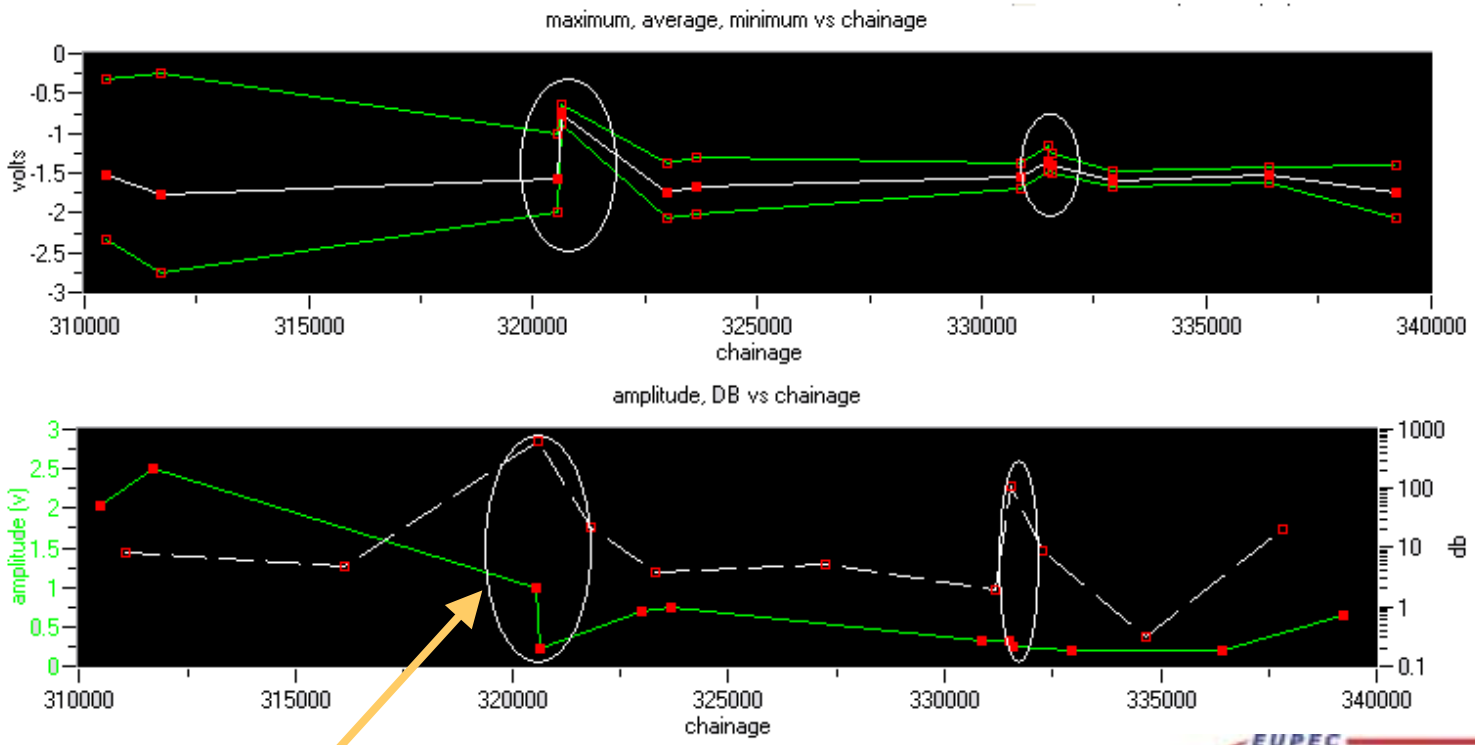

Amplitude & dB change confirm holiday

EUPEC RMS RISK MANAGEMENT SYSTEMS

EUPEC RMS

ATIS Remote Monitoring Unit

- **Monitors waveform and parameters**
- **Transmits data to server**
- **Automatic parameter based alarms**
- **Multiple communications means**
- **Ideal for High Consequence Areas**
- **Component of RMS 7/24 system**

EUPEC RMS
RISK MANAGEMENT SYSTEMS

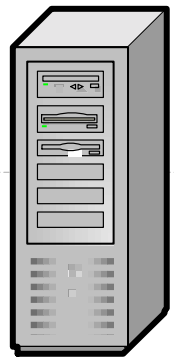

Server

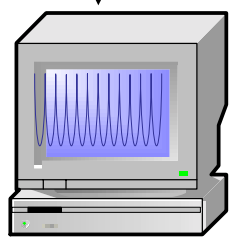

EUPEC Data Analysis

EUPEC RMS

Pipeline Integrity Analysis

- **EUPEC RMS FSC or RMU.**
- **Captures entire CP signal.**
- **Analyzes change.**
- **Identifies holidays.**
- **Identifies interference.**

EUPEC RMS RISK MANAGEMENT SYSTEMS

EUPEC RMS
Pipe Test Field
Pueblo, Colorado

4 pipes up to 250’.

Bare, FBE, (3-layer PE coming soon.)

Each pipe rectified.

Casing short, anomalies, interference.

EUPEC Pipeline Risk Assessment

CONCLUSIONS

1- Full wave form analysis allows a view of 360 degrees of pipe.

2- No loss of data through signal averaging such as with a volt meter.

3- More information faster since the equivalent of two surveys at once.

4- Ability to go test point to test point prioritizing segments for CIS.

EUPEC RMS RISK MANAGEMENT SYSTEMS

EUPEC Pipeline Risk Assessment

THANK YOU

EUPEC RMS RISK MANAGEMENT SYSTEMS

NEW WAVEFORM TECHNOLOGY FOR THE DIAGNOSTIC SURVEY AND REMOTE MONITORING OF CATHODICALLY PROTECTED UNDERGROUND GAS PIPELINES

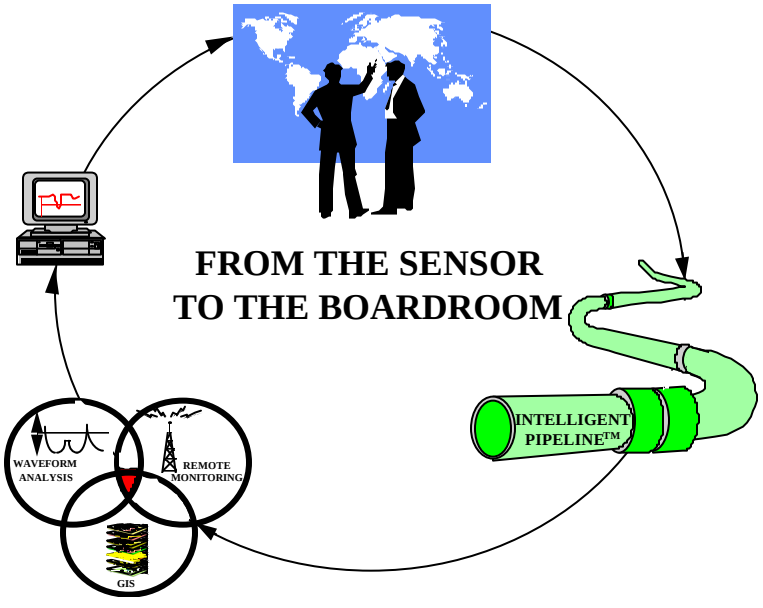

Submitted By:

Safet Hadzihasanovic - SarajevoGas Sarajevo, BiH
Muhamed Rizvanbegovic - SarajevoGas Sarajevo, BiH
Mark Flanery- TransWave International, Inc. Dayton, USA

June 16, 2000

1. SUMMARY

TransWave International, Inc. has developed a new technology for assessing buried underground structures that employ impressed cathodic protection (CP) for corrosion mitigation. This technology incorporates state of the art, computer driven filtering techniques and data analysis, as well as worldwide Internet communications capabilities. Technical advantages of this system are related to the ability to collect data automatically on 360? pipeline surface, 24 hour per day, while gathering more pipeline condition data for improved levels of pipeline analysis than any other technology provides. The technology was employed to perform diagnostic evaluations of gas pipeline coatings and cathodic protection conditions for the 8 bar natural gas pipeline system of SarajevoGas in the City of Sarajevo. This article describes the waveform technology used in the survey: how it works, what it does, and its capability for automated remote risk management on pipelines. This article also addresses results from the diagnostic survey of the 8 bar gas pipelines in Sarajevo. Of particular interest is the ability of waveform technology to identify multivariable stray current influences and measure the cathodic protection signal's propagation characteristics. This article consists of:

?? Technology for performing waveform pipeline assessments
?? Technology for performing automated remote risk management
?? The results of the 8 bar gas pipeline survey in Sarajevo

2. BASICS OF WAVEFORM TECHNOLOGY

2.1 Pipeline Circuitry Basics

For several decades the corrosion industry has used an overly simplified circuit schematic to explain cathodic protection analytical routines. The vast majority of service engineering companies use a variation of the following erroneous pipeline DC resistive circuit. See Figure 1.

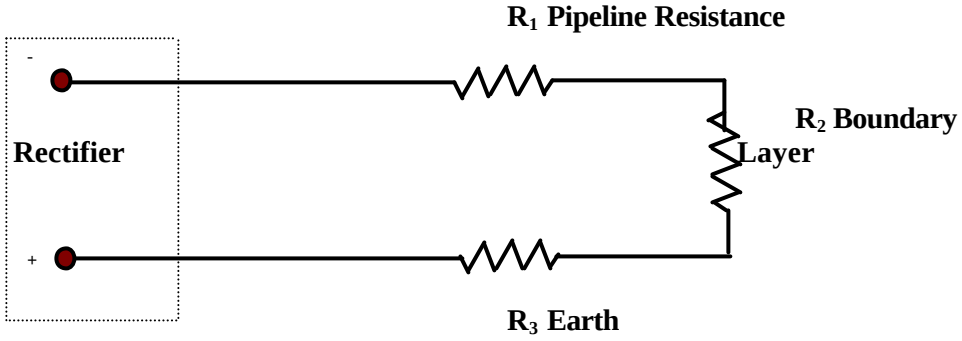

Figure 1

Unfortunately the above circuit does not take into account the series capacitance, the series inductance or the R_C network boundary layer interface circuit (polarisation zone of the pipeline). The corrected circuit is shown below. See Figure 2.

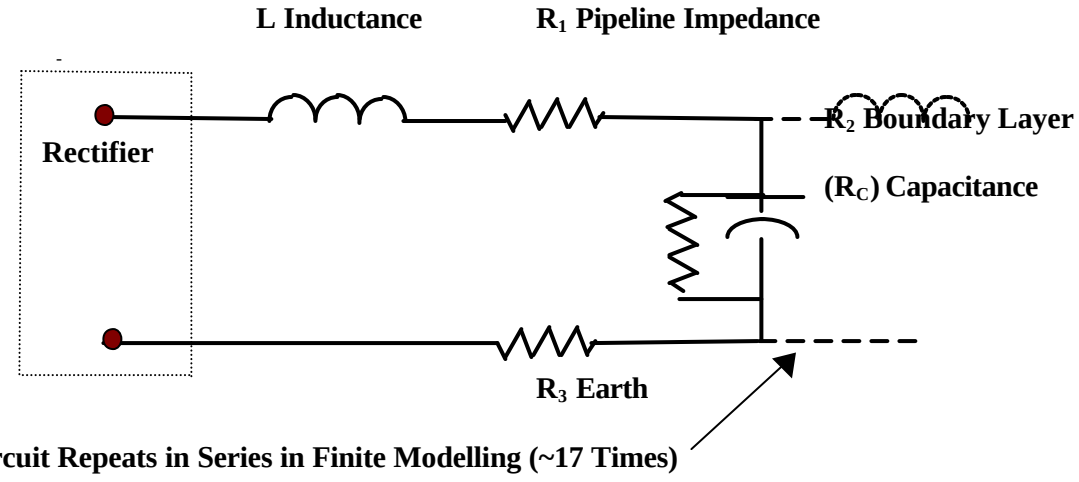

Figure 2

Average reading surveys capture data that is interpreted to the erroneous circuit shown in Figure 1. These averaging surveys can miss important CP operations that are found in the waveforms generated by the CP system. Interval surveys are made more definitive by capturing waveform data. Waveforms capture data that expose the subtleties of the corrected circuit in Figure 2. The result is more decisive information that is used during subsequent data reduction techniques.

While these techniques may be perceived as complex by nature, the pipeline signatures collected are more definitive and much less interpretative that average reading pipe-to-soil interval surveys. On a properly operating CP system the amplitudes of the waveform over distance should gradually increase as one approaches the rectifier. By measuring the gradually increasing amplitudes and drawing relationships between successive measurements the analysis reveals more useful data related to pipeline protection. For example average reading surveys are mostly ineffective at capturing, analysing and pinpointing coating defects. On large diameter pipelines (>14") the bottom half of the pipeline is shielded from averaging measurement inspection by the diameter alone. Shell Oil Research, having investigated these phenomena, found this to be the case .* The modified circuit, (Figure 2) takes into account the propagation ripple that is the CP rectifier output (AC component of the composite waveform – DC & AC). This waveform analysis provides the information that is contained in the AC responses of the CP waveform to changing pipeline conditions. The result is improved pipeline coating analysis.

CP waveform anomalies include full wave discrepancies, half wave operations at failed stacks and interference by kind (frequency mixing and other variations). Holidays (capacitive effects), inductive spiking (pulsing current dispersion), disbonded tape wraps (capacitive changes), corrosion conditions with bitumen coatings (relational waveform performance) and blistering on FBE and polyethylene tape coatings (dB variations – lack of consistency) are also indicated in waveform signature analysis.

The pipeline carries return electrical current from the anode bed back to the rectifier. The range of cathodic protection is dependent upon the coating quality (pipe to soil resistance) among other factors. The principal influence in current distribution across the pipeline is the coating quality and may be expressed as pipe-to-soil resistance or dielectric coating strength (i.e. ? /ft²). The waveform gradually builds peak-to-peak amplitude towards the rectifier's cad weld pipeline connection.

This current travels in multiple directions out from the groundbed location. Variances in this scenario expose current redistribution across the pipeline. This current redistribution is seen as upsets in ideal pipeline current flow. The changes and relationships may be measured in decibels (dB) and relational signature analysis. A pipeline may be refurbished by eliminating weakened areas in the coatings (i.e. excessive dB losses per unit section) thereby gaining more efficient control of the voltage propagation (CP protection) along the length of the pipeline. (See the charts in Section III, 4.2)

*[Shell Research, Houston, Texas and Battelle Labs – Engineering Studies]

2.2 Coating Types - Polyethylene Tape Wraps versus Cured (FBE/Coal Tar/Asphalt) Coatings

Polyethylene tape wraps have been found to present additional challenges with different propagation and current density characteristics than FBE, coal tar or asphalt coatings (cured coatings). Tape wraps have little or no moment of elasticity and can stretch and disbond. This situation sometimes provides shielded surfaces that can not be adequately protected by CP application. Extruded coatings can also perform in this manner. Temperature operations are a chief cause in coating degradation and disbonding. Tape wraps maintain a higher dielectric strength (pipe-to-soil resistance) than applied cured coatings. As a result localised tape wrap effects/defects are often more aggressive than the highly permeable cured applied powder or tar coatings. Polyethylene tapes are prone to highly localised defects with more aggressive behaviour than pipelines with cured coatings. Waveform analytical techniques take the above concerns into account. Waveform analysis accounts for the following:

1) the (series) capacitance of individual measurements taken above the pipeline,
2) the relationships over distance from differential measurements and
3) signatures of the individual waveforms

The CP propagation characteristics expose higher risk pipeline sections located between measurement points along the length of the pipeline. Waveform data collection techniques employ all of the basics described in section II of this paper in order to provide multivariable analyses. The basic tool used in data collection and analysis is the depiction of pipeline conditions as waveforms.

III. EMPLOYMENT OF FIELD SURVEY EQUIPMENT

To perform a field survey of a pipeline, a waveform field mobile laboratory is used. This laboratory has the capability to collect, analyse, and store all of the CP data related to the pipeline in computer files. These files can be put into various Microsoft office program formats, and e-mailed on the Internet.
The mobile field laboratory consists of the following equipment:

3.1 Mobile Field Laboratory Hardware

Six major components and the carrying case comprise the Mobile Field Laboratory. A pipeline locator is also included. The total laboratory consists of:

1. Oscilloscope
2. Cathodic Protection Analysis Unit
3. Laptop Computer with waveform analytical software
4. Remote Waveform Reader
5. Battery Power Supply
6. Copper/Copper Sulphate Half Cell

Contained in the case with these major components are connectors, test leads, and wiring. The wires, leads, and connectors supply electrical current from the 12 volt DC battery of the survey vehicle (plug directly into the vehicle cigarette lighter outlet), collect waveform information, and power individual system components.

The Mobile Field Laboratory is programmed with the standard waveform software package software package.? This software filters out competing signals and isolates the cathodic protection voltage. The software, working in conjunction with laboratory hardware, collects this signal over distance, in real time. The software program analyses and compares existing conditions, locates and identifies by type, breakdowns in cathodic protection efficiency or the existence and location of corrosion causing conditions.

*****All waveform software is the proprietary licensed property of TransWave International, Inc.

The CP is sampled by connecting to a test post and placing a reference cell in the ground. The technology uses computer engineered filtering so that only the CP signal is collected. The sampling rate is over 10,000 times per second, and the CP is viewed as an oscilloscopic waveform. The amplitude and physical shape of each wave is a replica of the actual CP signal on the pipe.

A two man survey crew performs the pipeline diagnostic analysis and operates the mobile waveform laboratory. This crew moves from test post to test post along any given pipeline. When there is an abnormal change in data from the last point surveyed to the present point, the survey stops. A reference cell attached to a spool of wire is run back towards the last surveyed point. After collecting several more waveforms, a location is verified as the point of the anomaly that caused the upset condition.

3.2 Waveform Analysis Data Reduction

After completing the collection of waveform data for an entire pipeline, the survey crew performs analysis operations. This analysis consists of reducing the data to usable graphic and tabular forms. Waveform data reduction takes into account several variables and is more varied and decisive than simplified DC averaging techniques. Waveform analytical patterns, signatures and interrelationships are analysed to produce the final survey findings. To this end a simplified scroll report of the pipeline under survey is constructed to provide an executive summary of the pipeline analysis. This tabular data graphically displays the propagation characteristics of the pipeline.

3.3 Propagation Performance and Anomalies of the CP System

Below is a brief explanation of some waveform analytical techniques, followed by examples of waveforms collected from a pipeline.

Polyethylene tape wraps degrades with time loosing dielectric strength. Studies have shown that the average resistance of new tape wraps is 1,115,000 ? ft². At 10-to15 years tape wraps have been measured to be 100,000 ? ft^2. Since the data is of an empirical nature that does not and can not take into account all variables, TransWave adopted a de facto standard. Initial engineering studies determined that new tape wraps operate at .2 to 2 dB/mile dependent upon installation procedures. At 6 dB the dielectric strength is adjudged to be 100,000 ? ft^2 or an order of magnitude change. TransWave suggests that any section of pipeline that displays performance in excess of 10 dB/mile should be reviewed and that excessively high dB changes or losses be further defined so that target digs in these locations are pinpointed for excavation.

Additionally excessive dB changes often result from CP interference when trams or electrically driven trolleys operate near pipelines. In reviewing the dB performance and rates of change on any subject pipeline, several sections of the pipeline are further analyzed during the remote risk management hardware installation process, and dig locations are pinpointed for excavation at that time.

3.4 Waveform Examples

Example 1.

A standard waveform. The X-axis represents time in milliseconds and the Y-axis represents voltage. The Maximum, average, and minimum are the pipe to soil potentials collected using waveform technology. The high sampling speed of TransWave's equipment permits the display of CP information as an oscilloscopic waveform. This waveform represent good condition of because potential doesn't exceed referral voltage – 0.850 V.

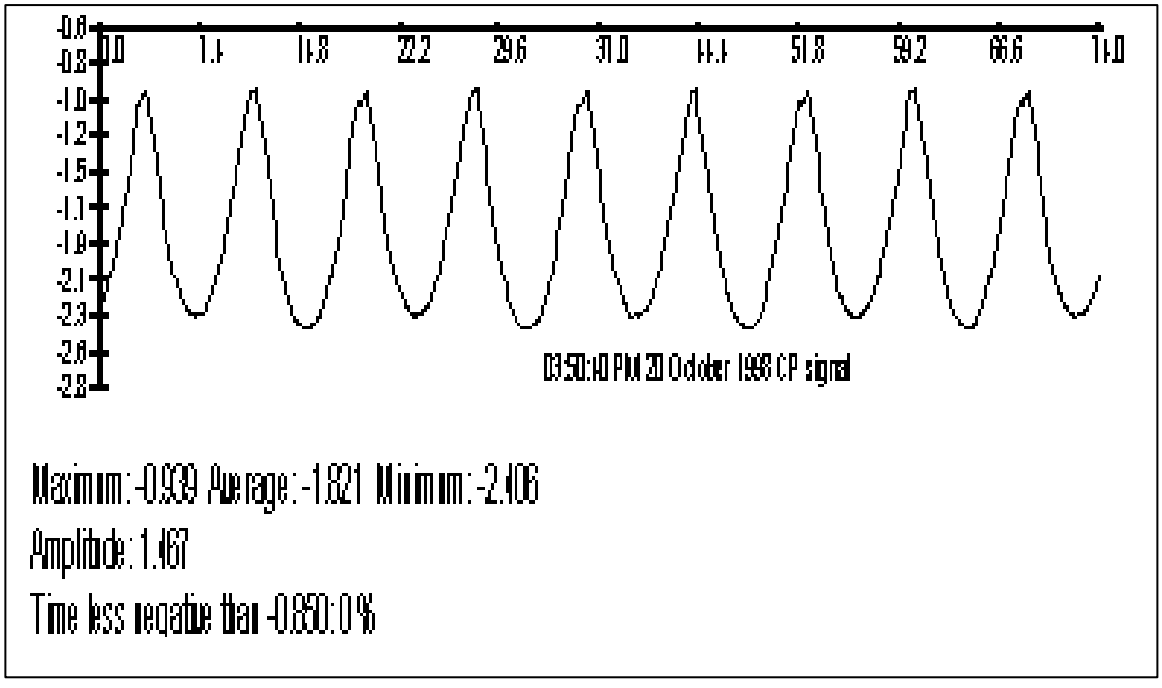

Example 1a.

Is an example of a waveform that exhibits positive spiking. The pipe to soil average potential is the data normally collected by traditional averaging voltmeters. In example 1a, this is –1.847, a good potential. However, the data collected by waveform technology shows that for 25% of the time, this CP is less than the required –0.850. For a period of time, the CP is not negative. The pipe is unprotected one quarter of the time, and conditions conducive to corrosion propagation are present.

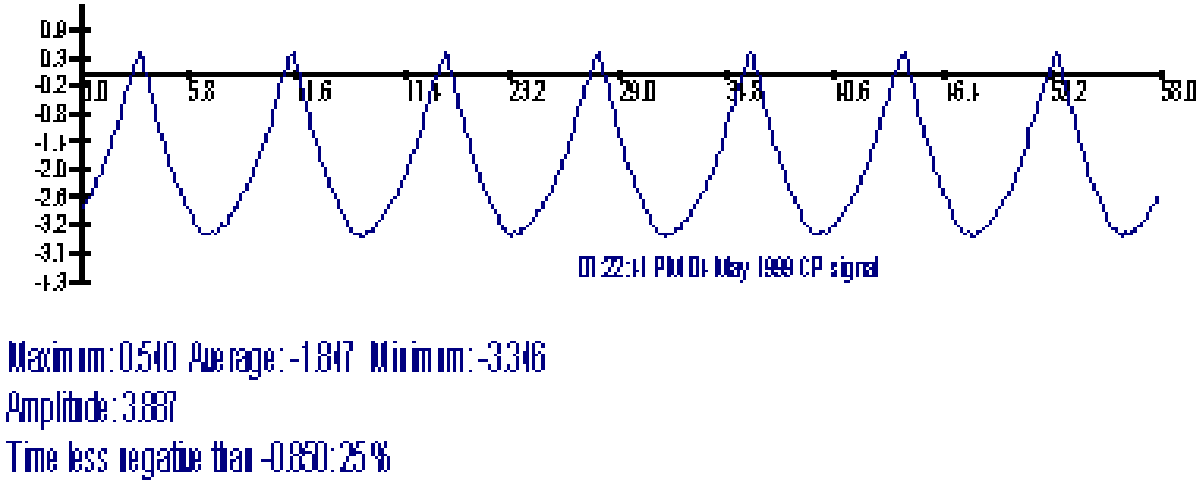

Example 1a.

3.5 Summary Graphs

The points on the graphs shown below represent individual pipeline locations where waveform data was collected, averaged, and analysed.

Waveform analytical software calculates the decibel (dB) propagation performance for sections of pipeline. Sections that show little or no dB loss by calculation cause a flat line to be graphed. A flat line dB response is actually a significant change in dB when one considers the series resistance of the pipeline. The absence of slope in the plots is a warning of significant length of pipeline with minimal coating quality and/or integrity. Consistent coatings subscribe to minimal but consistent dB slopes and are qualified and quantified by the dB values per mile of run. Better quality (new) tar coatings subscribe to a minimum consistent slope devoid of step functions and average less than three dB per mile.

Below is a graphic representation of a pipeline showing decibel and amplitude changes over distance. The decibel (dB) changes are generally in the hundreds along the short distance of pipeline analysed. Experience indicates that a dB change of thirty or less on a tape wrapped pipe 30+ years old is satisfactory. dB shifts in the hundreds are cause for concern. The areas with dB shifts between measured points that are in the hundreds represent pipeline sections that should be excavated and recoated. The location where dB shifts returned to thirty, or less, between test sites, and stayed there, is an indication that a section of good protective coating has been encountered.

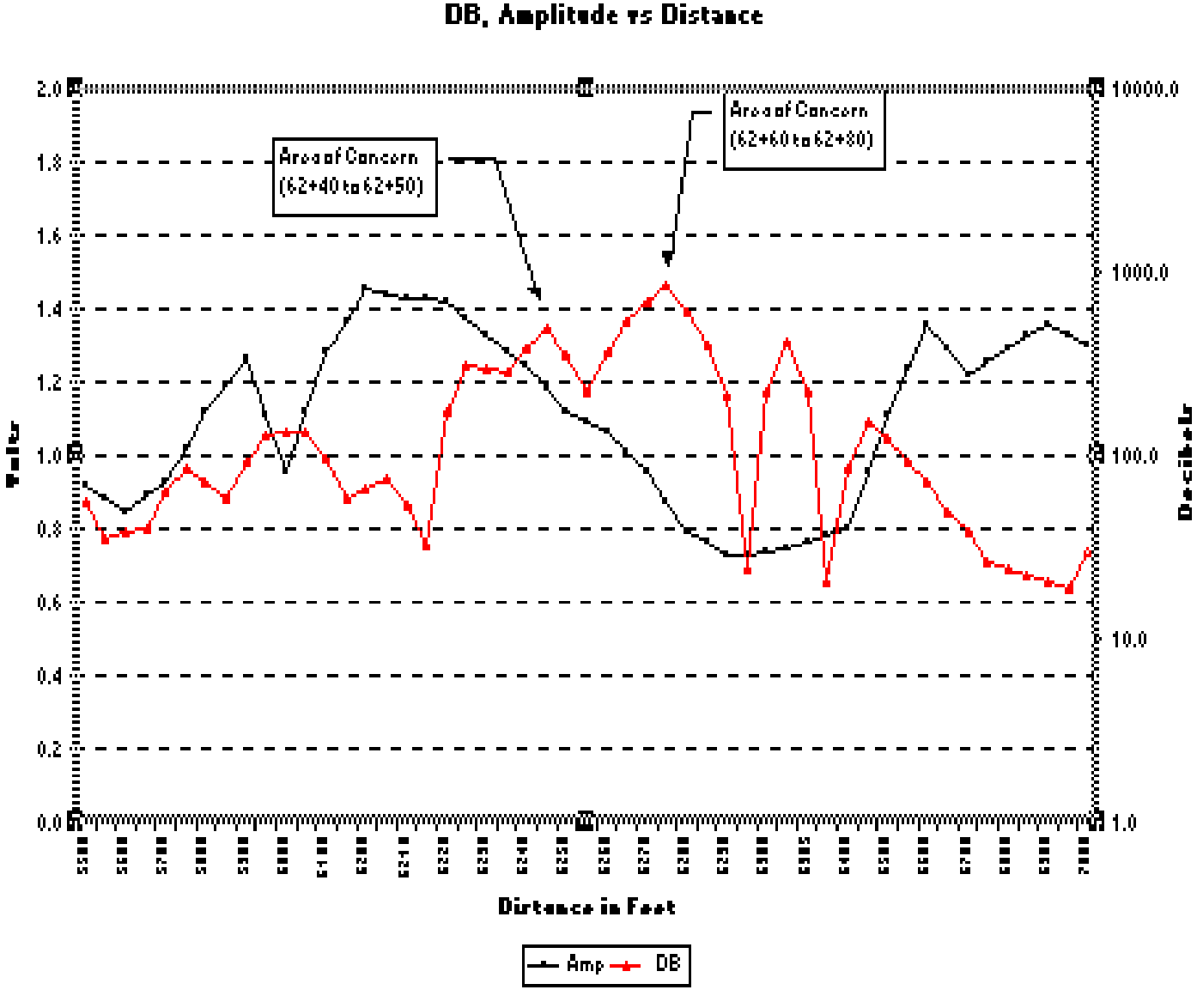

Graphic representation of a pipeline showing maximum, average, and minimum pipe to soil potentials over distance. The key point is that once the potentials begin to go positive, they do not significantly return to a satisfactory negative level (use the average potential black line as an example). This indicates that the CP is not staying on the pipe and protecting it after it passes the 5800 foot mark. This is another indication of poor coating. The location where pipe to soil potentials returned to more negative levels, and stayed there, is an indication that a section of good protective coating has been encountered.

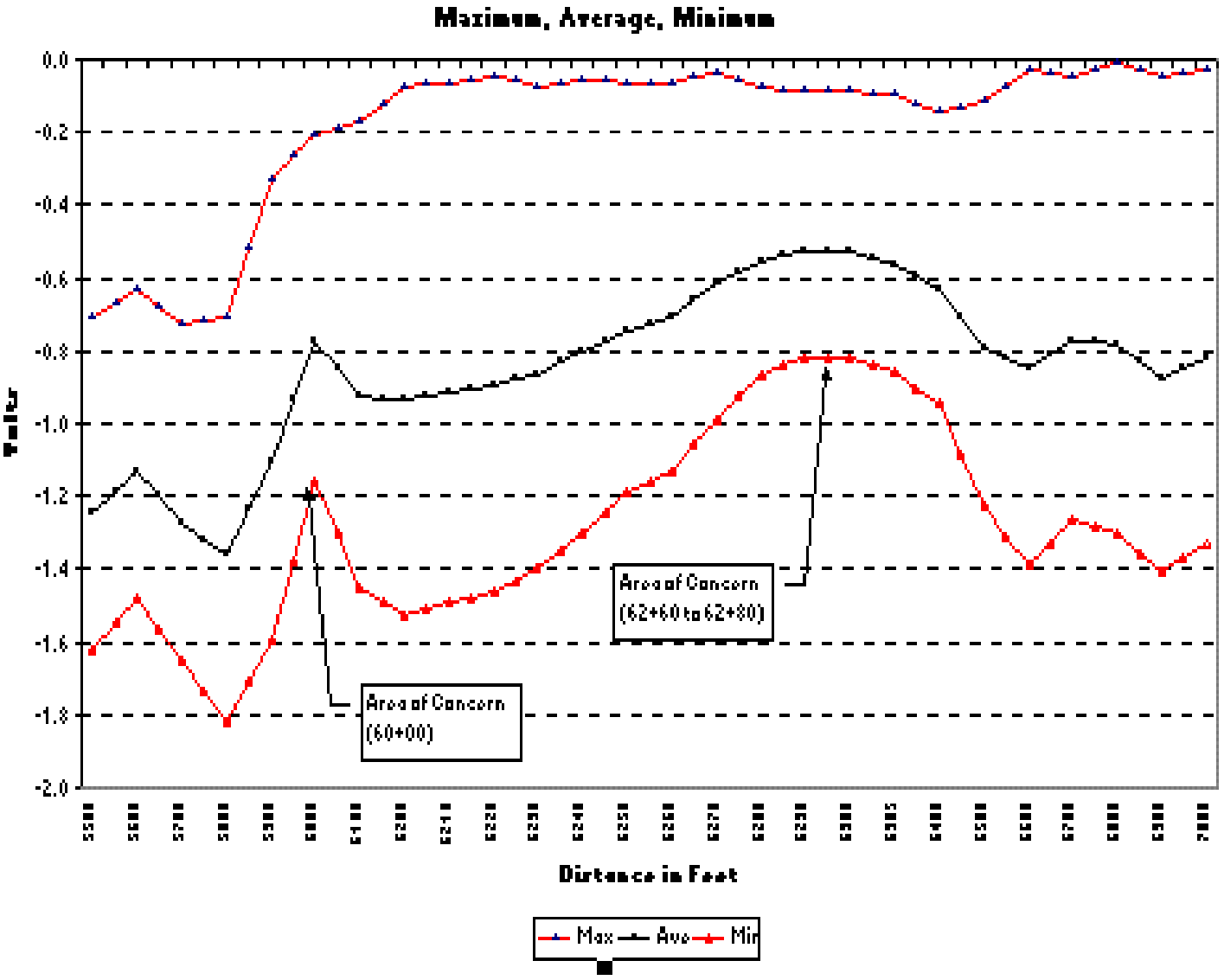

Upon excavation, pipelines have been found to have holidays, disbonded tape coatings and blistered conditions etc. These conditions are in keeping with capacitive measurement changes. Beneath these coatings are found films and pools of moisture. It is suggested that whenever this occurs, the "moisture" be pH tested, collected and/or referred to a laboratory for chemical analyses.

The reason for analysis is to verify solution chemistry and alkalinity. Alkaline solutions can be present when a pipeline is cathodically overdriven (over polarised) and these solutions are a principal reason for disbonding in (tape) coatings. In many digs alkaline residue is visible. The liquid solutions are clear and appear as water but can have an extremely high pH. These residue solutions dry to a brown rivulet. Should the liquids be highly alkaline then continuing the current CP practices can shorten the life of the remaining (tape) coatings and hence the pipeline. At this time consideration can be given to tuning the outputs of the power supplies.

4. SYSTEMS APPLICATIONS

After the initial survey is completed, the pipeline is populated with RWR microcomputers so that an automated alarming system can maintain the pipeline as a self-reporting sensor. Because degradation effects are highly localised upon tape wrapped pipelines and degradation can be ongoing with (cured) coated pipelines, a system should be installed when the baseline survey data is recent. Alarm point control will be most effective at this time and will continue into the future. Alarm points are set at several locations on the raw signal so that both AC and DC levels are captured. The survey gathered archived data set is loaded into the system central computer and is used as a basis for future operating parameters of the instrumented section. In this way the asset is better preserved for future prosperity.

4.1 The TERMS? Automated System

Upon completion of the waveform diagnostic analytical survey, TransWave's Expert Risk Management System (TERMS™) monitors, assesses and reports the performance of corrosion control systems on buried delivery and storage systems and any deviation from the baseline survey in real-time and on-line, 24 hours/day, 365 days/year. Below is a graphical view of the TERMS architecture:

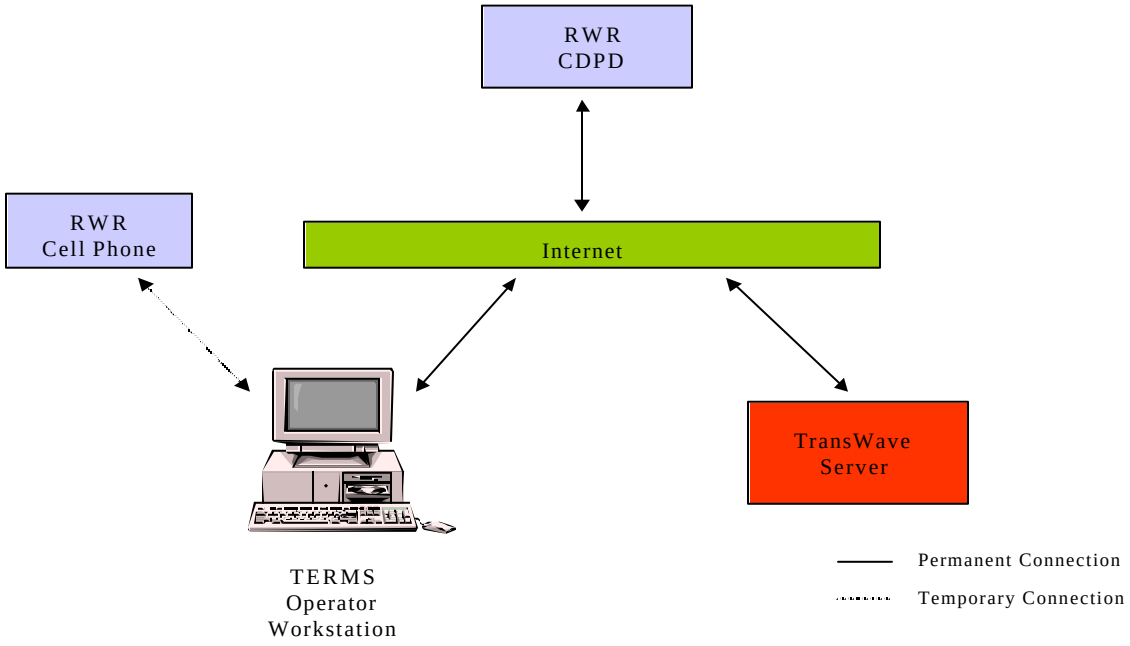

? ? RWR-The Remote Waveform Reader is a device used for remote data logging. These field devices are designed for outside installation

? ? CDPD (cellular digital packet data modems) and Cell Phone-These are the communications link between the RWRs and the TERMS workstation.

? ? TransWave server-The server protects unauthorised access to TERMS software and unauthorised access to RWRs.

? ? TERMS operator workstation-Pentium based computer with communication hardware and TransWave's TERMS software. This operates the TransWave TERMS system.

? ? Internet-The workstation must have a connection to the Internet to run the TERMS software. This is required to provide the connection to the TransWave server.

4.2 TERMS? Software

All of the inputs from the RWR's feed into a single base station that contains a monitoring computer. The waveform software analyzes, charts, graphs, and saves all incoming data. This data, when reduced to tabular and graphed data can be saved as excel files and e-mailed to other locations. Shown below is a display of the main TERMS screen, as it would appear on the monitoring computer main screen with the four major information windows:

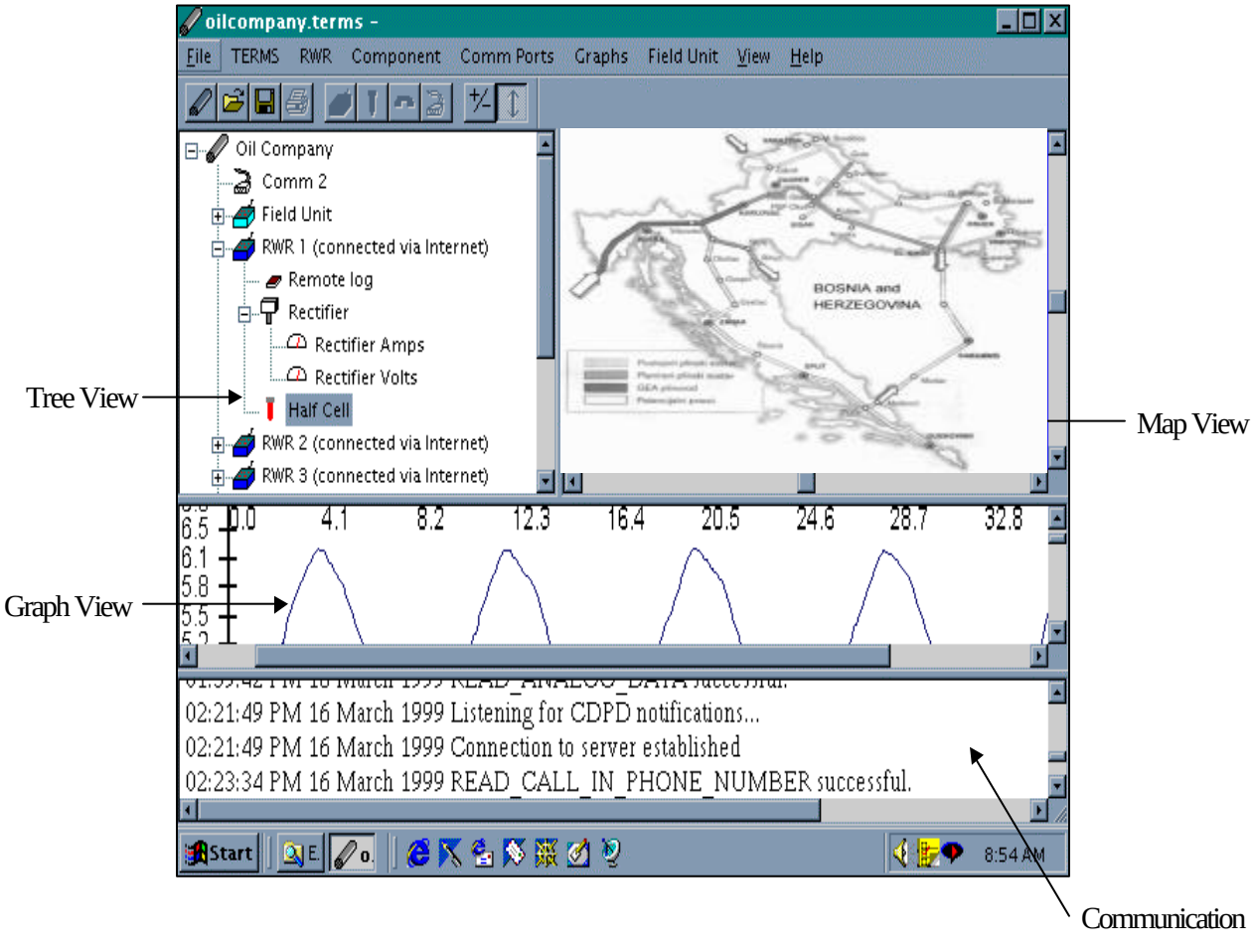

•Tree View-Shows all RWR's and communication ports defined on a system

•Graph View-Shows the waveforms collected and lets the user manipulate them

•Map View-Shows a graphical representation of the pipeline overlaid onto a digital map

•Communication View-Shows a log of communications; Will display whether the server connection was successful when the TERMS software is started; Shows the result of various communications between the TERMS workstation and RWRs.

5. CONCLUSION

Waveform technology was employed for Sarajevo Gas due to the existence of two major problems that would interfere with traditional pipeline survey and data acquisition methods. First was the fact that large areas of the pipeline right of way were covered with asphalt. At the same time, immediately following the siege of Sarajevo, large areas of right of way could not be entered due to the presence of minefields. Waveform survey methods provided the mechanism for analysing these restricted areas. Waveform techniques allowed the survey team to collect data on either side of restricted areas, and then employ the software to analyse the conditions between two test points based on CP propagation. The waveform software used the changes in propagation values between two points to calculate coating and CP conditions for the intervening pipeline distances.

At the conclusion of the waveform survey, the influence of three phased DC interference caused by the tram system was immediately observed as a major problem. This interference was directly responsible for corrosion hazards at several locations throughout Sarajevo. The data collection and analysis means employed with waveform technology located the areas of interference. Further studies of the tabular data collected, provided technical personnel with the means to measure the magnitude of the interference, and its sources. This data will be used in the design of interference mitigating systems that will protect the High Pressure Ring from future corrosion generated by three phase interference sources (Municipal Tram System).

By using waveform technology, Sarajevo Gas representatives were able to detect and measure threats to the Cathodic Protection system that would have been impossible using traditional measurement technologies. Waveform technical capabilities allowed for the collection of data from all 360º of the pipeline's surface. Waveform analytical software was able to measure the CP propagation characteristics of the pipeline's coating. This characteristic, when compared with interference characteristics, allowed technicians to precisely locate those areas where the city trams had the most destructive influence on the pipeline.

TERMS Further improvements moves to Geographical Information System (GIS) integration.

NACE International
THE CORROSION SOCIETY

NACE Standard TM0102-2002
Item No. 21241

Standard
Test Method

Measurement of Protective Coating Electrical Conductance on Underground Pipelines

Approved 2002-06-21
NACE International
1440 South Creek Dr.
Houston, Texas 77084-4906
+1 (281)228-6200

ISBN 1-57590-155-2

Foreword

This standard test method presents guidelines and procedures for use primarily by corrosion control personnel in the pipeline industry to determine the general condition of a pipeline coating. These techniques are used to measure the coating conductance (inverse of coating resistance) on sections of underground pipelines. This test method applies only to pipe coated with dielectric coatings.

When surveying a coated pipeline system, it may be necessary to determine the conductance of the coating. The conductance of a coating can vary considerably along the pipeline. Variations may be caused by changes in average soil resistivity, terrain, and quality of construction. To obtain data for coating conductance calculations, interrupted pipe-to-soil potentials and line current readings are taken at pre-selected intervals. It should be noted that the average soil resistivity has a direct effect on the coating conductance measurement. Because soil resistivity can affect the coating conductance, it must be known when evaluating a section of a pipeline coating.

This standard was prepared by NACE Task Group 030 on Coating Conductance. This Task Group was administered by Specific Technology Group (STG) 03 on Protective Coatings and Linings—Immersion/Buried. Sponsoring STGs also included STG 05 on Cathodic/Anodic Protection; STG 35 on Pipelines, Tanks, and Well Casings; and STG 62 on Testing and Monitoring Procedures. This standard is issued by NACE under the auspices of STG 03.

In NACE standards, the terms *shall*, *must*, *should*, and *may* are used in accordance with the definitions of these terms in the *NACE Publications Style Manual*, 4th ed., Paragraph 7.4.1.9. *Shall* and *must* are used to state mandatory requirements. *Should* is used to state something considered good and is recommended but is not mandatory. *May* is used to state something considered optional.

NACE International
Standard
Test Method

Measurement of Protective Coating Electrical Conductance on Underground Pipelines

Contents

NEW ELECTROMAGNETIC METHODS TO LOCATE AND ASSESS BURIED CP PROBLEMS

Gord W. Parker, C.E.T.
Radiodetection Ltd.
Calgary and Toronto, Canada; Bristol, U.K.

NACE International Seminar
Northern Area, Montreal Sector
AUGUST 26-27, 2002, PALACE ROYAL HOTEL, Quebec

Abstract

In this era of increased market competitiveness and the need for cost reduction strategies, natural gas pipeline and local distribution companies will soon be able to better control the growth of their Cathodic Protection (CP) pipeline maintenance costs with the emergence of two new productivity enhancement techniques. In the early 90's, corrosion control engineers at Southern California Gas Company (SoCal) were encouraged to find new methods to reduce the maintenance costs associated with the Company's approximately 173 million feet of cathodically protected pipelines, mains and services. Mindful of how the maintenance problems in their CP systems were typically being resolved and the annual dollars associated with these efforts, an intriguing concept was conceived that could potentially reduce these costs or increase productivity.

SoCal and the Pacific Gas and Electric Company (PG&E), in conjunction with the Gas Research Institute (GRI), in the mid 90's partnered with Radiodetection Corporation in the research and development of a new family of CP fault-finding technology.

Keywords: integrity, coating, evaluation, cathodic protection, current, pipeline, PCM, Pipeline Current Mapper, GPS, stray current

Introduction

This paper is going to describe two new CP diagnosis tools; where they work well; in what situations they do not work well; and how to use them to reduce the time required to track down troublesome contacts, shorts, holidays and interference in transmission and distribution pipeline systems.

Perhaps the strongest reason for considering this method and technology is that it was conceived, developed, proven and now sworn by, by corrosion engineers and technicians just like you.

Historically, the CP industry has looked at voltage, as it is the voltage (potential) level that protects our pipes. However, it is the flow of current (or lack thereof) that creates these potentials and knowing where the current is flowing shows the engineers and technicians why potentials may not be what they expect.

Pipeline Current Mapping

Generally, we still cannot detect absolute DC current flow through electromagnetic methods without an access to the pipe. The earth's magnetic field, effectively a DC field, provides too much of an interfering signal and masks the true value of the field coming from current flow on a pipe. For this reason, an alternating current (AC) or pulsed direct current (DC) must be used to create signals we need to read above ground. The source of these external signals is an external transmitter or interrupter associated with the system.

The first of the two techniques has been referred to as Pipeline Current Mapping (PCM). This technique is as simple as using appropriate equipment to detect electro-magnetic (EM) fields above ground resulting from the flow of current on a conductor (pipeline) buried beneath it. The EM information is processed to show the current magnitude creating it and then recorded. Analysis becomes very intuitive at this point, current has to go somewhere and any anomalous loss of current

along a span of pipe indicates problems. Kirchhoff's current law states: The sum of the currents into a point in a circuit equals the sum of the currents out (conservation of charge). This is perhaps more relevant than it initially appears to be. It requires that current in all parts of a series circuit is the same. Since a pipeline is effectively a long series circuit, it can closely be modeled like a transmission circuit of a long series resistor (the steel of the pipeline) and an infinite number of parallel resistors along its length (normal and anomalous leakage and losses).

The magnitude and direction of the current must be tightly controlled and thus the system requires a stable, calibrated source for the current. A law of physics comes into play at this point. The higher a frequency, the more it will leak across insulators and out through coatings. This leakage may be detected and reported, but isn't really happening to our DC, so to minimize erroneous responses, we must use an AC signal that is close in frequency to DC. The frequency chosen for this system is 4 Hz. This low frequency, while having the advantage of closely simulating the flow of our DC, is at a disadvantage when it comes to locating the pipe.

To track the current, we still need a locatable signal to follow the pipeline path above ground and four Hz. is too low to be picked up with antennas. Four Hz. is also too low to efficiently guide a technician walking and swinging a receiving device to quickly locate the pipe position. For this reason, an additional frequency is transmitted at the same time to allow locating the pipe. This second frequency can be any locatable signal, however for maximum distance and strength, a low frequency must be used and in this system, it is either 98 Hz. or 512 Hz.

Finally, in the case of distribution short locating where loops may exist, knowing the direction of the current flow on the pipe below us can provide very useful information. A specific example is covered in a following case study (#2). To determine Current Direction (CD), another frequency, exactly double the main current frequency is added to the output. Now by looking at the received signal and

comparing the relative phases of the four Hz. and eight Hz. frequency components, we can easily determine the current direction and use it to guide our troubleshooting.

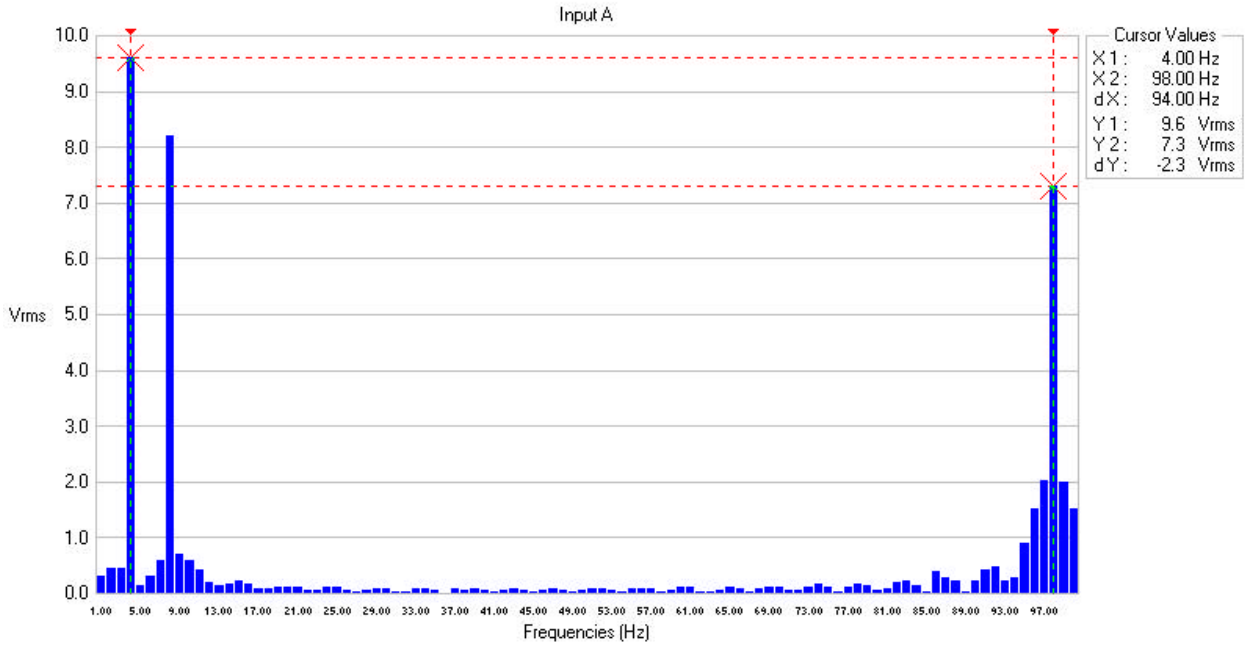

Figure 1: Spectrum of a PCM Output (ELF frequency with CD) at two Amperes into a 4.8 Ohm load.

NACE has included EM test methods in their recommended practice “Pipeline External Corrosion Direct Assessment Methodology” as being a suitable method of data collection for many situations that existing methods could not address.

THE TECHNOLOGY

The system consists of a portable transmitter and a user carried portable receiver.

The transmitter component is a stand-alone 0.1 to 3 Ampere current output device and locating signal generator and may be powered from a variety of sources. It is packaged in portable and weatherproof housing.

The receiver portion of the unit is packaged in two parts consisting of a unique hand-held pipe-locating receiver that can also be used as a Pearson type detector along with an attachable magnetometer module.

To remove the earth's magnetic field and other static fields from the PCMs current measurement function, the alternating current signal of 4Hz is transmitted onto the pipeline. The receiver's flux gate magnetometer module, using specialized signal processing techniques, is positioned directly above the target pipeline segment and accurately measures the 4Hz. magnetic field from which a corresponding current magnitude is electronically calculated. During the research portion of this development, it was confirmed that this alternating signal was sufficiently low in frequency to suffer negligible effects from the capacitance of the protected structure. In other words, the electrical characteristics of current attenuation and distribution on typical natural gas piping systems are virtually the same for this near DC signal as they would be for a comparable magnitude of DC.

Finally, we must remember that we are locating our transmitter signal, not the actual DC current. For cost and portability reasons, the transmitter is limited to 3.0 Amperes output. Although this may be substantially less than the rectifier for the system is capable of, our recorded current is directly proportionate to the actual DC. Simple cross multiplication is the most advanced math needed to relate PCM current to the equivalent DC values.

BENEFITS and STRENGTHS

Above ground, at any point, and with no ground disturbance we can easily find the current amount and direction on the piping under our feet. Previous methods of current spanning, use of large clamp-on ammeters, and installing shunt resistors to give a current proportionate voltage usually require access to the pipe. Ground disturbance is very expensive, especially when roadway detours, restoration, and

liability issues are concerned. Getting permission from land–owners, municipalities, other facility owners, and possibly transportation ministries is time consuming and usually expensive.

Non-invasive methods such as this paper describe have the potential for substantial improvements in time and cost savings.

Another advantage is that since we are tracing a specific transmitted signal, shorts between different CP zones are easily shown up by this method. As both zones may have adequate protection levels, reading potentials may not show up a faulted insulator. Since only one zone has the PCM transmitter, the mapping current will flow through any failed insulators quickly showing their existence. People may wonder why do we need to locate these if both zones are adequately protected, but the original designers must have had a reason to design them into the system, perhaps due to seasonal variations or future system changes.

The measured data is recorded internally and can be downloaded into a computer where the data is easily imported into a spreadsheet for advanced and automated graphing. Currents and current loss can be plotted out versus distance to aid in the analysis and detection of pipeline coating problems. Additional productivity enhancement can come from the GPS compatibility of the PCM system. By connecting the PCM to a data logging Global Positioning Satellite (GPS) receiver system, all the distances can be automatically calculated and recorded. The resulting positional data can be incorporated into a utilities' Geographic Information System (GIS). The measured current levels and rates of decay, recorded in the GIS, may also be used as a benchmark for future testing.

DIFFICULT APPLICATIONS

Because this process is completely dependent on the flow of current, areas where current is not flowing can create limitations. Often the information provided is still valuable, but always must be interpreted with respect to Ohm's and Kirchhoff's Laws.

A common desire is to find unwanted buried insulators such as 'Dresser' couplings. These couplings can often act as complete electrical insulators, preventing cathodic protection potentials from reaching sections of pipe. They will also prevent the flow of mapping currents. The information we do get regarding what current is flowing and where will still yield good information that is not available by any other means. For example, if we make a connection at a gas service line and find that virtually all of the current is flowing in one direction when the piping goes both ways, there **has** to be an insulator in the direction of little current flow. By repeating this process over several services, we can narrow down the position of the insulator. While this method will provide resolution down to the spacing between the two services, that may not be satisfactory when it comes time to rip up pavement. Based on the recorded decay of current flow, further testing is planned to find an empirical model correctly relating the physical position with respect to the reported current. Initial analysis is promising on this topic.

Other electromagnetic methods do exist and can give good results for detecting dresser positions. Use of a higher frequency can use to our advantage the relationship between frequency and current loss. By performing a similar survey while using a higher frequency, the abrupt loss of signal is usually more apparent. The PCM includes two frequencies that can be used for this purpose.

The flow of current does not necessarily guarantee adequate protection levels. While this process does an excellent job of telling us where our current is going, it cannot show if there is or is not sufficient

potentials. If there is little current flowing, it just could be very well insulated pipe that requires little current to be protected. Even if there is substantial current flowing, some pipe may require more current and we still may not be protected. Connected Magnesium anodes may continue to be connected but must be considered when analyzing data.

PCM CASE-STUDIES

The demonstrated productivity gains with the PCM system are impressive. Using the labour-intensive techniques and procedures of the past, corrosion technicians would often spend days in search of difficult foreign contact(s).

During the winter of '96-'97, CP specialists from two major US gas distribution companies were involved in the prototype PCM evaluations requested, from their various operating regions, notification of shorted CP areas that had proven difficult to resolve using traditional troubleshooting methods. The following case studies document some of these findings:

Case # 1

The CP potential reads in an extremely large distribution network of coated pipe had been reported "down" the prior month. After at least one week of extensive field investigative work by two technicians using traditional troubleshooting techniques, the problem failed to be resolved. Within three hours of the PCM equipment set-up, an evaluation team member determined that a two-inch main was shorted in the middle of a paved intersection. A subsequent excavation at the indicated location found that the main had come into parallel contact with a previously abandoned gas pipeline.

Case # 2

The CP area consisted of approximately 45,000 feet of two, three, and four-inch mains and 15,000 feet of service piping. System piping was in a compounded multiple loop configuration and coating conditions were fair to poor. Pipe-to-soil reads were below the established criteria. Approximately 100 hours had been spent in trying to resolve the problem. Line-dropping techniques had not been used to determine the problem. Instead, extensive Pearson detector surveys were performed without success.

The PCM transmitter was connected to the power supply and ground bed of the rectifier supplying current to the area. Due to the size of the area, the transmitter was set at its maximum output of three amperes. Using a systematic current mapping approach, an uninsulated meter set was found in approximately two hours. Protective levels were again re-established.

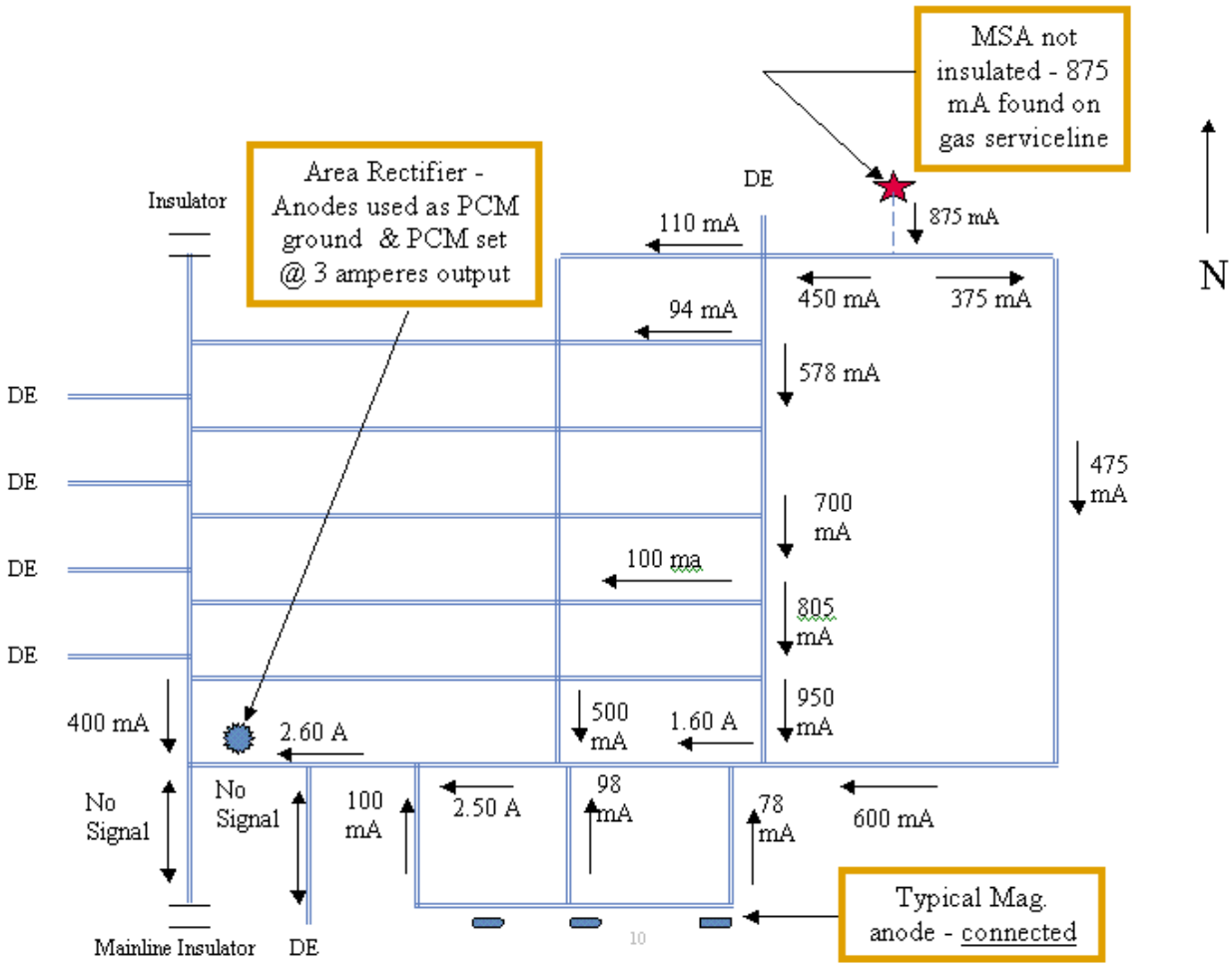

Figure 2: Layout of Case Study #2

Case # 3

The subject CP area consisted of approximately 18,000 feet of two, three, and four-inch mains and 6,000 feet of service piping. Area piping was in a multiple loop configuration and coating conditions were generally only fair. Pipe-to-soil voltage reads were found to be below the established criteria. After approximately 80 hours of investigation, using traditional troubleshooting methods, a missing meter set insulator had been located and corrected, however there were still problems.

Subsequent tests showed that even with the installation of another 20-pound magnesium anode, the potential reads were still low. Use of a Pearson detector had been difficult due to the high noise levels of alternating current interference from overhead electrical lines. Close interval line-dropping of the main was not economically feasible due to the lack of adequate contact points -- resultant from the area's large number of plastic replacement services.

Using an existing magnesium anode bank located near the middle of the area as a ground, the PCM transmitter was set at an output of one ampere.

Using a systematic current mapping approach, an underground contact was pinpointed. A subsequent excavation at this location found that a 6-inch diameter cast iron water main had come into contact with a three-inch gas main. The time to locate this contact with the PCM was approximately two and one-half hours. Pipe-to-soil measurements after the contact was cleared were higher than at any previous time.

Case # 4

The ability of the PCM to adequately determine coating quality of transmission pipelines and mains was documented while surveying a small diameter gas transmission line. Three separate problems were found, none of which were known to the owner. Referring to the graph ‘Case #4” we can see three separate problems. The shorted insulator to a compressor station is the largest loss. Also to be noted is the loss through two sloughs. The first slough is just past the edge of the station and the second slough is now dry and ¼ mile further. The current loss/distance has been calculated in a spreadsheet that the collected data was imported into and is expressed in millibels (1/100 of a dB) per foot.

Analyzing the data in terms of deci or millibels provides a better display of loss severity. If an anomaly causes 50% loss, at 2A input we lose 1A, but at 100mA input we only lose 50mA and the problem **looks** less severe. Displaying in terms of bels normalizes the loss against the source.

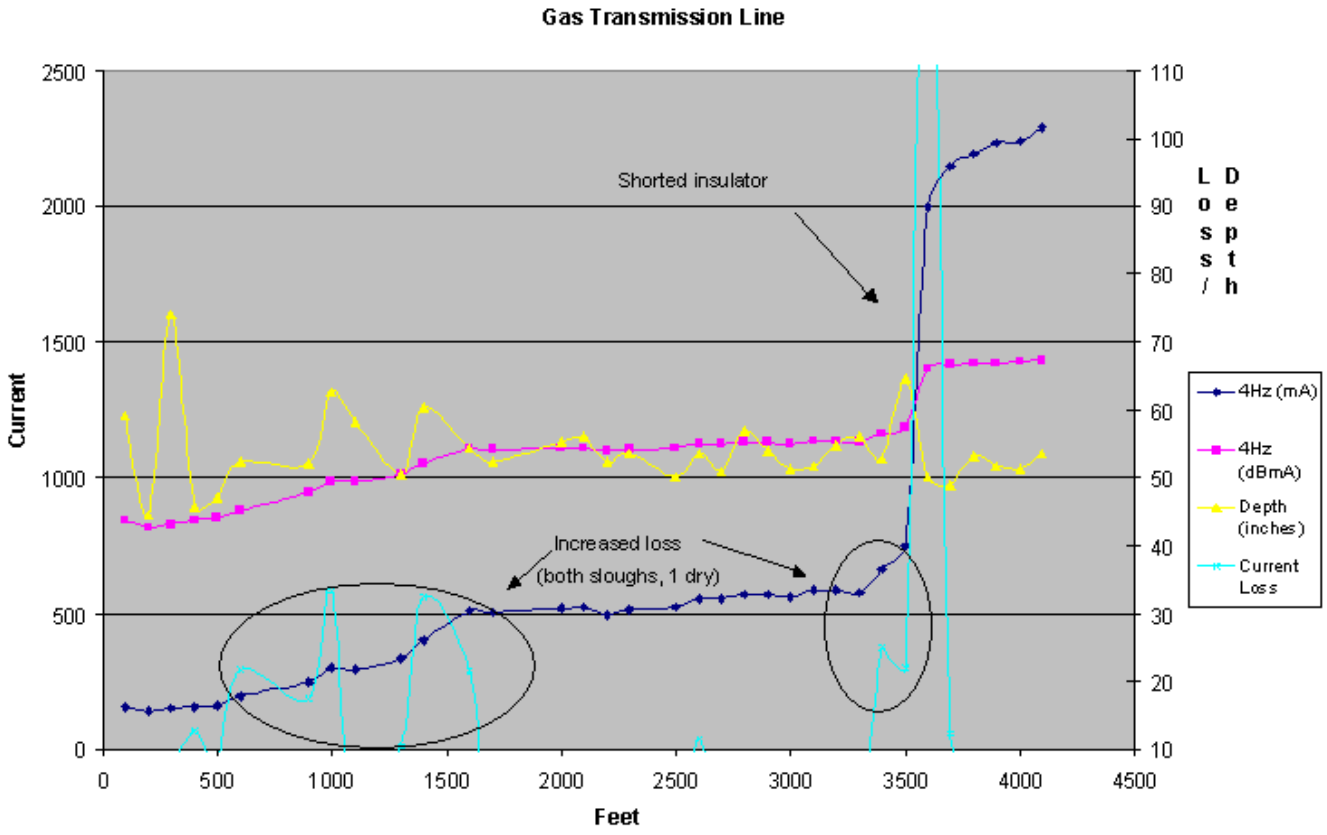

Figure 3: Results of Case Study #4

PCM CONCLUSIONS

The ability of the prototype PCM system to quickly, non-intrusively, and accurately measure the distribution of an impressed test current on a natural gas piping network is a quantum improvement in the methodology of troubleshooting CP areas. Feedback has been extremely positive:

"The technology to be able to quickly measure pipeline current flow and know its direction is unquestionably a major breakthrough in the approach to troubleshooting cathodic protections systems." said R.C. Skelton, cathodic protection consultant.

"We found it extremely useful to locate sections of poor coating, especially under concrete and pavement. The cost of excavation in these areas is very high and the PCM eliminates the guesswork." said, Ray Harding, Enbridge Consumers CP Technician.

Klaus Jeppesen, cathodic protection specialist #5448, Farwest Corrosion Control Co., said "The PCM provides a higher level of confidence than a conventional signal locator. The current direction feature has enabled me to quickly resolve problems that previously required calibrated current span work. The PCM has quickly become my troubleshooting tool of choice".

Midway through the field evaluation phase, it became clear to the development partners that the performance of the prototype PCM units had far exceeded initial productivity expectations. The original objective of developing a new CP device that could increase troubleshooting productivity by at least 25 percent was met. It has also been found that use of the PCM system significantly increases field technicians' working knowledge of cathodic protection, reduces safety and liability considerations inherent with previous troubleshooting techniques, and allows for some other operating cost reductions, i.e. -- the reduction in the current outputs of many urban impressed current systems (set high in the past to mask existing shorts) thereby also reducing the potential of stray current interference. Economic analyses have shown that a payback period of less than one year is a reasonable expectation for using this system. As the system also works as a regular pipe and cable locator, the value of a flexible tool like this is further increased for a shorter payback. Finally, the technology has been endorsed by both standards organizations and by operators of pipeline systems.

Stray Current Mapping

The second of the two techniques is referred to as Stray Current Mapping (SCM). As the name suggests, it uses similar processes to detect unwanted, non-designed currents that can cause very serious, dramatic and localized corrosion problems (figure 4). It resulted as a "spin-off' of the PCM technology.

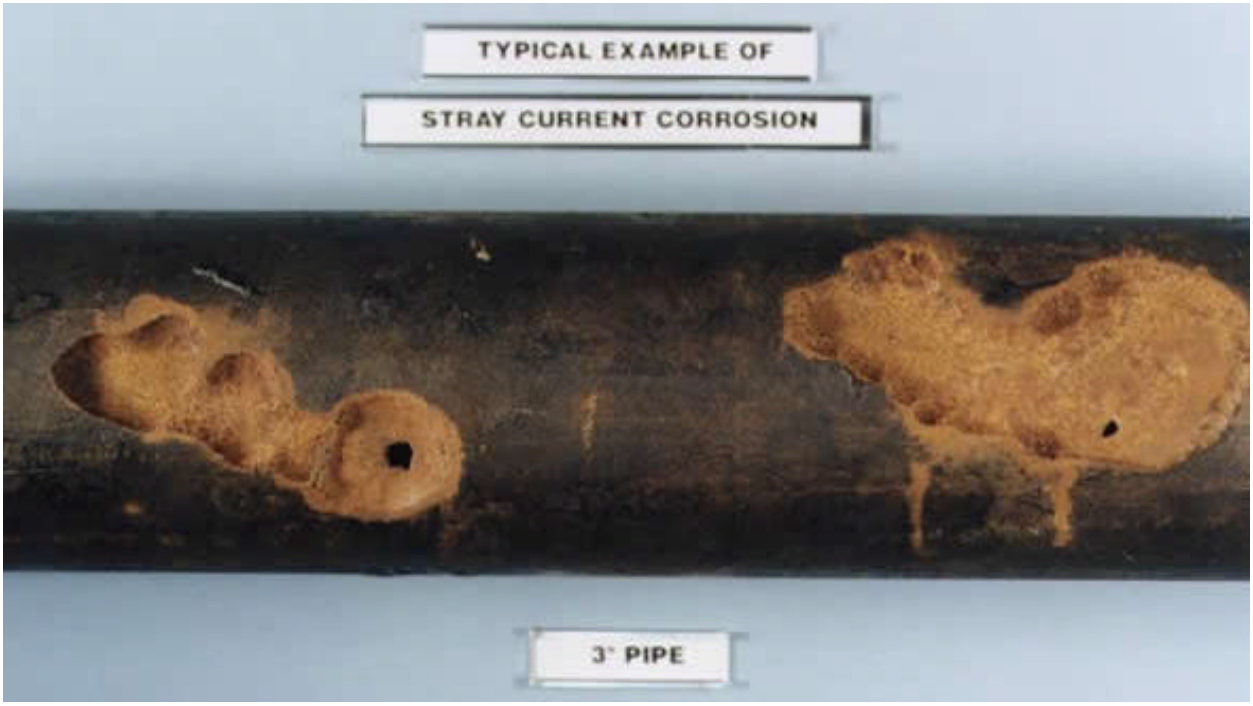

Figure 4: Typical pipeline failure due to highly localized corrosion caused by Stray Currents.

The two main sources for stray currents are other pipeline systems and electric rail systems. The SCM system is able to determine if and where stray currents are being forced onto a metallic piping system, the magnitude of this interference, and most important, the location(s) and magnitudes where this often detrimental current leaves an interfered-with system.

The technology is very similar to the PCM system. It uses magnetometers to detect very low frequency changes to the current along the pipeline. It includes data-logging technology and software to allow

analysis of the detected fields on standard laptop computers. Where the technology differs is that it records the actual current flow created by the systems CP rectifier. Since the CP current flow is DC and the earth's magnetic field is effectively DC, it could not be accurately detected. It also uses several sets of orthogonal magnetometer sensors along the length of the receiver bar to receive data and process it for accuracy. An analog voltage data logger was also included so that EM effects upon a pipeline could be easily related to actual fluctuations in the pipeline potential.

The method chosen to identify which is desired and which is stray CP current flow was to develop current interrupters that stop current flow with a periodic but unique 'patterns'. The SCM software 'sees' this pattern in the collected data and is able to accurately determine the related current. Since a typical pipeline may have multiple desired and stray current sources, there were multiple patterns defined in the software. To accurately determine how much of an effect other pipeline systems have on the system under test, interrupters must be placed on these other systems. This of course requires co-operation from the other companies.

Stray currents become quite easy to observe when the data is collected and presented (see figure 5).

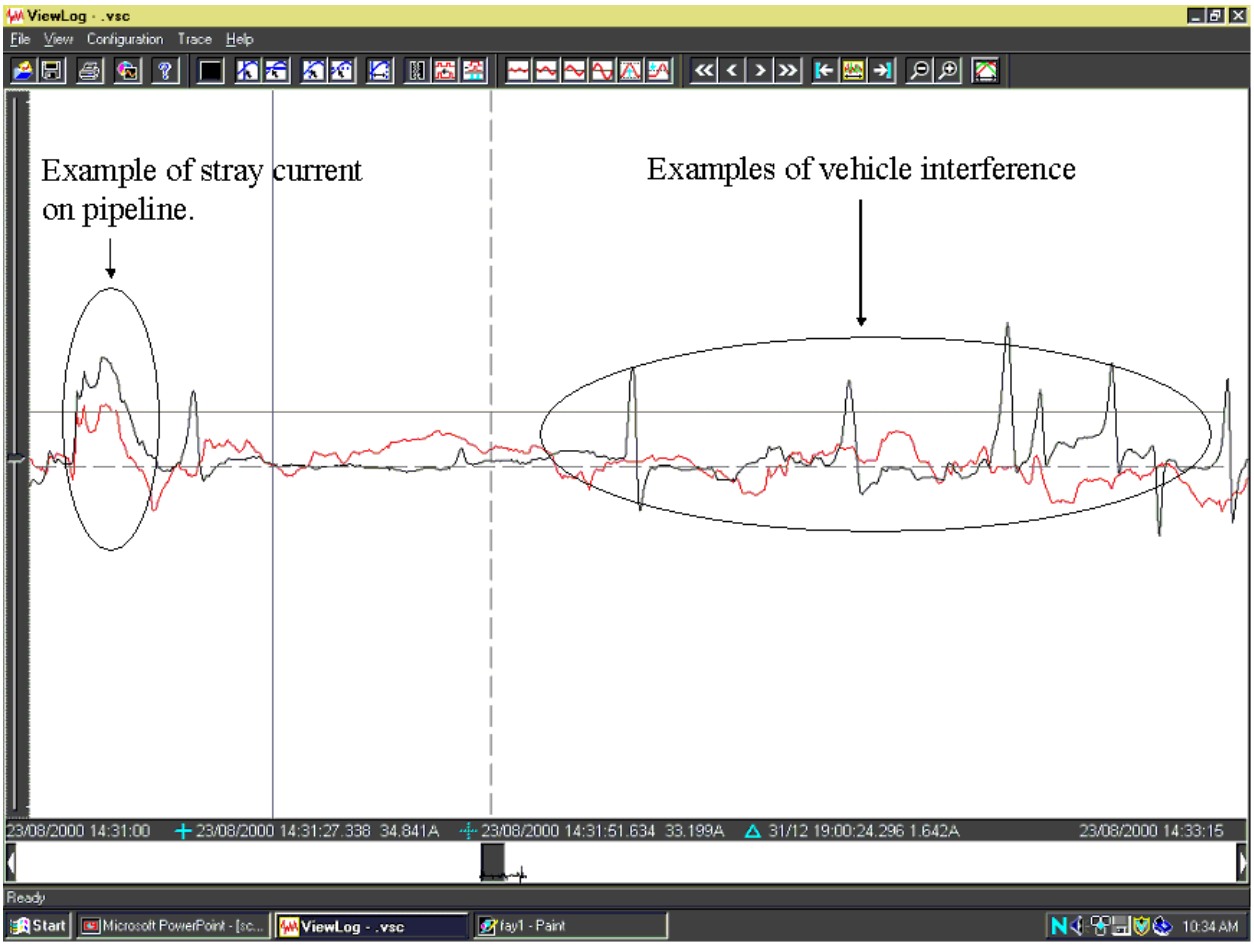

Figure 5: One example of data presentation.

In the case of rail-induced interference, it is obviously impossible to interrupt these currents. The method for detecting these relies on their large differential from the baseline magnetic field. When looking at long-term (6 hour +) recorded data, anomalous spikes become very apparent in the recorded magnetic field. These same spikes have been recorded as affecting the pipe-to-soil data as shown in figure 6.

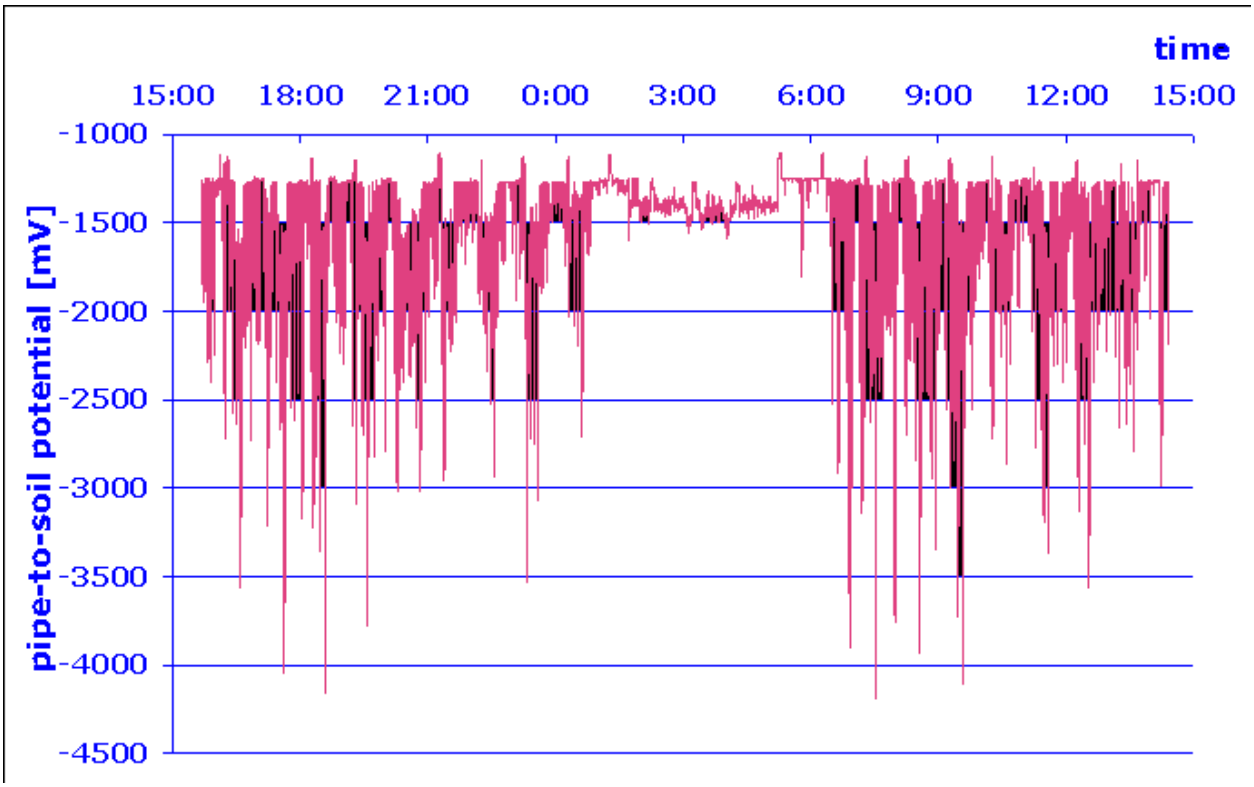

Figure 6: Stray current resulting from rail operation (Note time of inactivity).

As an added benefit, the interrupters were developed to work as a standard interrupter for close interval survey work. Absolute time stability is guaranteed in all modes due to the inclusion of a timing module based on the Global Positioning System clocks.

SCM CONCLUSIONS

Stray current mapping is very new but has progressed to a commercialized product. Unfortunately, as the technology is this new, real world case study data was not available at the time of writing this paper. Workshops and applications will be completed in the spring and summer of 2002 and further data from them will be presented at the conference.

Acknowledgements

The author would like to acknowledge the following people and sources whose prior work and material contributed greatly towards this paper:

Gas Research Institute (now Gas Technology Institute) of Des Plains, IL

Southern California Gas Company, Los Angeles, CA

Chuck Skelton, Southern California Gas Company, Los Angeles, CA

Pacific Gas and Electric, San Francisco, CA

Anton Kacicnik, Enbridge Consumers Gas, Ontario

Ray Harding, Enbridge Consumers Gas, Ontario

Klaus Jeppesen, Farwest Corrosion Control Co., Gardena, CA

Barney Walker, Radiodetection Ltd. Bristol, UK

Jim Walton, Radiodetection Corporation, Mahwah, NJ

New NACE Test Method *Pipeline Coating: Aboveground Techniques for the Underground Evaluation of Condition* (TG 294)

Gord Parker, C.E.T.
Radiodetection Ltd.

What it is

- It will be a Test Method
- Fits 'under' RPO502 (ECDA)
- Out for ballot in December '04
- Aiming for approval at NACE National in Houston, April '05
- This is as fresh as it gets

The document outline:

- Section 1 General
- Section 2 Definitions
- Section 3 AC Current Attenuation (EM)
- Section 4 AC Voltage Gradient
- Section 5 DC Voltage Gradient
- Section 6 Pearson Survey

- CIS has its own TM or RP
- - isn't necessarily part of ECDA

- I helped with ACCA and ACVG

5 sections each, Structure:

- Introduction
- Instrumentation and Equipment
- Survey Procedure
- Survey Results
- Data Analysis

ECDA Notes

- Several good projects complete
- Don’t expect it to be an order of magnitude cheaper then an ILI project
  - Properly done, can be very close in price
  - Still the only option for non-pigable lines

Defect Sizing

- A good idea is available but very precise sizing is still dependent on soil resistivity at the holiday and at the probes.
- Applying soil resistivity info to the results should help size the defects more accurately.
- This has been discussed by users, empirical data not yet available.

Section 3 – AC Current Attenuation

- The Electromagnetic part of this is only a means to measure current without contact to pipe or ground.
- The real data is how much current has been lost.
- When people hear ‘Electromagnetic’ they get worried. Don’t! It is just a way to measure current.
- The industry is used to wires & volts.
  - Trusting invisible EM fields is new to it.

Current Attenuation

- Doesn’t replace measuring potentials
- BUT… seeing where current is going can be a big help in trouble-shooting
- Measures the current and looks for losses

- Spacing - finer the better, especially for ECDA
- Newer equipment = better resolution
  - allows detection of smaller holidays.
- Spacing of 25-100’ is common
- A very coarse survey can be used for a baseline, even 1 reading per road x-ing

- A non-contact method for determining where current loss/gain is occurring along a pipeline or a distribution system.
- Proven very popular in areas where earth contact is not available
  - through concrete and high resistivity soils
- Modern equipment has improved rejection of interference and field distortion
  - it is a very user-friendly tool.

Transmission Example

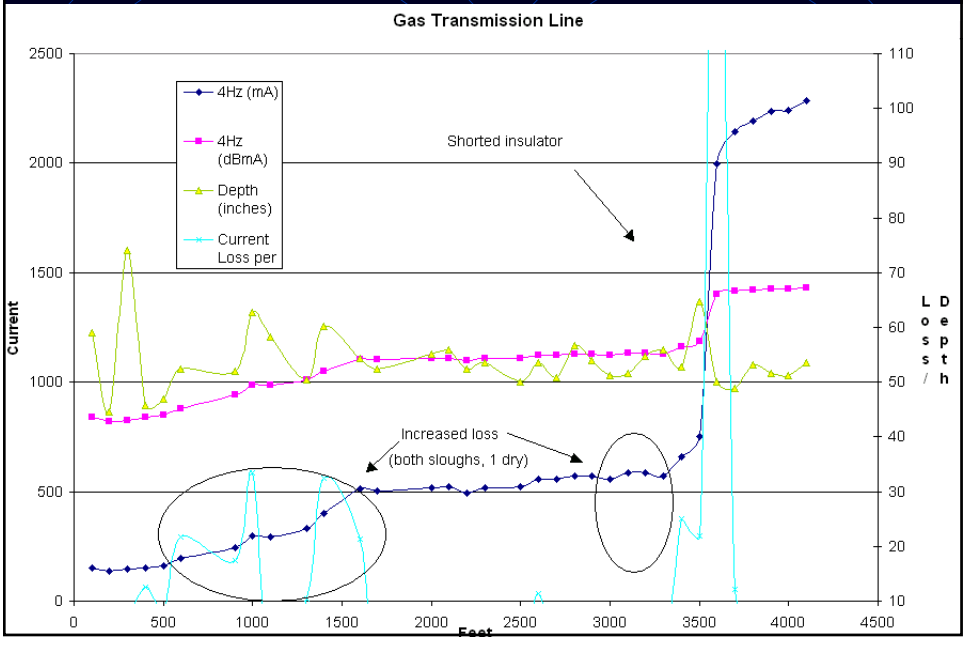

Distribution Example

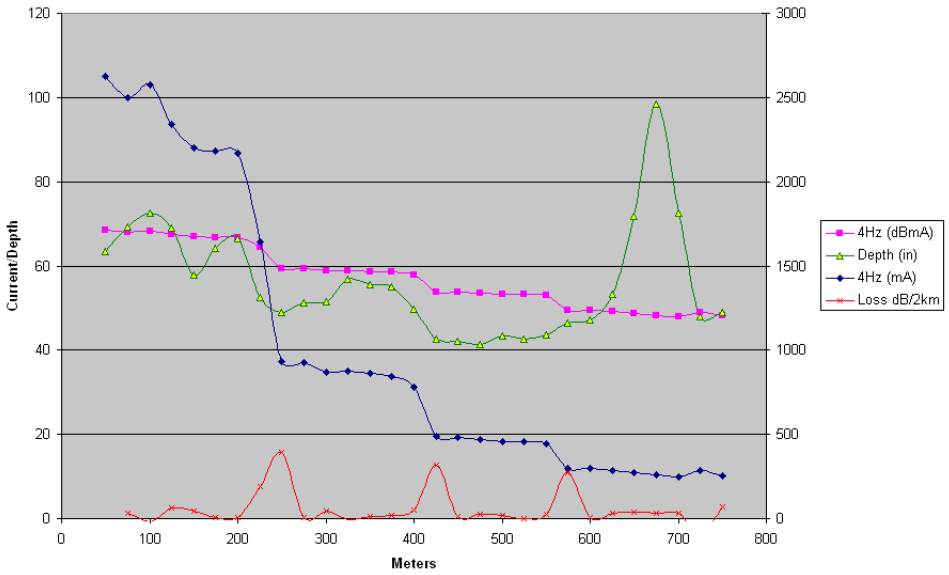

What's new in ACCA

- Adding pipeline diameter into current attenuation data to calculate loss per **square area**
  - Allows comparing all diameters to each other
  - Gives bigger database of coating qualities
- Adding soil resistivity data to help size defects based on loss

Cons

- Congested areas may have confusing EM fields.
  - Parallel lines
  - Other utilities if user not careful
- We need current flow, so open circuits can limit strength
  - Stubs & Dressers™

Stray Current Mapping

- We can also use a similar idea to detect current from other sources
- Magnetometers triangulate to get depth and amount of current
- Creating unique pattern in the current will allow identification.
- Separate product.

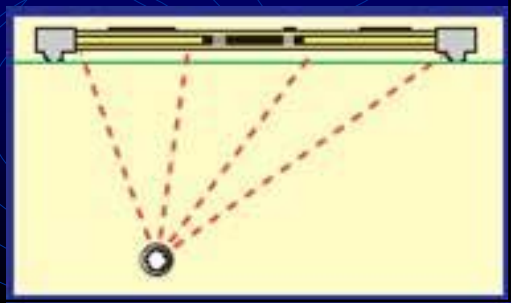

Section 4 AC Voltage Gradient

- Becoming very popular
- Extreme sensitivity
- Rejection of interference
- Very accurate location of faults
  - typically better then 6"
- Sometimes part of Current Attenuation equipment
- This method deserves to be considered as a solid tool for integrity and the ECDA process.

ACVG in Operation

- Both signal strength and direction arrows lead user to holiday.
- Fault value is proportional to holiday size and soil resistivity.

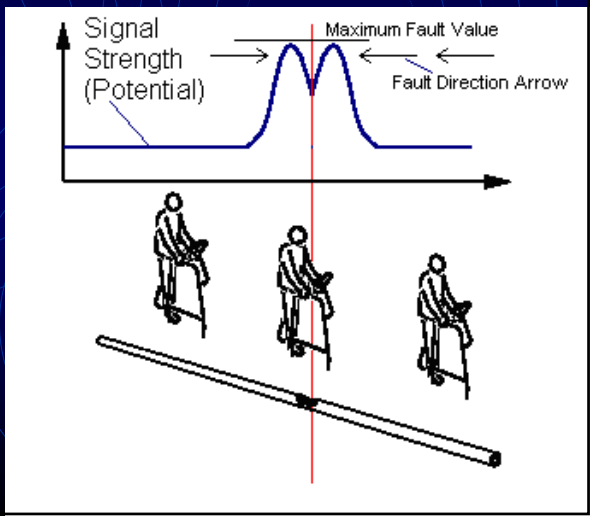

ACVG Tuning

- Older systems used a simple DMM
  - Does not tune to any one frequency
  - 60 Hz, cable earth faults, telecom noise Rx'd
- Very tight tuning in the signal generator and receiver effectively increases sensitivity as it ignores current from other sources
  - SNR improves

The END

- Questions?

- Gord Parker, C.E.T.
- Radiodetection Ltd. (Calgary, Alberta)
- 403-281-1808 cell: 403-606-5464
- gord.parker@radiodetection.spx.com
- www.radiodetection.ca

Analysis of Spread Spectrum Time Domain Reflectometry for Wire Fault Location

Paul Smith, *Member, IEEE*, Cynthia Furse, *Senior Member, IEEE*, and Jacob Gunther, *Member, IEEE*

***Abstract*—Spread spectrum time domain reflectometry (SSTDR) and sequence time domain reflectometry have been demonstrated to be effective technologies for locating intermittent faults on aircraft wires carrying typical signals in flight. This paper examines the parameters that control the accuracy, latency, and signal to noise ratio for these methods. Both test methods are shown to be effective for wires carrying ACpower signals, and SSTDR is shown to be particularly effective at testing wires carrying digital signals such as Mil-Std 1553 data. Results are demonstrated for both controlled and uncontrolled impedance cables. The low test signal levels and high noise immunity of these test methods make them well suited to test for intermittent wiring failures such as open circuits, short circuits, and arcs on cables in aircraft in flight.**

***Index Terms*—Aging wire detection, arc detection, sequence time domain reflectometry (STDR), spread spectrum time domain reflectometry (SSTDR), time domain reflectometry (TDR), wire fault detection.**

I. Introduction

FOR MANY years, wiring has been treated as a system that could be installed and expected to work for the life of an aircraft [1]. As aircraft age far beyond their original expected life span, this attitude is rapidly changing. Aircraft wiring problems have recently been identified as the likely cause of several tragic mishaps [2] and hundreds of thousands of lost mission hours [3]. Modern commercial aircraft typically have more than 100 km of wire [2]. Much of this wire is routed behind panels or wrapped in special protective jackets, and is not accessible even during heavy maintenance when most of the panels are removed.

Among the most difficult wiring problems to resolve are those that involve intermittent faults [4]. Vibration that causes wires with breached insulation to touch each other or the airframe, pins, splices, or corroded connections to pull loose, or "wet arc faults" where water drips on wires with breached insulation causing intermittent line loads. Once on the ground these faults often cannot be replicated or located. During the few milliseconds it is active, the intermittent fault is a significant impedance mismatch that can be detected, rather than the tiny mismatch observed when it is inactive. A wire testing method that could test the wires continually, including while the plane is in flight would, therefore, have a tremendous advantage over conventional static test methods.

Another important reason to test wires that are live and in flight is to enable arc fault circuit breaker technology [5] that is being developed to reduce the danger of fire due to intermittent short circuits. Unlike traditional thermal circuit breakers, these new circuit breakers trip on noise caused by arcs rather than requiring large currents. The problem is that locating the tiny fault after the breaker has tripped is extremely difficult, perhaps impossible. Locating the fault before the breaker trips could enable maintenance action.

This paper describes and analyzes one such method, based on spread spectrum communication techniques that can do just that. This method is accurate to within a few centimeters for wires carrying 400-Hz aircraft signals as well as MilStd 1553 data bus signals. Results are presented on both controlled and uncontrolled impedance cables up to 23 m long.

Early research on spread spectrum time domain reflectometry (SSTDR) [6] has considered fault location tests on high voltage power wires. Sequence time domain reflectometry (STDR) [7] has been studied and used to test twisted pairs for use in communications. More recently, it has been demonstrated for location of intermittent faults such as those on aircraft wiring [18]. These test methods could be used as part of a smart wiring system [2], and could provide continuous testing of wires on aircraft in flight, with automatic reporting of fault locations to facilitate quick wiring repairs. This could be done by integrating the electronics into either the circuit breaker or into "connector savers" throughout the system. In order for this to be feasible, the prototype system that has been described here is being redesigned as a custom ASIC, which should cost on the order of $10–$20 per unit in bulk. This paper focuses on the analysis of SSTDR and STDR. Parameters required for these methods to function as potential test methods on wires carrying 400-Hz ACor high speed digital data such as Mil-Std 1553 are discussed. This analysis is critical to determine the system tradeoffs between speed, accuracy, code length/system complexity, etc. This ideal analysis provides information on the expected accuracy, which is verified with tests of near-ideal lossless controlled impedance coax. The effect of realistic noncontrolled impedance cable is also evaluated, and sources of error within a realistic system are discussed.

Manuscript received April 10, 2004; revised September 14, 2004. This work was supported in part by the Utah Center of Excellence for Smart Sensors and in part by the National Science Foundation under Contract 0097490. The associate editor coordinating the review of this paper and approving it for publication was Prof. Michael Pishko.

P. Smith is with VP Technology, LiveWire Test Labs., Inc., Salt Lake City, UT 84117 USA (e-mail: psmith@livewiretest.com).

C. Furse is with the Department of Electrical and Computer Engineering, University of Utah, Salt Lake City, UT 84112 USA, and also with VP Technology, LiveWire Test Labs., Inc., Salt Lake City, UT 84117 USA (e-mail: cfurse@ece.utah.edu).

J. Gunther is with the Department of Electrical and Computer Engineering, Utah State University, Logan, UT 84322-4120 USA (e-mail: jake@ece.usu.edu).

Digital Object Identifier 10.1109/JSEN.2005.858964

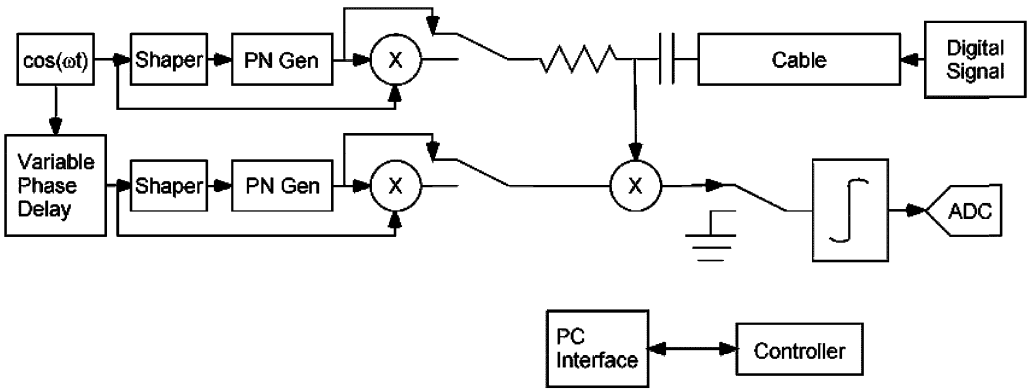

Fig. 1. S/SSTDR circuit diagram.

II. Current Wire Test Technology

There are several test technologies that can be used to pinpoint the location of wiring faults. Some of the most publicized methods are: time domain reflectometry (TDR) [8], standing wave reflectometry (SWR) [12], frequency domain reflectometry (FDR) [13], impedance spectroscopy [14], high voltage, inert gas [15], resistance measurements, and capacitance measurements. At the present time, these test methods cannot reliably distinguish small faults such as intermittent failures on noncontrolled impedance cables without the use of high voltage. In addition, the signal levels required to reliably perform these tests may interfere with aircraft operation if applied while the aircraft is in use [4]. Another test method is needed that can test in the noisy environment of aircraft wiring, and that can be used to pinpoint the location of intermittent faults such as momentary open circuits, short circuits, and arcs.

III. Spread Spectrum Wire Testing

Spread spectrum signals, both in baseband (STDR) [7] and modulated (SSTDR) [6], are detectable through cross correlation, even though they may be buried in noise. The ability to pick out the signal is due to processing gain, which for direct sequence spread spectrum (DSSS) can be expressed as

$$\mathrm{PG} = \frac{T_s}{T_c} = \frac{R_c}{R_s} = \frac{W_{\mathrm{ss}}}{2R_s}$$

where W_{ss} is the bandwidth of the spread-spectrum signal, T_s is the duration of one entire STDR/SSTDR sequence (considering the entire sequence equal to one bit in communication-system terms), T_c is the duration of a PN code chip, R_c is the chip rate in chips per second, and R_s is the symbol rate, which in this case is the number of full sequences per second [16].

Because of this processing gain, it is reasonable to assume that a spread spectrum test system could operate correctly in a noisy environment with 400-Hz 115-V ACor digital data on the wires. The test system could be designed such that it would not be damaged by or interfere with any of the signals already on the wires. For the analysis that follows, the digital data on the wires will be assumed to be Mil-Std 1553, a standard aircraft communication data bus that specifies a 1 Mbit/second data rate, a 2.25–20 V RMS signal level, normally operates on low-loss (3 dB/100 m) 70-Ω shielded twisted pair cable, and allows for a SNR of 17.5 dB [17].

The block diagram of the STDR/SSTDR block is shown in Fig. 1. A sine wave generator (operating at 30–100 MHz) creates the master system clock. Its output is converted to a square wave via a shaper, and the resulting square wave drives a pseudo-noise digital sequence generator (PN Gen). To use SSTDR, the sine wave is multiplied by the output of the PN generator, generating a DSSS binary phase shift keyed (BPSK) signal. To use STDR, the output of the PN generator is not mixed with the sine wave. The test signal is injected into the cable. The total signal from the cable (including any digital data or ACsignals on the cable, and any reflections observable at the receiver) is fed into a correlator circuit along with a reference signal. The received signal and the reference signal are multiplied, and the result is fed to an integrator. The output of the integrator is sampled with an analog-to-digital converter (ADC). A full correlation can be collected by repeatedly adjusting the phase offset between the two signal branches and sampling the correlator output. The location of the various peaks in the full correlation indicates the location of impedance discontinuities such as open circuits, short circuits, and arcs (intermittent shorts). Test data indicate that this test method can resolve faults in a noisy environment to within 1/10th to 1/100th the length of a PN code chip on the cable, depending on the noise level, cable length, and type of cable [4].

IV. STDR/SSTDR Analysis

The operation of STDR/SSTDR depends on the fact that portions of electrical signals are reflected at discontinuities in the characteristic impedance of the cable. A spread spectrum signal shown in Fig. 2 is injected onto the wires, and as with TDR, the reflected signal will be inverted for a short circuit and will be right-side-up for an open circuit [8]. The observed reflected signal is correlated with a copy of the injected signal. The shape of the correlation peaks is shown in Fig. 3. In this figure, the modulating frequency is the same as the chip rate. Note that the sidelobes in the correlation peak are sinusoids of the same amplitude as the off-peak autocorrelation of the ML code. This is due to the selected modulation frequency and synchronization. Use of a different modulation frequency or different synchronization will yield a different correlation pattern that may have higher side lobes [4]. Different PN sequences also have different peak shapes, as shown in Fig. 4 for ML and gold codes.

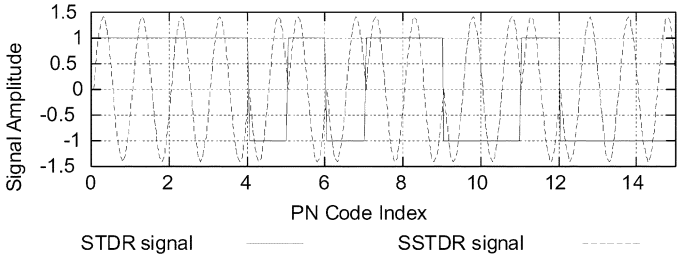

Fig. 2. STDR and SSTDR signals. The SSTDR signal is modulated with $1.0 \cdot F_{\mathrm{STDR}}$.

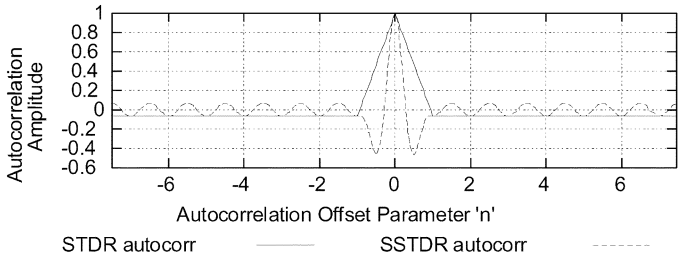

Fig. 3. Autocorrelations of STDR and SSTDR signals from Fig. 2.

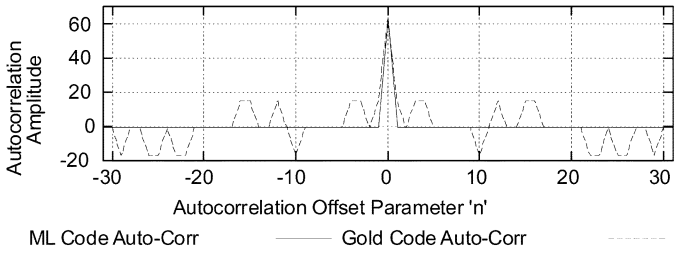

Fig. 4. Autocorrelations of ML and gold codes.

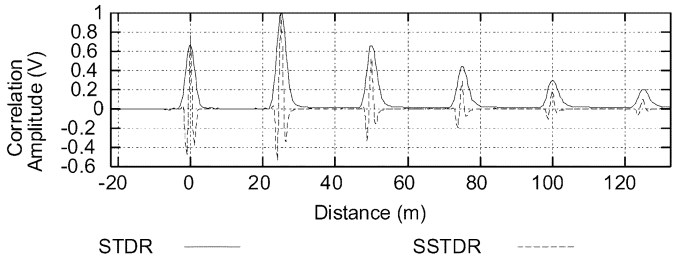

Fig. 5. Correlator output for STDR and SSTDR tests on 75-Ω coax cable with an open circuit 23 m down the cable. Note the peak at zero (connection between the test system and cable), multiple reflections, and definitive shape of the correlation peaks.

The location of the peaks in the correlator output in conjunction with an estimate of the velocity of propagation indicates the distance to impedance discontinuities. Fig. 5 shows normalized sample test data collected on 75-Ω coax cable. The correlation peaks after 23 m are due to multiple reflections in the 23-m cable. The response for noncontrolled impedance cable is not as clean, which is to be expected because of the variation in impedance and subsequent small reflections as well as minor variation in velocity of propagation down the length of the cable. Fig. 6(a) and (b) show the STDR and SSTDR correlation responses measured on two 22 AWG wires in a loosely bundled set of 22 wires that is 9.9 m long. The wires snake in and out within the bundle, and although they are roughly parallel throughout, they definitely do not have even spacing throughout the bundle. The response is not as smooth as that seen in Fig. 5, due to the multiple small reflections that occur within the uncontrolled impedance bundle. These multiple reflections as well as the variations in velocity of propagation that go with them will reduce the accuracy of the method somewhat for uncontrolled impedance cables, as we shall see later.

When a peak detection algorithm (to identify the approximate open circuit location) is coupled with a curve fitting approach (to determine its precise location), the length of the wires can be calculated very accurately as shown in Fig. 4(a) and (b) for the controlled and uncontrolled impedance wires, respectively. The maximum error observed for controlled impedance cables is 3 cm, and for the uncontrolled impedance wires is 6 cm. The minimum measurable length for both systems is approximately 3.5 m, as seen in these figures. This is because the initial and final peaks overlap. A more advanced curve fitting approach can be used to distinguish these overlapping peaks.

For the discussion that follows, the ideal case will be assumed where the cable is lossless. An additional assumption is that frequency dispersion is negligible in the cable. That is, that all frequencies travel down the cable at the same rate.

A. Expected Correlator Output With Generalized Noise

The correlator output can be analyzed in terms of the signal injected onto the cable, various reflections of that signal, and any unwanted signals (noise) received at the correlator input.

Let $S[n]$ be a recursive linear sequence of period K consisting of 1s and -1 s. Then let

$$s(t) = \sum_{n=-\infty}^{\infty} S[n] \cdot p(t - nT) \tag{1}$$

where

$$p(t) = \begin{cases} 1, & 0 \le t \le T_c \\ 0, & \text{otherwise} \end{cases} \tag{2}$$

so that $s(t)$ is a recursive linear signal (RLS) of period $T_s = KT_c$ consisting of 1s and -1 s. Here, T_c is the minimum duration of a 1 or -1, otherwise known as a "chip." Note that

$$s(t) = s(t + T_s) \tag{3}$$

for any t for a RLS of duration T_s.

The test system will send a signal $s(t)$ onto the cable, which will be reflected by some arbitrary number of impedance discontinuities in the cable. The reflected signals will return to the test system after some transmission delay. Along with the reflected signals will be some noise that will depend on the nature of the cable being tested, anomalies in the signal generation, and extraneous noise. The noise could be white noise, or it could contain signals such as Mil-Std 1553.

Let $x(t)$ be the received signal, defined as

$$x(t) = \sum_{k} a_k s(t - \tau_k) + n(t) \tag{4}$$

where a_k is the amplitude of reflected signal $a_k s(t-\tau_k)$ relative to $s(t), \tau_k$ is the time delay before receiving reflection k, and

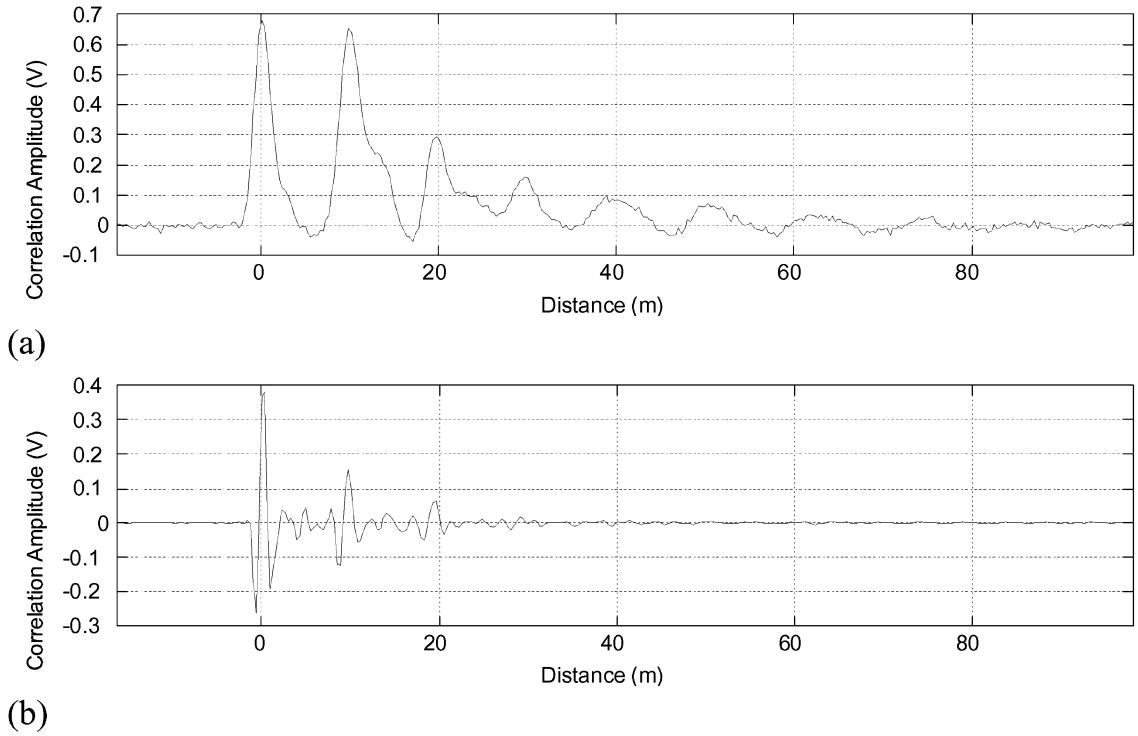

Fig. 6. (a) STDR and (b) SSTDR correlation response for an open circuit measured on two 22 AWG wires in a loosely bundled set of 22 wires that is 9.9 m long.

$n(t)$ is a noise signal of duration $T_n \gg T_s$, that is statistically uncorrelated to $s(t)$.

The correlator output will be

$$\begin{aligned} R_{sx}\tau &= \int_0^{T_s} s(t)x(t-\tau)\,dt \\ &= \int_0^{T_s} s(t)\sum_k a_x s(t-\tau-\tau_k)\,dt \\ &\quad + \int_0^{T_s} s(t)n(t-\tau)\,dt. \end{aligned} \tag{5}$$

As can be seen from (5), the correlator output will depend on the reflected signals and the noise, and is, therefore, determined by both deterministic and nondeterministic signals. The expected value $E(\cdot)$ of the correlation $R_{sx}\tau$ must, therefore, be considered

$$\begin{aligned} E\{R_{sx}\tau\} &= E\left\{\int_0^{T_s} s(t)\sum_k a_x s(t-\tau-\tau_k)\,dt \right. \\ &\quad \left. + \int_0^{T_s} s(t)n(t-\tau)\,dt\right\} \\ &= \int_0^{T_s} s(t)\sum_k a_x s(t-\tau-\tau_k)\,dt. \end{aligned} \tag{6}$$

In the last step in (6), the fact that $s(t)$ is zero mean and $n(t)$ is asynchronous to $s(t)$ was used.

The output of the correlator in the absence of noise is the sum of cross correlations of scaled and time-shifted copies of $s(t)$ and the original $s(t)$. The expected output in the presence of noise is the same as the output in the absence of noise, with some additional random noise term that is zero mean.

B. Correlator Output in the Presence of White Noise

The cross correlation of noise terms with $s(t)$ can be discussed in terms of the nature of the noise terms. If $n(t)$ is white Gaussian noise, the cross-correlation analysis can be described explicitly [11]. From (6), the cross correlation of $s(t)$ with $n(t)$ has mean

$$E\{R_{sn}\tau\} = E\left\{\int_0^{T_s} s(t)n(t-\tau)\,dt\right\} = 0 \tag{7}$$

and variance

$$E\{R_{sn}\tau^2\} = \frac{N_0}{2}E_s \tag{8}$$

where $N_0/2$ is the noise power received at the input, and E_s is the energy in the reference signal $s(t)$ over one period.

Thus, the effect of white noise in the system will be to add variation to the measurements proportional to the energy of the signal $s(t)$, but it will not cause a consistent DC offset.

C. Correlator Output in the Presence of Mil-Std 1553

As with white noise, the mean output of the correlator with Mil-Std 1553 as the noise source $n(t)$ is zero as shown in (6). The variance of the noise is a bit more involved to calculate since for Mil-Std 1553

$$E\{n(t_1-\tau)n(t_2-\tau)\} \text{ not proportional to } \partial(t_1-t_2) \tag{9}$$

which is not the same as it is for white noise, as shown in (8).

The signal used for correlation $s(t)$ will be integrated over a single period. It can, therefore, be considered to be an energy signal [11], and its energy spectral density is given by

$$G_{s(f)} = |F\{s(t)\}|^2 = |S(f)|^2 \tag{10}$$

where $S(f)$ is the Fourier transform of $s(t)$. Since $s(t)$ is of finite duration, its power spectral density (PSD) is only nonzero if considered only over the integration time T_s, in which case

$$\mathrm{PSD}_s(f) = \frac{|S(f)|^2}{T_s}. \tag{11}$$

The total energy in the signal $s(t)$ can be found in several ways as given by Rayleigh's theorem [11]

$$\begin{aligned} E_s &= \int_0^{T_s} s^2(t)\,dt = \int_{-\infty}^{\infty} |S(f)|^2\,df \\ &= T_s \int_{-\infty}^{\infty} \mathrm{PSD}_s(f)\,df. \end{aligned} \tag{12}$$

Let $n(t)$ be the noise signal due to Mil-Std 1553 operating on the wires. The Fourier transform of $n(t)$ is given by

$$N(f) = \int_{-\infty}^{\infty} n(t) e^{-j2\pi ft}\,dt. \tag{13}$$

Rayleigh's theorem gives the energy of the signal $n(t)$ as

$$\begin{aligned} E_n &= \int_{\kappa}^{\kappa+T_n} n^2(t)\,dt = \int_{-\infty}^{\infty} |N(f)|^2\,df \\ &= T_n \int_{-\infty}^{\infty} \mathrm{PSD}_n(f)\,df \end{aligned} \tag{14}$$

and the PSD defined over T_n as

$$\mathrm{PSD}_n(f) = \frac{|N(f)|^2}{T_n}. \tag{15}$$

As $n(t)$ is not a periodic function, the cross-correlation functions listed below that deal with $n(t)$ will be linear cross correlations. If both $s(t)$ and $n(t)$ or their derivatives are used in a cross correlation, it will be operating on one cycle of $s(t)$ and be defined over $0 \le t \le T_n$, unless otherwise specified. If only $s(t)$ is shown in a cross correlation or autocorrelation, it will be a circular cross correlation or autocorrelation, and will be nonzero only for $0 \le t \le T_s$. Since $T_n \gg T_s, T_n + T_s \approx T_n$, and will be treated as if $T_n + T_s = T_n$.

The Fourier transform of the cross correlation of $s(t)$ and $n(t)$ is

$$F\{R_{sn}(t)\} = F\{s(t) * n(-t)\} = S(f)N^*(f) \tag{16}$$

where $N^*(f)$ is the complex conjugate of $N(f)$.

The energy in this cross correlation is

$$E_{R_{sn}} = \int_{-\infty}^{\infty} |R_{sn}(t)|^2\,dt = \int_{-\infty}^{\infty} |S(f)|^2 |N(f)|^2\,df. \tag{17}$$

The expected energy in the cross correlation over time $0 \le t \le T_s$ is given by

$$\begin{aligned} E\{E_{R_{sn},T_s}\} &= \frac{T_s}{T_n} E\left\{ \int_{-\infty}^{\infty} |S(f)|^2 |N_{T_s}(f)|^2\,df \right\} \\ &= \frac{T_s}{T_n} \int_{-\infty}^{\infty} |S(f)|^2 |N(f)|^2\,df \approx E_{R_{sn},T_s} \end{aligned} \tag{18}$$

where $N_{T_s}(f)$ is the Fourier transform of the subsection of $n(t)$ used for the cross correlation for $0 \le t \le T_s$. Note that, in general, $N_{T_s}(f) \ne N(f)$ because the cross correlation may be over only a few bits of $n(t)$. However, the expected value for $N_{T_s}(f)$ is $N(f)$.

The expected noise power is

$$P_{R_{sn}} = \frac{E_{R_{sn},T_s}}{T_s} = \frac{E_{R_{sn}}}{T_n} = \frac{\int_{-\infty}^{\infty} |S(f)|^2 |N(f)|^2\,df}{T_n} \tag{19}$$

which is true for any noise source $n(t)$, including the Mil-Std 1553 signal.

It is clear that (19) indicates that spectral overlap between the noise and STDR/SSTDR signal results in unavoidable noise in the correlator output.

D. SSTDR Modulation

In order to perform a consistent cross correlation, a reference signal must be available. This brings us to the question of synchronization. If the reference signals modulation is off by 90° from the driving signals modulation, the cross correlation of the received signal and the reference signal would be zero, as the two signals would be orthogonal to each other. Another cross correlation of the same signal could return a different result, if the phase difference between the modulating frequency and the PN code changed. This would make the system very difficult to calibrate. Because the choice has been made to use PN codes, it makes sense to synchronize the modulating sinewave with the PN code [4]. By generating the signals in a consistent way, a reference signal can be generated which can be used consistently with the injected signal, providing for a system that gives consistent results under similar circumstances.

Sample aircraft cables tested with S/SSTDR have significant loss at high frequency. Noncontrolled impedance cables (discrete bundled wires) over 60 m long have been tested with STDR and over 15-m long have been tested with SSTDR (which has higher frequency content).

Another effect of realistic aircraft cable is the effect of variation in the velocity of propagation (VOP). Typical wires have VOP ranging from 0.66 to 0.76 times the speed of light [9]. If the type of wire is known, the correct velocity can be used to obtain the best possible calculation for the length of the wire. If the type of wire is not known, and average values are used, additional errors of up to 10% could be observed. Correlation peaks show higher dispersion if they are due to reflections farther down the cable, as shown in Fig. 2. This effect can be accounted for by changing the shape that is matched by the curve fitting algorithm as it is applied to reflections from different lengths down the cable.

Results for both controlled and uncontrolled impedance aircraft cables with a variety of signals on the line were tested [4]. Using curve fitting, both methods had errors on the order of 3 cm for controlled impedance coax and 6 cm for uncontrolled bundled cable with or without 60-Hz signals for both open and short circuited cables. However, as expected, SSTDR performs significantly better than STDR in the presence of the MilStd-1553 signal utilizing the uncontrolled impedance bundled wire (a worse case than normal, since MilStd 1553 would

normally be implemented on controlled impedance twisted pair wire). For an SNR of -24 dB, STDR has an error of about 24 cm, and SSTDR had less than 3 cm of error. SSTDR still had less than 6 cm of error down to and SNR of -53 dB below the MilStd 1553 data signal. Both methods could be used effectively, since the required SNR for MilStd 1553 is -17 dB, however the advantage of SSTDR for a high frequency noisy environment was clearly demonstrated.

V. Signal-to-Noise Ratio

The SNR is defined as the signal power divided by the average noise power. For a digital signal such as Mil-Std 1553, this would be expressed as

$$\frac{S}{N} = \frac{\text{Mil Std 1553 Power}}{\text{Background Noise Power}}. \tag{20}$$

In the case of STDR/SSTDR, the STDR and SSTDR signals are the desired signals, and other signals are noise. Therefore, considering the signal-to-noise power of the STDR and SSTDR signals in the presence of another signal (Mil-Std 1553 in this example), gives

$$\frac{S}{N} = \frac{\text{XCorr(STDR or SSTDR Signal)}}{\text{XCorr(Mil] Std 1553} + \text{Background Noise)}} \tag{21}$$

after correlation, where $\text{XCorr}(\cdot)$ means "cross-correlated power."

The reflection terms $g_k = a_k s(t-\tau_k)$ represent the reflections at various distances down the cable. To detect each of these signals, the correlator offset is set to time $t = \tau_k$. All other reflection terms are considered noise terms. The received signal after cross correlation is

$$R_{sg_k}(t_k) = a_k E_s. \tag{22}$$

From (22) and (19), the SNR is

$$\left(\frac{S}{N}\right) = \frac{a_k^2 E_s^2}{\frac{\int_{-\infty}^{\infty} |S(f)X(f)|^2\, df}{T_s}} = \frac{a_k^2 E_s^2 T_s}{\int_{-\infty}^{\infty} |S(f)X(f)^2\, df}. \tag{23}$$

The integral in (23) needs to be carried out for every signal of interest that could be a noise source. For spectrally narrow noise, such as the 115 V 400 Hz on aircraft, (23) simplifies to

$$\begin{aligned}\left(\frac{S}{N}\right) &= \frac{a_k^2 E_s^2 T_s}{\int_{-\infty}^{\infty} |S(f)X(f)|^2\, df} \\ &= \frac{a_k^2 E_s^2 T_s}{\int_{-\infty}^{\infty} \left|S(f)\sqrt{2}\frac{\delta(f-400\text{ Hz})+\delta(f+400\text{ Hz})}{2}\right|^2 df} \\ &= \frac{\sqrt{2}}{115}\frac{a_k^2 E_s^2 T_s}{(|S(400\text{ Hz})|^2 + |S(-400\text{ Hz})|^2)}.\end{aligned} \tag{24}$$

From this, it can be seen that if $S(f)$ has very little of its energy centered at ± 400 Hz, the SNR will be large.

For noise signals that are broad in frequency spectrum, the integral in (23) is quite involved, and is best handled numerically on a case-by-case basis.

The effects of changing certain parameters can be studied analytically in such a way as to provide excellent insight into factors other than signal and noise power that affect the SNR. These analyzes are carried out below.

A. Changing the Length of the STDR/SSTDR Signal

In order to approximate a signal with m times the number of chips as $s(t)$, let us define a new signal $s_m(t)$ such that $|S_m(f)|$ is proportional to $|S(f)|$, and let the duration of $s_m(t)$ be $mT_s = T_{s_m}$. Letting the amplitude of $s_m(t)$ be the same as $s(t)$

$$E_{s_m} = \int_{-\infty}^{\infty} |s_m(t)|^2\, dt = m\int_0^{T_s} |s(t)|^2\, dt = mE_s. \tag{25}$$

In the frequency domain

$$\begin{aligned}E_{s_m} &= \int_{-\infty}^{\infty} |S_m(f)|^2\, df = \int_{-\infty}^{\infty} |\sqrt{m}S(f)|^2\, df \\ &\therefore |S_m(f)| = |\sqrt{m}S(f)|\end{aligned} \tag{26}$$

which is what would be expected if the duration of $s(t)$ were increased by a factor of m by adding more chips to its sequence.

Letting

$$R_{s_m n}(t) = s_m(t) * n(-t) \tag{27}$$

gives

$$E_{R_{s_m n}} = \int_{-\infty}^{\infty} |S_m(f)|^2 |N(f)|^2\, df = mE_{R_{sn}} \tag{28}$$

which is the noise energy in the cross correlation of $s(t)$ with $n(t)$ over the time $0 \le t \le T_n$. The expected value of the noise power over the interval $0 \le t \le T_s$ is the noise power over the interval $0 \le t \le T_n$, given by

$$P_{R_{s_m n}} = \frac{E_{R_{s_m n}}}{T_n} = \frac{mE_{R_{sn}}}{T_n} = mP_{R_{sn}} \tag{29}$$

which is valid because $T_n \gg T_s$.

The central peak of the autocorrelation is given by

$$R_{s_m}(0) = E_{s_m} = mE_s. \tag{30}$$

The signal power is

$$(R_{s_m}(0))^2 = (mE_s)^2 = m^2 E_s^2. \tag{31}$$

From (31) and (29), the SNR is

$$\left(\frac{S}{N}\right)_m = \frac{m^2 E_s^2}{mP_{R_{sn}}} = m\frac{E_s^2}{P_{R_{sn}}} = m\left(\frac{S}{N}\right). \tag{32}$$

Equation (32) shows that doubling the length of the PN code while leaving all other parameters the same will double (increase by 3 dB) the SNR. This is true for any noise type including 400-Hz ac, Mil-Std 1553, and white noise.

B. Scaling the Frequency of the STDR/SSTDR Signal

Let $s_\psi(t) = s(\psi t)$, and $T_{s_\psi} = (T_s/\psi)$, where ψ is a constant. Using the scaling property of the Fourier transform and assuming $\psi \geq 1$

$$S_\psi(f) = \frac{1}{|\psi|} S\left(\frac{f}{\psi}\right) = \frac{1}{\psi} S\left(\frac{f}{\psi}\right). \tag{33}$$

The signal of interest after correlation is the peak value in the autocorrelation of $s_\psi(t)$, which is $R_{s_\psi}(0)$, and corresponds to the energy in $s_\psi(t)$, given by

$$R_{s_\psi}(0) = \int_0^{\frac{T_s}{\psi}} |s(\psi t)|^2 \, dt = \frac{1}{\psi} E_s. \tag{34}$$

Examining correlator noise output, we have

$$R_{s_\psi n}(t) = s_\psi(t) * n(-t) \tag{35}$$

and

$$E_{R_{s_\psi n}} = \frac{1}{\psi^2} \int_{-\infty}^{\infty} \left| S\left(\frac{f}{\psi}\right) \right|^2 |N(f)|^2 \, df. \tag{36}$$

If STDR is considered with the chip rate much greater than the Mil-Std 1553 data rate of 1 MHz, it can be assumed that $S(f)$ is approximately constant in the region where the majority of the power of $N(f)$ exists. Then, $(1/\psi)S(f/\psi)$ will also be approximately constant in that region if $\psi \geq 1$. With these assumptions, (36) can be written as

$$E_{R_{s_\psi n}} \approx \int_{-\infty}^{\infty} |S(f)|^2 |N(f)|^2 \, df = \frac{1}{\psi^2} E_{R_{sn}} \tag{37}$$

and the average noise power is

$$P_{R_{s_\psi n}} = \frac{E_{R_{s_\psi n}}}{T_n} \approx \frac{\frac{1}{\psi^2} E_{R_{sn}}}{T_n} = \frac{1}{\psi^2} P_{R_{sn}}. \tag{38}$$

The SNR from (38) and (34) is

$$\left(\frac{S}{N}\right)_\psi \approx \frac{\frac{1}{\psi^2} E_s^2}{\frac{1}{\psi^2} P_{R_{sn}}} = \frac{E_s^2}{P_{R_{sn}}} = \left(\frac{S}{N}\right). \tag{39}$$

Equation (39) states that in STDR mode, doubling the chip rate of the PN code while leaving all other parameters the same will have no appreciable effect on the SNR for STDR tests if the major noise contributor is Mil-Std 1553.

Attention is now turned to changing the chip rate and modulation frequency for SSTDR tests. For SSTDR with a chip rate much greater than the Mil-Std 1553 data rate of 1 MHz, scaling the SSTDR chip rate and modulation frequency by a factor ψ will change the slope near $f = 0$ by a factor $1/\psi$. So, in the region where the Mil-Std 1553 signal is significant

$$\left| S\left(\frac{f}{\psi}\right) \right| \approx \frac{1}{\psi} |S(f)|. \tag{40}$$

With this approximation

$$E_{R_{s_\psi n}} = \int_{-\infty}^{\infty} |S_\psi(f)|^2 |N(f)|^2 \, df = \frac{1}{\psi^4} E_{R_{sn}} \tag{41}$$

and the average noise power is

$$P_{R_{s_\psi n}} = \frac{E_{R_{s_\psi n}}}{T_n} \approx \frac{\frac{1}{\psi^4} E_{R_{sn}}}{T_n} = \frac{1}{\psi^4} P_{R_{sn}}. \tag{42}$$

The SNR from (42) and (34) is

$$\left(\frac{S}{N}\right)_\psi \approx \frac{\frac{1}{\psi^2} E_s^2}{\frac{1}{\psi^4} P_{R_{sn}}} = \psi^2 \left(\frac{S}{N}\right). \tag{43}$$

Equation (43) shows that in SSTDR mode, doubling the chip rate of the PN code and modulation frequency while leaving all other parameters the same will increase the SNR for SSTDR tests by 6 dB if the major noise contributor is Mil-Std 1553. This is vastly superior to the STDR results.

C. Self-Induced Noise

A certain amount of noise comes from the selection of a particular PN code. This is considered *noise*, because there is a deviation in the cross correlation of all PN codes from the ideal of a central peak with no side-lobes. Fig. 7 shows the autocorrelations of two identical-power PN sequences, one of which is using a ML code [10], and the other of which is using a gold code [10]. Note that the power in the two autocorrelations is not equal, even though the power in the signals used to generate them is equal. In fact, the power in the ML code autocorrelation is 56% the power in the gold code autocorrelation. This extra power in the gold code autocorrelation is self-induced noise power, and it reduces the SNR for STDR/SSTDR tests.

D. STDR/SSTDR Code Selection

The optimal PN code depends on the nature of the application. The PN code with the lowest side lobes in its autocorrelation is a ML code. It is, therefore, optimal for use when only one PN code will be used at a time.

The PN code with the next best autocorrelation properties is the Kasami code [11]. It is the best PN code choice when simultaneous tests on one or more conductors can interfere with each other. This is due to the high degree of orthogonality of signals in a Kasami set. If, however, the number of simultaneous tests exceeds the number of codes in the Kasami set, then codes with higher autocorrelation side-lobes, such as gold codes, may be used. One-shot codes, such as those similar to Barker codes, may also be used for STDR/SSTDR.

Many other PN codes are a poor choice for STDR/SSTDR due to high autocorrelation side lobes or the lack of a single autocorrelation peak.

E. STDR/SSTDR Using ML Codes

When the background noise is white noise, the total noise power after correlation is identical for both the STDR and SSTDR cases because the noise is spectrally flat. In this case, it is clear that there is little advantage of STDR over SSTDR or vice versa. However, when the noise is not spectrally flat, such as is the case with a Mil-Std 1553 or other digital data signal, the spectral overlap of the noise with the STDR/SSTDR signal will change the relative benefits of STDR versus SSTDR.

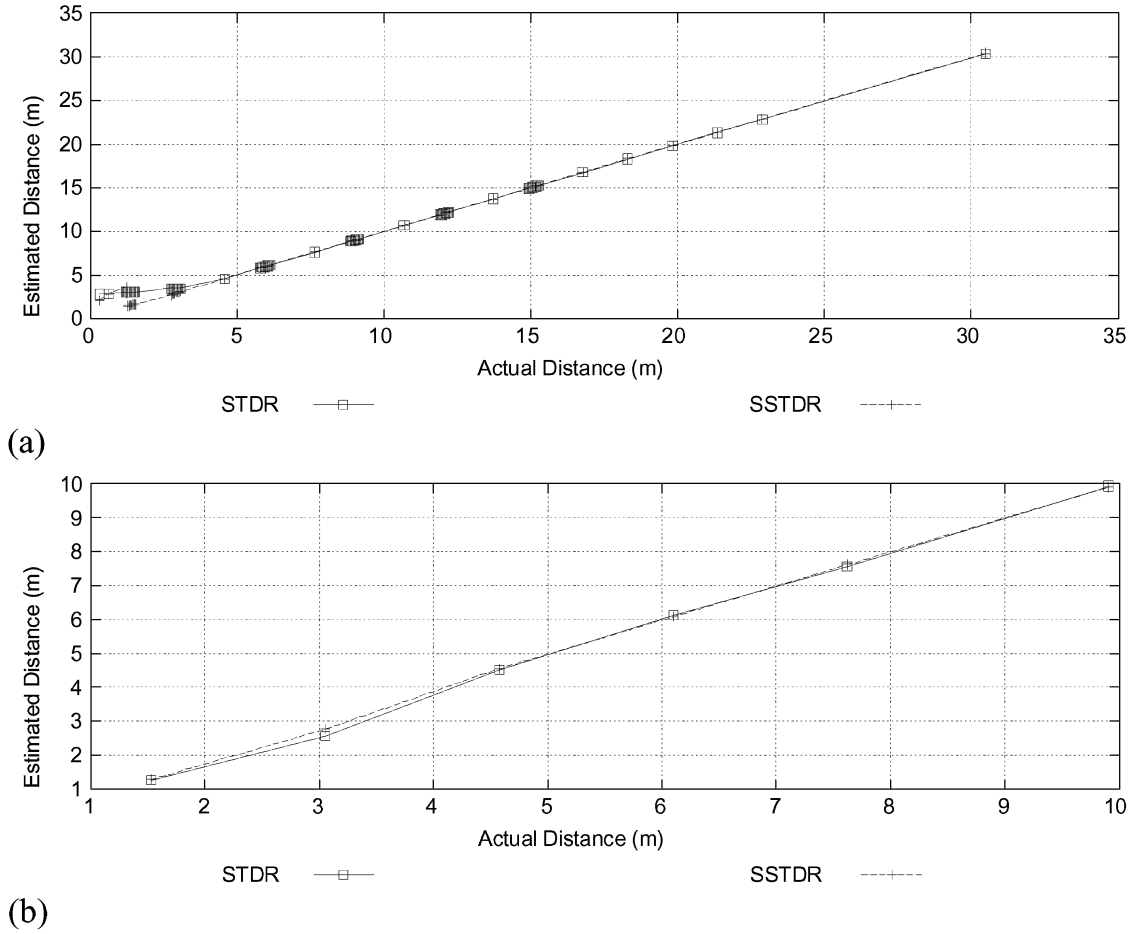

Fig. 7. Actual versus distance estimated with a curve-fit algorithm on (a) a 75-Ω cable and (b) a pair of two 22 AWG wires within a loose bundle of 22 wires tested with S/SSTDR.

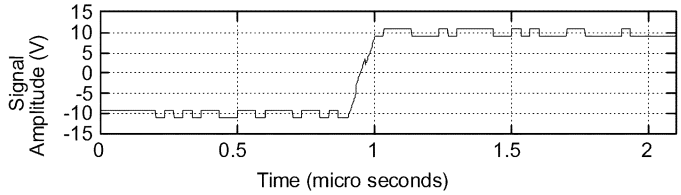

Fig. 8. ML code STDR signal at 1-V RMS, with a signal length of 63 chips at 30 MHz, operating in the presence of Mil-Std 1553 at 10-V RMS.

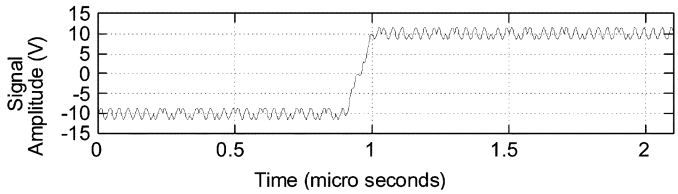

Fig. 9. ML code SSTDR signal at 1-V RMS, with a signal length of 63 chips at 30 MHz, operating in the presence of Mil-Std 1553 at 10-V RMS.

Fig. 8 shows a 1-V RMS STDR signal in the presence of 10-V RMS Mil-Std 1553. Since the Mil-Std 1553 signal is at 10-V RMS, it is 20 dB above the STDR signal level. The PN code length is 63 bits, which will give a processing gain of 36 dB. The chip rate in this figure is 30 MHz. The processing gain for longer STDR sequences is higher, so a lower power STDR signal can be used in an actual test system that will not interfere with the Mil-Std 1553 signal.

Fig. 9 shows a 1-V RMS SSTDR signal in the presence of 10-V RMS Mil-Std 1553. The PN code length used to generate this SSTDR signal is 63 bits.

Even after the 36 dB processing gain, the correlation peak shown in Fig. 10 is not clear due to the high noise level after correlation. Consider, however, the clarity of the correlation peak in Fig. 11. In both cases, the amplitude of the correlation peak is identical, but the background noise levels are significantly different.

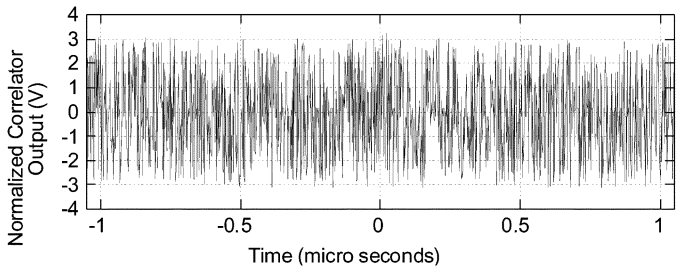

Fig. 10. Normalized cross correlation of a reference ML code STDR signal with the signal shown in Fig. 8.

To gain insights into the dramatic difference in background noise levels shown in Figs. 10 and 11, the spectral content of

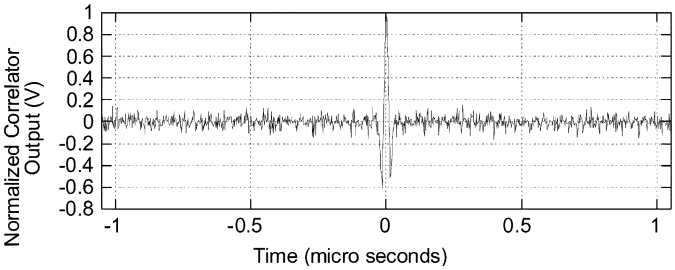

Fig. 11. Normalized cross correlation of a reference ML code SSTDR signal with the signal shown in Fig. 9.

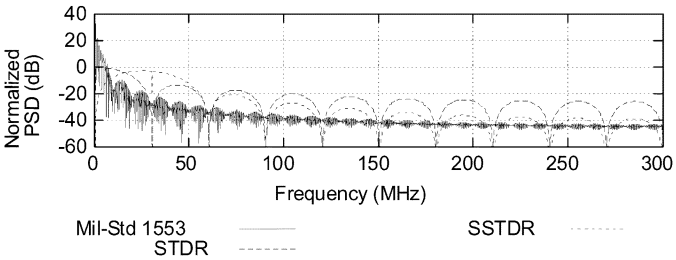

Fig. 12. Normalized PSD of a ML code STDR signal of length 63 chips at 30 MHz (1-V RMS), ML code SSTDR signal of length 63 chips at 30 MHz (1-V RMS), and Mil-Std 1553 (1-V RMS). Signals are normalized with respect to the peak STDR power.

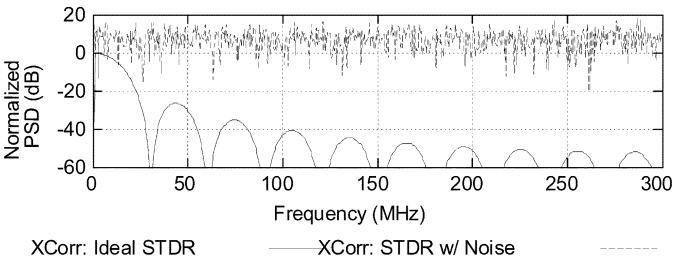

Fig. 13. Normalized PSD of the cross-correlator (XCorr) output for a pure ML code STDR (ideal case) signal of length 63 chips at 30 MHz (1-V RMS), and a 1-V RMS ML code STDR signal in the presence of a 10-V RMS Mil-Std 1553 signal.

the STDR and SSTDR signals with respect to the Mil-Std 1553 signal can be examined. The PSD of these three signals as used in the simulations is shown in Fig. 12, normalized to the peak STDR power.

In Fig. 12, it can be seen that the power in the Mil-Std 1553 signal is centered about 0 Hz, as is the power in the STDR signal. The SSTDR signal, however, slopes down to a spectral null at 0 Hz (dc). If this is considered in light of (19), it is clear that there will be significantly more unwanted power in the cross correlation of an STDR signal with Mil-Std 1553 than there will be in the cross correlation of an SSTDR signal with Mil-Std 1553.

To compare SSTDR with STDR, frequencies above the chip rate were not trimmed off prior to modulation, which caused some aliasing in the SSTDR case. Tests performed using bandlimiting prior to modulation did not show a significant difference in the SSTDR correlator output.

Fig. 13 shows the PSD of the cross correlation shown in Fig. 12, alongside the cross correlation of an STDR signal in the ideal case where there is no noise. The background noise completely dwarfs the desired signal. The frequency spectrum of the noise is broad due to the random sampling of the noise

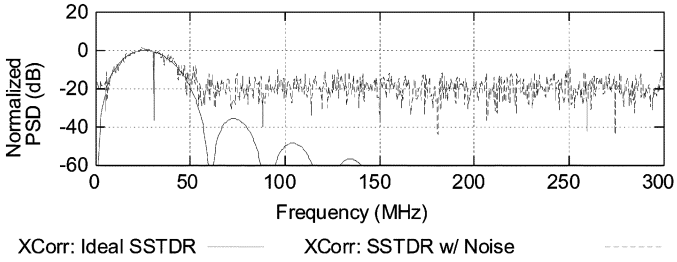

Fig. 14. Normalized PSD of the cross-correlator (XCorr) output for a pure ML code SSTDR (ideal case) signal of length 63 chips at 30 MHz (1-V RMS), and a 1-V RMS ML code SSTDR signal in the presence of a 10-V RMS Mil-Std 1553 signal.

that naturally occurs in a single sample per iteration correlator design.

Fig. 14 shows the PSD of the cross correlation shown in Fig. 11, alongside the cross correlation of an SSTDR signal in the ideal case where there is no noise. The background noise is significantly lower than the peak of the desired signal. Again, the frequency spectrum of the noise is broad due to the random sampling of the noise that naturally occurs in a single sample per iteration correlator design.

It is clear from these simulations that STDR and SSTDR can be used to find impedance changes in wiring. It is also clear that the spectral content of the SSTDR signal can be adjusted to avoid mutual interference between the SSTDR and digital signals on the wires. Tests with narrowband noise, such as 400-Hz 115-V ac, show a negligible effect on the correlator output compared to wideband noise such as the digital signals discussed above.

VI. Conclusion

This paper has examined STDR and SSTDR using ML codes. Equations were developed to enable system design by describing the interactions of the STDR/SSTDR signal and various types of noise in the correlator output. Simulations were performed for STDR and SSTDR tests for ML codes in the presence of a Mil-Std 1553 background signal to study the effects of this type of noise on STDR/SSTDR tests. Equations were developed to describe the effects of scaling test system parameters including the number of chips in the PN sequence and the PN sequence chip rate used for STDR and SSTDR. It was shown that doubling the PN code length doubles the SNR independent of the noise type, and that doubling the chip rate (and modulation frequency for SSTDR) in the presence of Mil-Std 1553 can have no appreciable effect on the SNR for STDR, but can increase the SNR for SSTDR by 6 dB.

ML codes were identified as the best code to use for testing single wires at a time due to the higher self-induced noise present with other code choices. Kasami codes are the optimal codes to use when performing multiple interacting tests simultaneously.

The work covered in this paper shows that SSTDR and STDR can be effective tools for locating defects on live cables, and this was demonstrated for both controlled and uncontrolled impedance cables carrying 60 Hz (similar to 400 Hz) and 1-MHz Mil Std 1553 signals. This discussion has shown that

STDR and SSTDR are equally suited for testing in the presence of white noise or low frequency signals (such as 60- or 400-Hz power), but that SSTDR is a better choice for testing in the presence of the high-frequency data signals typically found on aircraft cables.

The discussion in this paper suggests that STDR and SSTDR test system parameters could be adjusted so that the test signal levels are below the noise tolerance of other signals on the wires, while still providing a sharp correlation peak to detect changes in impedance along the length of the cables. These features make it feasible to use SSTDR and to a lesser degree STDR to test live wires on aircraft in flight. Because the tests can be performed continuously, intermittent failures such as open circuits, short circuits, and arcs could be detected and recorded when they occur, enabling maintenance personnel on the ground to quickly identify the nature and location of intermittent wiring problems so they can be resolved. Further evaluation of this method for locating intermittent "soft" faults can be found in [18]. Faults with lower impedance, either on a "hot" wire or on the ground return, have less reflection and, therefore, less SNR. Detection of these faults is limited by the SNR required for detection and the noise in the measured correlation.

REFERENCES

[1] R. Pappas, "Aging systems research program," presented at the DER Recurrent Seminar, Sep. 2000.

[2] C. Furse and R. Haupt, "Down to the wire," *IEEE Spectrum*, vol. 38, no. 2, pp. 34–39, Feb. 2001.

[3] S. Field, P. Arnason, and C. Furse, "Smart wire technology for aircraft applications," presented at the 5th Joint NASA/FAA/DoD Conf. Aging Aircraft, Orlando, FL, Sep. 2001.

[4] P. Smith, "Spread spectrum time domain reflectometry," Ph.D. dissertation, Dept. Elect. Comput. Eng., Utah State Univ., Logan, 2003.

[5] M. B. Djuric *et al.*, "Digital signal processing algorithms for arcing fault detection and fault distance calculation on transmission lines," *Elect. Power Energy Syst.*, vol. 19, no. 3, pp. 165–170, 1997.

[6] V. Taylor and M. Faulkner, "Line monitoring and fault location using spread spectrum on power line carrier," *Proc. Inst. Elect. Eng.*, vol. 143, pp. 427–434, Sep. 1996.

[7] K. Jones *et al.*, "Adaptive method and apparatus for transmission line analysis," U.S. Patent 20 020 169 585, Mar. 11, 2002.

[8] M. F. Iskander, *Electromagnetic Fields and Waves*. Englewood Cliffs, NJ: Prentice-Hall, 1992.

[9] Y. Chung, C. Furse, and J. Pruitt, "Application of phase detection frequency domain reflectometry for locating faults in an F-18 flight control harness," *Trans. IEEE Electromagn. Compat.*, vol. 47, no. 2, pp. 327–334, May 2005.

[10] R. C. Dixon, *Spread Spectrum Systems*. New York, NY: Wiley, 1984.

[11] J. G. Proakis and M. Salehi, *Communication Systems Engineering*. Englewood Cliffs, NJ: Prentice-Hall, 1994.

[12] P. J. Medelius and H. J. Simpson, "Non-intrusive impedance-based cable tester," U.S. Patent 5 977 773, Aug. 15, 1997.

[13] D. Bates, "Wireless communication and signal processing for aging aircraft wiring," M.S. thesis, Dept. Elect. Comput. Eng., Utah State Univ., Logan, 2002.

[14] K. Shull, L. C. Brinson, N. Nunalee, T. Bai, T. Mason, and S. Carr, "Aging characterization of polymeric insulation in aircraft wiring via impedance spectroscopy," in *Proc. 5th Joint NASA/FAA/DoD Conf. Aging Aircraft*, Sep. 2001, pp. 55–61.

[15] P. Smith, "Using inert gas to enhance electrical wiring inspection," presented at the 6th Joint FAA/DoD/NASA Conf. Aging Aircraft, San Francisco, CA, Sep. 2002.

[16] B. Sklar, *Digital Communications, Fundamentals and Applications*. Englewood Cliffs, NJ: Prentice-Hall, 1988.

[17] *Mil-Std-1553 Designers Guide*, 6th ed. New York: ILC Data Device Corp., 1998, pp. II-28–II-48.

[18] C. Furse, P. Smith, M. Safavi, and C. Lo, "Feasibility of spread spectrum sensors for location of arcs on live wires," *IEEE Sensors J.*, vol. 5, no. 6, pp. 1445–1450, Dec. 2005.

Paul Smith (M'02) received the M.B.A. degree in 1996 and the Ph.D. degree in 2003.

He is currently the President of LiveWire Test Labs., Inc., Salt Lake City, UT, which builds hardware for locating intermittent wire faults. He has over 11 years of experience designing cable and wire harness test equipment. He has been working on solutions to difficult wire test issues and holds patents, and has patents pending, in the field. He has a background in business management, electronic circuit design, electromechanical system design, electromagnetic theory, nonlinear inversion theory, microwaves, quantum mechanics, and optics.

Cynthia Furse (SM'99) received the Ph.D. degree in 1994.

She is the Director of the Center of Excellence for Smart Sensors, University of Utah, Salt Lake City, where she is also an Associate Professor in the Electrical and Computer Engineering Department. The Center focuses on embedded sensors in complex environments, particularly sensors for anomalies in the human body and aging aircraft wiring. She has directed the Utah "Smart Wiring" program, sponsored by NAVAIR and USAF, since 1997. She teaches electromagnetics, wireless communication, computational electromagnetics, microwave engineering, and antenna design.

Dr. Furse was the 2000 Professor of the Year at the College of Engineering, Utah State University, Logan, the 2002 Faculty Employee of the Year, a National Science Foundation Computational and Information Sciences and Engineering Graduate Fellow, IEEE Microwave Theory and Techniques Graduate Fellow, and Presidents Scholar at the University of Utah. She is the Chair of the IEEE Antennas and Propagation Society Education Committee and an Associate Editor of the IEEE TRANSACTIONS ON ANTENNAS AND PROPAGATION.

Jacob Gunther (M'99) was a Research Assistant with the Microwave Earth Remote Sensing Laboratory, Brigham Young University, Provo, UT, from 1992 to 1994. From 1994 to 1995, he was with Lockheed-Martin, Manassas, VA, where he worked on target detection algorithms, sonar systems, and satellite digital communication systems. From 1998 to 2000, he was with Merasoft, Inc., Provo, where he worked on speech recognition, speaker identification, and noise cancellation using microphone arrays. He joined the faculty of the Department of Electrical and Computer Engineering department, Utah State University, Logan, in 2000. His research interests include array signal processing for wireless communications, blind deconvolution and source separation, and system identification.